Identification and Characterisation of the Circadian Pacemaker of the Cockroach *Leucophaea maderae*

(Identifizierung und Charakterisierung des circadianen Schrittmachers der Schabe *Leucophaea maderae)*

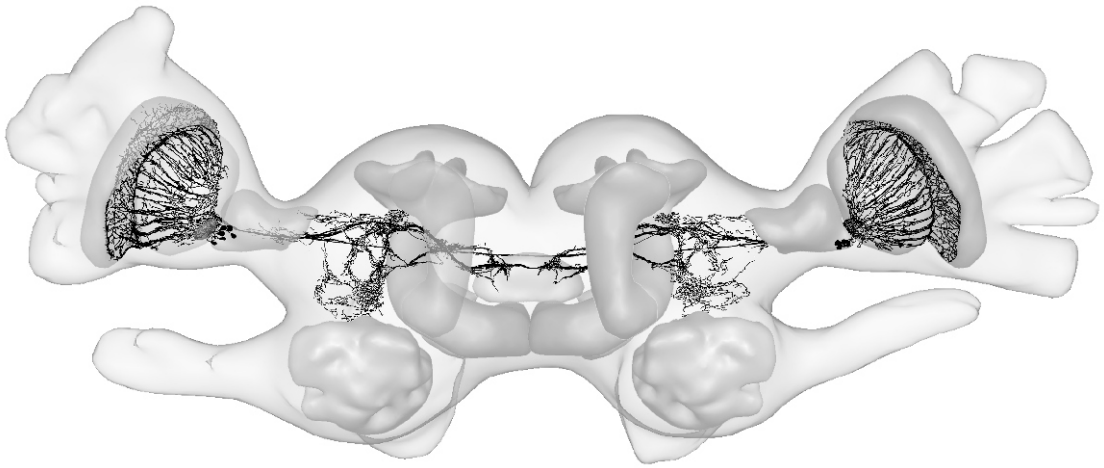

Dissertation zur Erlangung des Doktorgrades der Naturwissenschaften (Dr. rer. nat.), dem Fachbereich Biologie der Philipps-Universität Marburg vorgelegt von

Thomas Reischig
aus Eichstätt/Obb.

Marburg/Lahn, Juli 2003

Vom Fachbereich Biologie
der Philipps-Universität Marburg als Dissertation am 2003 angenommen.

Erstgutachterin: HD Dr. Monika Stengl
Zweitgutachter: Prof. Dr. Roland Brandl

Tag der mündlichen Prüfung am 2003.

Für Sabine.

Contents

Erklärung: Eigene Beiträge und veröffentlichte Teile der Arbeit

Laut Promotionsordnung der Philipps-Universität Marburg vom 29.11.1989 (idF. vom 12.4.2000) müssen bei den Teilen der Dissertation, die aus gemeinsamer Forschungsarbeit entstanden, die individuellen Leistungen des Doktoranden deutlich abgrenzbar sein. Diese Beiträge werden im folgenden näher erläutert.

Kapitel I: Morphology and pigment-dispersing hormone immunocytochemistry of the accessory medulla, the presumptive circadian pacemaker of the cockroach *Leucophaea maderae*: a light- and electron-microscopic study.

- Ausarbeitung, Durchführung und Auswertung der Experimente durch den Autor hauptsächlich im Rahmen der Diplomarbeit „Licht- und elektronenmikroskopische Analyse der akzessorischen Medulla, eines möglichen Schrittmacherzentrums der Schabe *Leucophaea maderae*“, Regensburg, 1995. Die Vervollständigung der elektronenmikroskopischen Experimente und der Auswertungen wurde während der Zeit der Dissertation durchgeführt.
- Verfassen der Veröffentlichung in Zusammenarbeit mit HD Dr. Monika Stengl.
- Veröffentlichung: Reischig T and Stengl M. 1996. Cell Tissue Res 285:305–319. Das vorliegende Kapitel entspricht der Veröffentlichung.

Kapitel II: Ultrastructure of pigment-dispersing hormone-immunoreactive neurons in a three-dimensional model of the accessory medulla of the cockroach *Leucophaea maderae*.

- Ausarbeitung, Durchführung und Auswertung aller Experimente durch den Autor. Verfassen der Veröffentlichung in Zusammenarbeit mit HD Dr. Monika Stengl.
- Veröffentlichung: Die Arbeit ist bei *Cell and Tissue Research* eingereicht worden. Das vorliegende Kapitel entspricht der überarbeiteten, eingereichten Version des Manuskripts, nachdem die Änderungsvorschläge der Gutachter eingearbeitet wurden. Das Manuskript wurde kurz vor Abgabe der Dissertation zur Veröffentlichung angenommen.

Kapitel III: Lesion of PDH-immunoreactive medulla neurons abolishes circadian rhythmic locomotor activity in the cockroach *Leucophaea maderae*.

- Ausarbeitung, Durchführung und Auswertung aller Experimente durch den Autor.

Kapitel IV: Ectopic transplantation of the accessory medulla restores circadian rhythmic behaviour in arrhythmic cockroaches (*Leucophaea maderae*).

- Ausarbeitung, Durchführung und Auswertung aller Experimente durch den Autor.
- Verfassen der Veröffentlichung in Zusammenarbeit mit HD Dr. Monika Stengl.
- Veröffentlichung: Reischig T and Stengl M. 2003. J Exp Biol 206:1877–1886. Das vorliegende Kapitel entspricht der Veröffentlichung.

Kapitel V: Scan periodogram analysis: a new method for an automated detection of short circadian rhythmic activity phases in long data records.

- Konzeption der Auswertung und Programmierung durch den Autor.

Kapitel VI: Optic lobe commissures in a three-dimensional brain model of the cockroach *Leucophaea maderae*: a search for the circadian coupling pathways.

- Ausarbeitung, Durchführung und Auswertung aller Experimente durch den Autor.
- Verfassen der Veröffentlichung in Zusammenarbeit mit HD Dr. Monika Stengl.
- Veröffentlichung: Reischig T and Stengl M. 2002. J Comp Neurol 443:388–400. Das Kapitel entspricht der Veröffentlichung.

Kapitel VII: Pigment-dispersing hormone (PDH)-immunoreactive neurons form a direct coupling pathway between the bilaterally symmetric circadian pacemakers of the cockroach *Leucophaea maderae*.

- Die Dextran-Injektionen an *wholemount*-Präparaten wurden durch Dr. Bernhard Petri durchgeführt und sind Teil seiner Dissertation „Neuronal organisation of a circadian clock: analysis of the clock which controls circadian locomotor behaviour in the brain of the cockroach *Leucophaea maderae*“, Regensburg, 1998. Aus dieser Arbeit wurde eine Abbildung (Fig. 3) übernommen. Die Konzeption und Durchführung aller übrigen Experimente sowie deren Auswertung, als auch die Erstellung aller anderen Abbildungen wurden vom Autor vorgenommen.
- Das Manuskript wurde in Zusammenarbeit mit HD Dr. Monika Stengl verfaßt und wird demnächst bei *Journal of Comparative Neurology* eingereicht. Das Kapitel entspricht dem Manuskript.

Im Zeitraum der Dissertation wurden durch den Autor Vorversuche zu Multielektroden (MEA)-Ableitungen an der akzessorischen Medulla, sowie immunzytochemische Färbungen und Westernblots mit verschiedenen Antiseren gegen das Uhrprotein PERIOD durchgeführt. Die Ergebnisse der MEA-Ableitungen sind Teil der Dissertation von Dr. Bernhard Petri. Die Immunfärbungen und Westernblots wurden von Julia Fischer bzw. Jana Zimmermann in ihren jeweiligen Diplomarbeiten fortgeführt. Diese Experimente wurden daher nicht in die Dissertation aufgenommen. Ferner wurde vom Verfasser der immunzytochemische Teil der Zulassungsarbeit „Untersuchungen zur Inneren Uhr von Insekten: Desoxyglukose-Markierung der akzessorischen Medulla in der Schabe *Leucophaea maderae* und PDH-immunzytochemische Untersuchungen“ von Andreas Meßner (Regensburg, 1998) betreut. Zwei Präparate, die im Laufe Arbeit entstanden, wurden in in die Fig. 1, Appendix A aufgenommen.

Der Verfasser ist Co-Autor des Reviews „Neural organisation of the circadian system of the cockroach *Leucophaea maderae*“, Homberg U, Reischig T, and Stengl M. 2003. Chronobiol Int 20:577–591.

Die Abfassung des Dissertation in englischer Sprache wurde vom Dekan des Fachbereichs Biologie am 13.06.2003 genehmigt.

Elektronische Adressen des Verfassers:

E-Mail: `thomas@reischig.de`
Web: `http://www.reischig.de`

Zusammenfassung

Läsionsexperimente in den 60er und 70er Jahren lokalisierten den circadianen Schrittmacher, der das Laufverhalten der Schabe *Leucophaea maderae* steuert, in den optischen Loben des Gehirns der Schabe. In dieser generellen Schrittmacherregion liegt die akzessorische Medulla (AMe; plural akzessorische Medullae, AMae). Die AMe wird dicht von Neuronen innerviert, welche durch ein Antiserum gegen das Oktadeka-Peptid *pigment-dispersing hormone* (PDH) aus Crustaceen angefärbt werden können. Die Somata dieser PDH-immunreaktiven (PDH-ir) Neurone befinden sich in den optischen Loben, wo sie vier Hauptgruppen bilden: zwei an der posterioren Lamina (dorsale und ventrale PDH-ir Laminaneurone, PDHLa), und zwei in der Nähe der AMe (anteriore und posteriore PDH-ir Medullaneurone, PDHMe).

Die vorliegende Dissertation hatte zum Ziel, die Struktur der AMe und ihrer PDH-ir Neurone sowie deren Funktion im circadianen System der Schabe *L. maderae* zu untersuchen. Die Arbeit besteht aus sieben Kapiteln, welche drei Hauptthemen umfassen:

- Beschreibung der Morphologie und Neuroarchitektur der AMe von *L. maderae* und ihrer PDH-ir Neurone auf licht- und elektronenmikroskopischer Ebene (Kapitel I und II).
- Identifizierung der AMe als circadianes Schrittmacherzentrum der Schabe *L. maderae* mit Läsions- und Transplantatonsexprimenten; dabei wurde eine neue Methode zur Auswertung sehr langer Aktivitätsaufzeichnungen entwickelt (Kapitel III-V).
- Charakterisierung aller direkten neuronalen Verbindungen zwischen beiden optischen Loben der Schabe, und Identifizierung einer Untergruppe der PDH-ir Neurone als Kopplungsneurone zwischen den beiden bilateral angelegten AMae (Kapitel VI und VII).

Kapitel I: Morphology and pigment-dispersing hormone immunocytochemistry of the accessory medulla, the presumptive circadian pacemaker of the cockroach *Leucophaea maderae*: a light- and electron-microscopic study.

Der Aufbau der AMe der Schabe *L. maderae* und ihrer assoziierten neuronalen Strukturen wurden auf licht- und elektronenmikroskopischer Ebene untersucht. Es ergab sich, daß die AMe im Gegensatz zu den großen optischen Neuropilen nicht retinotop organisiert ist. Sie besteht statt dessen aus einem dichten nodulären Neuropil, welches in internoduläres Neuropil eingebettet ist. Die gesamte Struktur ist von einem Hüllneuropil umgeben, welches sich in frontaler Richtung in ein anteriores Neuropil fortsetzt. Die elektronenmikroskopischen Untersuchungen ergaben, daß sich in der AMe außergewöhnlich viele neuronale Fortsätze befinden, die dicht mit *dense core* Vesikeln angefüllt sind. Diese *dense core* Vesikel konnten in mindestens vier Typen eingeteilt werden: Die granulären, kleinen, mittelgroßen und großen *dense core* Vesikel. Granuläre Vesikel kommen hauptsächlich in neuronalen Fasern des nodulären Neuropils vor, die wahrscheinlich lokalen Interneuronen angehören. Die anderen drei Typen beschränken sich auf Fasern des anterioren, Hüll- und internodulären Neuropils der AMe. Immunfärbungen auf licht- und elekronenmikroskopischer Ebene zeigten, daß dort auch die Verzweigungen der PDH-ir Fasern zu finden sind, nicht aber im nodulären Neuropil. Die PDH-ir Färbung ist in Fasern mit mittelgroßen und großen *dense core* Vesikeln lokalisiert. Dort ist die Färbung deutlich mit den Vesikeln assoziiert, was darauf hinweist, daß diese Vesikel das Peptid *pigment dispersing factor* als Ausgangssignal der PDHMe speichern und transportieren. Der Aufbau der AMe ähnelt in gewissen Zügen dem suprachiasmatischem Nukleus, dem circadianen Schrittmacherzentrum der Säugetiere.

Kapitel II: Ultrastructure of pigment-dispersing hormone-immunoreactive neurons in a three-dimensional model of the accessory medulla of the cockroach *Leucophaea maderae*.

Als Basis für neuroanatomische Studien der AMe wurde ein dreidimensionales Computermodell dieses Neuropils und dessen assoziierter Strukturen erstellt, welches eine verbesserte Bewertung und Darstellung der

anatomischen Befunde ermöglicht. Es zeigte sich, daß die anterioren PDHMe der AMe aufgrund verschiedener Kriteria in drei morphologisch unterscheidbare Gruppen von jeweils etwa vier Neuronen unterteilt werden können: den großen, mittelgroßen und kleinen anterioren PDHMe. Um zu untersuchen, welche synaptischen Verbindungen die verschiedenen Typen von PDH-ir Neuronen eingehen, wurden zuerst die synaptischen Verschaltungen von durch ihren Vesikelgehalt unterscheidbaren Neuronen der AMe elektronenmikroskopisch charakterisiert. Anschließende immuno-elektronenmikroskopische Studien ergaben, daß die großen und stark immunoreaktiven anterioren PDHMe die mittelgroßen *dense core* Vesikel enthalten und Eingangs- und Ausgangssynapsen zu neuronalen Fortsätzen vor allem im anterioren und Hüllneuropil der AMe bilden. Die mittelgroßen anterioren PDHMe enthalten große *dense core* Vesikel, und formen Eingangs- und Ausgangssynapsen haupsächlich im internodulären Neuropil der AMe. Die kleinen, schwach färbenden anterioren PDHMe gehören zur morphologischen Gruppe der distalen, frontoventralen Neuronen, wogegen die großen und mittelgroßen anterioren PDHMe den ventralen Neuronen der AMe angehören. Offensichtlich senden nur die beiden letzteren Gruppen Ausgangsverzweigungen in das Zentralhirn und/oder formen Eingänge in den kontralateralen optischen Lobus. Die Untersuchungen wiesen auf unterschiedliche Rollen der verschiedenen Untergruppen der PDH-ir Neuronen in der Funktion der Inneren Uhr hin und ermöglichten die Formulierung begründeter Hypothesen über die Beschaffenheit des neuronalen Netzwerkes der AMe.

Kapitel III: Lesion of PDH-immunoreactive medulla neurons abolishes circadian rhythmic locomotor activity in the cockroach *Leucophaea maderae*.

Um die Rolle der PDHMe in der Funktion der Inneren Uhr zu untersuchen, wurden Methoden zur gezielten Läsion der AMe von *L. maderae* und zugehöriger neuronaler Somata entwickelt, kombiniert mit nachfolgender PDH-immunhistologischer Auswertung der Gehirne. Nachdem die AMe mit speziell präparierten, feinen Glaspipetten ausgestanzt wurde, zeigten alle Tiere, denen durch Zerstörung der Somata der PDHMe die PDH-ir Verzweigungen im Zentralhirn fehlten, arhythmisches lokomotorisches Verhalten. Zwei Tiere mit teilweise reduzierten PDHMe und teilweise verbliebenen und/oder regenerierten PDH-ir Fasern im Zentralhirn zeigten postoperative Rhythmik; eines davon liefert den ersten Hinweis darauf, daß möglicherweise auch die posterioren, und nicht nur die anterioren PDHMe an der Erzeugung circadian rhythmischen Verhaltens beteiligt sein könnten. Die Daten unterstützen die Hypothese, daß die AMe der wichtigste Schrittmacher zur Erzeugung circadianer Aktivitätsrhythmen ist. Ferner zeichnete sich ab, daß durch Läsionsexperimente die Funktionen verschiedener Untergruppen von Neuronen der AMe im circadianen System der Schabe untersucht werden können. Testexperimente zeigten, daß die Verwendung eines Elektrokoagulators mit Wolfram-Elektroden zukünftig die beste Methode sein wird, um präzise und lokal begrenzte Läsionen der AMe zu erreichen.

Kapitel IV: Ectopic transplantation of the accessory medulla restores circadian rhythmic behaviour in arrhythmic cockroaches (*Leucophaea maderae*).

Durch ektopische Transplantationen von AMe-Gewebe aus erwachsenen Schaben konnte das circadiane Laufverhalten von Schaben, denen zuvor ihr eigener Schrittmacher entfernt wurde, wiederhergestellt werden. Die Aktivitätsdaten wurden mit einer neuentwickelten Methode ausgewertet, die eine automatisierte Erkennung rhythmischer Aktivität ermöglicht. Alle Tiere mit wiedererlangtem circadian rhythmischem Verhalten zeigten, sofern sie histologisch untersucht werden konnten, regenerierte PDH-ir Fasern, die aus dem Implantat heraus ihre ursprünglichen Zielgebiete im Zentralhirn innervierten. Die AMe konnte somit als circadianer Schrittmacher, der das Laufverhalten der Schabe steuert, identifiziert werden. Da postoperative Rhythmik deutlich mit dem Vohandensein regenerierter PDH-ir Fasern im superioren lateralen und medialen Protocerebrum korreliert war, sind diese Neurone sehr wahrscheinlich circadiane Schrittmacher- und Ausgangsneurone der AMe.

Kapitel V: Scan periodogram analysis: a new method for an automated detection of short circadian rhythmic activity phases in long data records.

Hier wird eine neue Methode vorgestellt, die eine automatische und objektivierte Erkennung kurzer circadian rhythmischer Aktivitätsepisoden in wochen- bis monatelangenlangen Aktivitätsdatenaufzeichnungen ermöglicht, die große Anteile von arhythmischem Verhalten beinhalten. Diese Analyse wird durch ein Computerprogramm bewerkstelligt, welches als ‚Add-In' für das Tabellenkalkulationsprogramm Microsoft Excel konzipiert ist, und in der Programmiersprache *Visual Basic for Applications* geschrieben wurde. Das Programm, genannt *Tempus*, führt fortschreitende χ^2-Periodogramm-Analysen mit kurzen Analyse-Intervallen

über die gesamten Datenaufzeichnungen durch. Durch Anwendung dieser ‚Periodogramm-Scan-Analyse' sowohl auf arhythmische als auch auf randomisierte Aktivitätsaufzeichnungen wurden Schwellenwerte für die Auswertung der *peaks* der einzelnen Periodogramme ermittelt, um rhythmische Aktivität in experimentellen Daten zu erkennen. In Transplantationsexperimenten konnten dadurch erfolgreich circadian rhythmische von arhythmischen Schaben unterschieden werden, wodurch die AMe als circadianer Schrittmacher für das lokomotorische Aktivitätsverhalten der Schabe identifiziert wurde. *Tempus* entwickelte sich zu einem umfassenden chronobiologischen Auswertprogramm, welches, bedingt durch seinen modularen Aufbau, leicht mit vielen weiteren Analysefunktionen versehen werden kann.

Kapitel VI: Optic lobe commissures in a three-dimensional brain model of the cockroach *Leucophaea maderae*: a search for the circadian coupling pathways.

Auf der Suche nach direkten neuronalen Kopplungswegen zwischen den AMae in beiden optischen Loben der Schabe *L. maderae* wurden mit *tracer*-Experimenten sieben Kommissuren gefunden, die die optischen Loben untereinander verbinden. Mindestens zwei, möglicherweise drei dieser Kommissuren verbinden beide AMae. Zwei davon ähneln im Muster der von ihnen abgehenden Verzweigungen den PDH-ir Neuronen. Zusammen mit physiologischen Daten begründet dies die Annahme, daß einige PDH-ir Neurone die auch Kandidaten für circadiane Schrittmacherneurone sind, einen direkten Kopplungsweg zur Synchronisation der beiden Inneren Uhren darstellen. Für eine verbesserte Darstellung der Kommissuren wurde ein dreidimensionales Computermodell des Schabengehirnes entwickelt, in das die konventionell rekonstruierten Trakte eingebettet wurden.

Kapitel VII: Pigment-dispersing hormone (PDH)-immunoreactive neurons form a direct coupling pathway between the bilaterally symmetric circadian pacemakers of the cockroach *Leucophaea maderae*.

Um nachzuweisen, ob tatsächlich eine Untergruppe der PDHMe beide AMae untereinander verbinden, wurde der Farbstoff Rhodamin-Dextran als neuronaler *tracer* in eine AMe injiziert, und die Gehirne darauffolgend mit anti-β-PDH-Antiserum immuncytochemisch angefärbt. Die Präparate wurden mit einem konfokalen Laser-Rastermikroskop ausgewertet. Das Vorkommen doppelt markierter Fasern im anterioren, im Hüll- und im internodulären Neuropil der AMe kontralateral zur injizierten AMe zeigte, daß PDH-ir Fasern beide AMae direkt miteinander verbinden. Diese Fasern stammen von drei PDHMe, welche alle den anterioren PDHMe, aber nicht den posterioren PDHMe angehören. Diese Untergruppe der PDHMe ist daher sehr wahrscheinlich am circadianen Kopplungsweg der bilateral organisierten Schrittmacherzentren beteiligt. Im Zentralhirn werden alle bis auf eines der typischen Projektionsgebiete von PDHMe beider Seiten innerviert. Die Daten unterstützen die Annahme, daß die anterioren PDHMe eine vielseitige Rolle bei der Erzeugung circadianer Rhythmen, der Übertragung von Zeitinformation in das Zentralhirn, sowie bei der gegenseitigen Synchronisation der circadianen Schrittmacher der Schabe *L. maderae* spielen.

Introduction

Introduction

Die vierundzwanzigstündige Periode, welche durch die regelmäßige Umdrehung unsres Erdkörpers auch allen seinen Bewohnern mitgeteilt wird, zeichnet sich besonders in der physischen Ökonomie des Menschen aus. In allen Krankheiten äußert sich diese regelmäßige Periode, und alle andern so wunderbar pünktlichen Termine in unsrer physischen Geschichte werden im Grunde durch diese einzelne vierundzwanzigstündige Periode bestimmt. Sie ist gleichsam die Einheit der Naturchronologie.[1]

— *Christoph Wilhelm Hufeland, 1796*

CIRCADIAN RHYTHMS: DAY AFTER DAY

Life processes of all organisms are temporarily organised in connected biological rhythms, i.e., repetitive incidences with characteristic periods. These periods cover time ranges from milliseconds (e.g., spontaneous rhythmic action potentials) up to several years (e.g., population cycles) and may be driven by endogenous and/or environmental processes. Biological rhythms are the subject of chronobiology, a research field that developed tremendously in the last decades.

Among the most important biological rhythms are circadian rhythms which are determined by the course of the day with its regular changes of illumination and temperature. These daily rhythms affect most of behavioural and physiological processes in such an apparently self-evident way, that their real significance to our whole way of life rarely becomes aware. It has long been assumed that internal daily rhythms such as wake/sleep cycles are only passively driven by the changes of day and night. First incidences that in fact endogenous clocks are able to control daily rhythms in living organisms, are presented in the 18^{th} century by the French naturalist Jean J. de Mairan (1729), who observed daily leave movements of a mimosa continuing for several days even under constant darkness. Nevertheless, it took two more centuries until the existence of internal clocks became generally accepted among life scientists. The pioneer works of Jürgen Aschoff, Ernst Bünning, and Colin S. Piddendrigh in the 1950s and 1960s (Bünning, 1973; Aschoff, 1984; Pittendrigh, 1993) revealed that living organisms are in fact able to self-generate rhythms with periods very close to, but not exactly matching the 24 hours of a day (hence, termed *circadian* rhythms).

These rhythms can be observed under constant environmental conditions without any external rhythmic cues (*freerunning* condition). The actual period lengths (τ) of circadian rhythms turned out to constitute species-specific properties, with a tendency to be slightly longer than 24 hours in diurnal, and shorter than 24 hours in nocturnal animals (Aschoff's rule; Pittendrigh, 1960). The period from one particular *phase reference point* (e.g., begin, maximum, or end of activity phases) to the next under freerunning condition is called the *circadian day*. It can be divided into 24 circadian hours of about one hour lenght. The subjective, circadian time (CT) experienced by an organism is expressed in numbers of circadian hours, which are generally defined in respect to a particular, easy recognisable phase reference point; e.g., the beginning of the locomotor activity of a freerunning nocturnal cockroach is defined as CT 12 h (Fig. 1A).

Because the period of endogenous clocks differ slightly from 24 hours, they have to be continuously synchronised to the environmental time by external daily rhythms (*Zeitgebers*). The most reliable and

[1] The twenty-four hours period, which is communicated to all its inhabitants by the regular revolution of our earth, is particularly apparent in the physiological economy of men. This regular period is expressed in all diseases, and all other so wonderful punctual incidences of our physical history are actually determined by this twenty-four hours period. It is, as it were, the unit of the natural chronology.

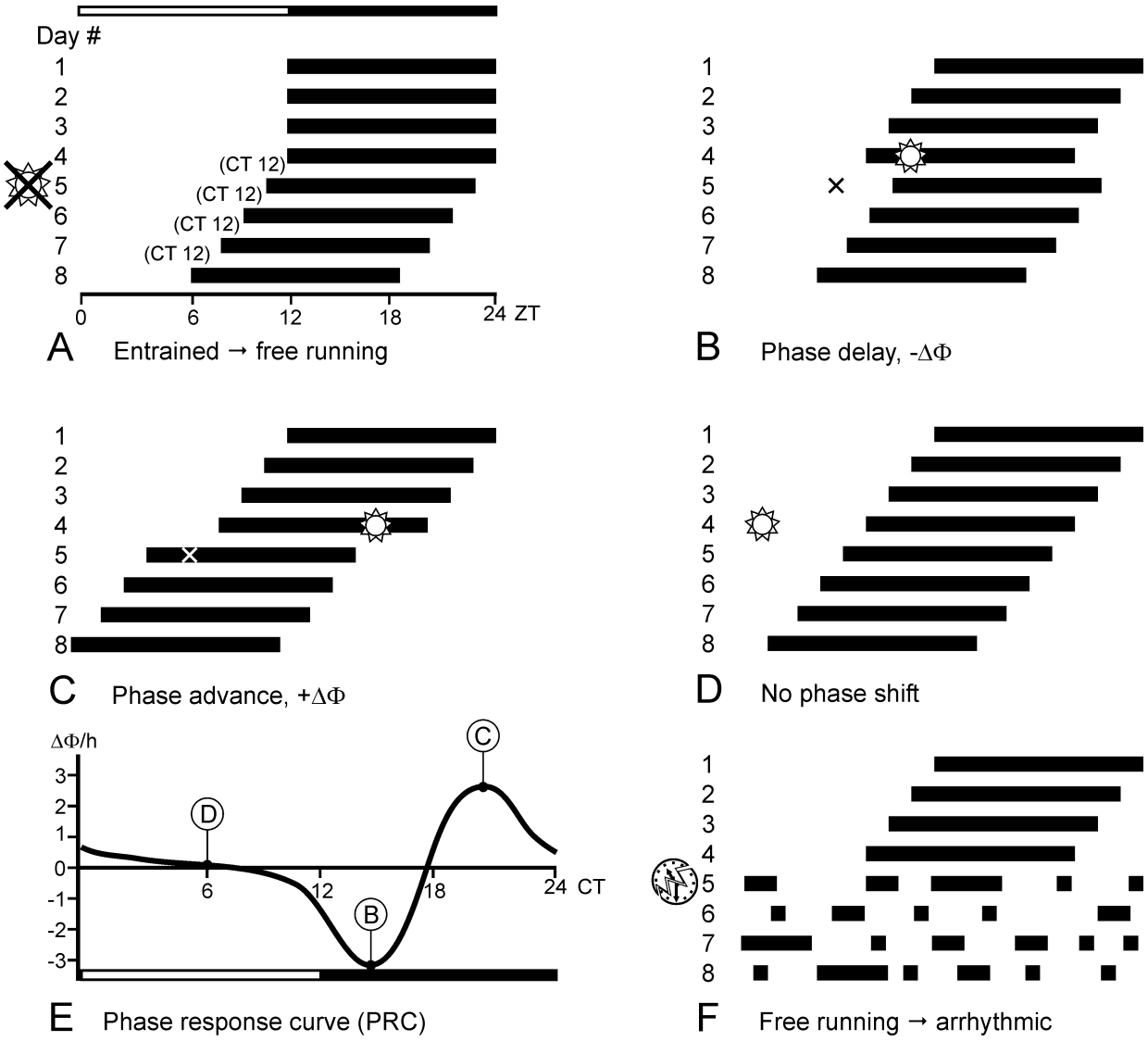

Fig. 1. Scheme of some basic circadian experiments(A–D, F), and construction of a phase response curve (PRC, E). Shown is the locomotor activity of a model night-active animal with a circadian period $\tau < 24$ hours like the cockroach *Leucophaea maderae*. **A:** In the actogram plot, activity phases appear as black bars. The activity recordings of consecutive days in real time (Zeitgeber time, ZT) are shown. The half white, half black bar above the activity plot represents light and dark phases during the course of a day. Until day 4, the light is switched on at ZT 0 and switched off at ZT 12. The animal is entrained to the light/dark cycle, and every day starts its activity phases at ZT 12. Beginning with day 5, the light remains off. In constant darkness, the internal clock of the animal begins to free-run, and, due to an enogenous τ shorter than 24 hours, the activity phase of every day starts earlier. In the freerunning condition, the start of activity is used as phase reference point and defined as circadian time (CT) 12. CT 0–12 is the subjective day, CT 12–24 the subjective night of the animal. **B:** The freerunning animal receives a light pulse with defined intensity and duration in the early subjective night of day 4. The following day 5, the activity onset is delayed in respect to the expected activity onset (cross). The phase delay is expressed as negative value of $\Delta\Phi$, which is calculated from the expected activity onset of day 5 to the actual activity onset. Since this phase shift occurs only once, the animal continues with its normal period. **C:** This freerunning animal receives a light pulse at its late subjective day. The activity onset of day 5 is advanced in respect to the expected activity onset (cross). The phase advance is expressed as positive value of $\Delta\Phi$ from the expected activity onset to the actual activity onset. **D:** A light pulse at the middle of the subjective day causes no phase shift. **E:** Defined light pulses or any other disturbances, which phase shift the internal clock (temperature changes, transmitter injections, noise, etc.), might be delivered at any circadian time of a freerunning animal, and the resulting phase shift can be measured. If these phase shifts are plotted against the animal's circadian time where the disturbances are applied, the respective PRC results. This model PRC for light pulses shows the typical bi-phasic shape, which is common for light PRCs for all day as well as night active animals examined so far. Light pulses at the early subjective night cause phase delays, while at the late subjective night they cause phase advances. At the subjective day, no or only minute phase shifts occur. The phase shifts with respective CT of the light stimuli of the model experiments in Figs. B–D are indicated. **F:** At the end of the activity phase of day 4, the circadian pacemaker is lesioned in a freerunning animal. Subsequently, the activity phases lose their temporal order and are randomly distributed; the animal behaves arrhythmic.

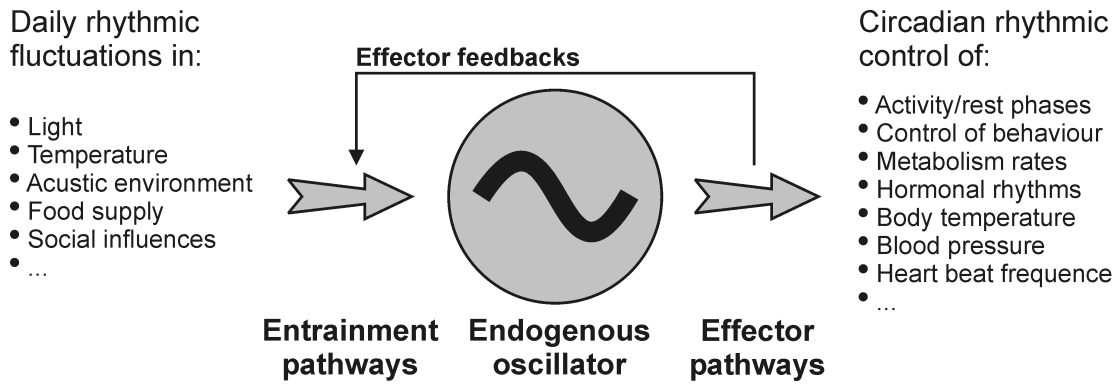

Fig. 2. The general model of an internal clock consists of a pacemaker generating a circadian rhythm, which is synchronised to daily environmental rhythms *via* entrainment pathways, and which controls behavioural and physiological daily rhythms *via* effector pathways. The actions of the effectors feed back to clock entrainment pathways.

hence, the most important external rhythms are the daily changes of light and dark, and temperature (Aschoff, 1960). These stimuli reset circadian oscillators by evoking phase shifts, caused by either temporarily slowing down (phase delaying) or accelerating (phase advancing) the oscillator. The amounts and directions of phase shifts, which can be evoked by a defined stimulus, are directly dependent on the actual phase of the circadian day, and are characteristic for this particular stimulus (Fig. 1B–D). These relations are described by so-called *phase response curves* (PRCs; Fig. 1E), which proved to be indispensable tools for describing properties of circadian clocks. For instance, light pulses of sufficient intensity and duration cause no or only slight phase shifts if delivered in the circadian day, but clear phase delays in the *early* circadian night, and phase advances in the *late* circadian night. This is characteristic for both diurnal and nocturnal animals, and leads to permanent maintenance of the specific phase relation of the endogenous rhythm to the external light/dark cycle, and thus, to synchronisation of the internal clock to the environmental day (Aronson et al., 1993).

In summary, the general model for the organisation of an internal clock includes an endogenous oscillator (*pacemaker*) which generates a self-sustained circadian rhythm (Fig. 2). Synchronisation of the internal pacemaker to the *Zeitgeber* time is processed and transmitted through *entrainment pathways*. Then, the time information of the pacemaker is delivered to the target organs by a system of *effector pathways*, which, to certain extend, feed back to the clock.

It was shown that circadian clocks constituted enormous evolutionary advantages very early in the phylogeny of living organisms, which do not only have to adapt to a spatial, but also to a temporal environment. It is obvious, that almost all organisms have species-specific activity phases, either at day or night, or at dawn or dusk. An internal clock allows for anticipation of activity or rest phases and hence, adequate physiological preparation, e.g., by adaptation of metabolism rates, right *before* a new phase begins. Hamsters with disturbed circadian rhythmicity die earlier than intact specimens (Hurd and Ralph, 1998). The significance of chronobiological aspects for human health care is still underestimated, but currently becomes more and more evident in the research on shift work, sleep pathology, jet lag, time-dependent drug application, and so on (Touitou and Haus, 1994).

Unrevealing the physiological correlates of internal clocks and exploring how they work, are a main subject of chronobiological research. These investigations are based on a variety of organisms, including humans and other mammals as mice and rats, but also invertebrate animals as snails and insects. It was in fact an insect, the cockroach *Leucophaea maderae*, where for the first time a circadian clock could be localised. Lesion studies found the pacemaker controlling circadian rhythmic behaviour in the brain's optic lobes of the cockroach (Nishiitsutsuji-Uwo and Pittendrigh, 1968b). Although it later turned out that the ability for generating circadian rhythms may be an inherent property of all cells of an organism (Schibler and Sassone-Corsi, 2002), it became obvious, that most higher animals carry superordinate and spatially distinct pacemakers in their central nervous systems (*master-clocks*). There, they are always closely attached to the visual systems, reflecting the importance of light as the main clock synchronising stimulus. Thus, research on internal clock functions is an important subject in neurobiology.

Again it was an insect, the fruitfly *Drosophila melanogaster*, where the molecular functions of generating circadian rhythms within single neurons

could first be deciphered, resulting in the PER/TIM feedback loop model (reviewed by Stanewsky, 2002). However, larger insects like cockroaches are important model organisms to determine neurophysiological properties of circadian clocks, because their single identifiable neurons are accessible to lots of experimental manipulations that are not achievable in fruitflies.

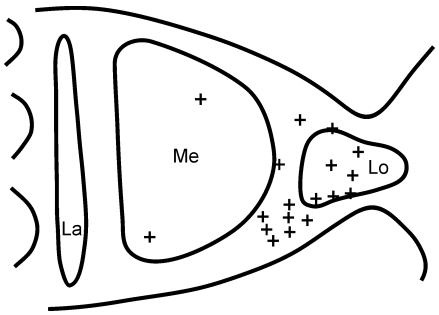

Fig. 3. Microlesions in the remaining optic lobes of cockroaches (*Leucophaea maderae*) which contralateral optic lobes have been removed, caused arrhythmic locomotor behaviour (scheme modified after Sokolove, 1975). The centres of lesions causing arrhythmicity are indicated by crosses. They lie ventrally between medulla (Me) and lobula (Lo), where the PDH-ir medulla neuron somata, the accessory medulla, and the lobula valley tract are located. La lamina.

THE CLOCK OF THE COCKROACH *LEUCOPHAEA MADERAE*

Lesion and transplantation studies, as well as electrophysiological observations in *L. maderae* located the circadian pacemaker driving rhythmic locomotor behaviour in the optic lobes of the brain, where it appeared to reside in a ventral area between medulla and lobula (Fig. 3; Nishiitsutsuji-Uwo and Pittendrigh, 1968b; Roberts, 1974; Sokolove, 1975; Page, 1982; Colwell and Page, 1990). The light entrainment of this pacemaker apparently occurs exclusively through the compound eyes of the animal (Roberts and De, 1965; Nishiitsutsuji-Uwo and Pittendrigh, 1968a). The phase information of the clock is transmitted by neuronal pathways to midbrain targets (Page, 1982). Furthermore, both bilaterally symmetric pacemakers are mutually coupled and synchronised by apparently neuronal pathways (Page, 1978, 1981, 1983b).

More than ten years ago, immunohistochemical stainings with an antiserum against the crustacean octadeca-peptide pigment-dispersing hormone (PDH, Dircksen et al., 1987; the substance causing PDH immunoreactivity in insects is termed pigment-dispersing factor, PDF) revealed 3–4 groups of conspicuous optic lobe neurons in several orthopteroid insects including the cockroaches *Periplaneta americana* and *Leucophaea maderae* (Fig. 4C; Chapter VI, Fig. 6A; Homberg et al., 1991; Stengl and Homberg, 1994). One of these groups with somata at the ventro-proximal medulla (PDH-immunoreactive medulla neurons, PDHMe) conspicuously share anatomical properties predicted for pacemaker neurons in orthopteroid insects. These properties include the position of the somata, which lie in the general pacemaker location. Furthermore, these neurons showed, untypically for medulla neurons, axonal projections widespread into various areas of the central brain; there, they may transmit timing information to descending neurons. Moreover, in cockroaches subpopulations of the PDH-immunoreactive (PDH-ir) neurons cross the midline of the brain and appear to connect both optic lobes. Thus, they could provide pathways to synchronise the strongly coupled bilateral optic lobe pacemakers of the cockroach (Stengl and Homberg, 1994). In contrast, the circadian pacemakers of crickets are only weakly coupled, and there are no heterolateral PDH-ir pathways (Stengl, 1995). Another feature of the PDHMe are apparently axonal ramifications that project tangentially through the distal layer of the optic lobe's medulla up to the lamina. There, they could serve for circadian modulation of the visual system (Pyza and Meinertzhagen, 1997). Thus, the PDHMe are strong candidates for circadian pacemaker neurons, as well as for output and/or coupling pathways of the clock (reviewed by Helfrich-Förster et al., 1998; Homberg et al., 2003).

Within the ventromedial medulla of the cockroach close to the PDHMe, a small neuropil shows a conspicuous aggregation of PDH-ir neuron processes. A similar neuropil was so far only known in some holometabolous insects and there, termed accessory medulla (AMe, plural form: accessory medullae, AMae; Pflugfelder, 1936). In these insects, the AMe serves as larval visual integration centre, but remains in adult insects (Hanström, 1940; Ehnbohm, 1948; Hagberg, 1986). Since a homology of the AMae in holometabolous and orthopteroid insects was assumed, this term was also introduced for the orthopteroid insects (Homberg et al., 1991; see Appendix A). Since its discovery, accumulating evidences point to the AMe as neuronal integration centre for internal and external timing information in insects. The AMe neurons may include pacemaker neurons, pacemaker coupling neurons, neurons delivering entrainment information, neurons mediating phase information to other brain centres, and interneurons connecting all these functions (reviewed by Helfrich-Förster et al., 1998; Homberg et al., 2003). The involvement of the AMe in the time sense of insects is further supported by the conspicuous integration of the AMe into the polarisation vision

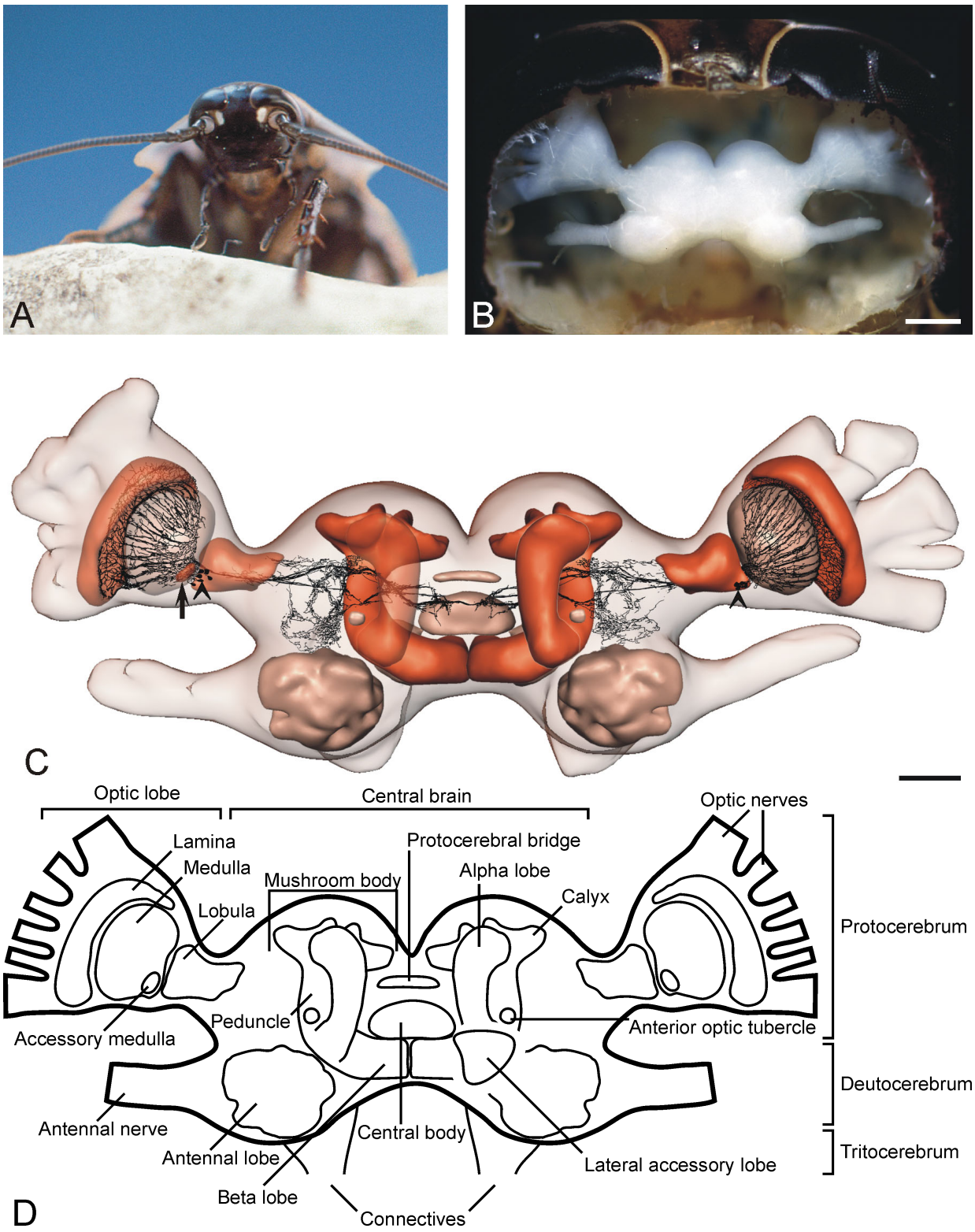

Fig. 4. The cockroach *Leucophaea maderae* (A) and its brain (supraoesophageal ganglion; B–D). **A:** From this fronto-ventral view, the head of the cockroach is visible. **B:** The brain of a cockroach is exposed by removing the clypeus, and subsequent removing of mandibular muscles, fat bodies, trachea, and the oesophagus. **C:** Three-dimensional model of the cockroach brain, obtained after segmentation of a 10-μm paraffin section series. A reconstruction of the PDH-ir neuron system is incorporated into the model. Further descriptions of soma groups, commissures, and output regions of this fibre system are presented in Chapter VI, Fig. 6A. The right (in respect to body axis) optic lobe neuropils and alpha-lobe are rendered transparent to enable the view onto internal and underlying structures. At the ventro-distal edge of the transparent medulla, the AMe is visible (arrow). Arrowheads: anterior PDH-ir medulla neuron somata. **D:** Scheme and descriptions of the main structures of the cockroach brain. Scale bars = 500 μm in B, 200 μm in C.

system of orthopteroids (Labhart and Petzold, 1993; Loesel and Homberg, 2001). Orientation in space with aid of the polarised light pattern of the blue sky is tightly coupled with orientation in time. Hence, the AMe seems to include all necessary clock functions. Nevertheless, the identity of the AMe with the circadian clock driving behavioural rhythms of cockroaches still remains to be confirmed.

This dissertation is aimed to get insights into the structure and function of the AMe and associated PDH-ir neurons as part of the circadian system of the cockroach *L. maderae*. The work consists of seven chapters, which address three main subjects:

- Chapters I and II elucidate the structure of the AMe and PDH-ir neurons on the light- and electron-microscopical level.
- Chapters III and VI are concerned with the identification of the AMe as circadian pacemaker centre of the cockroach with lesion and transplantation experiments; hereby, a new method for detection of rhythmic activity in long time data series containing arrhythmic activity was developed (Chapter V).
- To identify the neuronal pathways that couple both circadian pacemakers of the cockroach, in chapters VI and VII monosynaptic connections between the optic lobes of the cockroach were described, and it could be shown that a subset of the PDHMe indeed directly connects both bilaterally symmetric AMae.

The following three main sections of this part will introduce these three subjects and briefly review the results. The section afterwards combines the new and older findings about the neuronal pathways connecting the AMe to other brain areas. To view the results of this thesis in the light of the resent research on internal clock mechanisms of insects, the last section briefly resumes the current knowledge about PDF function in insects.

INSIDE THE CLOCK: THE STRUCTURE OF THE ACCESSORY MEDULLA

The central nervous system (CNS) of insects consists of a chain of ganglia (ventral nerve cord), which anterior ganglia are organised into a supra- and a suboesophageal ganglion. The supraoesophageal ganglion is probably developed after fusing of the first three ganglia of the ancestral ventral nerve cord due to a cephalisation process in the evolution of insects (Hennig, 1986). It is commonly termed the brain of the insect (Fig. 4B). Like all other ganglia, the brain consists of a cortex of neuronal and glial somata, which surround a core of neuropil. Due to the characteristic pseudounipolar morphology of insect neurons, the neuropil is almost completely formed by neuronal processes, and is the site of the synaptic interactions between insect neurons. Functionally dependent spatial arrangement of neuronal processes leads to the formation of distinct neuropils, which partly are separated by glia sheaths from the surrounding structures. Well-known neuropils of the central brain are the mushroom bodies, the central complex, and the antennal lobe glomeruli (Fig. 4C,D).

Laterally to the central brain reside the optic lobes, which are the primary visual integration centres of the compound eyes. They contain three large neuropils: the lamina as the first station of most photoreceptor outputs, followed by the medulla, and most proximally the lobula. They are serially connected by crossed nerve tracts (optic chiasma). The optic lobe neuropils are internally organised as retinotopic maps, i.e., single ommatidia of the compound eyes are represented by associated neuronal units, which maintain the ommatidia's spatial relationships. The arrangement of columnar and tangential neurons forms a layered appearance of the optic neuropils, which is easily recognisable in histological preparations. Retinotopic maps arranged in layers and columns are a principal organisation scheme of all CNS visual centres which are capable for image processing and movement detection (Douglass and Strausfeld, 1995; Logothetis and Sheinberg, 1996).

The AMe is not retinotopically organised

The AMe of the cockroach is located in an anterior, ventro-proximal edge of the medulla. It has a conspicuous pear-shaped appearance, extends about 90 μm over its longitudinal axis, and is easily recognisable on mass stained histological sections (Chapter I, Fig. 1; Chapter II, Fig. 1B). Anteriorly, ventrally, and medially to the AMe six main groups of AMe-associated neuronal somata could be described according to morphological criteria (Chapter I, Fig. 3B; Chapter II, Fig. 1B–F). They altogether comprise about 250 neurons. Additionally, some posterior neuron groups, which are less well characterised, are also associated to the AMe (e.g., posterior PDHMe, Chapter II, Fig. 1A, and MC III neurons, Chapter VI, Figs. 3D, 5E). Hence, the circadian clock of *L. maderae* appears to consist of at least some 300 neurons.

Further examinations and 3D computer reconstructions showed the AMe comprising an irregularly

shaped nodular core formed by dense neuropil, which is embedded in loose internodular neuropil (Chapter II, Fig. 1B–F). The whole structure is enveloped by a shell of loose neuropil. Anteriorly to the AMe lies a mass of loose neuropil (anterior neuropil), which can be interpreted as anterior continuation of the shell neuropil (Chapter I, Fig. 1C). Since the AMe shows no sign of any layered structure, it does not form a retinotopic map, similary to the suprachiasmatic nucleus (SCN), the main circadian pacemaker centre of mammals (reviewed by van Esseveldt et al., 2000; Moore et al., 2002). Thus, it is very unlikely that the AMe is involved in image processing or movement detection mechanisms of the insect visual system. However, it might still be involved in temporal integration of information about ambient illumination, as is necessary for the light entrainment of circadian clocks. The relation between the structure of the AMe and its putative pacemaker function is still not clear. Moreover, preliminary observations showed that the structure of the AMe might be quite diverse among the insect groups, thus emphasising the importance of comparative studies (see Appendix A).

The AMe function bases on parakrine peptide release

Also on the ultrastructural level, the AMe displays considerable differences compared to the main optic lobe neuropils. The AMe shows many synaptic interactions between different types of neurones (Chapter II, Figs. 5, 6). However, yet in light-microscopical peptide immunostainings it could be observed that fibre terminals of the AMe often show a beaded appearance, caused by serially arranged swellings of the fibres termed varicosities (Chapter I, Fig. 3). Varicosities indicate active output regions of nerve fibres. On the ultrastructural level it was shown that the varicosities contain accumulations of dense core vesicles (DCVs; Chapter I, Fig. 2C, 4A–D). The DCVs are storage sites and intracellular transport vehicles for peptides in neurons (reviewed by Nässel, 2002). Together with currently eight different peptide immunoreactivites found in the AMe of the cockroach so far (Petri et al., 1995; S. Hofer, unpublished), this demonstrates that neuromodulation by peptides plays an important role in the neuronal function of the AMe. This was also shown for the SCN of mammals (reviewed by van Esseveldt, Lehman et al., 2000).

Types of neuronal terminals in the AMe could be differentiated by the morphological properties of their DCVs and the distribution patterns of the DCVs within the varicosities (Chapter II, Fig. 4). It was shown, that the segregation of the AMe in nodular and loose neuropil compartments is the result of the differential distribution of larger output fibres and fine dendrites, but also of nerve terminals carrying different types of DCVs (Chapter I, Fig. 2). In the nodular neuropil of the AMe, mainly terminals containing DCVs with typically structured, granular content were found (granular DCVs). Terminals with granular DCVs are often clustered together (Chapter I, Fig. 4A; Chapter II, Fig. 6B,C). Additionally, many large axonal terminals occur that carry only few or no DCVs, but which are densely filled with the smaller synaptic clear vesicles. These terminals are surrounded by many small, postsynaptic processes (small dendrites; Chapter II, Fig. 6A). This altogether leads to a high aggregation of membrane material in the nodular neuropil and hence, to its darker appearance after staining with membrane-affinity histological dyes.

In the internodular and shell neuropil, preferentially varicosities filled with highly electron dense and rather unstructured DCVs occur (Chapter I, Fig. 4B–D; Chapter II, Fig. 6C–F). These terminals could be differentiated into three main groups according to size and distribution of their DCVs (small, medium-sized, and large DCVs), and specific distribution of these terminals within the internodular and shell neuropil. Varicosities with dark DCVs often carry synapses, but are never filled with so many clear vesicles as the axonal terminals in the nodular neuropil containing only few DCVs. Although also small, postsynaptic dendrites occur, the mean cross section size of these neuronal profiles seemed to be larger in the internodular and shell neuropil compared to the nodular neuropil. This leads to weaker and more uneven staining with membrane-affinity dyes in the loose neuropil.

The morphologically identifiable terminal types do certainly not represent all types of neurons of the AMe. Firstly, at least the granular and large DCVs show more than one peak in size distribution histograms (Chapter I, Fig. 5). Secondly, so far, eight peptide immunoreactivities are found in the AMe of *Leucophaea* (Petri et al. 1995, S. Hofer, unpublished), and, owing to findings in locusts, more may be expected (Würden, 1994). However, these morphological studies provide a reasonable framework to get insights into the multitude of neuronal interactions in the AMe (Chapter II, Figs. 5 and 6).

Structure and ultrastructure of the PDH-ir neurons

With an antiserum against crustacean β-PDH, four sets of neurons can be stained in the cockroach brain, which all have their somata in the optic lobes: the anterior and posterior PDHMe, and the dorsal and ventral PDH-ir lamina neurons (PDHLa). The ante-

rior PDHMe consist of about 12 neurons, which can be assigned to three groups (small, medium-sized, and large anterior PDHMe), each containing about four neurons (Chapter II, Fig. 2). They belong to two of the six morphologically characterised soma groups of the AMe (Chapter II, Fig. 1C–F). The small anterior PDHMe are a subgroup of the distal group of frontoventral neurons, whereas the medium-sized and large anterior PDHMe are a part of the ventral neurons (Chapter II, Fig. 3A). Evidences indicate that the small anterior PDHMe restrict their arborisations to the ipsilateral optic lobe and possibly may even be local interneurons of the AMe. In contrast, at least most of the medium-sized and large anterior PDHMe form also midbrain projections and, partly, arborisations in the contralateral optic lobe (Chapter VII, Fig. 4A–C). The targets of the posterior PDHMe, which consist of about 2–6 somata, are so far not well known. In the lesion studies (Chapter III) it could be shown, that their fibres arborise in the AMe and project *via* the distal fibre fan to the lamina; there is until now only one indication that they additionally project into the ipsilateral midbrain (Chapter III, Fig. 10). Of the PDHLa, both groups ramify in the lamina, but, at least partly, they project into the AMe through the distal fibre fan (Chapter III, Fig. 6).

In the AMe, PDH-ir projections were found mainly in the anterior, shell, and internodular neuropil, but only scarcely in the nodular neuropil. It turned out, that two types of DCVs are PDH-ir, namely a subpopulation of the large DCVs, and probably all medium-sized DCVs (Chapter II, Fig. 9). It was shown that the terminals with medium-sized DCVs at least partly belong to the large PDHMe (Chapter II, Fig. 7), and indirect evidences lead to the conclusion that a part of the varicosities with large DCVs belong to the medium-sized anterior PDHMe.

The projections of these anterior PDHMe subgroups are differentially distributed in the neuropil of the AMe, most likely reflecting different functions of these neurons. The PDH-ir terminals with medium-sized DCVs (hence, originating from the large PDHMe), could mainly be found in the anterior and shell neuropil of the AMe, where they form output and, most likely, also input synapses (Chapter II, Figs. 6F, 9A, B). The pre- and postsynaptic partners of the PDH-ir terminals with medium-sized DCVs are herein discussed to belong to the serotonergic neuron system of the AMe, which apparently consists of local interneurons (Chapter II, Fig. 11). Since half of the large PDHMe, which contain the medium-sized DCVs, form a monosynaptic neuronal pathway between both AMae (Chapter VII, Fig. 5), a larger population of varicosities with medium-sized DCVs observed in the AMe should origin from neurons of the contralateral AMe (see Appendix B).

The PDH-ir varicosities with large DCVs (originating from medium-sized PDHMe), could also be found in the anterior and shell neuropil of the AMe, but are more frequent in the internodular neuropil. They form synaptic connections to different types of neurones. Among them, at the transition to the nodular neuropil, are fibres with granular DCVs, which are assumed to belong to *Mas*-allatotropin-ir neurons and hence, to be involved in the light entrainment pathway (Petri et al., 2002; Chapter II, Fig. 3B). These connections may form the interface between the light entrainment pathway and the PDH-ir neurons; here, light synchronisation of the pacemaker neurons as well as circadian gating of the entrainment pathway might occur (Chapter II, Fig. 11).

However, since the hypotheses about the pre- and postsynaptic partners of the different PDHMe can so far only be formulated after indirect conclusions, much work remains to unravel their synaptic connections, e.g., by double and triple staining experiments on the electron-microscopic (EM) level. Furthermore, a part of the PDH-ir fibres in the AMe definitely belongs to the so far neglected posterior PDHMe, which require further investigations. Moreover, the nature of the PDH-ir AMe-projections originating from the small anterior PDHMe and of the PDHLa remains so far unknown, since they most likely where not observed on the EM level due to their low immunoreactivity even in preparations for light microscopy.

In this work it could be demonstrated, that the PDH-ir neurons communicate to other cells *via* two ways: firstly, *via* synaptic interactions most likely involving classical neurotransmitters, secondly *via* non-synaptic, parakrine neuropeptide release. Whether the same or different neurons are hereby addressed by one particular PDH-ir neuron, can only be determined by labelling target neurons carrying PDF receptors combined with PDH-immunocytochemistry on the EM level. However, it is reasonable to assume that increased synaptic output of PDH-ir neurons will be accompanied by increased PDF release, since synaptic output mechanisms involve intracellular increase of calcium levels, which is simultaneously the signal for the release of DCVs and hence, for peptide release into the intercellular space (Nässel, 2002). This could evoke modulation of long-term effects to neurons that are postsynaptic to the PDH-ir neurons as is required for the function of an internal clock, if these postsynaptic neurons additionally carry PDF-receptors. The short-lasting effects of synaptic excitations or inhibitions could therefore gate these long-term peptide ef-

fects. However, PDF-release could also provide feedback information to neurons presynaptically to the PDH-ir neurons, or even influence neurons, which are not directly connected to the PDH-ir neurons by synapses. To understand the complex neuronal network of the AMe, both the synaptic connections as well as the peptidergic interactions between the AMe neurons have to be investigated in the future.

IDENTIFICATION OF THE ACCESSORY MEDULLA AS CIRCADIAN PACEMAKER: WHERE THE CLOCK WORKS

With AMe-lesion and -transplantation studies combined with PDH immunocytochemistry in *Leucophaea maderae* it was investigated, whether the AMe and adjacent PDHMe in fact form a circadian pacemaker. In the lesion experiments (Chapter III), cockroaches which one optic lobe was removed, were placed into running-wheels in constant darkness. Locomotor activity was recorded with computer-aided devices connected to the running-wheels, until the animals showed a stable circadian rhythmic locomotor activity for several weeks. Then, the AMe of the remaining optic lobe was lesioned and the animals were further monitored in their running-wheels. Animals that behaved arrhythmic after lesions consistently showed damages of the PDHMe and AMe, and had either no or sparsely regenerated PDH-ir fibres in the midbrain (Chapter III, Figs. 5, 6).

However, it cannot be ruled out that other neurons near the PDHMe, which where not observed in these experiments but which were also affected by the lesions, establish rhythmicity. Furthermore, arrhythmicity occurring after lesions is no compelling evidence that the pacemaker itself is affected by the lesion. The lesion may only have destroyed output or auxiliary structures of the clock, what could also lead to the observed behavioural consequences. Hence, much more striking evidence that a certain tissue contains a circadian pacemaker is the ability of this tissue to restore circadian rhythmicity in animals, which own pacemaker(s) have been ablated. Therefore, pacemaker transplantation experiments were designed (Chapter IV). Nevertheless, although the lesion experiments were deferred in favour of AMe-transplantations, lesions are still a valuable instrument to get further information about the functional components of the internal clock, preferentially, if the clock's location is already confirmed by additional experiments. In many cases, it may even be more informative if animals remain rhythmic after setting of defined lesions (Chapter III, Figs. 7–10).

Transplantation experiments aimed to identify circadian pacemakers have been successfully applied to a variety of animals, such as cockroaches, rats, hamsters, and birds (Zimmerman and Menaker, 1979; Page, 1982; Drucker–Colin et al., 1984; Sawaki et al., 1984; DeCoursey and Buggy, 1989). However, Page (1982) transplanted large and intact brain pieces, namely whole optic lobes, among cockroaches. Herein, extirpated brain grafts consisting of only about 1000 neurons containing the AMe were transplanted into cockroaches which own pacemakers, after recording rhythmic forerun activity as described above, had been removed (Chapter IV). After performing the AMe-transplantations and control experiments it turned out, that significantly more animals with AMe-grafts regained circadian rhythmic activity according to specified criteria than control animals did, even if the AMae were transplanted into the antennal lobes of the hosts (Chapter IV, Figs. 2, 3, Table 1). Hence it could be concluded, that the AMe indeed is the circadian clock controlling activity rhythms in *Leucophaea*. Further, all postoperatively rhythmic animals, which brains could be processed for PDH-immunocytochemistry, showed PDH-ir somata at the transplantation sites as well as regenerated PDH-ir fibres in the superior protocerebra, where the PDHMe originally terminate (Chapter IV, Fig. 4B–D, Table 4). These findings show a correlation of rhythmicity and the presence of PDH-ir midbrain projections, as was previously demonstrated by Stengl and Homberg (1994). Further, it appears that the most important output regions for timing information of the PDH-ir neurons are the superior lateral and medial protocerebra, whereas PDH-ir innervations of the inferior lateral and ventrolateral protocerebra or of the posterior optic tubercles seem not to be crucial to maintain circadian rhythmic behaviour. Nevertheless, the assumption that the PDHMe belong to the pacemaker neurons that form the AMe, is still not unequivocally demonstrated, since the PDHMe constitute only about 1–2 % of all transplanted neurons, and other neurons that have not been identified may have re-established rhythmicity. However, the repeated demonstration of present PDH-ir fibres in several midbrain areas in correlation with regained circadian rhythmic behaviour strongly supports the assumption that the PDHMe, or at least a subset of them, are circadian pacemaker neurons. This is also concordant with the demonstrated identity of PDH-ir and *per*-expressing pacemaker neurons in *Drosophila* (Helfrich-Förster, 1995).

In transplantations of whole optic lobes between cockroach populations with different circadian period lengths by Page (1982) it was possible not only to restore circadian locomotor behaviour in the hosts, but also to establish the overt period lengths of the donors. This was not the case in the ex-

periments described herein, where postoperatively rhythmic hosts showed a variety of period lengths (Chapter IV, Table 2). The main explanation for this is that the grafts obviously suffer disintegration of the AMe neuropil and partly decease of AMe neurons. Assuming that the individual pacemaker neurons couple each other inside the AMe neuropil to produce the overt period length, hence forming a multiple oscillator system, loss of this coupling in the grafts and regeneration of processes of only few of the original pacemaker neurons might lead to the observed period lengths. That the individual neurons of a circadian pacemaking structure indeed can produce periods which are not equal to the overt period of the pacemaker, is already shown for the SCN of rats (Honma et al., 1998).

The partly disintegration of the AMe-grafts and regeneration of processes of only a part of its neurons may also be the case for that circadian rhythmicity in AMe-transplanted animals re-established only transiently, and was sometimes difficult to detect on actogram printouts due to ragged activity onsets and arrhythmic background activity. This caused the problem of unbiased separation of postoperatively rhythmic and arrhythmic specimens among AMe-transplanted and control animals. For this reason, a computer analysis was created which automatically separated rhythmic from arrhythmic animals ("scan periodogram analysis with Rhythm Detector"; Chapter V). This analysis involves scanning of the whole data tracks with sequential χ^2-periodograms covering small analysis intervals of 8–12 days (Chapter V, Figs. 15, 16). The χ^2-periodogram analysis with its built-in statistical test is a common method in circadian rhythm research to detect the presence of rhythmicity, as well as for determining of its period length (Sokolove and Bushell, 1978; Klemfuss and Clopton, 1993; Chapter V, Fig. 11). The Rhythm Detector determined whether the peaks of single periodograms exceeded the Sokolove significance level that indicates rhythmicity, and determined heights and widths of these peaks (Chapter V, Fig. 12). Since small periodogram peaks exceeding the significance threshold also occur to certain extend in arrhythmic activity recordings, the periodogram peak heights and width of arrhythmic as well as of generically rhythmic, but randomised activity recordings were measured and averaged (Chapter V, Fig. 14). These values were used to determine thresholds for the decision, whether a certain periodogram peak in an actual Rhythm Detector scan indicates rhythmicity or not. This Rhythm Detector analysis successfully sorted postoperatively rhythmic from arrhythmic animals, and only with this analysis it could be clearly shown, that significantly more AMe-transplanted animals regained circadian rhythmic locomotor behaviour than control animals did.

SEARCH FOR THE COUPLING PATHWAYS: HOW CLOCKS COMMUNICATE

Mutual coupling of the bilaterally organised circadian pacemakers is required to synchronise both internal clocks. Otherwise, the pacemaker's phases would drift apart due to small differences in their period lengths, and cause undesirable splitting of circadian behaviour (Wiedenmann, 1983). Since the discovery of PDH-ir neurons in insects, the PDHMe are discussed to provide a direct neuronal connection between both AMae, because they reach the contralateral brain hemispheres *via* two commissures, the anterior and the posterior optic commissure. However, the staining pattern known from the PDHMe (Fig. 4) is the result of morphologically different neurons with partly overlapping projections. Hence, it could not be clearly discerned only by studying the immunostainings whether a subset of PDHMe reaches the contralateral AMe or optic lobe, or if they just terminate in the contralateral midbrain hemisphere. First incidences that the PDHMe in fact project to the contralateral AMe are supplied by tracer injections in the AMe combined with PDH-immunocytochemistry by Petri (1998; Chapter VII, Fig. 3). He showed that up to three PDHMe-somata were labelled after dextran injection into the opposite AMe. However, since the histological evaluations of these experiments were performed on whole-mount preparations only, PDH-ir fibres in the AMe originating from contralateral PDHMe, as required for a direct neuronal connection, could not be shown. Furthermore, other neurons, which were not PDH-ir, also appeared to connect both AMae.

To characterise all existing direct neuronal connections between both optic lobes, a series of conventional tracer experiments was designed (Chapter VI). In the first set of these experiments, one optic lobe of a group of cockroaches was cut, and the tracer horseradish peroxidase (HRP) was applied to the optic lobe stumps by means of suction pipettes (Chapter VI, Fig. 1B). In the second experimental series, HRP or biotin-labelled dextran was injected into one AMe (Chapter VI, Fig. 1C). Seven tracts (tracts 1–7) directly connecting both optic lobes were found, and, except tract 3, could be compared with existing anatomical correlates and physiological data of cockroaches and other insects (Chapter VI, Figs. 2–5). Three tracts, namely tracts 3, 4, and 7, converge proximally to the lobula in the lobula valley tract (LoVT), which leads to the AMe, and hence, are candidates for direct connections between both

AMae. The tracts 4 and 7 pass the midbrain *via* the anterior and posterior optic commissure, respectively, and their midbrain and optic lobe projections together strongly resemble the arborisation pattern of the PDH-ir neurons (Chapter VI, Fig. 6).

In the vicinity to the AMe, three groups of neuronal somata were stained after tracer injection into the contralateral AMe, and termed medulla cells groups I–III (MC I–III). The MC I consist of up to four somata and belong to the ventral neurons of the AMe (Chapter II, Fig. 1E) as the anterior PDHMe. Projections of these neurons even reach the lamina of the optic lobe contralaterally to the injected AMe through the distal (former: anterior) fibre fan; this is probably the first incidence for a contralateral lamina connection in insects (Chapter VI, Fig. 5D). The MC II, containing up to 35 somata, are identical to the ventroposterior neurons (Chapter II, Fig. 1E). They comprise a population of light and, partly, polarisation sensitive neurons (Loesel and Homberg, 2001), which have been also characterised in crickets (Labhart and Petzold, 1993), and form the so-called contralateral middle layer fibre system of the medulla (Chapter VI, Fig. 5E). The MC III are situated posteriorly to the LoVT at a similar location as the posterior PDHMe. The origin of the interoptical commissure tract 3 is so far unknown except for one soma at the dorso-proximal base of the lobula that contributes to this tract. It is also not yet clear whether this tract indeed connects both AMae. Since the MC III turned out to be not identical with the posterior PDHMe (see below), they may belong to this tract.

Despite striking morphological evidences, the identity of MC I somata and their tract 4/7 projections with the PDH-ir neuron system remained to be demonstrated by combined tracer labelling and PDH-immunocytochemistry. These experiments are the subject of Chapter VII. Three anterior PDHMe were found to connect the ipsi- to the contralateral AMe, two belonging to the large, and one to the medium-sized anterior PDHMe (Chapter VII, Fig. 4A). A fourth MC I additionally connects both AMae but is not PDH-ir. The posterior PDHMe do not project to the contralateral AMe (Chapter VII, Fig. 7B). In the AMe, contralateral PDH-ir fibres could be found mainly in the anterior neuropil, but also in the shell neuropil and, rarely, in the internodular neuropil (Chapter VII, Figs. 4B,C, 6). These contralateral PDH-ir fibres further extend *via* the distal fibre fan of the medulla up to the lamina. In the central brain, most but not all areas innervated by the PDH-ir neuron system receive PDH-ir fibres from both AMae (Chapter VII, Fig. 8). Hence, pacemaker coupling occurs not only at the level of the AMae, but also the major central output regions of the PDH-ir neurons receive outputs from both AMae (Chapter VII, Fig. 9). The nature of the fourth MC I soma projecting to the contralateral AMe is so far unknown, but it is very likely that it belongs to the FMRFamid-ir fibre system of the AMe. Computer models of coupled PER/TIM feedback loops require two reciprocally acting coupling forces to achieve the coupling properties, which can be observed experimentally (Petri and Stengl, 2001). This counterpart may be provided by the fourth MC I neuron.

It was formerly proposed that the bilateral optic lobe pacemakers of *L. maderae* do not only exchange information about the current phase, but also receive entraining light information from the contralateral eye (Page, 1978, 1983a,b). It appears, that the phase information is transmitted by the MC I neurons through a pathway containing the contralateral projecting PDHMe (PDHMe-like pathway). In electrophysiological experiments, all neurons belonging to this pathway did not or only faintly react to light pulses so far (Loesel and Homberg, 2001). Contrarily, neurons of a pathway containing the MC II neurons (VMNe-like pathway, see below) showed prominent and fast reaction to changes of light intensity. Hence, these two AMe-connecting pathways appear to constitute the morphological correlates of the two functionally different pathways connecting the circadian optic lobe pacemakers of *Leucophaea*, which were proposed in earlier works (Page 1983 a,b).

NEURONAL PATHWAYS OF THE ACCESSORY MEDULLA

Combining all morphological observations on the AMe of *Leucophaea* (Petri et al., 1995, 2002; Loesel and Homberg, 2001; Chapters I–III, VI–VII), a comprehensive map of the input and output pathways of the AMe could be created (Fig. 5). Three main pathways connect the AMe to regions of the ipsilateral optic lobe, to the midbrain, and to the contralateral optic lobe.

One pathway consists of the distal tract of the AMe (green in Fig. 5) and is restricted to the ipsilateral optic lobe. Morphological evidences indicate that it is an unidirectional pathway providing input into the nodular neuropil of the AMe. The distal tract connects the medulla with the AMe, and shows conspicuous γ-amino butyric acid (GABA)-immunoreactivity. It is discussed to be a light entrainment pathway into the AMe due to anatomical and physiological indications (Petri et al., 2002).

The second pathway (PDHMe-like pathway, red in Fig. 5) contains the PDH-ir, FMRFamid-ir, and leucokinin-ir neurons (Petri et al., 1995) of the AMe. Within the ipsilateral optic lobe, it contains also

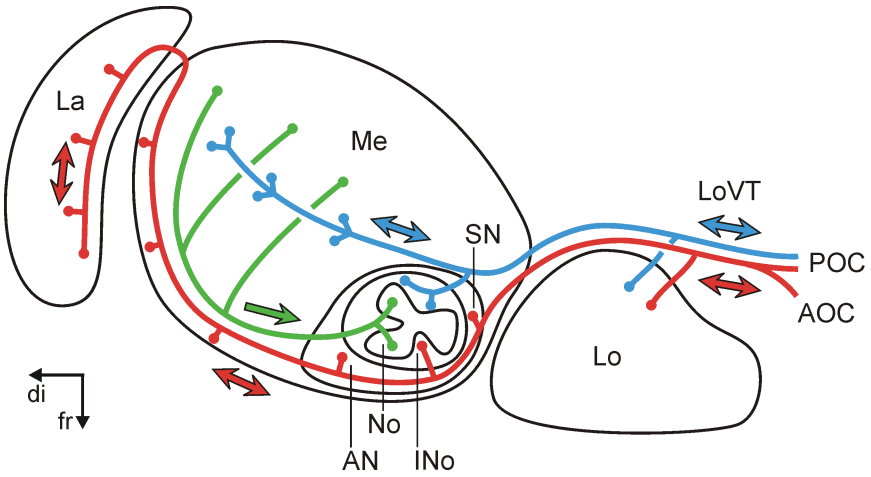

Fig. 5. Input and output pathways of the AMe. The scheme shows a horizontal view of the optic lobe neuropils lamina (La), medulla (Me), and lobula (Lo), and of the subcompartments of the accessory medulla (AN anterior neuropil; INo internodular neuropil; No nodular neuropil; SN shell neuropil). The accessory medulla is enlarged to about twice its size in respect to the other neuropils. Three pathways connect the accessory medulla to other optic lobe neuropils, two of them provide connections to the midbrain and contralateral optic lobe *via* the lobula valley tract (LoVT). Input and output regions of the pathways are indicated by circles; information flows of bidirectional pathways are indicated by double-headed arrows, of the monodirectional pathway by a single-headed arrow. The distal tract pathway (green) is supposed to carry light information to the nodular neuropil of the accessory medulla. The PDHMe-like pathway (red) connects the anterior, shell, and internodular neuropil of the accessory medulla to the distal layer of the medulla and to the lamina and lobula, as well as to anterior and posterior midbrain areas, and to the contralateral optic lobe and accessory medulla. The VPNe-like pathway (blue) connects the posterior and distal internodular neuropil of the accessory medulla to middle layers of the medulla and to the lobula, and to the contralateral accessory medulla and optic lobe. AOC, POC: pathways to the anterior and posterior optic commissure, respectively. Coordinates: di distal, fr frontal.

processes of the PDHLa, and probably, processes of FMRFamid-ir and serotonin-ir lamina neurons, which share a similar morphology to the PDHLa (Petri et al., 1995). The midbrain and contralateral optic lobe connections of this pathway, however, appear to be established solely by neurons with somata in the vicinity of the AMe. These centripetal projections run through the LoVT, which bifurcates between midbrain and proximal lobula (Chapter VII, Fig. 9). From this bifurcation, one portion of fibres joins the posterior optic tract and runs *via* the posterior optic tubercles and the posterior optic commissure. The other fibres head to more anterior midbrain areas and run through the anterior optic commissure. Midbrain projections emerging from this pathway appear to be output structures, but since contralateral connections between both AMae use the PDHMe-like pathway, it is in total a bidirectional pathway. In the optic lobe, this pathway extends through the distal layer of the medulla, there forming the typical fibre-fan, to the lamina. These fanshaped fibres in the distal layer of the medulla are not only transmitting information between the AMe and lamina, but are most likely active output structures into the medulla due to the varicosities formed by the PDH-ir and FMRFamid-ir fibres passing this region. Some neurons of the PDHMe-like pathway, like the leukokinin-ir neurons are restricted to the ipsilateral optic lobe (Petri et al., 1995). Since also neurons with somata in the lamina project *via* the distal layer to the AMe, probably delivering output information to the AMe (Chapter III, Fig. 6A), also in the optic lobe this pathway appears to function in a bidirectional way. In the AMe, the main input and output regions of the PDHMe-like pathway are the anterior, shell, and internodular neuropil. Generally, all neurons belonging to the PDHMe-like pathway seem not or only faintly respond to light stimuli (Loesel and Homberg, 2001).

The third pathway (ventromedial neuron (VMNe)-like pathway; blue in Fig. 5) contains populations of neurons that are sensitive to light and, partly, to e-vector rotation of polarised light. Most of their somata belong to the group of ventroposterior neurons (Chapter II, Fig. 1E), which are largely, if not totally identical with the MC II neurons (Chapter VI, Fig. 5E). These neurons use the LoVT to reach the midbrain like the neurons of the PDHMe-like pathway, which therefore is probably the only tract providing centripetal pathways for the AMe in *Leucophaea*. They project *via* the posterior optic tract and the posterior optic commissure to areas of the posterior midbrain and to the contralateral optic lobe, but do not project to anterior parts of the midbrain (Chapter VI, Fig. 5C). In the optic lobe, fibres emerging from this pathway

arborise in middle layers of the medulla and do not reach the lamina. Since at least most, if not all, neurons belonging to this pathway connect both optic lobes and partly both AMae, they are assumed to have their input region in one optic lobe (most likely where the soma lies), and the output region in the opposite optic lobe. Hence, this pathway functions bidirectionally in both its midbrain and optic lobe portions. Additionally, neurons with somata in the *pars intercerebralis* use the posterior optic tract and LoVT to reach the AMe (Loesel and Homberg, 2001; Chapter VI, Fig. 5C). Since they strongly react to light, they are herein assigned to the VMNe-like pathway. The AMe is entered by the VMNe-like pathway from the posterior side. The main input and output regions of the VMNe-like pathway in the AMe appear to be the internodular neuropil and distal shell neuropil of the AMe (Chapter VII, Figs. 4B, C, 7A).

THE FUNCTION OF PDF

All information obtained throughout this work strongly support the assumption that the PDHMe act as pacemaker, output, and clock-coupling neurons in the cockroach circadian system, and that PDF release is the circadian output signal of these neurons. These assumptions are consistent with findings in the fruitfly *Drosophila*, the main insect model organism for research on molecular clock function (reviewed by Taghert, 2001). Eight of the nine clock protein (i.e., PER, TIM, CLOCK, and CYCLE) expressing ventral lateral neurons (LN_vs) of one *Drosophila's* optic lobe also express PDF (Helfrich-Förster, 1995). The PDF expression is differentially affected in *per* and *tim* mutants, respectively, indicating that PER and TIM regulate PDF-expression at posttranscriptional level. The small LN_vs show circadian fluctuation of PDH-immunoreactivity in the midbrain terminals, indicating PDF-release in the early subjective night (Park et al., 2000). In the marine snail *Bulla gouldiana*, isolated retinal pacemaker cells show circadian rhythmicity in membrane conductance (Michel et al., 1993). It is likely that also in the insect pacemaker neurons circadian changes in membrane conductance occur and thus, regulate action potential activity and DCV release. Gynander experiments revealed fruitflies, which miss the LN_vs of one optic lobe. They showed large LN_vs projecting to the contralateral optic lobe (C. Helfrich-Förster, unpublished), similar to the conditions found here for the cockroach. Evidences for a physiological function of PDF were delivered by PDF-injections into the optic lobes of cockroaches monitored in a running-wheel assay, which resulted in a monophasic phase response curve with a maximum phase-delay at the late subjective day (Petri and Stengl, 1997). Since this PRC is dissimilar to the PRC obtained with light pulses, a non-photic input to the clock by PDF was concluded by the authors, which probably, if combined with the morphological data presented herein, reflects a clock-coupling function of the PDF output.

In this work it was shown that PDF most likely functions as non-synaptic but parakrine intercellular signal (Chapters I, II). Several lines of evidence suggest, that PDF acts to target neurons envolving protein phosphorylation pathways. Evidences by genetic experiments point to a function of the intracellular protein kinase A (PKA) pathway in the circadian output controlling locomotor rhythms in *Drosophila* (Majercak et al., 1997). This would assume preceded binding of PDF to G-protein coupled receptors (GPCRs); this receptor appears to be identified among about three dozen orphan GPCRs in *Drosophila* (Hewes and Taghert, 2001; P. Taghert, personal communication). Further, recent data suggest a function of the *neurofibromatosis-1* gene product (NF1) acting through the mitogene-activated protein kinase (MAPK) in mediating circadian output controlling locomotor activity in *Drosophila* (Williams et al., 2001). A clear circadian rhythm of phospho-MAPK immunostaining was found in the vicinity of the PDH-ir central brain projections, indicating a functional relation between circadian PDF-release and Ras/MAPK signalling.

Phosphorylation of the clock proteins PER and TIM through the doubletime- and shaggy-kinases, respectively, is crucial for clock function in *Drosophila* (Price et al., 1998; Kloss et al., 2001; Martinek et al., 2001). Mutations in both kinases, which slow down phosphorylation rates, resulted in prolonged circadian periods in *Drosophila*. Further, the mathematical models of oscillator coupling published by Petri and Stengl (2001) demonstrated, that stable coupling through phase delays, as can be evoked by PDF-injections in *Leucophaea* (Petri and Stengl, 1997), can only be achieved by reduction of the phosphorylation rates of PER and TIM. Putting all together, it is most likely that PDF acts through phosphorylation pathways both in the midbrain outputs of the PDHMe, as well as in the pacemaker coupling input into the AMe provided by the PDHMe.

The bilaterally symmetric circadian pacemakers of the cockroach are spatially separated, contrarily to the nearly inseparable SCN hemispheres of mammals. Hence, the coupling pathways of the cockroach's internal clock driving behavioural rhythms are well accessible to anatomical and physiological studies. Due to these morphological advantages,

combined with its robustness and size, the cockroach *Leucophaea maderae* is expected to play an important role in the exploration of general circadian pacemaker coupling and output mechanisms in the future.

LITERATURE CITED

Aronson BD, Bell-Pederson D, Block GD, Bos NPA, Dunlap JC, Eskin A, Garceau NY, Geusz ME, Johnson KA, Khalsa SBS, Koster-Van Hoffen G, Koumenis C, Lee TM, LeSauter J, Lindgren KN, Liu Q, Loros JJ, Michel SH, Mirmiran M, Moore RY, Ruby NF, Silver R, Turek FW, Zatz M, and Zucker I. 1993. Circadian rhythms. Brain Res Rev 18:315–333.

Aschoff J. 1960. Exogenous and endogenous components in circadian rhythms. In Cold Spring Harbor Symposia on Quantitative Biology: Volume XXV. Biological clocks. New York: Cold Spring Harbor Press. p 11–28.

Aschoff J. 1984. Circadian timing. Ann NY Acad Sci 423:442–468.

Bünning E. 1973. The physiological clock – circadian rhythms in biological chronometry. New York, Heidelberg, Berlin: The English Universities Press Ltd.; Springer Verlag.

Colwell CS and Page TL. 1990. A circadian rhythm in neural activity can be recorded from the central nervous system of the cockroach. J Comp Physiol 166:643–649.

de Mairan JJ. 1729. Observation botanique. Histoire de l'Académie Royale des Sciences Paris, 35–36.

DeCoursey PJ and Buggy J. 1989. Circadian rhythmicity after neural transplant to hamster third ventricle: specificity of suprachiasmatic nuclei. Brain Res 500:263–75.

Dircksen H, Zahnow CA, Gaus G, Keller R, Rao KR, and Riem JP. 1987. The ultrastructure of nerve endings containing pigment-dispersing hormone (PDH) in crustacean glands: identification by an antiserum against a synthetic PDH. Cell Tissue Res 250:377–387.

Douglass JK and Strausfeld NJ. 1995. Visual motion detection circuits in flies: peripheral motion computation by identified small-field retinotopic neurons. J Neurosci 15:5596–5611.

Drucker–Colin R, Aguilar-Roblero R, Garcia-Hernandez F, Fernandez-Cancino F, and Bermudez Rattoni F. 1984. Fetal suprachiasmatic nucleus transplants: diurnal rhythm recovery of lesioned rats. Brain Res 311:353–37.

Ehnbohm K. 1948. Studies on the central and sympathetic nervous system and some sense organs in the head of neuropteroid insects. Opusc Entomol [Suppl] 8:1–162.

Hagberg M. 1986. Ultrastructure and central projections of extraocular photoreceptors in caddiesflies. Cell Tissue Res 245:643–648.

Hanström B. 1940. Inkretorische Organe, Sinnesorgane und Nervensystem des Kopfes einiger niedriger Insektenordnungen. Kungl Sven Vetensk Akad Handl Ser 3 18:1–265.

Helfrich-Förster C. 1995. The period clock gene is expressed in central nervous system neurons which also produce a neuropeptide that reveals the projections of circadian pacemaker cells within the brain of *Drosophila melanogaster*. Proc Natl Acad Sci USA 92:612–616.

Helfrich-Förster C, Stengl M, and Homberg U. 1998. Organisation of the circadian system in insects. Chronobiol Int 15:567–594.

Hennig W. 1986. Taschenbuch der speziellen Zoologie. Wirbellose II. Gliedertiere. Thun, Frankfurt: Harri Deutsch.

Hewes RS and Taghert PH. 2001. Neuropeptides and neuropeptide receptors in the *Drosophila melanogaster* genome. Genome Res 11:1126–1142.

Homberg U, Reischig T, and Stengl M. 2003. Neural organisation of the circadian system of the cockroach *Leucophaea maderae*. Chronobiol Int, in press.

Homberg U, Würden S, Dircksen H, and Rao KR. 1991. Comparative anatomy of pigment-dispersing hormone-immunoreactive neurons in the brain of orthopteroid insects. Cell Tissue Res 266:343–357.

Honma S, Shirakawa T, Katsuno Y, Namihira M, and Honma K. 1998. Circadian periods of single suprachiasmatic neurons in rats. Neurosci Lett 250:157-160.

Hufeland CW. 1776. Makrobiotik oder Die Kunst, das menschliche Leben zu verlängern. Munich: Insel Taschenbuch, licensed by Matthes und Seitz Verlag, 1984.

Hurd MW and Ralph MR. 1998. The significance of circadian organisation for longevity in the golden hamster. J Biol Rhythms 13:430–446.

Klemfuss H and Clopton PL. 1993. Seeking tau: A comparison of six methods. J interdiscipl Cycle Res 24:1–16.

Kloss B, Rothenfluh A, Young MW, and Saez L. 2001. Phosphorylation of period is influenced by cycling physical associations of double-time, period, and timeless in the *Drosophila* clock. Neuron 30:699–706.

Labhart T and Petzold J. 1993. Processing of polarised light information in the visual system of crickets. In Wiese K, Gribakin FG, Popov AV, and Renninger G, editors. Sensory system of arthropods. Basel: Birkhäuser Verlag. p 158–169.

Loesel R and Homberg U. 2001. Anatomy and physiology of neurons with processes in the accessory medulla of the cockroach *Leucophaea maderae*. J Comp Neurol 439:193–207.

Logothetis NK and Sheinberg DL. 1996. Visual object recognition. Annu Rev Neurosci 19:577–621.

Majercak J, Kalderon D, and Edery I. 1997. *Drosophila melanogaster* deficient in protein kinase A manifests behaviour-specific arrhythmia but normal clock function. Mol Cell Biol 17:5915–5922.

Martinek S, Inonog S, Manoukian AS, and Young MW. 2001. A role for the segment polarity gene shaggy/GSK-3 in the *Drosophila* circadian clock. Cell 105:769-779.

Michel S, Geusz ME, Zaritsky JJ, and Block GD. 1993. Circadian rhythm in membrane conductance expressed in isolated neurons. Science 259:239–241.

Moore RY, Speh JC, and Leak RK. 2002. Suprachiasmatic nucleus organisation. Cell Tissue Res 309:89–98.

Nässel DR. 2002. Neuropeptides in the nervous system of Drosophila and other insects: multiple roles as neuromodulators and neurohormones. Prog Neurobiol 68:1–84.

Nishiitsutsuji-Uwo J and Pittendrigh CS. 1968a. Central nervous system control of circadian rhythmicity in the cockroach. III. The pathway of light signals that entrain the rhythm. Z vergl Physiol 58:1–13.

Nishiitsutsuji-Uwo J and Pittendrigh CS. 1968b. Central nervous system control of circadian rhytmicity in the cockroach. II. The optic lobes, locus of the driving oscillator? Z vergl Physiol 58:14–46.

Page TL. 1978. Interactions between bilaterally paired components of the cockroach circadian system. J Comp Physiol A 124:225–236.

Page TL. 1981. Effects of localised low-temperature pulses on the cockroach circadian pacemaker. Am J Physiol 240:R144-R150.

Page TL. 1982. Transplantation of the cockroach circadian pacemaker. Science 216:73–75.

Page TL. 1983a. Effects of optic-tract regeneration on internal coupling in the circadian system of the cockroach. J Comp Physiol 153:353–363.

Page TL. 1983b. Regeneration of the optic tracts and circadian pacemaker activity in the cockroach *Leucophaea maderae*. J Comp Physiol A 152:231–240.

Park JH, Helfrich-Förster C, Lee G, Liu L, Rosbash M, and Hall JC. 2000. Differential regulation of circadian pacemaker output by separate clock genes in *Drosophila*. Proc Natl Acad Sci USA 97:3608–3613.

Petri B. 1998. Neuronal organisation of a circadian clock. Analysis of the clock which controls circadian locomotor behaviour of the cockroach *Leucophaea maderae*. Dissertation: University of Regensburg, Germany.

Petri B, Homberg U, Loesel R, and Stengl M. 2002. Evidence for a role of GABA and *Mas*-allatotropin in photic entrainment of the circadian clock of the cockroach *Leucophaea maderae*. J Exp Biol 205:1459–1469.

Petri B and Stengl M. 1997. Pigment-dispersing hormone shifts the phase of the circadian pacemaker of the cockroach *Leucophaea maderae*. J Neurosci 17:4087-4093.

Petri B and Stengl M. 2001. Phase response curves of a molecular model oscillator: implications for mutual coupling of paired oscillators. J Biol Rhythms 16:125–141.

Petri B, Stengl M, Würden S, and Homberg U. 1995. Immunocytochemical characterisation of the accessory medulla in the cockroach *Leucophaea maderae*. Cell Tissue Res 282:3–19.

Pflugfelder O. 1936. Vergleichend-anatomische, experimentelle und embryologische Untersuchungen über das Nervensystem und die Sinnesorgane der Rynchoten. Stuttgart: Schweizerbart'sche Verlagsbuchhandlung.

Pittendrigh CS. 1960. Circadian rhythms and the circadian organisation of living systems. In Cold Spring Harbor Symposia on Quantitative Biology: Volume XXV. Biological clocks. New York: Cold Spring Harbor Press. p 159–182.

Pittendrigh CS. 1993. Temporal organisation: Reflections of a Darwinian clockwatcher. Annu Rev Physiol 55:17–54.

Price JL, Blau J, Rothenfluh A, Abodeely M, Kloss B, and Young MW. 1998. *double-time* is a novel Drosophila clock gene that regulates PERIOD protein accumulation. Cell 94:83–95.

Pyza E and Meinertzhagen IA. 1997. Neurites of period-expressing PDH-cells in the fly's optic lobe exhibit circadian oscillations in morphology. Eur J Neurosci 9:1784-1788.

Roberts SK. 1974. Circadian rhythms in cockroaches: Effects of optic lobe lesions. J Comp Physiol 88:21–30.

Roberts SK and De F. 1965. Photoreception and entrainment of cockroach activity rhythms. Science 148:958–959.

Sawaki Y, Nihonmatsu I, and Kawamura H. 1984. Transplantation of the neonatal suprachiasmatic nuclei into rats with complete bilateral suprachiasmatic lesions. Neurosci Res 1:67–72.

Schibler U and Sassone-Corsi P. 2002. A web of circadian pacemakers. Cell 111:919–922.

Sokolove PG. 1975. Localisation of the cockroach optic lobe circadian pacemaker with microlesions. Brain Res 87:13–21.

Sokolove PG and Bushell WN. 1978. The chi square periodogram: its utility for analysis of circadian rhythms. J Theor Biol 72:131–160.

Stanewsky R. 2002. Clock mechanisms in *Drosophila*. Cell Tissue Res 309:11–26.

Stengl M. 1995. Pigment-dispersing hormone-immunoreactive fibres persist in crickets which remain rhythmic after bilateral transection of the optic stalks. J Comp Physiol A 176:217–228.

Stengl M and Homberg U. 1994. Pigment-dispersing hormone-immunoreactive neurons in the cockroach *Leucophaea maderae* share properties with circadian pacemaker neurons. J Comp Physiol A 175:203–213.

Taghert PH. 2001. How does the circadian clock send timing information to the brain? Semin Cell Dev Biol 12:329–341.

Touitou Y and Haus E. 1994. Biological rhythms in clinical and laboratory medicine. Berlin, Heidelberg, New York: Springer Verlag.

van Esseveldt KE, Lehman MN, and Boer GJ. 2000. The suprachiasmatic nucleus and the circadian time-keeping system revisited. Brain Res Brain Res Rev 33:34–77.

Wiedenmann G. 1983. Splitting in a circadian activity rhythm: the expression of bilaterally paired oscillators. J Comp Physiol A 150:51–60.

Williams JA, Su HS, Bernards A, Field J, and Sehgal A. 2001. A circadian output in Drosophila mediated by *neurofibromatosis-1* and Ras/MAPK. Science 293:2251–2256.

Würden S. 1994. Funktionelle, anatomische und neurochemische Organisation der akzessorischen Medulla der Heuschrecke, *Schistocerca gregaria*. Dissertation: University of Regensburg, Germany.

Zimmerman NH and Menaker M. 1979. The pineal gland: a pacemaker within the circadian system of the house sparrow. Proc Natl Acad Sci USA 76:999–1003.

I. Morphology and pigment-dispersing hormone immunocytochemistry of the accessory medulla, the presumptive circadian pacemaker of the cockroach *Leucophaea maderae*: a light- and electron-microscopic study.

Reischig T and Stengl M. 1996. Cell Tissue Res 285:305-319

Cell Tissue Res (1996) 285:305–319

Cell & Tissue Research

Morphology and pigment-dispersing hormone immunocytochemistry of the accessory medulla, the presumptive circadian pacemaker of the cockroach *Leucophaea maderae:* a light- and electron-microscopic study

Thomas Reischig, Monika Stengl

Institut für Zoologie, Biologie 1, Universität Regensburg, D-93040 Regensburg, Germany

Received: 30 November 1995 / Accepted: 23 March 1996

Abstract. To provide a framework for a cellular analysis of the accessory medulla, which is the presumptive circadian pacemaker of hemimetabolous insects, we have studied this neuropil and its associated neuronal structures by light- and electron-microscopy in the cockroach *Leucophaea maderae*. The accessory medulla is situated at the ventromedial edge of the medulla and shows no evidence of a retinotopical organization. Instead, it is composed of dense noduli that are embedded in internodular neuropil. The distal fiber tract, which appears to originate from the lamina and the medulla, provides a possible visual input to the accessory medulla. Electron-microscopic studies show that the accessory medulla contains accumulations of at least four types of dense-core vesicles, viz., granular, small, medium-sized, and large. Granular vesicles occur almost exclusively in processes of the nodular neuropil and are apparently confined to local neurons; the other three types are restricted to the internodular and loose neuropil that surrounds the accessory medulla. Immunostaining for light- and electron-microscopy has demonstrated that arborizations of presumptive pacemaker neurons, viz., neurons immunoreactive for the pigment-dispersing hormone, are restricted to the internodular and the loose neuropil of the accessory medulla. Immunoreactivity for pigment-dispersing hormone is found only in subpopulations of terminals containing medium-sized or large dense-core vesicles, in association with the vesicles.

Key words: Nervous system, insect – Optic lobe – Neuropil – Circadian rhythm – Dense-core vesicles – Pigment-dispersing hormone – *Leucophaea maderae* (Insecta)

This research was supported by DFG grant Ste 531/1-1 to M. Stengl.

Correspondence to: M. Stengl (Tel.: +49–941–9433117; Fax: +49–941–9433304)

Introduction

One of the most important goals in rhythm research is the identification of the morphological correlates of the relevant pacemakers. Hemimetabolous insects were among the first groups of animals in which the approximate position of the pacemaker was localized (Nishiitsutsuji-Uwo and Pittendrigh 1968a,b). Lesion studies have shown that the brain of the cockroach *Leucophaea maderae* contains two mutually coupled pacemakers in the optic lobes, positioned ventrally between the lobula and the medulla (Nishiitsutsuji-Uwo and Pittendrigh 1968a,b; Roberts 1974; Sokolove 1975; Colwell and Page 1990; for a review, see Page 1984). These pacemakers control circadian locomotor activity and circadian fluctuations in the sensitivity of the compound eyes via neuronal pathways (Nishiitsutsuji-Uwo and Pittendrigh 1968a,b; Page 1983a,b; Wills et al. 1986; Colwell and Page 1990). The bilaterally symmetric pacemakers are entrained by unidentified photoreceptors in or near the ipsilateral and contralateral compound eyes (Nishiitsutsuji-Uwo and Pittendrigh 1968a; Page 1978). Therefore, at least three output pathways of the pacemakers must be present, one to the ipsilateral compound eye, one to the central brain (with a connection to descending neurons), and one to the contralateral pacemaker. These features of the circadian system have also been found in other cockroaches (Roberts 1974; Lukat and Weber 1979) and in crickets (Loher 1972; Sokolove and Loher 1975; Tomioka and Chiba 1986).

Neurons that fulfil all the anatomical criteria for circadian pacemaker cells in cockroaches have been identified immunocytochemically (Homberg et al. 1991) with an antiserum against the crustacean octadecapeptide pigment-dispersing hormone (PDH; Dircksen et al. 1987). In crustaceans, PDH released from the sinus glands triggers chromatophoral pigment migration (Mangerich et al. 1987; Rao and Riehm 1988, 1989). It also appears to synchronize the circadian migration of retinal screening pigment (Arechiga and Mena 1975; Fingerman and Fingerman 1977; Larimer and Smith 1980; Rao and Riehm

1989). In cockroaches, two clusters of PDH-immunoreactive (PDH-ir) neurons lie frontally and ventrally near the posterior lamina. The third group of immunostained neurons fulfils several morphological criteria proposed for the circadian pacemaker (Homberg et al. 1991; Stengl and Homberg 1994). The somata of these PDH-ir medulla neurons (termed PDHMe neurons) lie frontoventrally between the lobula and the medulla, where lesion studies have localized the pacemaker. The PDHMe neurons send processes to the optic lobes and to various areas in the central brain, including neuropils directly connected to the central complex (an apparent locomotor control center) and possible sites of overlap with arborizations of neurosecretory cells. The presence of few or no PDH-ir commissural fibers in crickets correlates with the weak coupling of the two bilaterally paired pacemakers, whereas many PDH-ir commissural fibers in cockroaches (Homberg et al. 1991) can be correlated with strong coupling (Loher 1972; Roth and Sokolove 1975; Page 1978, 1981, 1982, 1983a,b; Wiedenmann 1983, 1984; Chiba and Tomioka 1987). In the midbrain of cockroaches, the regeneration of PDH-ir fibers, that have degenerated after the severance of both optic stalks, occurs concomitantly with the restoration of circadian locomotor activity (Stengl and Homberg 1994). Following the severance of both optic stalks in crickets circadian singing and locomotor activity rhythms remain, but with an altered period, and the PDH-ir fibers of the midbrain do not degenerate (Stengl 1995). The PDH-ir neurons of *Drosophila* express the period gene (Helfrich-Förster 1995), which plays a role in the molecular mechanisms of circadian rhythm generation (for reviews, see Hall and Kyriacou 1990; Hall 1995). The morphology of these cells is changed in mutants with abnormal rhythmic behavior (Helfrich-Förster and Homberg 1993).

In all the insect species studied, dense PDH-ir arborizations, apparently originating from the PDHMe neurons, innervate the accessory medulla, a small neuropil area at the ventromedial edge of the medulla (Homberg et al. 1991). The accessory medulla is situated near the somata of the PDHMe neurons in the presumed region of the circadian pacemaker. Injections of PDH into the vicinity of the accessory medulla cause specific phase-shifts in locomotor rhythms of cockroaches only during the late subjective day (Petri and Stengl 1996), indicating that PDH release in the accessory medulla plays an important role in the mechanisms of the circadian clock. However, the manner in which PDH-ir neurons contribute to the neuropil of the accessory medulla remains unknown.

Accessory medullae were first described in holometabolous insects (Pflugfelder 1936; Hanström 1940; Ehnbohm 1948; Hagberg 1986; Ichikawa 1994) and are assumed to be the remnants of the larval visual system. Larval stemmata and extraocular imaginal photoreceptors, which might play a role in the light-entrainment of the circadian clock (Schulz et al. 1984; Hagberg 1986; Fleissner et al. 1993), terminate in the accessory medulla of holometabolous insects (Schulz et al. 1984; Hagberg 1986; Hofbauer and Buchner 1989; Fleissner et al. 1993). The accessory medulla in hemimetabolous insects was first discovered because of its dense innervation by PDH-ir neurons (Homberg et al. 1991). However, whether it receives direct or only indirect visual inputs via the lamina or the medulla has not been elucidated. Furthermore, its internal organization and the somata or fiber tracts in the vicinity are undescribed.

Here, we present a detailed morphological and PDH-immunocytochemical investigation of the accessory medulla, a little known brain area in hemimetabolous insects. Light- and electron-microscopic studies have characterized the neuropil structure, aspects of innervation, distribution of PDH-ir fibers, and intracellular localization of PDH immunoreactivity in *L. maderae*. We attempt to provide a framework for past and future single-cell studies and to obtain insights into the contribution of PDH-ir fibers to the presumptive clock. Parts of this study have been reported in abstract form (Reischig and Stengl 1995).

Materials and methods

Animals

Adult male cockroaches (*Leucophaea maderae*) were obtained from laboratory colonies at the University of Regensburg. They were reared under the following conditions: 25°C, 30% humidity, and light-dark cycles of 12:12 h with lights on from 6 a.m. to 6 p.m., with dried dog food, bread, and water ad libitum. Most preparations were performed at the end of the light phase. The nomenclature of brain structures follows the terminology used by Strausfeld (1976). The orientation of the figures is always indicated relative to the longitudinal axis of the animal.

Conventional light-microscopy

After being anesthetized with CO_2, the animals were decapitated and the heads mounted on a Petri dish coated with a wax/rosin mixture. Dissection of the brains was carried out under fixative (glutaraldehyde 2.5% in 0.1 M sodium phosphate buffer; Serva, Heidelberg, Germany). The brains were fixed overnight with the same fixative in 0.1 M sodium phosphate buffer. When not otherwise stated, the pH of all solutions was 7.4. The brains were post-fixed with 2% OsO_4 in the same phosphate buffer for 1 h, dehydrated in a series of ethanols and embedded in Epon (Serva). Whole brains or optic lobes were sectioned (Diatome, Switzerland) at a thickness of 2 µm in frontohorizontal, horizontal, or sagittal planes. The sections were mounted on microscope slides, stained with a mixture of 0.5% azur II, 0.5% methylene blue, 0.5% borax, and 40% saccharose at 60°C (modified after Richardson et al. 1960), and mounted with Epon under glass coverslips. The sections were analyzed and photographed using a Zeiss Axiophot microscope. Reconstructions of fiber tracts were performed using a camera lucida attachment.

Conventional electron-microscopy

The fixation procedure, embedding, and cutting of semithin sections followed the same procedures as described above. The best tissue preservation was obtained with a fixative consisting of 2% glutaraldehyde, 2% paraformaldehyde, 0.1% picric acid (first fixation), and 1% OsO_4 (postfixation) in 0.1 M sodium cacodylate buffer (modified after Langford and Coggeshall 1980) at pH 6.9. For electron-microscopy, individual semithin sections containing

the accessory medulla were photographed and attached with cyanacrylate glue to preformed resin blocks. Sections with a silver or a gray interference color were cut on an ultramicrotome (Reichert, Austria). The sections were collected on slot grids coated with Budvar (Bio Rad, Watford, USA) and stained with aqueous uranyl acetate (2%) and lead citrate (Reynolds 1963). The sections were studied with a Zeiss EM 10 CR electron-microscope at an acceleration tension of 60 kV.

Diameters of dense-core vesicles (dcvs) were measured with a scaled magnifying glass on micrographs at a final magnification of ×78 000. To avoid mistakes by measuring calottes (sections with less than the full diameter) of vesicles, only vesicles with clearly visible membranes were taken into account. For the frequency distribution histograms of dcv diameters, the dcvs of 44 fiber profiles were counted and used for the calculation. The percentage of measured vesicles (y-axis) per size group of vesicle diameters (x-axis, with 6-nm bins) were estimated. Four clearly distinguishable size groups were discerned; these were significantly different from each other (one way-ANOVA, Scheffe multiple range test, significance level $P<0.05$).

Immunocytochemistry for light microscopy

For light-microscopy, preembedding immunocytochemistry was performed on free-floating Vibratome sections by means of the indirect peroxidase-antiperoxidase (PAP) method (Sternberger 1979) as described previously (Petri et al. 1995). Incubation of the tissues with anti-PDH serum preabsorbed with 10 nmol synthetic β-PDH per 1 µl anti-PDH prevented immunolabeling. Dissected brains were fixed overnight with 2.5% glutaraldehyde in 0.1 M sodium phosphate buffer (pH 7.4). The anti-PDH serum was diluted 1:80 000 in 0.1 M TRIS HCl/0.3 M NaCl containing 2% normal goat serum and 0.5% Triton X-100, and was applied to 30-µm thick Vibratome sections of gelatine-albumin-embedded brains (4.8% gelatine and 12% ovalbumin in H_2O; fixation of the embedding medium overnight in 10% formaline in 0.1 M sodium phosphate buffer at 4°C) and for 18–20 h at room temperature. The sections were incubated at room temperature for 1 h in goat-anti-rabbit IgG at 1:100 and for 1 h in rabbit PAP (Dakopatts, Hamburg, Germany) at 1:300. The diaminobenzidine reaction was performed as described previously (Homberg and Hildebrand 1989). Sections containing the accessory medulla were postfixed in 2% OsO_4 in the same sodium phosphate buffer, dehydrated in ethanol, and infiltrated with Epon. The sections were embedded between acetate sheets, polymerized at 60°C for at least 24 h, and remounted on resin blocks. Serial sections of 4 µm thickness were cut in the original cutting direction. The semithin sections were mounted on glass slides and counterstained with Richardson's blue as described above.

Immunocytochemistry for electron-microscopy

For electron-microscopy, postembedding on-grid staining was performed on ultrathin sections (silver interference color) collected on Budvar-coated nickel slot grids. Brains were fixed overnight in 2% glutaraldehyde, 2% paraformaldehyde, and 0.1% picric acid in 0.1 M sodium cacodylate buffer. Preparations were used with or without postfixation in 1% OsO_4 in 0.1 M sodium cacodylate buffer for 10 min. The brains were embedded in LR White (London Resin, England) using air-tight cups and were polymerized under UV light at 366 nm for 3–4 days. Ultrathin sections were cut directly from the block. All incubation steps were carried out in a moist chamber with grids floating on drops of incubation solution. Postfixed sections were previously etched with 4% Na-*meta*-periodate in H_2O for 10 min, washed in H_2O, and subsequently in 0.01 M sodium phosphate buffer. The sections were preincubated with normal goat serum (dilution 1:30) in 0.01 M phosphate buffer for 15 min, rinsed and incubated in anti-PDH serum diluted 1:12 000 overnight at 4°C. After a further rinse, the sections were incubated with the secondary antibody (gold anti-rabbit G10; Auroprobe Amersham, Belgium; dilution 1:80) for 2 h at room temperature. Controls were performed on consecutive sections, incubated either with anti-PDH serum or with normal rabbit serum (diluted at 1:12 000) and further treated as above. The sections were briefly counterstained with uranyl acetate and lead citrate.

Results

Organization of the neuropil

On Richardson's blue-stained semithin sections, the accessory medulla stands out as a distinct neuropil at the frontal medioventral edge of the medulla (Fig. 1A). The accessory medulla has an elongated pear-shaped form and lies about 80 µm below the anterior surface of the optic lobe. Its longitudinal axis inclines medially at an angle of about 45° to the horizontal axis of the animal. Along its longitudinal axis, the accessory medulla measures 78–100 µm (mean 90 µm, n=5). The mean distal to medial extension is dorsally 34 µm, and ventrally 40 µm. The mean frontal to caudal extension (along the longitudinal axis of the animal) is dorsally 31 µm (n=3) and ventrally 51 µm (n=7).

The medulla and the accessory medulla are enclosed by a common glia sheath that forms the medial, ventral, and frontoventral borders of the accessory medulla (Fig. 1). Frontodorsally, a layer of fibers, viz., the anterior fiber network (20–30 µm thick), spreads between the accessory medulla and the glia sheath (Fig. 1C). Distally and ventrocaudally, the accessory medulla is surrounded by the tissue of the medulla. No separating glial layer between the accessory medulla and the neuropil of the medulla is visible. The root of the posterior optic tract forms the dorsal boundary of the accessory medulla (Fig. 1D).

In contrast to all other optic neuropils, the neuropil of the accessory medulla shows no stratification. The main mass of the accessory medulla consists of two subdivisions containing dense neuropil with a nodular appearance (Fig. 1A,B,D). A dozen smaller noduli with diameters of 10–15 µm can be distinguished in the ventral bulge of the accessory medulla. In addition, one larger "frontal nodulus" lies in the frontal region of the accessory medulla (Fig. 1B). Together, the ventral noduli and the frontal nodulus form one subdivision of the accessory medulla. The larger "dorsal nodulus" (Fig. 1B,D) appears darker than the rest of the accessory medulla and constitutes the second subdivision. The dorsal nodulus is split by a fissure into a larger distal and a smaller medial portion; these portions are connected by a stalk of dense neuropil (Fig. 1D). The space between the noduli is filled with internodular neuropil (Figs. 1D, 2). A thin layer of loose neuropil completely envelops the accessory medulla (Fig. 2). Coarse neuropil fills the center and, distally, the space between the dorsal nodulus and ventral noduli. Fibers from the coarse neuropil extend into the distal fiber tract (Fig. 1C). Thus, the accessory medulla resembles a cauliflower with the coarse neuropil forming its stalk.

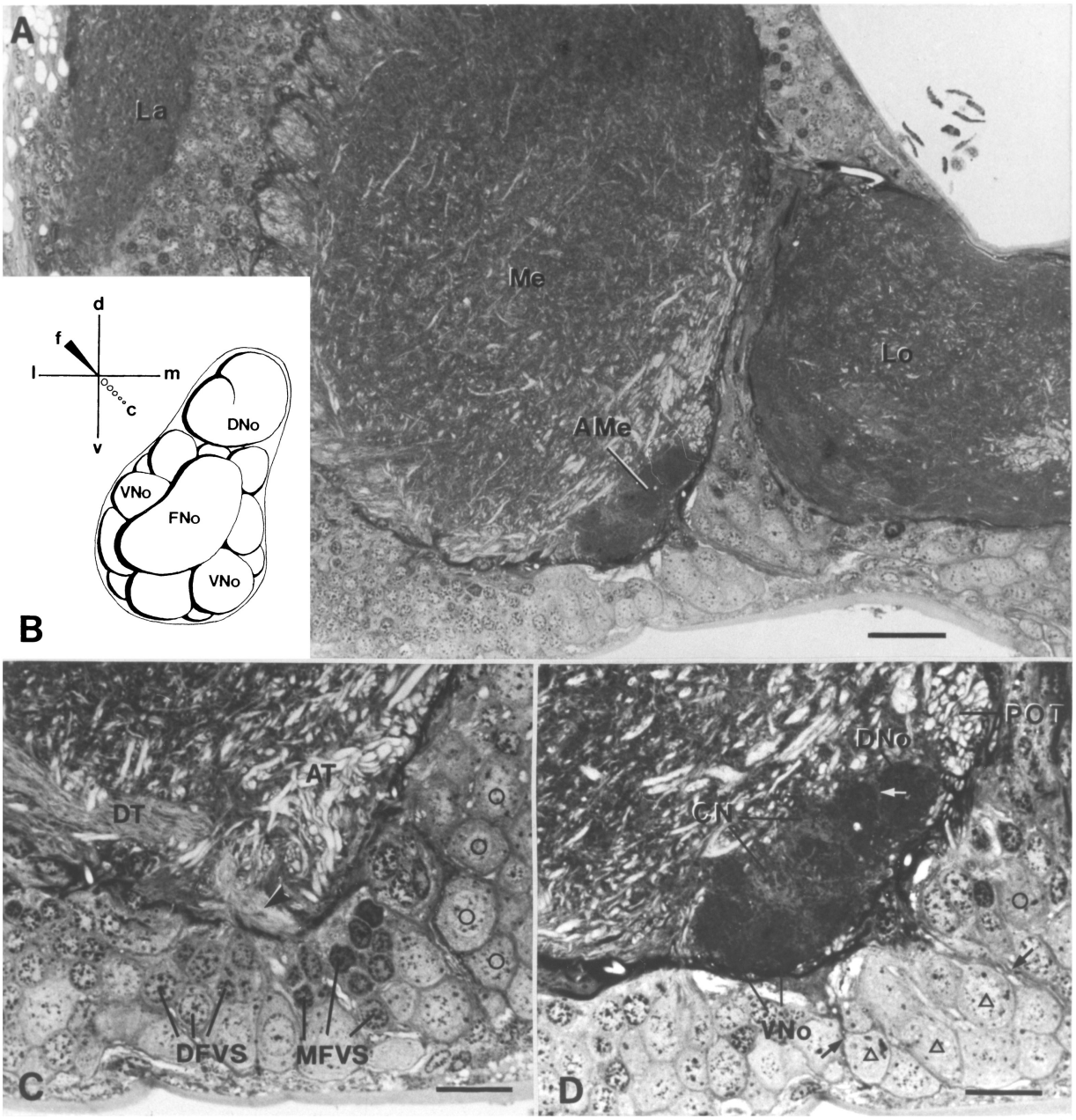

Fig. 1. **A** Frontohorizontal semithin section (2 µm) of the right optic lobe of *Leucophaea maderae* showing the accessory medulla (*AMe*) as a distinct pear-shaped neuropil at the ventromedial edge of the medulla (*Me*). *La*, Lamina; *Lo*, lobula. **B** Diagram of the internal nodular organization of the neuropil of the AMe with orientations indicated as used throughout the study. *c*, Caudal (posterior); *d*, dorsal; *f*, frontal (anterior); *l*, lateral (distal); *m*, medial; *v*, ventral; *DNo*, dorsal nodulus; *FNo*, frontal nodulus; *VNo*, ventral noduli. **C** A section taken 20 µm frontally from the accessory medulla shows the anterior tract (*AT*), which dorsally turns into the posterior optic tract. The anterior tract is the most prominent part of the anterior fiber network lying frontodorsal to the accessory medulla. The distal tract (*DT*) appears to originate near the lamina. *Open circles*, Median neurons. The medial (*arrowhead*) and distal frontoventral bundles originate from the medial and distal frontoventral somata (*MFVS*, *DFVS*) and turn toward the accessory medulla. **D** The ventral noduli (*VNo*) are visible some 32 µm posterior to the first section through the accessory medulla. The ventral noduli surround the coarse neuropil (*CN*) and are separated from each other by internodular neuropil. The *white arrow* marks a fissure that divides the dorsal nodulus (*DNo*) into two parts. Glia sheaths (*small arrows*) isolate the ventral neurons (*open triangles*) from neighboring neurons, such as the median neurons (*open circles*). *POT*, Posterior optic tract. *Scale bars*: **A** 50 µm, **C, D** 25 µm

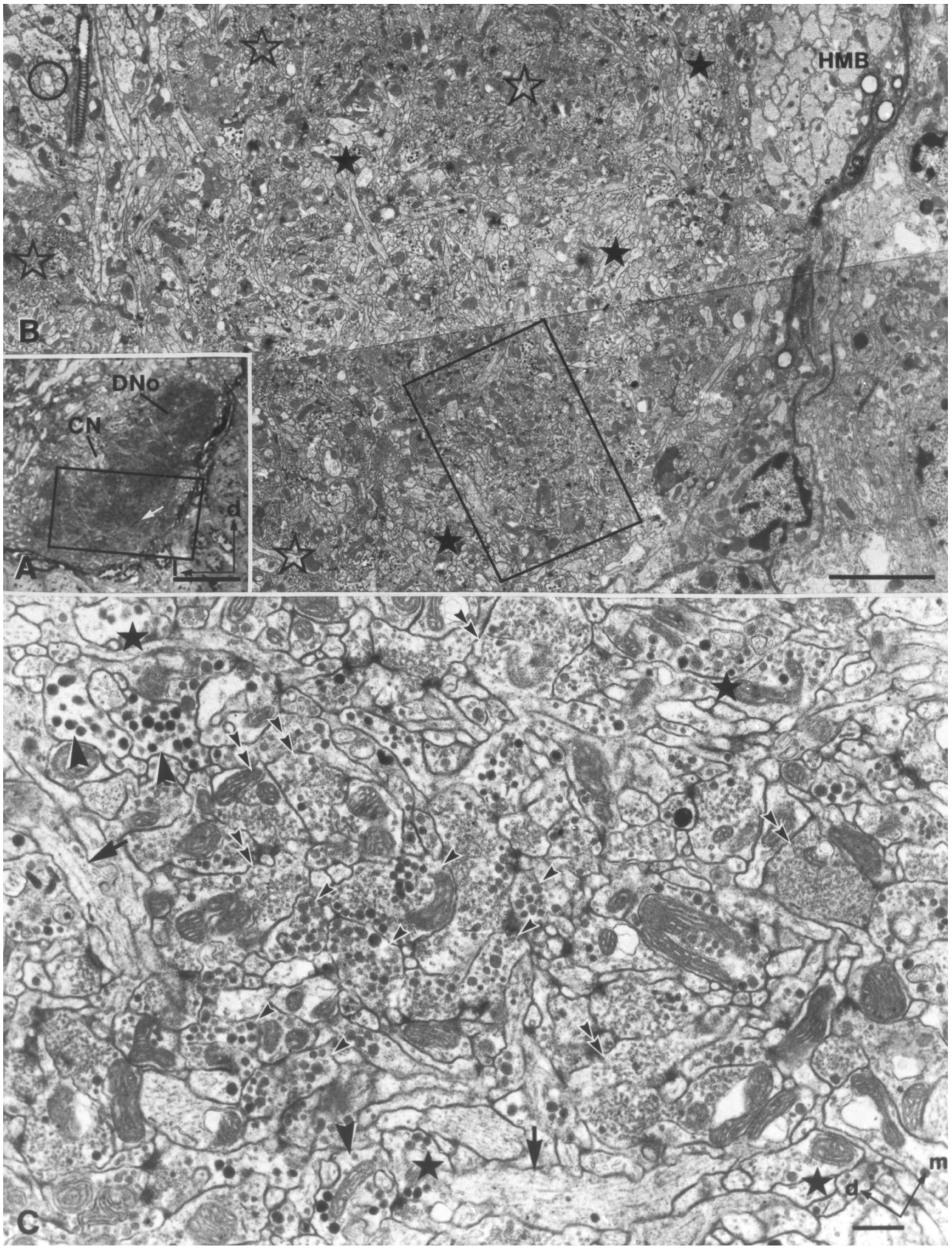

Fig. 2A–C (for legend see next page)

Fiber tracts and somata associated with the accessory medulla

The accessory medulla is surrounded by several fiber bundles most of which consist of primary neurites of neurons in the cell cortex, frontally, ventrally, and medially to the accessory medulla (Figs. 1, 3B). The anterior fiber network covers the accessory medulla fronto-dorsally. It is formed in part by a large fiber tract, the anterior tract, which runs dorsally to the accessory medulla, and which merges with the posterior optic tract (Fig. 1C). The anterior tract appears to be largely composed of primary neurites from somata in the anterior cell cortex (not shown). These cell bodies have diameters of 13.5–20 µm (mean 16.6 µm, n=16).

Two fiber bundles, the medial and distal frontoventral bundles, arise from two conspicuous groups of somata, the medial and distal groups of frontoventral somata (Figs. 1C, 3B). The medial group of the frontoventral somata consists of small cells (8.5–12.5 µm, mean 10.0 µm, n=19) with dark cytoplasm. The nuclei are densely filled with large stacks of heterochromatin. The cells of the distal group are slightly larger (10–13.5 µm, mean 12.5 µm, n=13), their cytoplasm also being darkly stained. The two frontoventral bundles turn dorsally into the anterior fiber network and head in a distal and dorsal direction. They could only be reconstructed over a short distance.

The only tract with a clear connection to the neuropil of the accessory medulla is the distal tract, which arises from the coarse neuropil in the center of the accessory medulla and leads distally toward the medulla and lamina (Fig. 1C). Cell bodies associated with fibers of the distal tract could not be identified.

Further posteriorly, two bundles of primary neurites, the medial and distal ventral bundles, enter the anterior fiber network of the accessory medulla. They originate from somata of the ventral neurons frontoventrally and ventrally to the accessory medulla (Figs. 1D, 3B). These neurons have a similar size to the anterior neurons (13–25 µm, mean 16.0 µm, n=14). Dorsally, the tracts merge with the large anterior tract. The horizontal median bundle, which is partly composed of primary neurites from anterior neurons, leads in anterior-posterior direction, medially between the glia sheath and neuropil of the accessory medulla to an unknown target (Fig. 2A,B).

The neurites that compose the ventromedian bundle arise from neurons located ventromedially to the accessory medulla (Fig. 3B). Some of the neurites of the ventromedian neurons (soma diameter: 10–20 µm, mean 14.2 µm, n=15) seem to join the horizontal median bundle; others turn dorsally and project behind the dorsal nodulus. A population of neurons, the median neurons (16.5–28 µm, mean 22.1 µm, n=14), apparently do not send neurites to the accessory medulla (Figs. 1D, 3B) and are separated, at least from ventral neurons, by a glial layer.

Fine structure of the neuropil

In electron micrographs, the reason for the conspicuous density of the noduli becomes apparent (Fig. 2). The relatively large fiber profiles within the noduli (diameters between 1 and 1.5 µm) are densely filled with clear vesicles, dcvs, and mitochondria. The internodular neuropil and the loose neuropil that surrounds the accessory medulla consist of profiles that are either filled with dcvs or that contain only a few dcvs and many microtubules (Fig. 2C). The coarse neuropil (Fig. 2A, B) consists of larger profiles (about 1 µm) that are enveloped by glia. They contain microtubules and only a few dcvs. Synapses are frequent in the noduli, in the internodular neuropil, and in the loose neuropil surrounding the accessory medulla, but not in the coarse neuropil.

More than half of all fiber profiles in the accessory medulla are densely filled with dcvs. At least four types of which can be distinguished (Figs. 4, 5), with those of the noduli being less electron-dense (Fig. 4A) than the dark dcvs (Fig. 4B–D). The former have a structured granular content and are therefore termed as being granular (Fig. 4A). These vesicles appear to be highly fixation-sensitive because their membranes are often ruptured. Vesicle diameters measure between 56 and 125 nm (mean±SD: 81±11 nm; n=151). The histogram of vesicular-size distribution shows at least two peaks (Fig. 5A). Moreover, profiles on micrographs can be distinguished as having granular dcvs of different sizes. The granular dcvs mostly occur in large numbers together with clear vesicles in large profiles (0.5–1.8 µm). These profiles are almost exclusively found in the noduli, where they appear to group together. All other dcvs, which mainly occur in the internodular and loose neuropil around the accessory medulla, are darker and homogeneously electron-dense (Fig. 4B–D). At least three main types of dark dcvs can be distinguished according to apparent size differences (Figs. 4, 5): small, between 50 and 113 nm (mean±SD: 73±12 nm; n=162), medium-sized, between 69 and 125 nm (mean 93±12 nm; n=156), and large, between 69 and 150 nm (mean±SD: 107±15 nm; n=206).

Fig. 2. Frontohorizontal semithin section of the accessory medulla (**A**) and electron micrographs of ultrathin sections (**B, C**), cut from the same section. **A** The *frame* outlines the part shown as an electron micrograph in **B**. The *white arrow* marks the ventral nodulus, which is magnified in **C**. *CN*, Coarse neuropil; *DNo*, dorsal nodulus. **B** Overview of the ventral part of the accessory medulla. The *open stars* indicate the dense noduli of the framed area in **A**. The *filled stars* indicate areas of loose neuropil. The *circle* marks coarse neuropil, which consists of large diameter fibers that often contain a few dense-core vesicles (dcvs). *HMB*, Horizontal median bundle. **C** Magnification of the neuropil outlined in **B**. Loose internodular neuropil, which is marked by *filled stars*, contains profiles with dark dcvs (*large arrowheads*) and axonal fibers with or without a few dcvs or clear vesicles, and many parallel microtubules (*arrows*). The loose neuropil surrounds a neuropil area that appears as a dense nodulus on semithin sections (*white arrow* in **A**). This area mainly consists of clustered profiles that are densely filled with clear vesicles (*double arrowheads*), or with granular dcvs (*small arrowheads*; compare Fig. 3) that are more electron lucent than the darker dcvs of the loose neuropil. *d*, Dorsal; *l*, lateral; *m*, medial. *Scale bars*: **A** 25 µm, **B** 5 µm, **C**0.5 µm

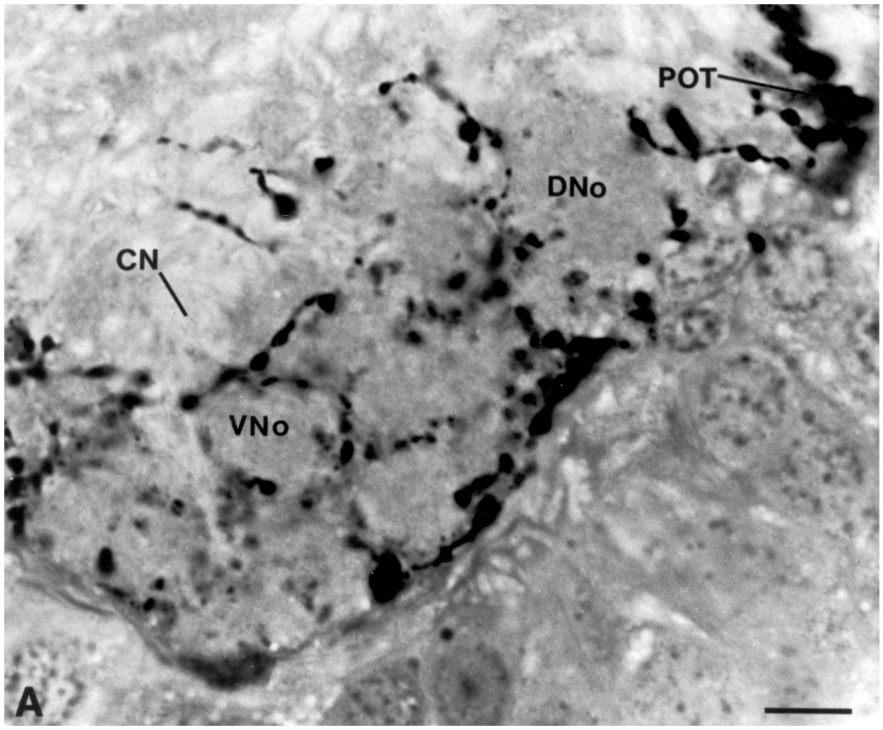

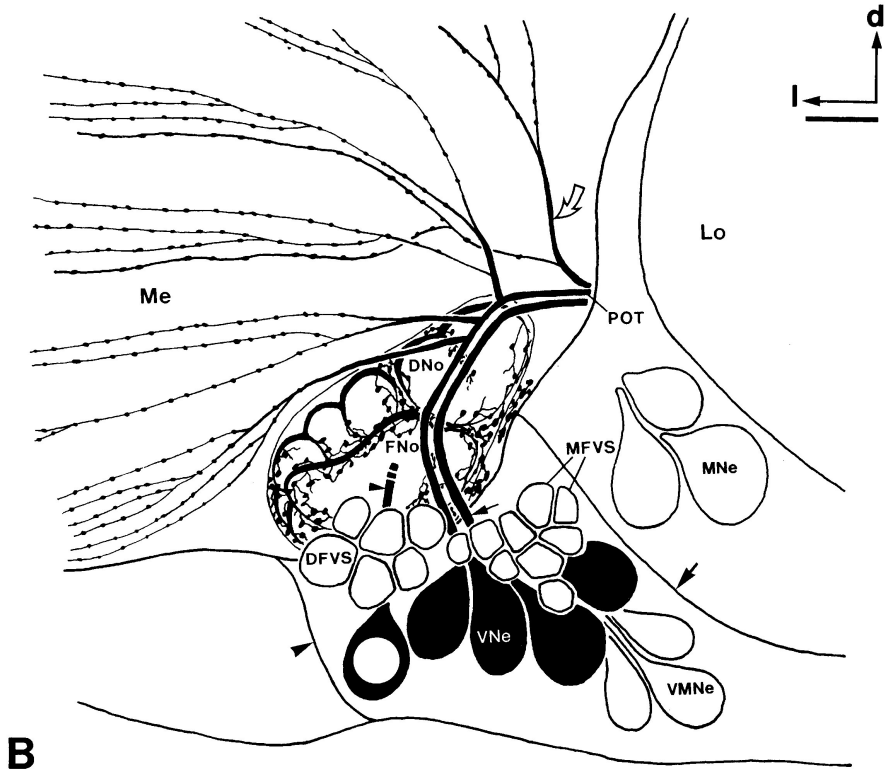

Fig. 3. PDH immunoreactivity on a frontohorizontal semithin section (4 µm), counterstained with Richardson's blue (**A**), and a partial schematic drawing of PDH-ir fibers in the area of the accessory medulla. **A** PDH-ir fibers are mainly restricted to the internodular and loose neuropil. *CN*, Coarse neuropil; *DNo*, dorsal nodulus; *POT*, posterior optic tract; *VNo*, ventral nodulus. **B** The PDH-ir arborizations in the internodular and loose neuropil of the accessory medulla are shown, but the branches of PDH-ir fibers covering the surface of the accessory medulla are omitted. The PDH-ir medulla cells (partially represented by *filled somata*) are a subgroup of the ventral neurons (*VNe*). The neurites of the weakly stained somata (partially represented by a *filled soma with a white dot*) contribute to the distal ventral bundle (*small arrowhead*), and the strongly and moderately stained somata (*filled somata*) pass through the medial ventral bundles (*small arrow*), which combine dorsally with the anterior tract. The median ventral bundles turn to the posterior optic tract (*POT*) after sending a fan of collaterals distally to the first layer of the medulla (*Me*). More intensely stained PDH-ir fibers (*open arrow*) arise from the posterior optic tract (apparently originating from contralateral PDH-ir neurons) and contribute to the fiber fan. The distal and medial frontoventral somata (*DFVS*, *MFVS*), the ventromedian (*VMNe*), and median neurons (*MNe*) are not PDH-ir. *Large arrow*, Glia sheath separating the median neurons from other soma groups; *large arrowhead*, glia sheath, separating neurons of the accessory medulla from other, more distal neurons (not shown) of the optic lobe; *DNo*, dorsal nodulus; *FNo*, frontal nodulus; *Lo*, lobula; *d*, dorsal; *l*, lateral. *Scale bars*: **A** 10 µm, **B** 20 µm

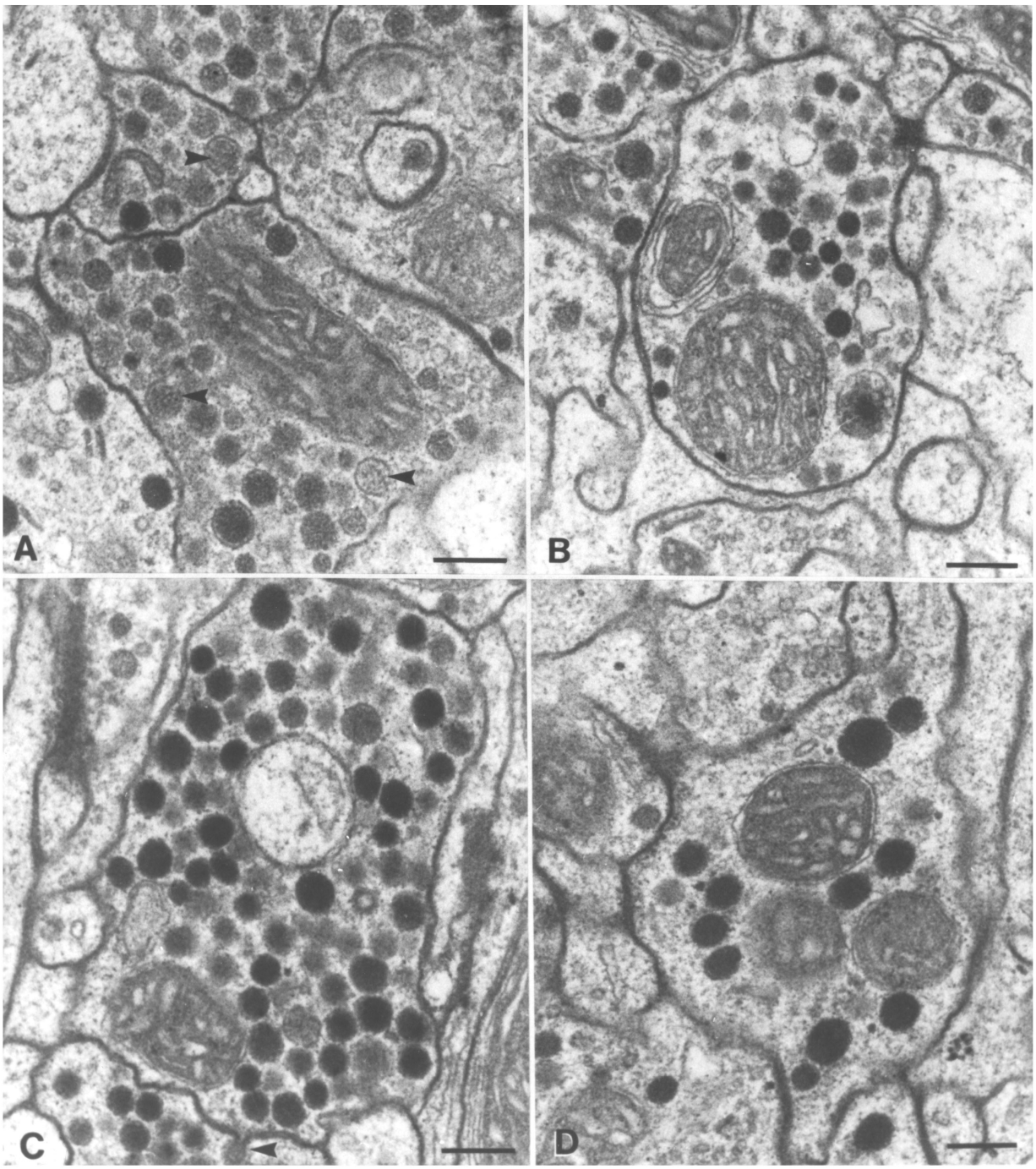

Fig. 4A–D. The four different types of dcvs of the accessory medulla. All micrographs were taken from the same section. **A** Four clustered profiles of a ventral nodulus contain granular dcvs. The membranes of granular dcvs are often ruptured (*arrowheads*). **B–D** Profiles from the loose neuropil with the dark type. **B** Profile containing the densely packed small type. **C** Profile containing the densely packed medium-sized type. The *arrowhead* marks a coated pit. **D** Large dcvs are typically loosely packed. *Scale bars*: 0.2 µm

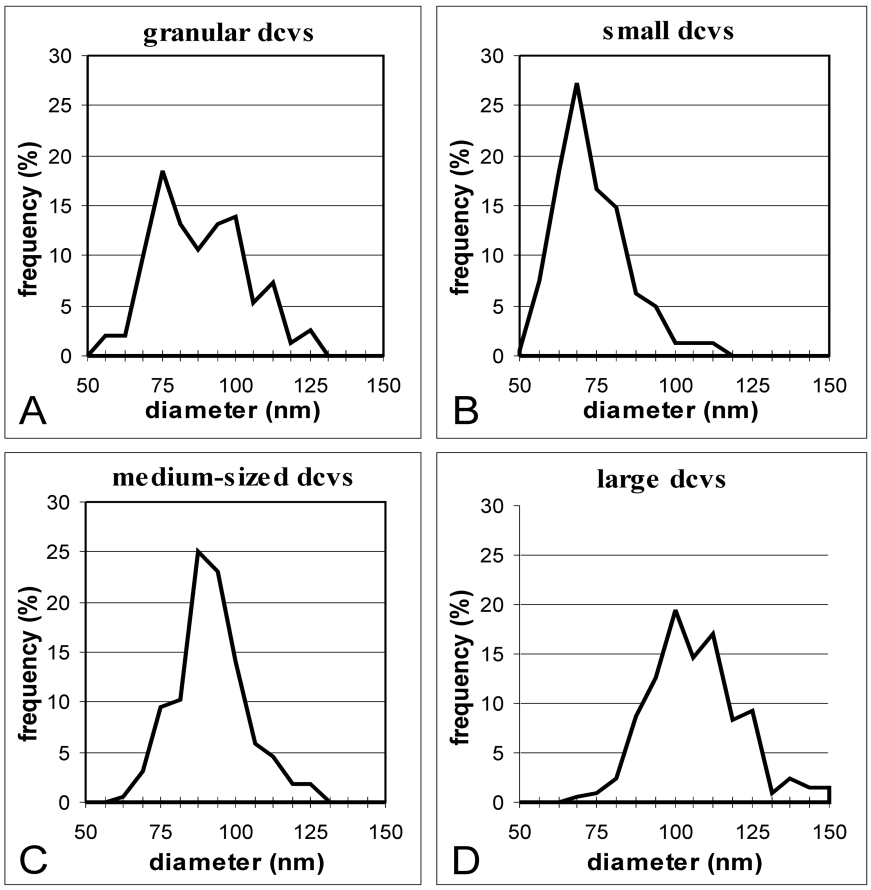

Fig. 5A–D. Histograms of size distributions of the dense-core vesicles (*dcvs*). The *abscissa* indicates the diameters, the *ordinate* shows the relative frequency of the respective *dcvs* in percentage. **A** Granular *dcvs* show a heterogeneous size-distribution with at least two maxima at 75 and 100 nm, and another possible maximum at 113 nm. **B**, **C** Small and medium-sized *dcvs* show single maxima at 69 nm and at 87 nm. **D** The histogram of large *dcvs* appears more irregular with possibly three peaks at 100, 113, and 125 nm

Profiles containing small and medium-sized dcvs have a distinctly large diameter (1–2 µm) and contain large numbers (up to 70) of densely packed vesicles (Fig. 4B,C). Profiles with both vesicle types occur in the surrounding loose neuropil between the glia sheath and dense neuropil, medially and ventrally to the accessory medulla, and in the anterior fiber network, but rarely in the internodular neuropil.

The fiber profiles with large dcvs always carry fewer vesicles (≤10–15; Fig. 4D). These profiles are often smaller. They are the most abundant profiles with dark dcvs within the accessory medulla. They occur in the loose neuropil around the accessory medulla and in the internodular neuropil.

Distribution of PDH-immunoreactive fibers in the accessory medulla

A reconstruction of PDH immunostaining in the brain of *L. maderae* has been published previously by Stengl and Homberg (1994). A more detailed reconstruction within the surrounding of the accessory medulla shows that fibers arising from the PDH-ir medulla cells (PDHMe) send processes to the central brain and, at the same time, contribute to the fan-like structure of PDH-ir fibers in the distalmost layer of the medulla (Fig. 3B). Some thick, darkly stained fibers of this fan appear to originate from the posterior optic tract and do not have connections to the PDHMe.

Even in thick Vibratome sections, the uneven distribution of PDH-ir fibers within the accessory medulla becomes apparent (Petri et al. 1995). Reembedded and counterstained semithin sections show that PDH-ir processes lie nearly exclusively in the loose and internodular neuropil and do not enter the noduli (Fig. 3A). Many varicose fibers exhibit strong PDH-ir in the loose neuropil between the accessory medulla and the medial glia sheath. The highest density of PDH-ir fibers does not occur in the accessory medulla, but in the anterior fiber network covering the accessory medulla frontally.

As previously reported by Petri et al. (1995), the PDH-ir somata that lie frontoventral and ventral to the accessory medulla can be divided into three subpopulations according to size and intensity of staining. Their primary neurites contribute to the medial and distal ventral bundles (Fig. 3B). The neurites of the strongly and moderately stained somata pass through the medial bundle, the neurites of the weakly stained somata, via the distal ventral bundle (Fig. 3B). The distal tract, the ven-

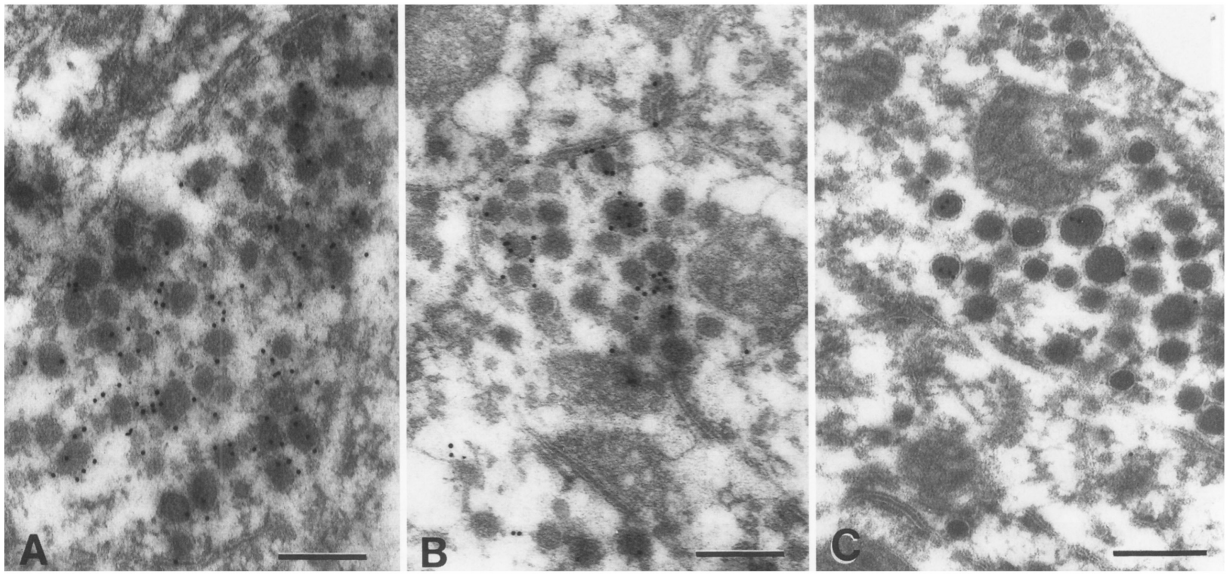

Fig. 6A–C. Electron micrographs of PDH-ir profiles showing the intracellular localization of PDH immunoreactivity; no postfixation. **A** This immunoreactive profile contains medium-sized dcvs. **B** Another example of an immunostained profile. The staining is more clearly confined to the medium-sized dcvs. **C** Large dcvs also show PDH immunoreactivity. The staining intensity is lower than for medium-sized dcvs. *Scale bars:* 0.2 µm

tromedian bundle, and the horizontal median bundle do not show PDH immunoreactivity. Furthermore, the PDH-ir fibers do not enter the internodular neuropil in a distinct bundle. The PDH-ir processes in the accessory medulla originate from collaterals of fibers in the loose neuropil surrounding the accessory medulla.

Localization of PDH immunoreactivity in nerve terminals

In immunogold preparations that were not postfixed with OsO_4, a nearly background-free staining of PDH-ir profiles was obtained (Fig. 6). The PDH immunoreactivity was associated exclusively with profiles carrying dcvs. The staining was largely confined to the vesicles (Figs. 6, 7).

Without postfixation, the granular dcvs were completely destroyed and the other dcvs shriveled. For a better identification of the PDH-ir dcvs, preparations that had undergone a brief OsO_4 postfixation were used (see Materials and methods). In these preparations, tissue preservation was improved and the staining intensity decreased without changing the staining pattern. Fiber profiles with granular and small dcvs were never immunopositive (Fig. 7A–D), whereas a subpopulation of profiles containing medium-sized dcvs exhibited PDH immunoreactivity (Figs. 6A,B, 7). These immunoreactive profiles were found mainly in the loose neuropil around the accessory medulla, and to a lesser extent in the internodular neuropil. Moreover, a subpopulation of profiles with large dcvs were PDH-ir (Fig. 6C). The staining of large dcvs appeared less intense than that of the medium-sized type and could be clearly identified only in preparations without postfixation. The immunoreactive profiles with large dcvs were found in the loose neuropil surrounding the accessory medulla and in the internodular neuropil.

Discussion

In comparison with other neuropils of the insect optic lobes, little is known about the neuronal organization of the accessory medulla, which was first described in hemimetabolous insects by Homberg et al. (1991) and which was suggested to be the circadian pacemaking center in insects. This investigation is the first general analysis of the neuronal architecture of the accessory medulla of the cockroach *Leucophaea maderae* at the light- and electron-microscopic levels.

One aim of this paper has been to characterize the internal neuropil of the accessory medulla, the soma groups, and the fiber tracts in the vicinity, in order to provide a framework for previous and future single cell studies. Moreover, the description of the accessory medulla and its surrounding somata enables neurons of this brain region to be identified in primary cell cultures (Petri and Stengl 1996). The second aim of this paper has been to examine the way in which presumptive pacemaker candidates, viz., the PDH-ir neurons, innervate the accessory medulla, in order to gain insights into their contribution to the network of the accessory medulla. Furthermore, we have examined the various types of

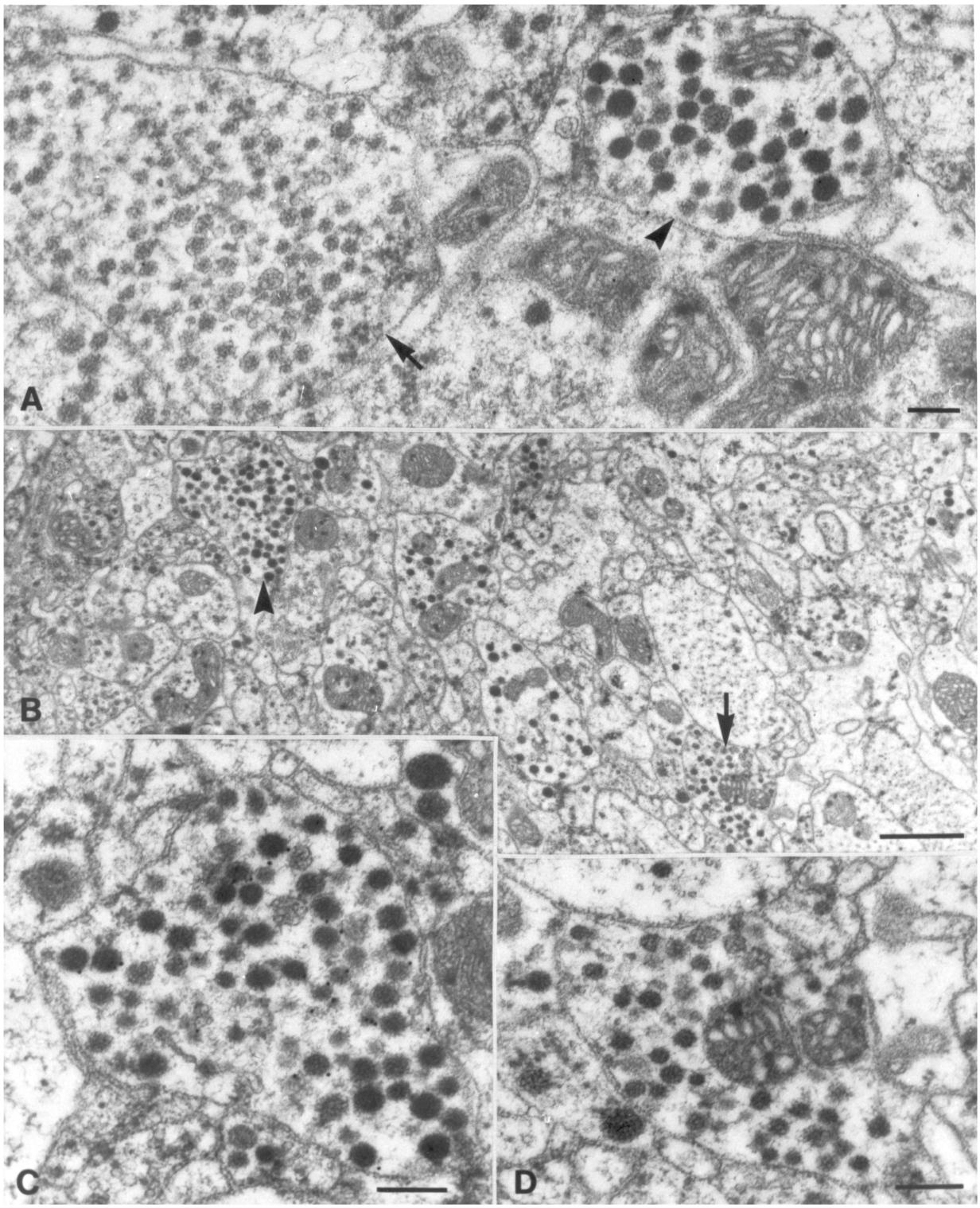

Fig. 7A–D. Electron micrographs of PDH-ir profiles in postfixed preparations. The staining intensity has decreased, whereas tissue preservation has improved. **A** Comparison between an unstained profile with granular dcvs (*arrow*) and a labeled profile with medium-sized dcvs (*arrowhead*). **B** Comparison between an immunostained profile with medium-sized dcvs (*arrowhead*, magnified in **C**) and an unstained profile with small dcvs (*arrow*, magnified in **D**). *Scale bars*: **A** 0.2 µm, **B** 1 µm, **C, D** 0.2 µm

dcvs of PDH-ir profiles and of other profiles in the accessory medulla in order to obtain morphological markers at the electron-microscopical level for the identification of local and output neurons of the accessory medulla.

The neuropil of the accessory medulla

The most conspicuous features of both the dorsal and ventral subdivisions of the accessory medulla are its nodular appearance and its apparent lack of retinotopic organization. The noduli of the accessory medulla are not "glomeruli" as are the glomeruli of the mushroom bodies (Schürmann 1987), or the glomeruli of the antennal lobes, which are formed by dense arborizations of fine fibers (Schürmann and Wechsler 1969; Tolbert and Hildebrand 1981; Boeckh and Ernst 1987; Homberg et al. 1989). They are rather densities of the neuropil, resulting from the accumulation of intracellular structures such as the many dcvs. The lamina, the medulla, and at least the distal lobula show a retinotopic organization that enables processing of retinal images (Strausfeld 1976; Strausfeld and Nässel 1981). The apparent lack of a retinotopic organization in the accessory medulla makes it unlikely that this neuropil is involved in visual-image processing. This is supported by intracellular recordings from neurons of the accessory medulla in *L. maderae* (Lösel and Homberg 1995) and *Schistocerca gregaria* (Würden and Homberg 1995). These neurons never show responses to moving objects or small field stimuli.

In holometabolous insects, the accessory medulla is part of the larval visual system and receives inputs from the larval stemmata, but also persists to the adult stage (Pflugfelder 1936; Hanström 1940; Ehnbohm 1948; Hagberg 1986; Ichikawa 1994). In hemimetabolous insects, a specific larval visual system does not exist. Because of the similar localizations of the neuropils in holometabolous and hemimetabolous insects, they may be homologous structures, but this remains to be established from comparative analysis.

Not only the neuropil structure of the accessory medulla, but also the morphology of the nerve terminals differs largely from other optic neuropils, because the former contain exceedingly large numbers of at least four different types of dcvs. In the other optic neuropils (own observations), only a few profiles contain scattered dcvs (Strausfeld and Campos-Ortega 1973; Burkhardt and Braitenberg 1976; Bishop and Bishop 1981). Similarly large numbers of dcvs are seen in the central complex (Kerwien and Schürmann 1990), the pars intercerebralis (Nishiitsutsuji-Uwo 1961) and the corpora cardiaca and corpora allata, the neurohemal organs of insects (Nishiitsutsuji-Uwo 1961; Scharrer 1963; Lafon-Cazal and Arluison 1976).

Evidence is accumulating that dcvs contain neuropeptides that are released non-synaptically by exocytosis (Hökfelt et al. 1980; Zimmermann 1993). In insects, peptide immunoreactivities that have been localized to dcvs and the colocalization of peptide immunoreactivities within single dcvs have been reported (Ude and Eckert 1988; Ude and Agricola 1995). The accessory medulla of *L. maderae* is immunoreactive to antisera against several peptides that are partly colocalized (Petri et al. 1995). Therefore, the accumulation of dcvs and the immunocytochemical results indicate that many neuropeptides are present in the accessory medulla of *L. maderae*. Subpopulations of the medium-sized and the large dcvs are PDH-ir. Thus, even more subgroups among the four different types of dcvs may be distinguished in future immunocytochemical studies. Since the granular dcvs occur only in neurons that innervate the nodular neuropil, these neurons may be local to the accessory medulla. They might contain allatotropin and leucokinin immunoreactivity, because these immunoreactivities are restricted to the noduli (Petri et al. 1995). Because of the multitude of neuropeptide immunoreactivities and the high density of profiles containing dcvs, we assume that neuromodulation plays an important role in the function of the accessory medulla. However, we have never observed exocytosis of dcvs, possibly because of the methods employed (Kerwien and Schürmann 1990; Schürmann et al. 1991).

Fiber tracts and somata of the accessory medulla

The general map of soma groups and fiber bundles in the vicinity of the accessory medulla provided here should aid future anatomical studies and should allow recent immunocytochemical results to be integrated into a general anatomical scheme (Nässel et al. 1991; Stengl and Homberg 1994; Petri et al. 1995). The distal fiber tract appears to connect the lamina with the accessory medulla and might, therefore, provide photic input to the accessory medulla. Unfortunately, we have not been able to determine the origin of these fibers. Petri et al. (1995) have shown that PDH-ir, FMRFamide-ir, gastrin-ir, and serotonin-ir fibers connect the accessory medulla to the medulla and lamina. These fibers apparently do not project via the distal tract, but via a fan-shaped fiber array from the proximal basis of the medulla to the lamina. As judged from varicose fiber specializations (Peters et al. 1986; Leitch et al. 1992), these fibers are outputs from the accessory medulla to the medulla and lamina (Petri et al. 1995).

The large anterior fiber tract continues into the posterior optic tract and therefore, forms a possible connection between the accessory medulla and central brain areas. Some of the anterior neurons that contribute to the anterior fiber tract might be identical to the FMRFamide-ir and PDH-ir cells of the accessory medulla, cells that send fibers to the posterior optic tract (Petri et al. 1995). The anterior fiber tract also seems to be the origin of fibers that contribute to the fiber fan of the distal medulla (see also below). Most neurons that connect the accessory medulla to other brain areas apparently join the anterior fiber tract.

The large, darkly stained median neurons that have never been observed to send processes directly to the accessory medulla might send processes to the central

brain. A corresponding location in *Periplaneta americana* has been demonstrated for a group of large GABA-ir neurons, that project processes caudally between the medulla and lobula to the posterior optic tract (Füller et al. 1989). The medial and distal ventral fiber bundles, which dorsally join the anterior fiber tract, appear to be identical in size and location to the neurites of PDH-ir, and also some FMRFamide-ir and leucokinin-ir neurons (Petri et al. 1995).

PDH-ir fibers of the accessory medulla

Detailed reconstructions of the PDH-ir fibers within the accessory medulla from semithin sections have failed to solve the question of their origin. The PDHMe neurons send processes over the medulla to the ipsilateral lamina and also to central brain areas via the posterior optic tract, but it remains unclear which somata actually contribute to PDH-ir processes in the accessory medulla. All ipsilateral and contralateral PDH-ir cell groups are possible candidates. Our reconstruction of PDH-ir fibers in the optic lobe suggests that the darkly stained fibers with few ramifications that arise from the posterior optic tract originate from contralateral PDH-ir neurons. Intracellular recordings combined with PDH immunocytochemistry should test this hypothesis.

In *L. maderae* single cells whose somata lie near the accessory medulla and that resemble PDHMe send apparently dendritic sidebranches into the ipsilateral accessory medulla (Lösel and Homberg 1995). Moreover, PDH-ir fibers do not enter the accessory medulla via a distinct tract, but rather send sidebranches from fibers surrounding the accessory medulla. The interesting branching pattern of the varicose PDH-ir fibers that arborize over wide areas in the loose and internodular neuropil suggests that peptides are released from the varicosities and that they act as paracrine neuromodulators on most or all synapses of the accessory medulia.

Intracellular localization of PDH immunoreactivity

In the accessory medulla, PDH immunoreactivity is localized in dcvs, as has been demonstrated for PDH-ir terminals in the crustacean sinus gland (Dircksen et al. 1987). Subgroups of profiles with medium-sized and large dcvs exhibit PDH immunoreactivity, but none of the profiles with small or granular vesicles are PDH-ir. The two types of PDH-ir dcvs may reflect colocalization with different peptides, such as leucokinin or FMRFamide, as has been demonstrated at the light-microscopic level by Petri et al. (1995). We assume that the large PDH-ir profiles are identical to the PDH-ir varicosities visible by light microscopy. Their marked accumulations of dcvs further indicate that they are peptide-release sites. Further experiments will focus on improving tissue preservation, while maintaining staining intensity, to elucidate the synaptic connections between PDH-ir neurons and other neurons in double-label experiments.

A comparison of the insect accessory medulla with the vertebrate suprachiasmatic nucleus

Previous evidence has suggested that the accessory medulla, which is innervated by presumptive pacemaker neurons (the PDH-ir cells), is the locus of the circadian clock in insects (Homberg et al. 1991; Helfrich-Förster and Homberg 1993; Stengl and Homberg 1994; Helfrich-Förster 1995; Petri et al. 1995; Stengl 1995; Würden and Homberg 1995). As in the main circadian pacemaker of mammals, viz., the suprachiasmatic nucleus (SCN), the accessory medulla is also subdivided into two main portions with no apparent retinotopical organization (Moore 1983; Reghunandanan et al. 1993). The SCN, which is closely associated with the visual system, shows three functional components: photic afferents for entrainment of the pacemaker, which are formed by the retino- and geniculo-hypothalamic tracts, intrinsic elements, and efferent projections serving as output-elements of the clock (Card and Moore 1984; Meijer 1990; Albers 1991b; Morin 1994). Moreover, in the accessory medulla of insects, the close association with the visual system is readily seen and, as previously described, various connections to visual neuropils and central brain areas are known (Schulz et al. 1984; Hagberg 1986; Hofbauer and Buchner 1989; Homberg et al. 1991; Nässel et al. 1991; Fleissner et al. 1993; Stengl and Homberg 1994; Helfrich-Förster 1995; Lösel and Homberg 1995). Furthermore, both the SCN and the accessory medulla appear to share an exceptionally high density of neuropeptides (Albers et al. 1991a,b; Reghunandanan et al. 1993; Petri et al. 1995; Würden and Homberg 1995). The colocalizing peptides of the SCN have been shown to phase-shift circadian activity rhythms (Albers et al. 1991a,b; Reghunandanan et al. 1993; Piggins et al. 1995). In addition, injections of the accessory medulla peptide PDH phase-shift the locomotor rhythms of the cockroach *L. maderae* (Petri and Stengl 1996). Current lesion experiments combined with immunocytochemistry and behavioral studies will now test whether the accessory medulla is indeed the circadian clock and necessary for circadian locomotor behavior in *L. maderae*.

Acknowledgements. We are grateful to Dr. Heiner Dircksen for the generous gift of the anti-PDH serum. We also thank H. Hallmer and S. Buchhauser for excellent photographic work, G. Thies for help with the electron-microscopical methods, and Dr. U. Homberg for considerable improvement of the manuscript.

References

Albers HE, Liou S-Y, Stopa EG, Zoeller RT (1991a) Interaction of colocalized neuropeptides: functional significance in the circadian timing system. J Neurosci 11: 846–851

Albers HE, Liou S-Y, Stopa EG, Zoeller RT (1991b) Neurochemistry of circadian timing. In: Klein DC, Moore RY, Reppert SM (eds) Suprachiasmatic nucleus. The mind's clock. Oxford University Press, Oxford New York, pp 263–288

Arechiga H, Mena F (1975) Circadian variations of hormonal content in the nervous system of the crayfish. Comp Biochem Physiol 52A: 581–584

Bishop CA, Bishop LG (1981) Vertical motion detectors and their synaptic relations in the third optic lobe of the fly. J Neurobiol 12: 281–296

Boeckh J, Ernst KD (1987) Contribution of single unit analysis in insects to an understanding of olfactory function. J Comp Physiol A 161: 549–565

Burckhardt W, Braitenberg V (1976) Some peculiar synaptic complexes in the first visual ganglion of the fly, *Musca domestica*. Cell Tissue Res 173: 287–308

Card JP, Moore RY (1984) The suprachiasmatic nucleus of the golden hamster: immunohistochemical analysis of cell and fiber distribution. Neuroscience 13: 415–431

Chiba Y, Tomioka K (1987) Insect circadian activity with special reference to the localization of the pacemaker. Zool Sci 4: 945–954

Colwell CS, Page TL (1990) A circadian rhythm in neural activity can be recorded from the central nervous system of the cockroach. J Comp Physiol A 166: 643–649

Dircksen H, Zahnow CA, Gaus G, Keller R, Rao KR, Riem JP (1987) The ultrastructure of nerve endings containing pigment-dispersing hormone (PDH) in crustacean sinus glands: identification by an antiserum against a synthetic PDH. Cell Tissue Res 250:377–387

Ehnbohm K (1948) Studies on the central and sympathetic nervous system and some sense organs in the head of neuropteroid insects. Opusc Entomol [Suppl] 8: 1–162

Fingerman SW, Fingerman M (1977) Circadian variations in the levels of red pigment-dispersing hormone and 5-hydroxytryptamine in the eyestalks of the fiddler crab, *Uca pugilator*. Comp Biochem Physiol 56C: 5–8

Fleissner G, Fleissner G, Frisch B (1993) A new type of putative non-visual photoreceptors in the optic lobe of beetles. Cell Tissue Res 273: 435–445

Füller H, Eckert M, Blechschmidt K (1989) Distribution of GABA-like immunoreactive neurons in the optic lobes of *Periplaneta americana*. Cell Tissue Res 255: 225–233

Hagberg M (1986) Ultrastructure and central projections of extraocular photoreceptors in caddiesflies (Insecta: Trichoptera). Cell Tissue Res 245: 643–648

Hall JC (1995) Tripping along the trail to the molecular mechanisms of biological clocks. Trends Neurosci 18: 230–240

Hall JC, Kyriacou CP (1990) Genetics of biological rhythms in *Drosophila*. Adv Insect Physiol 22: 221–298

Hanström B (1940) Inkretorische Organe, Sinnesorgane und Nervensystem des Kopfes einiger niederer Insektenordnungen. Kungl Sven Vetensk Akad Handl Ser III 18: 1–265

Helfrich-Förster C (1995) The period clock gene is expressed in central nervous system neurons which also produce a neuropeptide that reveals the projections of circadian pacemaker cells within the brain of *Drosophila melanogaster*. Proc Natl Acad Sci USA 92: 612–616

Helfrich-Förster C, Homberg U (1993) Pigment-dispersing hormone-immunoreactive neurons in the nervous system of wild-type *Drosophila melanogaster* and of several mutants with altered circadian rhythmicity. J Comp Neurol 337: 177–190

Hofbauer A, Buchner E (1989) Does *Drosophila* have seven eyes? Naturwissenschaften 76: 335–336

Hökfelt T, Johannson O, Ljungdahl Å, Lundberg JM, Schultzberg M (1980) Peptidergic neurons. Nature 284: 515–521

Homberg U, Hildebrand JG (1989) Serotonin immunoreactivity in the optic lobes of the sphinx moth *Manduca sexta* and colocalization with FMRFamide and SCP_B immunoreactivity. J Comp Neurol 288: 243–253

Homberg U, Christensen TA, Hildebrand JG (1989) Structure and function of the deutocerebrum in insects. Annu Rev Entomol 34: 477–501

Homberg U, Würden S, Dircksen H, Rao KR (1991) Comparative anatomy of pigment-dispersing hormone-immunoreactive neurons in the brain of orthopteroid insects. Cell Tissue Res 266: 343–357

Ichikawa T (1994) Reorganization of visual interneurons during metamorphosis in the swallowtail butterfly *Papilio xuthus*. J Comp Neurol 340: 185–193

Kerwien P, Schürmann FW (1990) Nichtsynaptische Exocytose im Hirn und in den Corpora cardiaca von *Gryllus bimaculatus*: Eine Tannin-Studie. In: Elsner N, Roth G (eds) Brain, perception, cognition. Thieme, Stuttgart New York, p 312

Lafon-Cazal M, Arluison L (1976) Localization of monoamines in the corpora cardiaca and the hypocerebral ganglion of locusts. Cell Tissue Res 172: 517–521

Langford LA, Coggeshall RE (1980) The use of potassium ferricyanide in neural fixation. Anat Rec 197: 297–303

Larimer JL, Smith JTF (1980) Circadian rhythm of retinal sensitivity in crayfish: modulation by the cerebral and optic ganglia. J Comp Physiol 136: 313–326

Leitch B, Laurent G, Shepherd D (1992) Embryonic development of synapses on spiking local interneurons in locusts. J Comp Neurol 324: 213–326

Loher W (1972) Circadian control of stridulation in the cricket *Teleogryllus commodus* Walker. J Comp Physiol 79: 173–190

Lösel R, Homberg U (1995) Anatomische und physiologische Charakterisierung von Neuronen im Bereich der akzessorischen Medulla der Schabe *Leucophaea maderae*. Verh Dtsch Zool Ges 88: 204

Lukat R, Weber F (1979) The structure of locomotor activity in bilobectomized cockroaches (*Blaberus fuscus*). Experientia 35: 38–39

Mangerich S, Keller R, Dircksen H, Rao KR, Riehm JP (1987) Immunocytochemical localization of pigment-dispersing hormone (PDH) and its coexistence with FMRFamide-immunoreactive material in the eyestalks of the decapod crustaceans *Carcinus maenas* and *Orconectes limosus*. Cell Tissue Res 250: 365–375

Meijer JH (1990) Physiological basis for photic entrainment. Eur J Morphol 28: 308–316

Moore RY (1983) Organization and function of a central nervous system circadian oscillator: the suprachiasmatic hypothalamic nucleus. Fed Proc 42: 2783–2789

Morin LP (1994) The circadian visual system. Brain Res Rev 67: 101–127

Nässel DR, Shiga S, Wikstrand EM, Rao KR (1991) Pigment-dispersing hormone-immunoreactive neurons and their relation to serotonergic neurons in the blowfly and cockroach visual system. Cell Tissue Res 266: 511–523

Nishiitsutsuji-Uwo J (1961) Electron microscopic studies on the neurosecretory system in Lepidoptera. Z Zellforsch 54: 613–630

Nishiitsutsuji-Uwo J, Pittendrigh CS (1968a) Central nervous system control of circadian rhythmicity in the cockroach. II. The pathway of light signals that entrain the rhythm. Z Vergl Physiol 58: 1–13

Nishiitsutsuji-Uwo J, Pittendrigh CS (1968b) Central nervous system control of circadian rhythmicity in the cockroach. III. The optic lobes, locus of the driving oscillation? Z Vergl Physiol 58: 14–46

Page TL (1978) Interactions between bilaterally paired components of the cockroach circadian system. J Comp Physiol 124: 225–236

Page TL (1981) Effects of localized low-temperature pulses on the cockroach circadian pacemaker. Am J Physiol 240: R144-R150

Page TL (1982) Transplantation of the cockroach circadian pacemaker. Science 216: 73–75

Page TL (1983a) Regeneration of the optic tracts and circadian pacemaker activity in the cockroach *Leucophaea maderae*. J Comp Physiol 152: 231–240

Page TL (1983b) Effects of optic tract regeneration on internal coupling in the circadian system of the cockroach. J Comp Physiol 153: 353–363

Page TL (1984) Neuronal organization of a circadian clock in the cockroach *Leucophaea maderae*. In: Porter R, Collins GM

(eds) Photoperiodic regulation of insect and molluscan hormones. Pitman, London, pp 115–135
Peters BH, Römer H, Marquart V (1986) Spatial segregation of synaptic inputs and outputs in a locust auditory interneuron. J Comp Neurol 254: 34–50
Petri B, Stengl M (1996) Is pigment-dispersing hormone a component of the circadian system of *Leucophaea maderae?* In: Elsner N, Schnitzler HU (eds). Brain and Evolution, p28 1996, in press
Petri B, Stengl M, Würden S, Homberg U (1995) Immunocytochemical characterization of the accessory medulla in the cockroach *Leucophaea maderae*. Cell Tissue Res 282: 3–19
Pflugfelder O (1936) Vergleichend-anatomische, experimentelle und embryologische Untersuchungen über das Nervensystem und die Sinnesorgane der Rhynchoten. Zoologica 34: 1–102
Piggins HD, Antle MC, Rusak B (1995) Neuropeptides phase shift the mammalian circadian pacemaker. J Neurosci 15: 5612–5622
Rao KR, Riehm JP (1988) Pigment-dispersing hormones: a novel family of neuropeptides from arthropods. Peptides 9: 153–159
Rao KR, Riehm JP (1989) The pigment-dispersing hormone family: chemistry, structure-activity relations, and distribution. Biol Bull 177: 225–229
Reghunandanan V, Reghunandanan R, Singh PI (1993) Neurotransmitters of the suprachiasmatic nucleus: role in the regulation of circadian rhythms. Prog Neurobiol 41: 647–655
Reischig T, Stengl M (1995) Light- and electron microscopic analysis of the accessory medulla of the cockroach *Leucophaea maderae*. In: Elsner N, Menzel R (eds) Göttingen neurobiology report 1995. Thieme, Stuttgart New York, p 252
Reynolds ES (1963) The use of lead citrate at high pH as an electron-opaque stain in electron microscopy. J Cell Biol 17: 208–212
Richardson KC, Jarett I, Finke EH (1960) Embedding in epoxy resins for ultrathin sectioning in electron microscopy. Stain Technol 35: 313–323
Roberts SK (1974) Circadian rhythms in cockroaches. Effects of optic lobe lesions. J Comp Physiol 88: 21–30
Roth RL, Sokolove PG (1975) Histological evidence for direct connections between the optic lobes of the cockroach *Leucophaea maderae*. Brain Res 87: 23–39
Scharrer B (1963) Neurosecretion. XIII. The ultrastructure of the corpus cardiacum in the insect *Leucophaea maderae*. Z Zellforsch 60: 761–796
Schulz WD, Schlüter U, Seifert G (1984) Extraocular photoreceptors in the brain of *Epilachna varivestis* (Coleoptera, Coccinellidae). Cell Tissue Res 236: 317–320
Schürmann FW (1987) The architecture of the mushroom bodies and related neuropils in the insect brain. In: Gupta PG (ed) Arthropod brain. Wiley, New York, pp 231–264
Schürmann FW, Wechsler W (1969) Elektronenmikroskopische Untersuchungen am Antennallobus des Deutocerebrums der Wanderheuschrecke *Locusta migratoria*. Z Zellforsch 95: 223–248
Schürmann FW, Sandemann R, Sandemann D (1991) Dense core vesicles and non-synaptic exocytosis in the central body of the crayfish brain. Cell Tissue Res 265: 493–501
Sokolove PG (1975) Localization of the cockroach optic lobe circadian pacemaker with microlesions. Brain Res 87: 13–21
Sokolove PG, Loher W (1975) Role of eyes, optic lobes, and pars intercerebralis in locomotory and stridulatory circadian rhythms of *Teleogryllus commodus*. J Insect Physiol 21: 785–799
Stengl M (1995) Pigment-dispersing hormone-immunoreactive fibers persist in crickets which remain rhythmic after bilateral transection of the optic stalks. J Comp Physiol A 176: 217–228
Stengl M, Homberg U (1994) Pigment-dispersing hormone-immunoreactive neurons in the cockroach *Leucophaea maderae* share properties with circadian pacemaker neurons. J Comp Physiol A 175: 203–213
Sternberger LA (1979) Immunocytochemistry. Wiley, New York
Strausfeld NJ (1976) Atlas of an insect brain. Springer, Berlin Heidelberg New York
Strausfeld NJ, Campos-Ortega JA (1973) L3, the 3rd 2nd order neuron of the 1st visual ganglion in the 'neural superposition' eye of *Musca domestica*. Z Zellforsch 139: 397–403
Strausfeld NJ, Nässel DR (1981) Neuroarchitecture of brain regions that subserve the compound eyes of crustaceans and insects. In: Autrum H (ed) Handbook of sensory physiology, vol VII, part 6B. Springer, Berlin Heidelberg New York, pp 1–132
Tolbert LP, Hildebrand JG (1981) Organization and synaptic ultrastructure of glomeruli in the antennal lobes of the moth *Manduca sexta*: a study using thin sections and freeze-fracture. Proc R Soc Lond B 213: 279–301
Tomioka K, Chiba Y (1986) Circadian rhythm in the neurally isolated lamina-medulla-complex of the cricket, *Gryllus bimaculatus*. J Insect Physiol 32: 747–755
Ude J, Agricola H (1995) FMRFamide-like and allatostatin-like immunoreactivity in the lateral heart nerve of *Periplaneta americana*. Colocalization at the electron microscopic level. Cell Tissue Res 285: 69–80
Ude J, Eckert M (1988) Submicroscopic characterization of proctolin-like immunoreactivity in the nervous system of the cockroach *Periplaneta americana* L. Cell Tissue Res 254: 197–202
Wiedenmann G (1983) Splitting in a circadian activity rhythm: the expression of bilaterally paired oscillators. J Comp Physiol A 150: 51–60
Wiedenmann G (1984) Zeitgeber and circadian activity rhythms of cockroaches: a system of unipolar coupled oscillators. J Interdiscipl Cycle Res 15: 69–80
Wills SA, Page TL, Colwell CS (1986) Circadian rhythms in the electroretinogram of the cockroach. J Biol Rhythms 15: 25–37
Würden S, Homberg U (1995) Immunocytochemical mapping of serotonin and neuropeptides in the accessory medulla of the locust, *Schistocerca gregaria*. J Comp Neurol 362: 305–319
Zimmermann H (1993) Synaptic transmission. Thieme, Oxford Stuttgart New York, pp 31–34

II. Ultrastructure of pigment-dispersing hormone-immunoreactive neurons in a three-dimensional model of the accessory medulla of the cockroach *Leucophaea maderae*.

Reischig T and Stengl M. 2003. Cell Tissue Res, in press.

Ultrastructure of pigment-dispersing hormone-immunoreactive neurons in a three-dimensional model of the accessory medulla of the cockroach *Leucophaea maderae*

Thomas Reischig and Monika Stengl

ABSTRACT

Locomotor activity rhythms of the cockroach *Leucophaea maderae* are orchestrated by two bilaterally paired and mutually coupled circadian pacemakers in the brain's optic lobes, which are confined to the accessory medulla (AMe) ventro-medially to the medulla. The AMe is innervated by about 12 pigment-dispersing hormone (PDH)-immunoreactive anterior medulla neurons (PDHMe), which are circadian pacemaker candidates in the fruitfly and the cockroach. Here, we developed a three-dimensional computer model of the AMe and associated structures, as a framework for current and future neuroanatomical studies. Thus, our greatly improved understanding of this structure in space allowed to further subdivide the PDHMe into three subgroups, the large, medium-sized, and small PDHMe. In subsequent light- and electron-microscopical studies the synaptic connections of two of these subgroups were described within subcompartments of the AMe. We found that the large, intensely staining anterior PDHMe contain medium-sized dense core vesicles and form input and output synapses primarily in the anterior and shell neuropil of the AMe with profiles densely filled with clear vesicles. The medium-sized, anterior PDHMe contain large dense core vesicles, and constitute input and output synapses preferentially in the internodular neuropil of the AMe either with profiles densely filled with clear vesicles, or with profiles containing granular dense core vesicles. The small, weakly staining anterior PDHMe belong to another morphological group as the large and medium-sized PDHMe, and could not be further identified on the electron microscopic level due to their weak PDH-immunoreactivity.

Indexing terms: Pigment-dispersing hormone, visual system, insects, cockroaches, accessory medulla, circadian rhythms

The locomotor activity rhythm of the cockroach *Leucophaea maderae* is controlled by two bilaterally symmetric, mutually coupled circadian pacemaker centres in the optic lobes (Nishiitsutsuji-Uwo and Pittendrigh, 1968b; Roberts, 1974; Sokolove, 1975; Page, 1982; Page, 1984; Chiba and Tomioka, 1987). Transplantation and regeneration studies located the circadian pacemaker in the accessory medulla (AMe) with associated pigment-dispersing hormone-immunoreactive (PDH-ir) medulla neurons (PDHMe) at the ventromedial edge of the medulla (Stengl and Homberg, 1994; Reischig and Stengl, 2003). The PDH-ir neurons contain circadian clock proteins, such as PERIOD, TIMELESS, CLOCK and CYCLE in *Drosophila melanogaster* and are thought to be circadian pacemaker cells as well as clock outputs in fruitflies and cockroaches (Homberg et al., 1991; Stengl and Homberg, 1994; Helfrich-Förster, 1995; Renn et al., 1999; Taghert et al., 2001; Reischig and Stengl, 2003; Reviews: Helfrich-Förster

et al., 1998; Stanewsky, 2002; Homberg et al., 2003). In the last years, the investigation of the molecular function of the circadian clock made astounding progress. However, little is known about the neuroanatomical structure and neurophysiological function of the neuronal network of the circadian pacemaker centre. Most neuroanatomical details of the insect circadian clock, the AMe, are known in the cockroach *L. maderae*. As a framework for all neuroanatomical data and to distinguish the 12 PDHMe, we developed a three-dimensional (3D) model of the AMe with associated PDH-ir somata. Several studies suggest that PDHMe form output pathways from the AMe to different midbrain regions as well as to the contralateral circadian clock (Homberg et al., 1991; Stengl and Homberg, 1994; Petri et al., 1995; Reischig and Stengl, 2002). Thus, to further elucidate the functional connections within the AMe we characterised the types of synaptic connections between neuronal profiles with different dense core vesicles (DCVs; as characterised in Reischig and Stengl, 1996) in the AMe. Then, we identified PDH-ir neurons at the electron microscopic (EM) level and studied their synaptic connections in the AMe. We show that two types of PDH-ir processes with either large or medium-sized DCVs form input as well as output synapses in distinct subcompartments of the AMe. Thus, PDH-ir neurons subserve different neuronal circuits within the AMe.

MATERIALS AND METHODS

Animals

Adult male cockroaches (*Leucophaea maderae*) were chosen from laboratory colonies. They were reared at 25 °C, 30 % relative humidity, and light-dark cycles of 12:12 h, with lights on at 6 AM. The animals were fed with dried dog food, potatoes, and water *ad libidum*. Most preparations were performed at the end of the subjective day.

Abbreviations

AMe(ae)	Accessory medulla(e)
DCV(s)	Dense core vesicle(s)
DFVNe	Fronto-ventral neurons, distal group
-ir	-immunoreactive
LPT(s)	Large presynaptic terminal(s)
MFVNe	Fronto-ventral neurons, medial group
MNe	Medial neurons
PDF	Pigment-dispersing factor
PDH	Pigment dispersing hormone
PDHLa	PDH-ir lamina neurons
PDHMe	PDH-ir medulla neurons
VMNe	Ventro-medial neurons
VNe	Ventral neurons
VPNe	Ventroposterior neurons

The nomenclature for anatomical orientation (left and right, dorsal, ventral etc.) is used according to the longitudinal axis of the animal. Only the previously termed "anterior layer" of the medulla is now ontogenetically more correctly termed "distal layer" (containing the distal PDH-ir fibre-fan).

The 3D-computer modelling

For 3D-reconstruction of the optic lobe and detailed analysis of the morphology of the PDH-ir neurons, 34 cockroaches were decapitated after anesthetising with CO_2, and the heads were mounted in the mould of a small dish filled with dental wax. To preserve the original shape and orientation of brain structures, the heads were opened and instantly covered with fixation solution (Bouin's solution, modified after Hollande (Romeis, 1989). Then, the brains were removed, washed in 0.1 M phosphate buffer (PB), pH 7.4, dehydrated in an ethanol series, and embedded in paraffin (Paraplast plus, Sigma, Germany). Serial frontal 10 μm-paraffin sections of the brains were obtained as ribbons, mounted on microscope slides, deparaffinised with xylene and rehydrated in descending ethanols. The anti-PDH immunostaining was performed after the three step method of Sternberger (1979) with diaminobenzidine as chromogen and modified as described below. All incubation steps were carried out on slides. The anti-*Uca*-β-PDH antiserum (# 3B3; Dircksen et al., 1987) was used at a concentration of 1:10,000. To visualise background structures, the sections were counterstained with 1 % methylene blue solution. For further correlation of immunocytochemically identifiable neuron groups with groups characterised by histological mass staining, we performed additional immunostainings on five brains with anti *Mas*-allatotropin antiserum (# 13-3-91; Veenstra and Hagedorn, 1993) at a dilution of 1:1,000 on paraffin sections with the same method. For 3D reconstruction, an anti-β-PDH stained brain section series was chosen for overall quality of staining and tissue preservation as well as for completeness and integrity of the single sections. Because 3D-reconstructions and size measurements of different soma groups were always performed with the same respective preparations, we measured relative size differences and did not attempt to obtain absolute values. Therefore, tissue shrinkage compensation was not employed. For sizes of intact cells of the AMe see Petri and Stengl (1999). The sections were consecutively photographed as 24 bit RGB images with a Polaroid (Cambridge, MA, USA) 2M-pixel camera mounted on a Zeiss Axioplan light microscope using a Zeiss 10x Plan-Neofluar lens. The images were digitally aligned by

means of the 3D visualisation software Amira™ 2.3 (Indeed-Visual Concepts GmbH, Berlin, Germany; http://www.amiravis.com), which was also used for surface reconstructions. Contours of the optic lobe's neurolemma and the glia sheaths around the optic neuropils (lamina, medulla, and lobula) were labelled by manual segmentation with the program's image segmentation editor (see also Reischig and Stengl, 2002). Surface models of these structures were calculated, simplified to about 10 % of the original triangle quantity, smoothed, and each object was saved as a separate file. The stained PDH-ir fibres were segmented by grey value thresholding, after the underlying image stack was adjusted to emphasise stained fibres against background in Adobe Photoshop 6.0. These adjustments included selective removing of the blue color out of the image stack, converting the images to 8 bit greyscales, and subsequent sharpness and contrast enhancement. The image stack was again loaded into Amira, an appropriate grey value threshold was determined, and an isosurface model of the segmented fibres was calculated. No further surface simplification or smoothing was applied. The somata of the PDH-ir fibres were segmented manually and stored as a separate file. After all, surface models of optic lobe's neurolemma, neuropils, fibres, and somata were superimposed in Amira for visualisation.

The reconstruction of the AMe neuropil with associated structures was performed basing on 53 consecutive 2 μm sections of a representative Richardson's blue stained semithin section series, which was attained as described below. The AMe and surrounding structures were consecutively photographed using the Zeiss 40x Plan-Neofluar lens, and images were saved as 8 bit greyscales. The images of the stack were subjected to contrast equalising in Photoshop, and digitally aligned. Glia sheaths, neuropils, tracts, and neuronal soma groups were labelled by manual segmentation, as described above. The nodular neuropil of the AMe was separated from the loose internodular neuropil by the difference of grey values and textures, as can be seen in Fig. 1B. The soma groups were identified and separated according to the criteria presented in Reischig and Stengl (1996). Single somata were pursued and labelled across the image stack, then all somata belonging to a group were combined, and a surface covering the soma group was calculated. The surface models of all structures and soma groups were simplified and smoothed as described above, stored in separate files, and superimposed in Amira for visualisation.

Conventional electron microscopy

After being anesthetised with CO_2, the cockroaches were decapitated, and the brains were dissected under EM-fixative (2 % glutaraldehyde, 2 % paraformaldehyde, 0.1 % picric acid in 0.1 M sodium cacodylate buffer (NaCaco) at pH 7.2, modified after Langford and Coggeshall (1980). The brains were further fixed overnight in the same fixative. Following washing in NaCaco the brains were postfixed with 1 % OsO_4 solution (Electron Microscopy Science, USA) in NaCaco for 1 h, washed again, dehydrated in a series of ethanols, and embedded in Epon (Serva, Germany) *via* acetone as intermedium. Then, the optic lobes were semithin sectioned (3 μm section thickness) in frontohorizontal plane with a diamond knife. The sections were mounted as series on microscope slides and stained with a mixture of 1 % azur II, 1 % methylene blue, 1 % borax, and 40 % saccharose at 60 °C (modified after (Richardson et al., 1960). The sections were analysed and photographed using a Zeiss Axiophot microscope. For conventional electron-microscopy, individual semithin sections containing the AMe were selected and attached with cyanacrylate glue to preformed resin blocks. Serial sections with silver or a grey interference color were cut with a diamond knife on an ultramicrotome (Reichert, Austria). These sections were collected on slot grids coated with Butvar™ (Solutia, USA) and stained with aqueous uranyl acetate (2 %) and lead citrate (Reynolds 1963).

PDH-Immunocytochemistry for electron microscopy

We performed immunostaining with the anti-β-PDH antiserum on the electron microscopic level with both pre- and postembedding techniques. To guarantee a clear distinction of different sizes of DCVs we defined all size categories with pre- as well as postembedding techniques all within corresponding preparations to avoid mistakes due to different tissue preservation. Though PDH immunostaining appeared to be very sensitive to OsO_4 postfixation (Reischig and Stengl, 1996), we were now able to achieve a good compromise between structure preservation and staining intensity by use of low OsO_4-concentrations in postembedding stainings, thus achieving a nearly background-free labelling. Nevertheless, we recognised that not all fibres could be reliably stained with this technique, so we additionally used the more sensitive preembedding technique.

For postembedding immunocytochemistry, ongrid staining was performed on ultrathin sections collected on Butvar-coated nickel slot grids. Brains

($N = 35$) were dissected and fixed for EM as described above. Preparations were postfixed in low concentrated OsO_4 (0.005, 0.01, or 0.05 %) in NaCaco for 1 h. The brains were embedded in Epon (*via* acetone as intermedium), or Durcupan (Fluka, Germany; *via* propylenoxide as intermedium). Semithin sections (3 μm) from the optic lobes were prepared and stained as described above. Sections containing the AMe were selected, remounted, and cut as described above. All following immunocytochemical incubation steps were carried out in a moist chamber with grids floating on drops of incubation solution. The sections were previously etched with 8 % Na-*meta*-periodate in H_2O for 1 hour, washed in H_2O, and subsequently in 0.01 M phosphate buffered saline (PBS), pH 7.4. The sections were preincubated with normal goat serum (dilution 1:30) in PBS for 15 min, rinsed, and incubated in anti-β-PDH serum diluted 1:1000 overnight at 4 ℃. After a further rinse, the sections were incubated with the secondary antibody (gold anti-rabbit G10; Auroprobe Amersham, Belgium; dilution 1:80) for 2 h at room temperature, then washed, and dried. Then, the sections were briefly counterstained with uranyl acetate and lead citrate. The best compromise between immunocytochemical staining intensity and ultrastructure preservation was achieved with an OsO_4-concentration of 0.05 %, together with the use of Durcupan as embedding medium.

In preembedding experiments, immunocytochemistry was performed on free-floating vibratome sections by means of the indirect peroxidase-antiperoxidase (PAP) method (Sternberger 1979). Brains ($N = 7$) were dissected under EM fixative (see above), further fixed *in vitro* overnight, embedded in gelatine/albumine, and sectioned with a vibratome at 30 μm. The free-floating sections were washed in PB and preincubated in 2 % normal goat serum, which was diluted in Tris-buffered saline, pH 7.4 (TBS: 0.1 M Tris-HCl/0.3 M NaCl) containing 0.01 % Triton X-100 (TrX). Anti-β-PDH polyclonal antiserum (Dircksen et al., 1987) was diluted at 1:5,000–1:60,000 in the TBS containing 1 % normal goat serum, and was applied to the sections for 18–20 h at room temperature. After washing in TBS, the sections were incubated at room temperature for 1 h in goat-anti-rabbit IgG (Dako, Denmark) at 1:100, and, after subsequent washing in TBS, for 1 h in rabbit PAP (Dako, Denmark) at 1:300. The diaminobenzidine/H_2O_2 staining reaction was performed as described elsewhere (Homberg and Hildebrand, 1989). Sections containing the AMe were postfixed in 0.05 % OsO_4 in NaCaco 0.1/7.4 for 1 h, dehydrated in ethanol, and infiltrated with Epon. The vibratome sections were embedded in Epon droplets between acetate sheets, polymerised at 36 ℃ for at least 3 days, and remounted on resin blocks. Serial semithin sections of 3–4 μm were cut in the original cutting direction. The sections were mounted on microscope slides and counterstained with Richardson's Blue as described above. Due to the low TrX-100 concentration used to preserve membrane structure, only semithin sections from the surfaces of the original vibratome sections showed satisfying staining intensity. From these sections, serial ultrathin sections were cut, collected, stained, and analysed as described below.

Evaluation and visualisation

The sections were studied with a Zeiss EM 10 CR electron microscope at an acceleration voltage of 60 kV. The photonegatives were digitised as 8 bit greyscale images on a flatbed scanner equipped with a transmission light device at high resolution (1200 dpi). In Adobe Photoshop 6.0, grey values were inverted, and contrast and sharpness of the micrographs were optimised. The coherences of immunostainings and synapses were always checked on consecutive sections. Identity and direction of chemical synapses were determined according to four criteria (Westfall, 1987; Peters and Palay, 1996): Presences of (i) pre- and (ii) postsynaptic densities, (iii) presynaptic clear vesicles and (iv) a synaptic cleft between the pre- and postsynaptic membranes.

RESULTS

For a detailed analysis of the internal structure of the AMe, the circadian pacemaker centre of the cockroach *Leucophaea maderae*, we performed conventional and immunohistological electron microscopy, as well as 3D computer modelling. Furthermore, because several studies suggested that a subgroup of PDH-ir neurons forms direct circadian coupling pathways between both AMae (Stengl and Homberg, 1994; Reischig and Stengl, 2002), we examined whether PDH-ir neurons (Fig. 1A) form input and output synapses within one AMe.

The 3D-model of the AMe with associated PDH-ir neurons displays its nodular structure, and the locations of adjacent soma groups and main input and output tracts could be clearly demonstrated (Fig. 1). Different types of neuronal somata and processes were distinguished by size and vesicle contents, and by their synaptic connections in specific regions of the AMe (Figs. 2–7). In addition, two different types of PDH-ir processes with their synaptic connections were identified (Figs. 8–11). They show that PDH-ir neurons apparently fulfill functions as output and

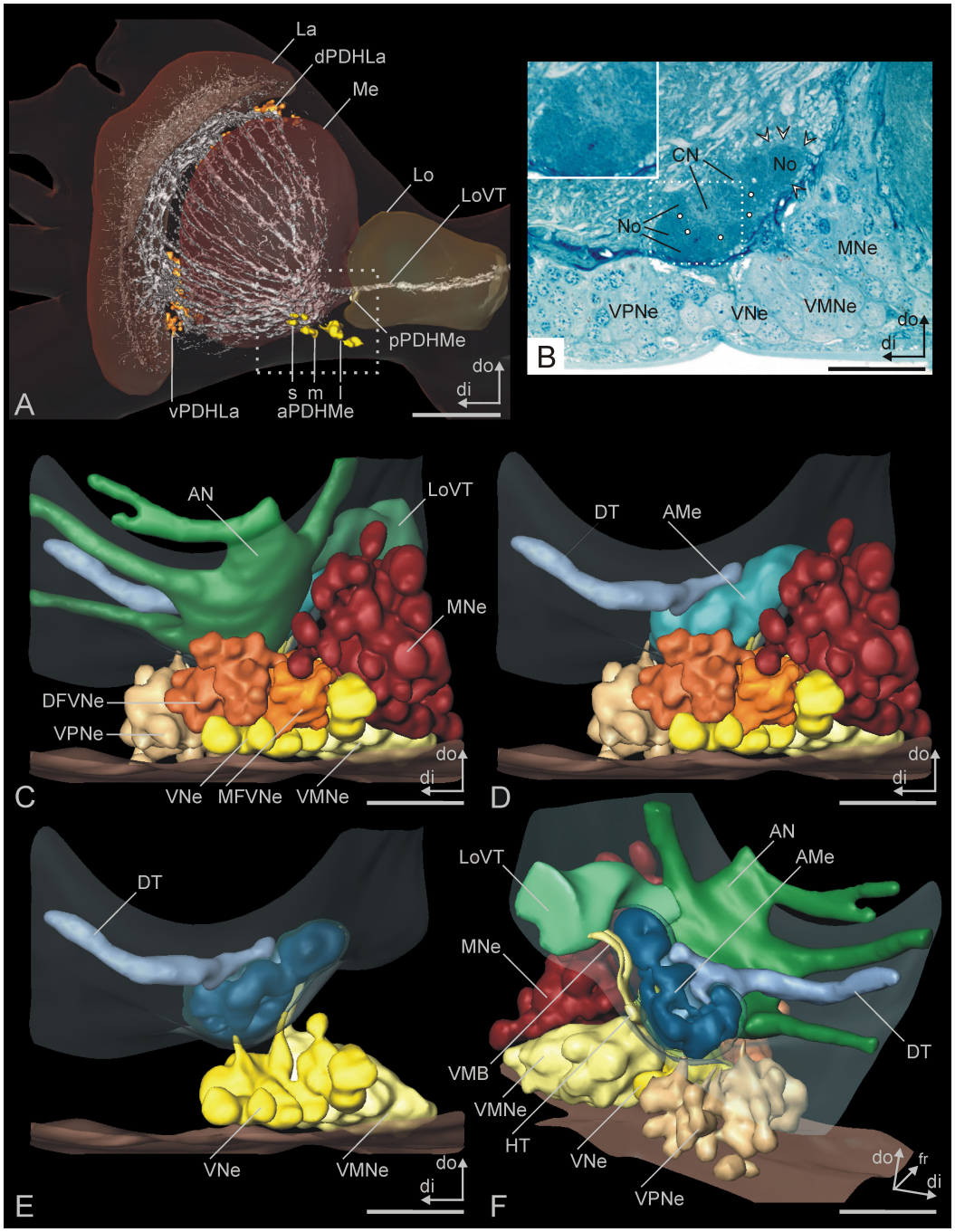

Fig. 1. Three-dimensional (3D) model of the optic lobe with PDH-ir neurons (A), and of the accessory medulla (AMe, C–F) of the cockroach *L. maderae*. **A:** Frontal view of a transparent optic lobe with reconstruction of the arborisations of the four different PDH-ir soma groups, the small (s), medium-sized (m), and large (l) anterior PDH-ir medulla cells (aPDHMe), of the posterior PDH-ir medulla cells (pPDHMe), and of the dorsal and ventral PDH-ir lamina cells (dPDHLa and vPDHLa, respectively). di distal, do dorsal, Me medulla, La lamina, Lo lobula, LoVT lobula valley tract. The AMe with associated soma groups (dotted window) is shown within detail in B–F. **B:** Semithin section of the AMe as used for the modeling studies. The inset (top left) enlarged the neuropil of the AMe (dotted square). The noduli of the AMe (No) are separated by loose internodular neuropil (white circles) and enveloped by loose shell neuropil (arrowheads). The coarse neuropil (CN) is formed by the distal tract, which enters the noduli. MNe Medial neurons, VMNe ventro-medial neurons, VNe ventral neurons, VPNe ventro-posterior neurons. **C–E:** Frontal 3D-reconstructions of the AMe with adjacent tracts and soma groups with consecutive anterior structures removed. **C:** The anterior neuropil (AN) continues distally and dorsally into the fanshaped fibre system (green) of the medulla. Medially, it continues into the LoVT. Grey = transparent glial sheath of the medulla. DFVNe and MFVNe, distal and medial frontoventral neurons, respectively. **D:** With the anterior neuropil removed, the accessory medulla (AMe), surrounded by its shell neuropil, and the distal tract (DT) become visible. **E:** After removal of the DFVNe, MFVNe, MNe, and VPNe, the nodular neuropil of the AMe (dark blue) is visible. The shell neuropil is rendered transparent to reveal the structure of the nodular neuropil. **F:** Posterior-dorsal view of the AMe with associated structures. Horizontal tract (HT), ventromedian bundle (VMB). Coordinates: do dorsal, fr frontal, di distal. Scale bars = 200 μm in A, 50 μm in B–F.

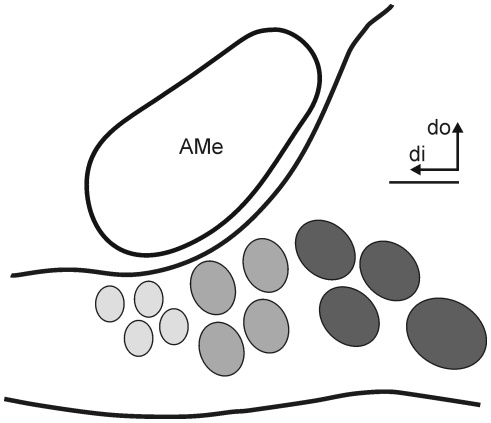

Fig. 2. Scheme of the accessory medulla (AMe) and the arrangement of the three groups of PDH-ir anterior medulla neurons (anterior PDHMe). The anterior PDHMe consist of about four small, weakly PDH-immunoreactive somata (light grey), about four medium-sized and more intensly PDH-immunoreactive somata (medium grey), and about four large, most intensely immunoreactive somata (dark grey). The most proximal soma is considerably larger than the others. Coordinates: di distal, do dorsal. Scale bar = 20 μm.

input pathways as well as internal elements of the circadian clockwork.

The 3D-model of the AMe

The 3D computer reconstruction of the PDH-ir neuron system in the optic lobe (Fig. 1A) was obtained from image stacks of 10 μm consecutive frontal paraffin sections stained with anti-β-PDH-antiserum (see Materials and Methods). The AMe models (Fig. 1C–F) were constructed from 2 μm semithin sections of methylene blue-stained tissue (Fig. 1B). In the optic lobe, four groups of PDH-ir neurons were distinguished (Fig. 1A): the anterior and posterior PDH-ir medulla neurons (PDHMe), and the dorsal and ventral PDH-ir lamina neurons (PDHLa). The anterior PDHMe ($n = 11.6 \pm 1.1$, mean $\pm$ standard deviation; from 7 optic lobes of 4 animals) can be further subdivided into three subgroups according to position, size, immunohistochemical staining intensity, and distinct bundles of their primary neurites (Figs. 1A, 2, 3A). The large and most intensely staining anterior PDHMe ($n = 3.9 \pm 0.7$; soma diameter $\varnothing = 18.9 \pm 3.8\,\mu$m) lie more proximally to the central brain. In many preparations, one of the large anterior PDHMe is conspicuously larger than the others (up to 26 μm) and it takes the position most proximally to the central brain. Further distally the medium-sized anterior PDHMe are located, which stain slightly weaker ($n = 4.1 \pm 0.7$; $\varnothing = 14.7 \pm 3.3\,\mu$m). Closest to the AMe, often in an anterior and ventral position, lie the faintly staining small anterior PDHMe ($n = 3.6 \pm 0.5$; $\varnothing = 10.7 \pm 1.6\,\mu$m). Within the AMe, varicose PDH-ir fibres arborise in the loose internodular neuropil, but more densely in the shell neuropil, especially in the anterior neuropil (Figs. 1C,F, 3A; Reischig and Stengl, 1996). From there, they fan out into the distalmost layer of the medulla towards the posterior rim of the lamina, invade the proximal lamina, touch the lamina organ (a putatively photoreceptive structure anteriorly to the first chiasm (Fleissner et al., 2001), and send sidebranches into more distal layers of the lamina. Additionally, middle layers of the medulla were invaded by few PDH-ir fibres. The PDH-ir fibres reach the central brain *via* the lobula valley tract (Figs. 1C,F). For an illustration of the complete PDH-ir neuron system in the central brain of *L. maderae*, see Reischig and Stengl (2002). The branching pattern of the PDHLa could not be distinguished from the branching pattern of the anterior PDHMe.

The AMe with associated soma groups and tracts is shown in a semithin section (Fig. 1B) and a 3D-model from an anterior (Figs. 1C–E) and an elevated distal-posterior perspective (Fig. 1F). On mass stained semithin sections six groups of somata can be morphologically distinguished by heterochromatin contents of the nuclei, by cytoplasm staining intensity, and by sizes of somata and nuclei, as described previously for five of the six groups (Reischig and Stengl, 1996). Most frontally the distal (DFVNe, 29 ± 10 somata; $\varnothing = 9.9 \pm 1.8\,\mu$m, $n = 68$ neurons from 3 optic lobes) and medial frontoventral neurons (MFVNe, 49 ± 7 somata; $\varnothing = 7.7 \pm 1.3\,\mu$m, $n = 81$) are associated with the AMe. The medial neurons (MNe, 56 ± 12 somata; $\varnothing = 17.9 \pm 3.3\,\mu$m, $n = 79$) are the medial-most, largest soma group facing the lobula. They are separated by a glial sheeth from the ventral neurons (VNe, 24 ± 5 somata; $\varnothing = 16.1 \pm 2.7\,\mu$m, $n = 59$) which lie more posterior, as do the ventroposterior neurons (VPNe, 36 ± 9; $\varnothing = 11.7 \pm 2.2\,\mu$m, $n = 80$), and the ventromedial neurons (VMNe, 35 ± 5 somata; $\varnothing = 13.8 \pm 2.6\,\mu$m, $n = 69$). The VMNe send their primary neurites *via* the ventromedian bundle to the upper-posterior edge of the AMe. One part of the ventromedian bundle (VMB in Fig. 1F) joins the lobula valley tract; the other part joins a tract leading in a horizontal plane along the proximal face of the AMe (HT in Fig. 1F). The VPNe are a heterogeneous group of somata, which send their primary neurites separately or in small bundles to ventro-distal regions of the AMe.

The 3D-model of the AMe with associated PDH-ir neurons illustrates its nodular structure. The AMe consists of an inner nodular neuropil and a loose internodular neuropil (Fig. 1E,F). The loose shell neuropil and the anterior neuropil surround the AMe, while the coarse neuropil is the continuation of the distal tract that terminates in the noduli (Reischig

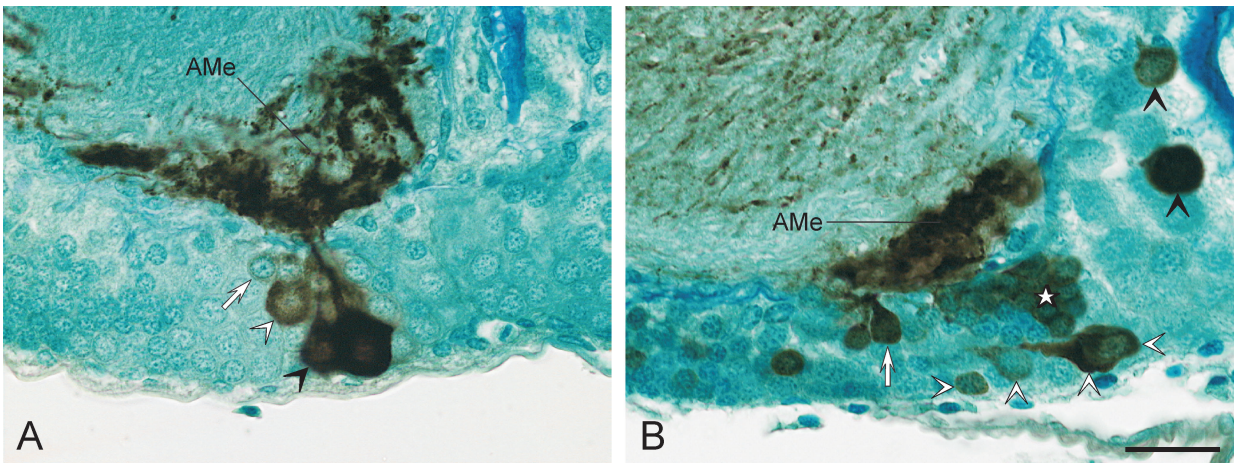

Fig. 3. Anti-β-PDH (A) and anti-*Mas*-allatotropin (B) immunostainings of the accessory medulla (AMe) on 10 μm paraffin sections, counterstained with methylene blue. **A:** While the small, weakly immunoreactive anterior PDHMe (arrow) belong to the DFVNe, the medium-sized (open arrowhead) and large anterior PDHMe (filled arrowhead) belong to the VNe. **B:** A composite image of *Mas*-allatotropin-ir neurons of the AMe was combined from three consecutive sections. *Mas*-allatotropin-ir somata are found among the DFVNe (asterisk), the MFVNe (arrow), the VNe (open arrowheads) and the MNe (filled arrowheads). Scale bar in B = 50 μm in A,B.

and Stengl, 1996). The shell neuropil continues into the anterior neuropil. However, as the main structural difference, the anterior neuropil is passed through by large primary neurits of neurons adjacent to the AMe like that of the anterior PDHMe.

The nodular neuropil forms knobs and interstices, with the dorsal part (the dorsal nodulus) as its most compact and dense substructure. While the distal tract is the main input pathway from the medulla into the noduli of the AMe, the lobula valley tract is the main input/output pathway from the internodular and shell neuropil of the AMe to the midbrain and contralateral optic lobe. In addition, the anterior neuropil extends into the fan-shaped distal layer fibre system of the medulla (Fig. 1A,C,F); the latter appears to constitute mainly an output system for the PDHMe to the medulla due to the many varicosities of the PDH-ir fibres which are storage and release sites of the pigment dispersing factor (PDF) also in the AMe (see below).

Immunocytochemically stained somata of the AMe on paraffin sections counterstained with methylene blue could be assigned to two of the six distinct neuronal soma groups associated with the AMe (Fig. 3A,B). It could be shown that the VNe contain the 3–6 large, strongly immunoreactive anterior PDHMe (Fig. 3A), as well as the 3–5 weaker immunoreactive medium-sized anterior PDHMe, since none of their primary neurites run *via* the ventromedian bundle like the VPNe, but form 2–3 separate bundles, which join the anterior neuropil of the AMe (Reischig and Stengl, 1996; Reischig and Stengl, 2002). However, the 3–5 weakly PDH-ir small PDHMe belong to the DFVNe (Fig. 3A), because of the characteristic location and size of their somata. In addition, their nuclei are more densely filled with heterochromatin, as is typical for DFVNe, but not for VNe.

To assign identified local interneurons to the morphological neuron groups of the AMe, we performed additional immunostaining with *Mas*-allatotropin antiserum on paraffin sections of the brain of *L. maderae*. We wanted to know whether output and local neurons can be assigned to different, characteristic soma groups of the AMe. Contrarily to anti-PDH staining, *Mas*-allatotropin-immunoreactivity is largely confined to the nodular neuropil of the AMe (Fig. 3B). Four *Mas*-allatotropin-ir soma groups lie adjacent to the AMe (Fig. 3B). More than half of the MFVNe, and about one third of the DFVNe were labelled. In addition, 2–4 of the MNe, and 3–4 of the VNe were allatotropin-ir. Although the neurits of the *Mas*-allatotropin-ir MNe somata could hardly be detected, it could be shown that at least two of them, but probably all, extended their primary neurites posteriorly to the LoVT and did not reach the AMe. The primary neurites of all other somata projected into the AMe. None of the axons appeared to project into the midbrain.

Synapses in the AMe

The neuropil of the AMe contains many fibres and varicosities filled with an astoundingly large amount of dense core vesicles (DCVs; Fig. 4). Generally, one can distinguish large axonal processes containing output synapses from small dendrites with input synapses. The axon terminals can be distinguished according to their DCV contents, while the

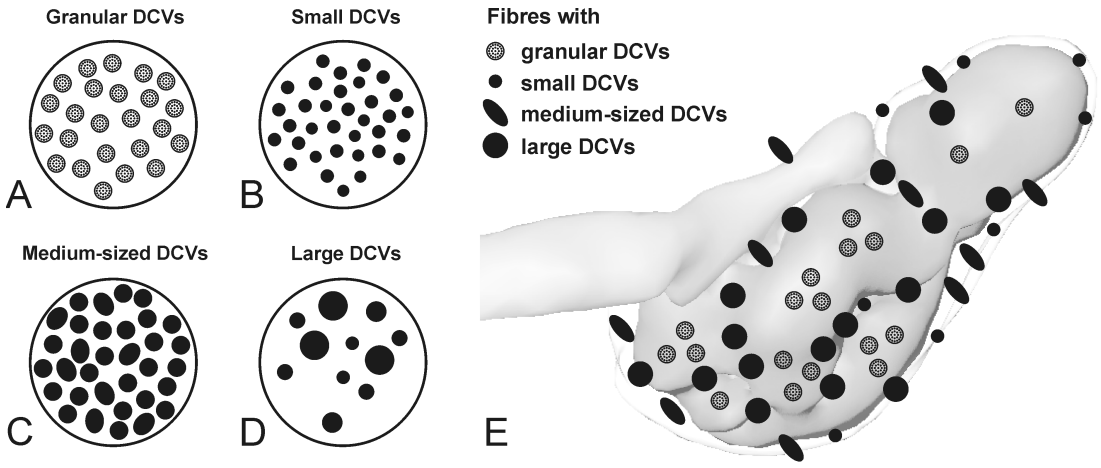

Fig. 4. Summary of the different types of dense core vesicles (DCVs) in neuronal profiles of different subcompartments of the AMe. **A:** Granular DCVs. **B:** Small DCVs. **C:** Medium sized DCVs. **D:** Large DCVs. **E:** Profiles with granular DCVs are confined to the noduli of the AMe, while small and medium-sized DCVs are preferentially found in the shell and anterior neuropil, and profiles with large DCVs in the internodular neuropil.

small dendrites are usually not identifiable, because they contain either no or only a small number of DCVs. The DCV-containing neurons, which regularily also contain some small, clear vesicles, can be separated into at least four types, according to size and structure of their DCVs (Fig. 4A–D), as described in Reischig and Stengl (1996). Neuron profiles with granular, small, medium-sized, and large DCVs can be distinguished, which branch in different regions of the AMe (Fig. 4E). While the granular DCVs appear to form a heterogeneous size group of at least two different DCV diameters, and almost exclusively occur in the noduli of the AMe, the small and medium sized DCVs belong to homogeneous size groups and were preferentially observed in the anterior neuropil and the shell neuropil surrounding the AMe, but also, to a lesser extend, in the internodular neuropil (Reischig and Stengl, 1996). The large DCVs, which also can be further differentiated into at least two different size groups (Reischig and Stengl, 1996), are very common in the internodular neuropil as well as in the shell and anterior neuropil. The large profiles ($\varnothing \approx 0.5$–$3\,\mu$m) filled with DCVs generally correspond to the beaded, immunostained, peptidergic axonal processes (varicosities; Fig. 3A). They frequently form output synapses to small dendrites as well as to other axonal terminals. Additionally, many large presynaptic terminals (= LPTs) with no or few DCVs are filled with numerous clear, synaptic vesicles. They occur mainly in the nodular neuropil and synapse with not identifiable small dendrites. Additionally, a large number of neurons, which cannot easily be assigned to either of these types, arborise in the AMe. They contain either no or few unclassifiable DCVs. Most of them are small postsynaptic dendrites.

The most common types of synaptic connectivities are summarised in Fig. 5, examples of electron micrographs are given in Fig. 6. Except one (Figs. 5H, 6F), all types of synaptic connections could be observed at least three times altogether, but generally, they were observed much more frequently; the types shown in Fig. 4A–D were observed in any preparation on nearly any section. Most commonly in the AMe are output synapses from LPTs (filled with clear synaptic vesicles) to small dendrites (Figs. 5A, 6A). They can be observed mainly in the noduli, most notably in the dorsal nodulus. The LPTs are often surrounded by many dendrites, and frequently form dyadic output synapses. Also, mainly in the nodular neuropil, preferentially in its ventral part, axon terminals with granular DCVs are grouped together, often associated with LPTs with clear synaptic vesicles. Output synapses of axon terminals with granular DCVs to unidentified small dendrites are very common (Figs. 5B, 6B). Some output synapses of axon terminals with large DCVs to profiles with granular DCVs were observed at the transition between nodular and internodular neuropil (Figs. 5D, 6C).

Varicosities with large, medium-sized, and small DCVs occur mainly in the anterior and shell neuropil of the AMe and in the internodular neuropil. Axonal terminals with large DCVs are the most abundant among these varicosities. Because of differences in profile sizes and vesicle contents (size, frequency, and distribution of the DCVs), they most likely belong to different types of neurons. They very frequently form output synapses to non-identified small dendrites and to terminals with granular DCVs (Figs. 5C,D; 6C). Also, but in fewer cases, synapses occur between axons with large DCVs (Figs. 5E, 6D). Ax-

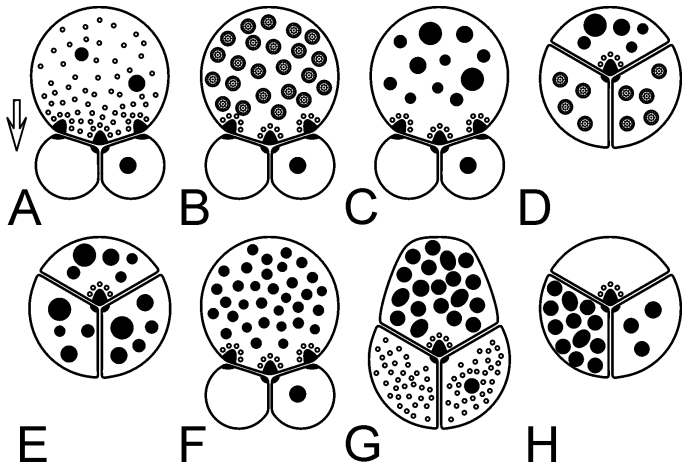

Fig. 5. Scheme of the main types of synaptic contacts found in the accessory medulla. The presynaptic site is always in the profile on the top, the arrow in A indicates information flow. **A:** In the centre and at the border of the noduli very frequently presynaptic terminals densely filled with clear vesicles and only few dense core vesicles (DCVs) form output synapses with small non-specified dendrites. **B:** Axonal profiles with granular DCVs form synapses with small, non-specified dendrites, mainly in the nodular neuropil. **C:** Axonal profiles with large DCVs form synapses with small non-specified dendrites in the internodular and shell neuropil. **D:** Axonal profiles with large DCVs form synapses with axonal profiles containing granular DCVs at the border of the noduli. **E:** Axon terminals with large DCVs form synapses on each other in the internodular and shell neuropil. **F:** Axonal profiles with small DCVs form synapses with small dendrites, preferentially in the shell, but also in the internodular neuropil. **G:** Axonal profiles with medium-sized DCVs form output synapses to axonal profiles with clear vesicles and few DCVs in the shell neuropil. **H:** Axonal profiles without DCVs form synapses with axonal profiles which contain medium-sized DCVs in the shell neuropil. A, B, C and D are the most abundant types of synaptic connections in the AMe and can be observed on almost every section throughout the AMe.

onal terminals with small and medium-sized DCVs occur mainly in the shell neuropil between the glia sheath and dense neuropil medially and ventrally to the AMe, as well as in the anterior neuropil, but also, to a lesser extend, in the internodular neuropil. Output synapses of profiles with small DCVs to small dendrites were sometimes observed (Figs. 5F, 6E). Output synapses from axon terminals with medium-sized DCVs to axons containing only clear vesicles were found more frequently (Fig. 5G), but until now, only one input synapse onto an axonal profile with medium-sized DCVs was observed (Figs. 5H, 6F).

Synapses of the PDH-ir neurons in the AMe

We performed immunostaining with anti-β-PDH antiserum on the electron microscopic level with both pre- and postembedding techniques. With both techniques we could confirm that PDH-immunoreactivity was restricted to two DCV types, the medium-sized and the large DCVs (Figs. 7–11), as shown previously in Reischig and Stengl (1996). The PDH-ir neurons with medium-sized DCVs were less abundant and predominated in the anterior and shell neuropil of the AMe, while fibres with PDH-ir large DCVs were more frequently observed, and arborised preferentially in the anterior and internodular neuropil (Figs. 4, 8–11). In both neuron types the PDH-immunoreactivity is largely confined to the DCVs, indicating that the DCVs contain the peptide. All varicosities containing medium-sized DCVs exhibited PDH-immunoreactivity, while less than one third of all varicosities with large DCVs were PDH-ir. The more intensely staining medium-sized PDH-ir DCVs could be found in somata of the large anterior PDHMe, which are also darker in PDH-immunostained preparations for light microscopy (Fig. 7A,B). PDH-immunoreactivity was found in the golgi apparatus and in premature vesicles exocytosing from the golgi. In the AMe, the PDH-ir neurons with medium-sized DCVs form large ($\varnothing \approx 3\,\mu$m) varicosities. In four cases we observed dyadic output synapses to LPTs with clear vesicles (Figs. 5G, 9A,B). In one case we observed an output synapse from a PDH-ir neuron with medium-sized DCVs to an LPT with clear vesicles, which on its part synapsed on a terminal with large DCVs (not shown). The large DCVs showed very faint PDH-immunoreactivity, which however, could not be confirmed on consecutive sections.

The PDH-ir neurons with large DCVs (Fig. 9C,D) are more abundant, but less intensely immunoreactive compared to the medium-sized DCVs. The PDH-ir neurons with large DCVs were found mainly in the internodular and anterior neuropil, but also in the shell neuropil of the AMe. In many cases we found output synapses of these neurons to smaller neurons with granular DCVs (Figs. 5D, 9C, D). Also,

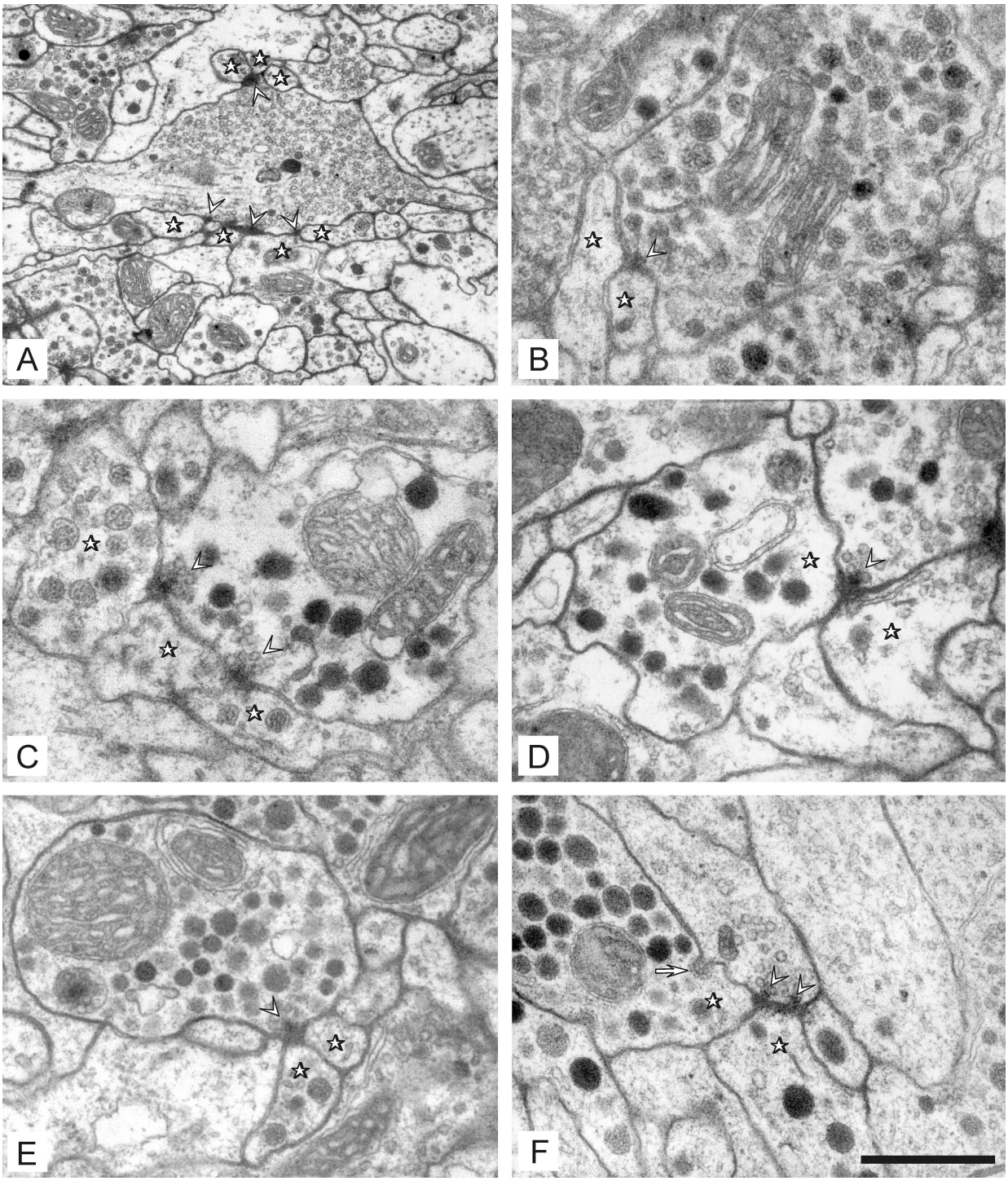

Fig. 6. Electron micrographs of synaptic connections between neuronal profiles with different vesicle types in the AMe. Arrowheads indicate presynaptic densities, asterisks mark postsynaptic profiles. **A:** An axonal profile densely filled with clear synaptic vesicles forms output synapses with small dendritic profiles in the nodular neuropil. **B:** An axonal profile with granular DCVs forms a dyadic output synapse to two small dendritic profiles in the nodular neuropil. **C:** An axonal profile with large DCVs forms dyadic output synapses to three profiles containing granular DCVs at the border of the noduli. **D:** An axonal profile with large DCVs forms dyadic output synapses to two axonal profiles in the internodular neuropil. One of them also contains large DCVs. **E:** An axonal profile with small DCVs forms dyadic output synapses with two small dendrites in the internodular neuropil. **F:** An axonal profile with clear vesicles and no DCVs forms synapses with two axonal profiles with medium-sized DCVs in the shell neuropil. The arrow points to a coated pit, possibly indicating release of neuropeptides from the postsynaptic cell. Scale bar in F = 1 μm in A, 0.5 μm in B–F.

output synapses to neurons without DCVs or with single unidentified DCVs were observed (Fig. 5C).

Additionally, input synapses to PDH-ir neurons in the AMe could be observed. The postsynaptic PDH-ir neurons are either large, axonic varicosities with large DCVs (Fig. 10A,B), or small dendrites with single or few DCVs (Fig. 10C,D); the latter cannot be clearly assigned to one of the known DCV types. In the first case the synaptic inputs are delivered from LPTs filled with clear vesicles. Inputs to small PDH-ir dendrites are formed by large terminals containing large DCVs. As shown for PDH-ir output fibres, the PDH-ir fibres receiving inputs are mainly found in the anterior, shell, and internodular neuropil, but not in the centre of the noduli.

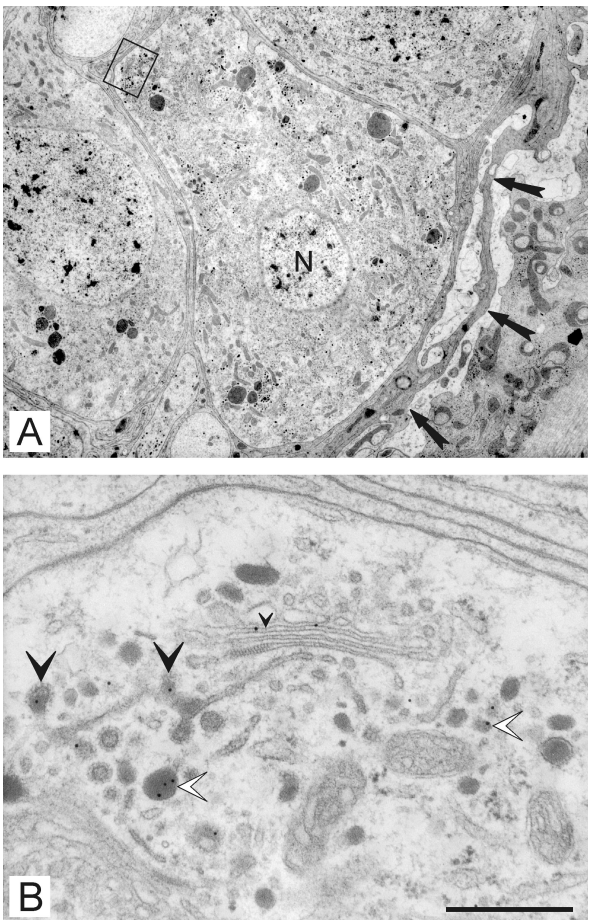

Fig. 7. A: This soma of the strongly stained large PDH-ir medulla cells contains medium-sized DCVs. Arrows: inner border of neurolemma. N nucleus. The rectangle defines the close-up shown in B. **B:** Medium-sized DCVs of different developmental states are PDH-ir. Small arrowhead: In the golgi apparatus PDH-immunoreactivity is detectable. Large arrowheads: Exocytosis of PDH-ir DCVs from the golgi. Open arrowheads: Fully differentiated DCVs. Scale bar in B = 7.5 μm in A, 0.5 μm in B.

DISCUSSION

In immuno-electron microscopical studies combined with 3D-reconstructions, the synaptic connections of PDH-ir neurons were examined to learn about their possible functions within the network of the AMe, the circadian pacemaker centre of the cockroach *L. maderae* (Stengl and Homberg, 1994; Reischig and Stengl, 2003). It was known that the main input region from the ipsilateral medulla into the AMe are GABA-ir fibres of the distal tract (Reischig and Stengl, 1996; Petri et al., 1995) terminating in the noduli. In contrast, the anterior and shell neuropils around the AMe, which continue into the internodular neuropil, appear to be contralateral input regions into the AMe (Reischig and Stengl 2002). These compartments also constitute output regions of the AMe *via* the lobula valley tract to midbrain targets. In addition, local neurons of the AMe with somata among the frontoventral neurons such as the *Mas*-allatotropin-ir neurons arborise in the noduli. Thus, we wanted to determine in which of the functional subcompartments of the AMe the different PDHMe synapse to learn about their possible functions. Here, we showed that there are three different groups of PDHMe, which can be distinguished according to their soma sizes and their DCV contents. While PDH-ir terminals with medium-sized DCVs originating from the large PDHMe form synaptic connections with fibres with clear vesicles mostly in the anterior and shell neuropil, the PDH-ir terminals with large DCVs originating from the medium-sized PDHMe form output synapses to profiles containing either clear vesicles or granular DCVs mostly in the internodular neuropil. Both of these PDHMe subgroups send processes to the midbrain and to the contralateral optic lobe. Thus, both of these PDHMe subgroups that belong to the ventral neurons appear to be involved in output pathways as well as in contralateral input pathways into the circadian clock. In contrast to these subgroups, the small PDHMe belong to the frontoventral neurons and might also be local interneurons of the AMe, such as the allatotropin-ir neurons.

The 3D-methods

After reconstructing a whole brain model of *L. maderae* (Reischig and Stengl, 2002; http://www.reischig.de) we now reconstructed the optic lobe, the AMe, and the PDH-ir neuron system in more detail to obtain insights into the network-functions of the circadian pacemaker centre. In contrast to the generally used 3D brain reconstruction techniques employing immunofluorescent labelling

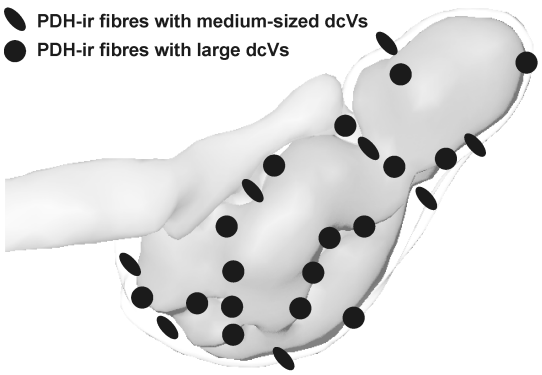

Fig. 8. The distribution of the two types of PDH-ir terminals differs in the AMe. While PDH-ir terminals with medium-sized DCVs are preferentially distributed in the anterior and shell neuropil, the more abundant varicosities with PDH-ir large DCVs are mostly found in the internodular neuropil.

and confocal laser scan microscopy (Galizia et al., 1999; Chiang et al., 2001; Rein et al., 2002), we used series of brain sections obtained with classical histological methods. Thus, we obtained non-bleaching, permanent preparations with more details of the labelled cells in addition to visualisation of all other brain neuropils. A section thickness of 10 μm in the paraffin series and 2 μm in the semithin series was suitable for most of the structures of interest, except for the fine PDH-ir processes in the paraffin series. These fibre reconstructions can be viewed from all angels, but can only be presented in the z-direction. With these 3D techniques it is possible to use all histological specimens with complete, intact sections of high quality for fast and easy 3D reconstructions without the need for expensive laser scanning microscopy.

Subgroups of PDH-ir neurons connect the clock to different targets

The 3D reconstructions of the PDH-ir neuron system allowed to clearly distinguish not only the PDHLa from the anterior and posterior PDHMe, but also to differentiate three subgroups of anterior PDHMe somata according to soma size and staining intensity. The four strongest stained large PDHMe, as well as the four medium-sized PDHMe could be assigned to the VNe of the AMe, while the four weakly PDH-ir, small PDHMe clearly belong to the DFVNe. This suggests that the subgroups of PDHMe serve in different neuronal circuits of the AMe.

Also previous counts of PDH-ir fibres in different fibre tracts suggested diverse functional groups of PDH-ir neurons (Petri et al., 1995). A first group of PDH-ir neurons restricts their arborisations to the ipsilateral optic lobe, while the remaining groups join the lobula valley tract and project to different midbrain targets (Petri et al., 1995). Backfills, lesion studies, as well as tract counts suggested that the PDHLa, all posterior-, but only a subgroup of the anterior PDHMe restrict their arborisations to the ipsilateral optic lobe (Petri et al., 1995; Reischig and Stengl, 2002; T. Reischig, unpublished). Because the small PDHMe belong to the DFVNe, they might be identical to this subgroup of anterior PDHMe cells that restricts their arborisations to neuropils of the optic lobe. This assumption is confirmed by the characteristic branching patterns of other DFVNe neurons such as the *Mas*-allatotropin- and the leucokinin-ir neurons, which restrict their arborisations mostly to the neuropil of the AMe and medulla (Petri et al., 1995). Moreover, one of the small PDHMe cells is also leucokinin-ir (Petri et al., 1995).

Thus, very likely all of the about eight PDH-ir fibres in the lobula valley tract, which project to the midbrain, originate from the four large and the four medium-sized PDHMe. Current tract counts and dye injection studies showed that among the eight anterior PDHMe which project into the midbrain, a subgroup forms commissures directly connecting both optic lobes and also both AMae *via* the posterior and the anterior optic commissures, while the remaining PDHMe end in midbrain targets (Reischig and Stengl, 2002). If one compares the numbers of PDH-ir fibres in the lobula valley tract and in both the anterior and posterior commissure at the midline, or close to the optic stalk, it becomes apparent that one PDH-ir neuron per side runs *via* the posterior optic commissure and projects into the contralateral optic lobe. In addition, among the about three PDH-ir neurons per side that project *via* the anterior commissure, one ends in the midbrain, while two project into the contralateral optic lobe (Petri et al., 1995; Reischig and Stengl, 2002; T. Reischig and M. Stengl, in preparation). The PDHMe which project into the contralateral optic lobe could possibly directly connect both AMae and, thus, form a circadian coupling pathway which was predicted by behavioural experiments (Page et al., 1977). An important prerequisite for this function would be that these cells form input and output synapses within the same AMe.

Synaptic contacts of PDH-ir neurons within the AMe

Current lesion studies indicate that all PDH-ir soma groups, the PDHLa as well as anterior and posterior PDHMe, branch in the AMe (T. Reischig and M. Stengl, unpublished). Nevertheless, it was possible to distinguish the origin of different PDH-ir and DCV-containing terminals in the AMe. Also

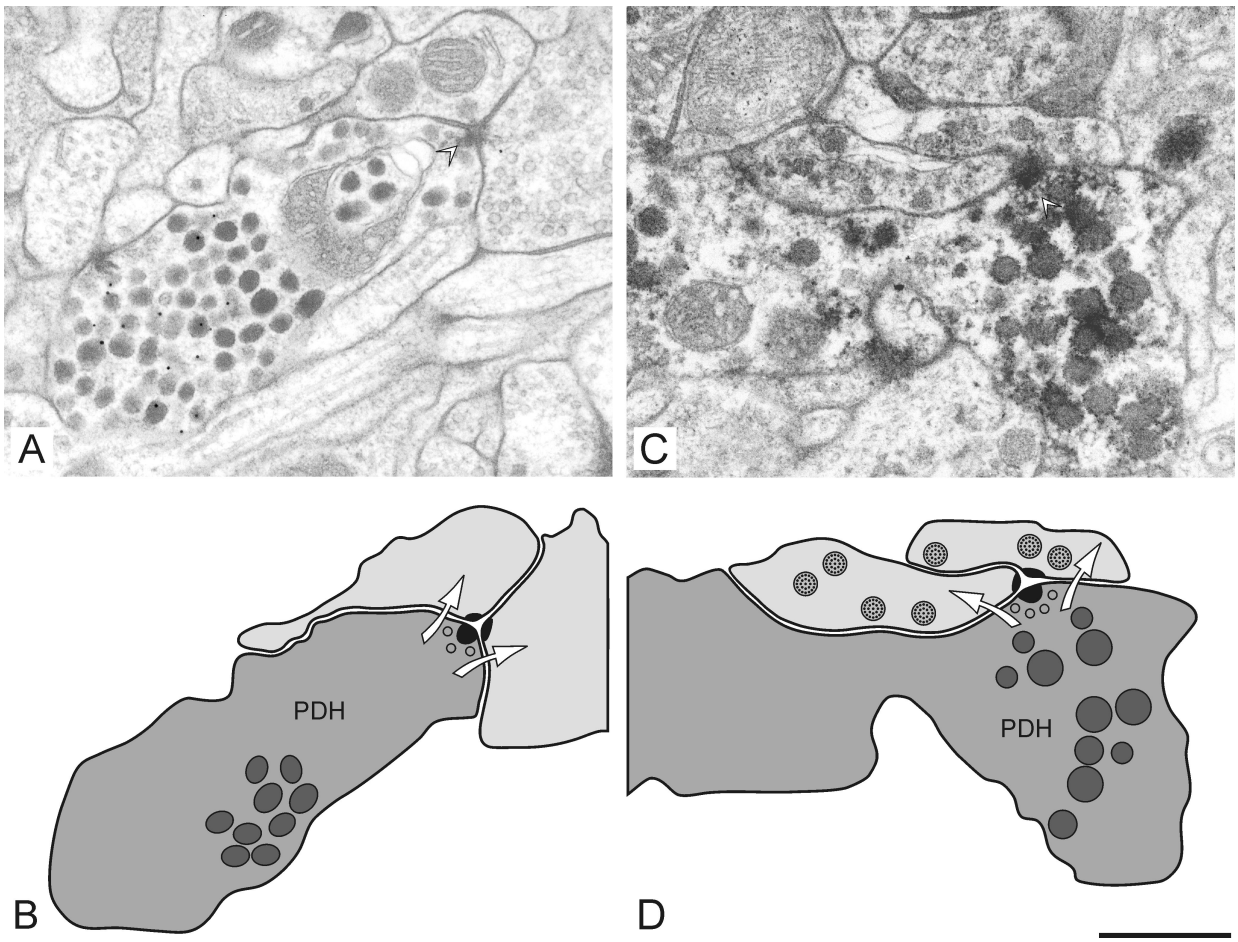

Fig. 9. Electron micrographs (**A,C**) with respective schemes (**B,D**) of PDH-ir profiles with output synapses in the AMe. The arrows in B and D represent the direction of information flow. PDH-ir profiles are shaded (PDH). **A,B:** An axonal profile containing PDH-ir medium-sized DCVs in a post-embedding preparation forms a dyadic output synapse (arrowhead in A) with two larger profiles filled with clear synaptic vesicles in the shell neuropil. **C,D:** The PDH-ir axonal profile with large DCVs in a preembedding preparation forms a dyadic output synapse (arrowhead in C) with two profiles containing granular DCVs at the border of the noduli. Scale bar in D = 0.5 μm in A–D.

considering the differential staining intensity, it became clear that the strongly PDH-ir terminals with medium-sized DCVs belong to the strongly staining large anterior PDHMe somata (Fig. 7). These large anterior PDHMe mostly arborise in the shell and anterior neuropil, in direct neighborhood to serotonin-ir processes of apparently local interneurons (Petri et al., 1995, 2002). Thus, it is likely that the large anterior PDHMe form outputs to serotonergic axon terminals (Fig. 11). This assumption is supported by injection studies that showed for both PDH and serotonin all-delay type phase response curves. Thus, it suggests involvement and interaction of both neuron systems in a non-photic input pathway such as a circadian coupling pathway (Page, 1987; Petri and Stengl, 1997). Therefore, serotonin-ir neurons are likely candidates for post- and possibly also presynaptic partners of the large PDHMe cells in the anterior and shell neuropil of the AMe.

The more numerous, weaker staining PDH-ir fibres with large DCVs, which occur mostly in the internodular neuropil, belong to the weaker staining PDH-ir medium-sized PDHMe somata, and possibly also to the posterior PDHMe. The PDH-ir terminals with large DCVs form synapses with small dendrites as well as with other axon terminals containing granular DCVs and apparently also large DCVs in different subcompartments of the AMe, and therefore, might interact with different partners. Thus, they appear to be strongly involved in local network interactions within the AMe. Because not all of the profiles with large DCVs are PDH-ir and because the large DCVs form different size groups (Reischig and Stengl, 1996), their different pre- and postsynaptic partners need to be identified in double-label experiments.

Throughout our investigations, direct synaptic contacts between PDH-ir neurons were not found.

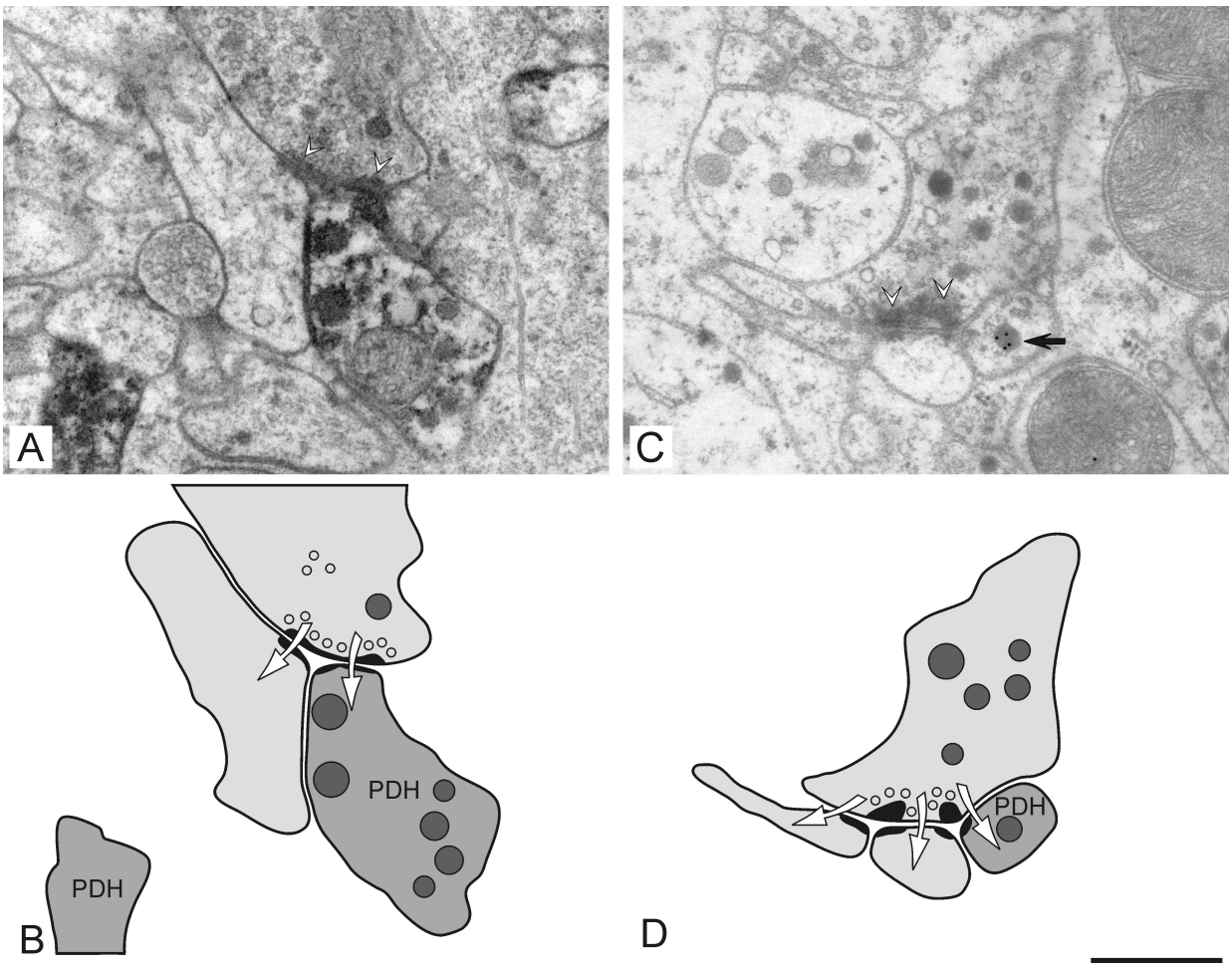

Fig. 10. Electron micrographs (**A,C**) with respective schemes (**B,D**) of PDH-ir profiles with input synapses in the AMe. The arrows in B and D represent the direction of information flow. PDH-ir profiles (PDH) are shaded. **A,B:** A large unstained profile densely filled with synaptic vesicles in a preembedding preparation forms output synapses (arrowheads in A) with a PDH-ir profile containing large DCVs, and with another non-stained profile in the internodular neuropil. **C,D:** A non-stained profile with large DCVs in a postembedding preparation forms output synapses (arrowheads in C) with a small dendritic profile containing a PDH-ir dense core vesicle (arrow), and with two other non-stained dendrites in the shell neuropil. Scale bar in D = 0.5 μm in A–D.

This suggests that coupling information between PDH-ir neurons has to be transmitted *via* interneurons, such as the serotonin-ir neurons. However, it is also possible that all neurons in the AMe possess PDF receptors and are affected by non-synaptically released PDF without the necessity for direct synaptic contacts. In addition, since we could not recognise the weakly PDH-ir small neurons, we cannot exclude direct synaptic contacts between PDH-ir neurons. Thus, identification of the PDF-receptors, as well as physiological experiments will be necessary to identify all the PDF-responsive cells in the AMe. Because our PDF-injections caused phase-delays of the onset of locomotor activity only during the middle of the day, it is possible that all PDHMe subgroups serve the same delay-function in the AMe, but within different functional circuits. Possibly, locomotor activity rhythms are only affected by one of the functional groups of PDHMe, comparably to the small ventrally located lateral neurons (LN_vs) in *Drosophila melanogaster*.

Thus, it could be assumed that according to morphological criteria the large PDHMe with the medium-sized DCVs are homologous to the large LN_vs of *Drosophila*, which project to the contralateral AMe, and the medium-sized PDHMe with large DCVs correspond to the small LN_vs of the fruitfly, which provide arborisations in the superior protocerebrum (Renn et al., 1999; Park et al., 2000; Helfrich-Förster et al., 2000). However, since both PDH-ir terminal types with medium-sized and large DCVs form input and output synapses in the AMe, it is possible that both contribute to local circuits as well as to circadian coupling pathways, but with

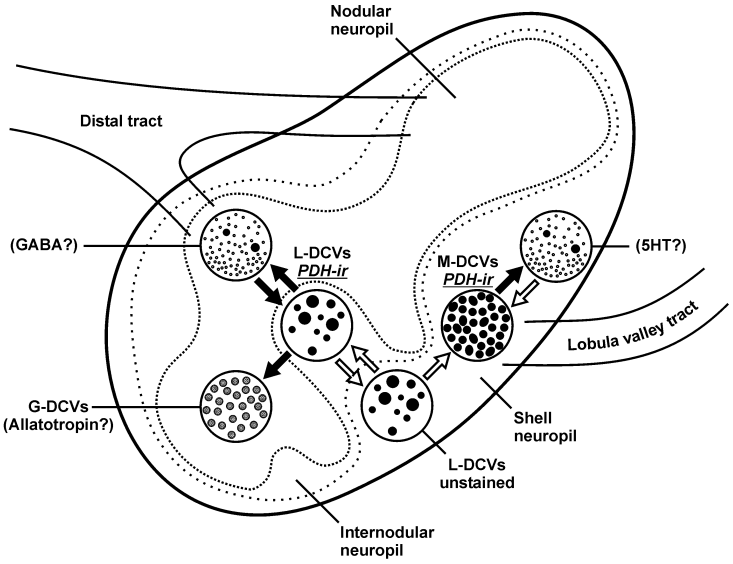

Fig. 11. Scheme of observed (filled arrows) and likely synaptic connections (open arrows) of PDH-ir neurons in the different subcompartments of the AMe. It is assumed that PDH-ir neurons with medium-sized DCVs (M-DCVs) form circadian coupling pathways between the bilaterally symmetric pacemakers. They might synchronise all pacemaker neurons of both AMae *via* synaptic connections to serotonin (5HT)-ir neurons and *via* non-synaptic neuropeptide release into the shell neuropil of the AMe. In contrast, the PDH-ir fibres with large DCVs (L-DCVs) are assumed to take part in local circuits of the AMe, possibly in the gating of the ipsilateral light input to the pacemaker. In the internodular neuropil they might be connected with GABA-ergic and *Mas*-allatotropin-ir profiles which appear to carry ipsilateral light input into the noduli of the AMe. Filled arrows indicate observed connections of PDH-ir profiles, while open arrows indicate connections based on the observation of non-immunostained synaptic partners with specified DCVs.

different pre- and postsynaptic partners. The small PDHMe probably do not correspond to either of *Drosophila's* LN_v groups, since they seem to arborise only in the ipsilateral optic lobe.

Light entrainment pathways and processing of light information in the AMe

Circadian clocks in all organisms are strongly connected to the visual system, because light input entrains the endogenous rhythms of the internal clocks to the external day/night cycle. In the cockroach both pacemakers can be entrained by photoreceptors in or near the compound eyes (Roberts and De 1965; Nishiitsutsuji-Uwo and Pittendrigh, 1968a; Page et al., 1977; Page, 1983a,b). However, no histaminergic photoreceptor terminals end in the AMe (Loesel and Homberg, 1999). Thus, the distal tract, which connects the noduli of the AMe with the medulla and the lamina, appears to be the main ipsilateral visual input pathway to the circadian clock. Because it was shown that the distal tract terminating in the noduli of the AMe is γ-aminobutyric acid (GABA)-ir, it is likely that a large population of the LPTs filled with many small clear vesicles, which mainly occur in the noduli, are GABA-ir processes (Petri et al., 2002). Since neurons with apparently the same morphology as GABA-ir neurons with dense arborisations in the AMe respond to light and connect the AMe to the medulla and the lamina (Loesel and Homberg, 2001; Petri et al., 2002), it is likely that the GABA-ir neurons form, mostly *via* the distal tract, the main light entrainment pathway of the ipsilateral compound eye to the circadian clock in *L. maderae.* This hypothesis is further supported by the finding of light-like phase response curves with GABA-injections into the vicinity of the AMe (Petri et al., 2002). In addition to GABA, also neurons immunoreactive to an antiserum against the neuropeptide *Mas*-allatotropin appear to be involved in the light entrainment pathway. Also, *Mas*-allatotropin-injections produced light-like biphasic phase response curves (Petri et al., 2002), and are restricted to the noduli (Fig. 3B), where mainly processes with granular DCVs occur. Thus, it is likely that the *Mas*-allatotropin-ir neurons contain granular DVCs, and are postsynaptic to the GABA-ir neurons. Therefore, the noduli appear to process information about light entrainment (Petri et al., 1995, 2002).

At the transition between nodular and internodular neuropil, it is likely that some of the outputs of LPTs with clear vesicles to PDH-ir profiles with large DCVs (Fig. 10A,B) could constitute direct GABA-dependent light entrainment of PDH-ir pacemaker neurons (Fig. 11). This hypothesis is supported by intracellular recordings which showed that PDH-like neurons responded with a weak inhibition to ipsilateral light (Loesel and Homberg, 2001). Furthermore, the synaptic output of PDH-ir neurons with large DCVs to nodular neurons with either clear vesicles or granular DCVs (Fig. 9C,D; Fig. 11) might suggest that PDF modulates or gates light entrainment (Petri et al., 2002).

In summary, we assume that ipsilateral light input from the compound eye is processed in the noduli, while contralateral light inputs enter preferentially *via* the shell neuropil. Circadian phase information

between ipsi- and contralateral pacemaker neurons appears to be mediated *via* the anterior and the shell neuropil, while outputs appear to leave the circadian pacemaker from the internodular neuropil *via* the anterior neuropil. Future studies will test these hypotheses.

ACKNOWLEDGEMENTS

We are very grateful to Dr. H. Dircksen (University of Bonn, Germany) for providing the anti-β-PDH antiserum. This work was supported by Deutsche Forschungsgemeinschaft (DFG) grants STE 531/7–1, 2, 3, and Human Science Frontier.

LITERATURE CITED

Chiang AS, Liu YC, Chiu SL, Hu SH, Huang CY, and Hsieh CH. 2001. Three-dimensional mapping of brain neuropils in the cockroach, *Diploptera punctata*. J Comp Neurol 440:1–11.

Chiba Y and Tomioka K. 1987. Insect circadian activity with special reference to the localisation of the pacemaker. Zool Sci 4:945–954.

Dircksen H, Zahnow CA, Gaus G, Keller R, Rao KR, and Riem JP. 1987. The ultrastructure of nerve endings containing pigment-dispersing hormone (PDH) in crustacean glands: identification by an antiserum against a synthetic PDH. Cell Tissue Res 250:377–387.

Fleissner G, Loesel R, Fleissner G, Waterkamp M, Kleiner O, Batschauer A, and Homberg U. 2001. Candidates for extraocular photoreceptors in the cockroach suggest homology to the lamina and lobula organs in beetles. J Comp Neurol 433:401–414.

Galizia CG, McIlwrath SL, and Menzel R. 1999. A digital three-dimensional atlas of the honeybee antennal lobe based on optical sections acquired by confocal microscopy. Cell Tissue Res 295:383–394.

Helfrich-Förster C. 1995. The period clock gene is expressed in central nervous system neurons which also produce a neuropeptide that reveals the projections of circadian pacemaker cells within the brain of *Drosophila melanogaster*. Proc Natl Acad Sci USA 92:612–616.

Helfrich-Förster C, Stengl M, and Homberg U. 1998. Organisation of the circadian system in insects. Chronobiol Int 15:567–594.

Helfrich-Förster C, Täuber M, Park JH, Muhlig-Versen M, Schneuwly S, and Hofbauer A. 2000. Ectopic expression of the neuropeptide pigment-dispersing factor alters behavioural rhythms in *Drosophila melanogaster*. J Neurosci 20:3339–3353.

Homberg U and Hildebrand JG. 1989. Serotonin immunoreactivity in the optic lobes of the sphinx moth *Manduca sexta* and colocalisation with FMRFamide and SCP immunoreactivity. J Comp Neurol 288:243–253.

Homberg U, Reischig T, and Stengl M. 2003. Neural organisation of the circadian system of the cockroach *Leucophaea maderae*. Chronobiol Int., in press.

Homberg U, Würden S, Dircksen H, and Rao KR. 1991. Comparative anatomy of pigment-dispersing hormone-immunoreactive neurons in the brain of orthopteroid insects. Cell Tissue Res 266:343–357.

Langford LA and Coggeshall RE. 1980. The use of potassium ferricyanide in neural fixation. The Anatomical Record 197:297–303.

Loesel R and Homberg U. 1999. Histamine-immunoreactive neurons in the brain of the cockroach *Leucophaea maderae*. Brain Res 842:408–418.

Loesel R and Homberg U. 2001. Anatomy and physiology of neurons with processes in the accessory medulla of the cockroach *Leucophaea maderae*. J Comp Neurol 439:193–207.

Nishiitsutsuji-Uwo J and Pittendrigh CS. 1968a. Central nervous system control of circadian rhythmicity in the cockroach. III. The pathway of light signals that entrain the rhythm. Z vergl Physiol 58:1–13.

Nishiitsutsuji-Uwo J and Pittendrigh CS. 1968b. Central nervous system control of circadian rhytmicity in the cockroach. II. The optic lobes, locus of the driving oscillator? Z vergl Physiol 58:14–46.

Page TL. 1982. Transplantation of the cockroach circadian pacemaker. Science 216:73–75.

Page TL. 1983a. Effects of optic-tract regeneration on internal coupling in the circadian system of the cockroach. J Comp Physiol 153:353–363.

Page TL. 1983b. Regeneration of the optic tracts and circadian pacemaker activity in the cockroach *Leucophaea maderae*. J Comp Physiol A 152:231-240.

Page TL. 1984. Neuronal organisation of a circadian clock in the cockroach *Leucophaea maderae*. In: Photoperiodic regulation of insect and molluscan hormones, Ciba foundation symposium 104. London: Pitman. p 115–135.

Page TL. 1987. Serotonin phase-shifts the circadian rhythm of locomotor activity in the cockroach. J Biol Rhythms 2:23–34.

Page TL, Caldarola PC, and Pittendrigh CS. 1977. Mutual entrainment of bilaterally distributed circadian pacemakers. Proc Natl Acad Sci USA 74:1277–1281.

Park JH, Helfrich-Förster C, Lee G, Liu L, Rosbash M, and Hall JC. 2000. Differential regulation of circadian pacemaker output by separate clock genes in *Drosophila*. Proc Natl Acad Sci USA 97:3608–3613.

Peters A and Palay SL. 1996. The morphology of synapses. J Neurocytol 25:687–700.

Petri B, Homberg U, Loesel R, and Stengl M. 2002. Evidence for a role of GABA and *Mas*-allatotropin in photic entrainment of the circadian clock of the cockroach *Leucophaea maderae*. J Exp Biol 205:1459–1469.

Petri B and Stengl M. 1997. Pigment-dispersing hormone shifts the phase of the circadian pacemaker of the cockroach *Leucophaea maderae*. J Neurosci 17:4087–4093.

Petri B and Stengl M. 1999. Presumptive insect circadian pacemakers i*n vitro*: immunocytochemical characterisation of cultured pigment-dispersing hormone-immunoreactive neurons of *Leucophaea maderae*. Cell Tissue Res 296:635–643.

Petri B, Stengl M, Würden S, and Homberg U. 1995. Immunocytochemical characterisation of the accessory

medulla in the cockroach *Leucophaea maderae*. Cell Tissue Res 282:3–19.

Rein K, Zockler M, Mader MT, Grubel C, and Heisenberg M. 2002. The *Drosophila* standard brain. Curr Biol 12:227–231.

Reischig T and Stengl M. 1996. Morphology and pigment-dispersing hormone immunocytochemistry of the accessory medulla, the presumptive circadian pacemaker of the cockroach *Leucophaea maderae*: a light- and electron- microscopic study. Cell Tissue Res 285:305–319.

Reischig T and Stengl M. 2002. Optic lobe commissures in a three-dimensional brain model of the cockroach *Leucophaea maderae*: a search for the circadian coupling pathways. J Comp Neurol 443:388–400.

Reischig T and Stengl M. 2003. Ectopic transplantation of the accessory medulla restores circadian locomotor rhythms in arrhythmic cockroaches (*Leucophaea maderae*). J Exp Biol 206:1877–1886.

Renn SC, Park JH, Rosbash M, Hall JC, and Taghert PH. 1999. A pdf neuropeptide gene mutation and ablation of PDF neurons each cause severe abnormalities of behavioural circadian rhythms in *Drosophila*. Cell 99:791–802.

Reynolds ES. 1963. The use of lead citrate at high pH as an electron-opaque stain in electron microscopy. J Cell Biol 17:208–212.

Richardson KC, Jarett I, and Finke EH. 1960. Embedding in epoxy resins for ultrathin sectioning in electron microscopy. Stain Technol 35:313–323.

Roberts SK. 1974. Circadian rhythms in cockroaches: effects of optic lobe lesions. J Comp Physiol 88:21–30.

Roberts SK and De F. 1965. Photoreception and entrainment of cockroach activity rhythms. Science 148:958–959.

Romeis B. 1989. Mikroskopische Technik. Munich: Verlag Urban und Schwarzenberg.

Sokolove PG. 1975. Localisation of the cockroach optic lobe circadian pacemaker with microlesions. Brain Res 87:13–21.

Stanewsky R. 2002. Clock mechanisms in *Drosophila*. Cell Tissue Res 309:11–26.

Stengl M and Homberg U. 1994. Pigment-dispersing hormone-immunoreactive neurons in the cockroach *Leucophaea maderae* share properties with circadian pacemaker neurons. J Comp Physiol A 175:203–213.

Sternberger LA. 1979. Immunocytochemistry. New York: Wiley & Sons.

Taghert PH, Hewes RS, Park JH, O'Brien MA, Han M, and Peck ME. 2001. Multiple amidated neuropeptides are required for normal circadian locomotor rhythms in *Drosophila*. J Neurosci 21:6673–6686.

Veenstra JA and Hagedorn HH. 1993. Sensitive enzyme immunoessay for *Manduca* allatotropin and the existence of an allatotropin-immunoreactive peptide in *Periplaneta americana*. Arch Insect Biochem Physiol 23:99–109.

Westfall JA. 1987. Ultrastructure of invertebrate synapses. In Ali MA, editor. Nervous systems in invertebrates. New York: Plenum Press. p 3–28.

III. Lesion of PDH-immunoreactive medulla neurons abolishes circadian rhythmic locomotor activity in the cockroach *Leucophaea maderae*.

Lesion of PDH-Immunoreactive Medulla Neurons Abolishes Circadian Rhythmic Locomotor Activity in the Cockroach *Leucophaea maderae*

Thomas Reischig

ABSTRACT

The presence of an endogenous circadian clock in the brain of an animal was first demonstrated in the optic lobes of the cockroach *Leucophaea maderae*. However, the clock's cellular basis remained elusive, until pigment-dispersing hormone-immunoreactive medulla neurons (PDHMe) were proposed as pacemaker candidates. Their homologues in *Drosophila* express the clock genes *period* and *timeless*. The PDHMe are closely associated with the accessory medulla (AMe), a small neuropil in the optic lobe, which was suggested to be a circadian clock neuropil. To investigate the role of the PDHMe in clock function and to analyse the components of the circadian clock in the cockroach, methods for lesioning the AMe and adjacent neuron somata were developed, combined with subsequent histological examination. After punching out the AMe with fine glass pipettes, all animals that lacked central PDH-ir projections due to removal of the respective PDHMe somata remained postoperatively arrhythmic. Two animals with partial reduction of the PDHMe and surviving PDH-ir fibres in the midbrain remained rhythmic, one of them providing the first evidence that also posterior PDHMe may be involved in rhythm generation. The data further support the hypothesis that the AMe is the circadian pacemaker controlling activity rhythms in the cockroach. Due to the small number of animals tested, however, more experiments will be necessary to finish this work. Preliminary studies showed that electro-cauterisation by a coagulator equipped with tungsten microelectrodes will be the best method to achieve precise and locally restricted lesions in future experiments.

Indexing terms: Circadian rhythms, accessory medulla, locomotor activity rhythms, pigment-dispersing hormone, pacemakers, cockroaches, *Leucophaea maderae*

Lesion and transplantation experiments demonstrated that the circadian locomotor activity rhythm of the cockroach *Leucophaea maderae* is controlled by two bilaterally paired and mutually coupled endogenous circadian pacemakers, which reside in the brain's optic lobes (Nishiitsutsuji-Uwo and Pittendrigh, 1968; Roberts, 1974; Sokolove, 1975; Page, 1982; Chapter IV; reviewed by Helfrich-Förster et al., 1998; Homberg et al., 2003). One optic lobe comprises four sets of neurons which are immunoreactive (-ir) to an antiserum against the crustacean pigment-dispersing hormone (PDH; Homberg et al., 1991). Two sets are located near the dorsal and ventral rim of the lamina, respectively (PDH-ir lamina neurons, PDHLa), both groups together consisting of about 43–136 somata (Petri et al., 1995; Chapter II). The other two reside ventromedially at the medulla (PDH-ir medulla neurons, PDHMe), one group in an anterior position, the other more posteriorly behind the lobula valley tract (Chapter II). They are associated with the accessory medulla (AMe), a small neuropil situated in the anterior, ventromedial edge

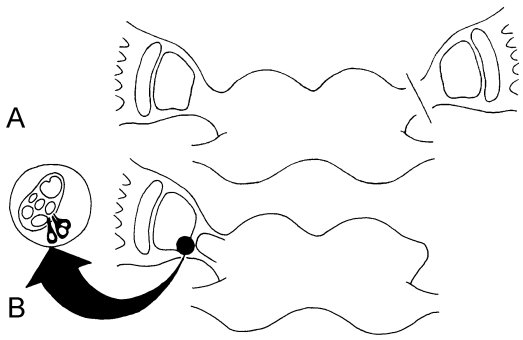

Fig. 1. The location of the lesion. **A:** Prior to the lesion experiments, the left (in respect to the body axis) optic lobe was removed. Circadian locomotor activity was assayed for at least three weeks before the lesion. **B:** In rhythmic cockroaches, the AMe with adjacent neuronal somata was punched out with a glass pipette. For lesions with a needle or the coagulator, the needle or electrode was stuck into the soma region of the AMe. See Materials and Methods for details.

of the medulla of the optic lobe (Homberg, et al., 1991; Petri and Stengl, 1995; Reischig and Stengl, 1996). The anterior PDHMe consist of about 12 somata, which can be further divided into three subgroups according to morphological criteria (Chapter II). They share properties predicted for circadian pacemaker neurons, e.g., position of somata, projections into various areas of the central brain, and connections to the contralateral optic lobe (Homberg, 1991; Stengl and Homberg, 1994; Reischig and Stengl, 2002; Chapter VII; reviewed by Homberg et al., 2003). In *Drosophila melanogaster* PDH-ir lateral neurons contain the clock proteins PERIOD and TIMELESS, and have been suggested to be circadian pacemaker neurons in fruit flies (reviewed by Stanewsky, 2002). The anterior PDHMe of the cockroach appear to be homologous to the fruit fly's lateral neurons and also appear to be circadian pacemakers and/or output elements of the circadian clock (Stengl and Homberg, 1994; Chapters IV, VII). To investigate of the role and the function of the AMe and different PDHMe in generating circadian rhythmic activity, the PDHMe and AMe were lesioned in cockroaches, which free-running locomotor activity was monitored in running-wheels. Subsequently, brains of lesioned animals were histologically examined and compared with the resulting postoperative activity. All lesioned animals with complete degeneration of the PDH-ir central brain projections showed arrhythmic locomotor activity. Several lesion techniques were investigated in order to achieve more precise lesions for future experiments.

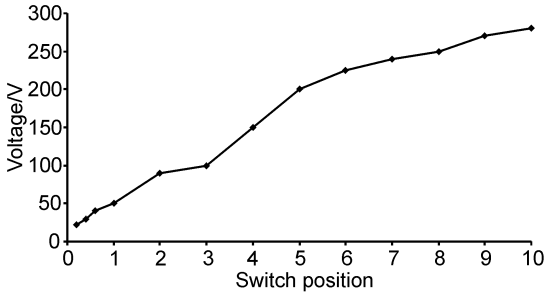

Fig. 2. Diagram of the relation between settings of the power selector knob of the coagulator and the resulting source voltages measured between lesion current output connector and reference electrode (see Materials and Methods).

MATERIALS AND METHODS

Animals

Adult male cockroaches (*Leucophaea maderae*) were chosen from laboratory colonies. They were reared at 25 °C, 30 % relative humidity, and light-dark cycles of 12:12 h, with lights on at 6 AM. The animals were fed with dried dog food, potatoes, and water *ad libidum*. The nomenclatures for anatomical orientations (left and right, dorsal, ventral etc.) are always quoted according to the longitudinal axis of the animal.

Surgery

All operations were performed on male cockroaches under steady CO_2 anesthesia. For surgery, the animals were fixed in special metal tubes, which were mounted under a stereoscopic dissecting microscope. Cell culture medium (L 15, Gibco, Germany) containing penicillin and streptomycin was used to rinse the wounds. For the initial left optic lobe resection (Fig. 1A), the optic lobe was exposed by cutting three sides of a small rectangular flap of the overlying head cuticle with a razorblade fragment. The cuticle flap was bend sidewards and fixed in this position. With an iridectomy scissor, the optic nerves and the optic stalks were cut, the optic lobe was removed, the cuticle was flapped back, and sealed with wax. Then, the animals were placed into running-wheels to record locomotor activity. When showing stable circadian rhythmic locomotor activity for at least three weeks, an experimental animal was removed from its running-wheel, anesthetised with CO_2, and fixed in the metal tube. The right optic lobe was exposed as described above. The location of the AMe was recognisable by a characteristic trachea near the surface of the optic lobe (Petri and Stengl, 1997). After lesion, the cuticle was flapped back and sealed with wax. The AMe-lesions were performed by one of the following methods:

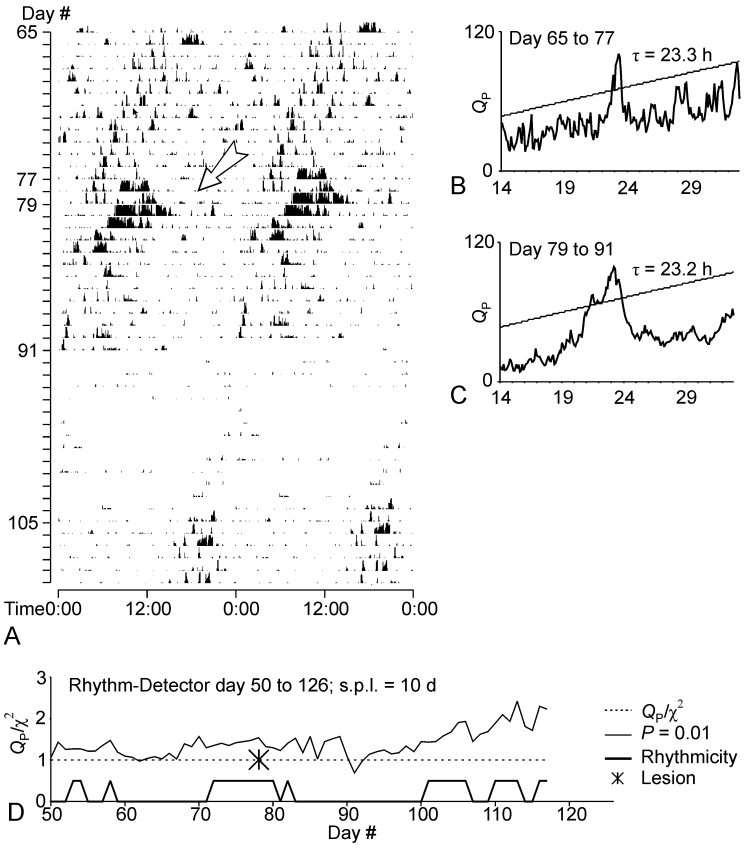

Fig. 3. Locomotor activity of a sham operated control animal (animal ID 06 in Table 2), which continues to be rhythmic after the operation. **A:** The double-plot activity histogram shows circadian rhythmic wheel-running activity ($\tau = 23.3$ h) in constant darkness before the operation (**B:** χ^2-periodogram, day 65–77). After the sham operation (see Material and Methods) at day 78 (arrow, A), rhythmic activity continues with a period of 23.2 h (**C:** χ^2-periodogram, day 79–91) and is also present after episodes with decreased activity (day 105). **D:** Postoperative rhythmicity is also documented by the Rhythm Detector. The scan periodogram curve (Q_P/χ^2) beginning with day 50 until the end of the wheel-running recording (day 126) detects rhythmic activity in consecutive 10-day-χ^2-periodograms (solid line, rhythmicity) immediately after the operation. s.p.l. = single periodogram length. For histology, see Fig. 4.

For lesions with glass pipettes (Fig. 1B), the perineurium above the AMe was opened with fine forceps. Fine glass pipettes were prepared from borosilicate glass capillaries (Hilgenberg, Germany; ∅ 1 mm) with an edged tip opening of 150–300 μm. The opposite opening of the pipette was attached to a flexible tube to apply negative pressure by means of mouth suction. The tip was placed on the surface of the optic lobe above the AMe, negative pressure was applied carefully, and simultaneously, the pipette was moved forward through the tissue. Then, the pipette was retracted with the punched out tissue remaining in the tip.

For lesions with a needle, the perineurium above the AMe was opened with fine forceps. The tip of a fine needle (as generally used for mounting of small insects in collections) was attached to a holder, its tip was stuck by hand into the area of the AMe, and fine circling movements were applied. This method was preliminary tested in a couple of animals, but was applied to only two experimental animals.

Lesions by electro-cauterisation were applied with a special electro coagulation device (Coagulateur de Wyss, J. Monti, Geneva, Switzerland) equipped with tungsten microelectrodes (1.1 MΩ; the shafts of the electrodes were isolated, only the tip was left blank at a length of 30 μm; World Precision Instruments, Sarasota, Florida, USA). The coagulator generated sinusoidal high frequency voltages (0–280 V, 0.5 MHz) adjustable by a power dialer knob, which was directed to the microelectrode and a reference electrode. The relation between source voltage and setting of the power dialer of the coagulator was measured with a conventional multimeter instrument and is shown in Fig. 2. The resulting high frequency current leads to heat production in the tissue at the tip of the electrode, causing coagulation of a limited area of tissue. The coagulation currents with the high resistance electrodes used is below the detection range of the coagulator's inbuild ampéremeter, which is optimised for the use of low-resistance electrodes. To find applicable settings for lesions with 1.1 MΩ electrodes in cockroaches, the recommendation of the coagulator's manual was followed that neither formation of steam-bubbles at the tips of the electrodes should occur nor adherent tissue should be found at the tips of the electrodes after lesion. In preliminary experiments, several coagulator settings were tested by varying application times and power of the coagulation current. At power settings between 2.5 and 3, and current delivered for 10 or more seconds, bubble formation combined with recognisable wrinkling of the neurolemma was observed around the electrode penetration site. Therefore, a reasonable configuration was suggested by setting the power dialer to 1 and current applied

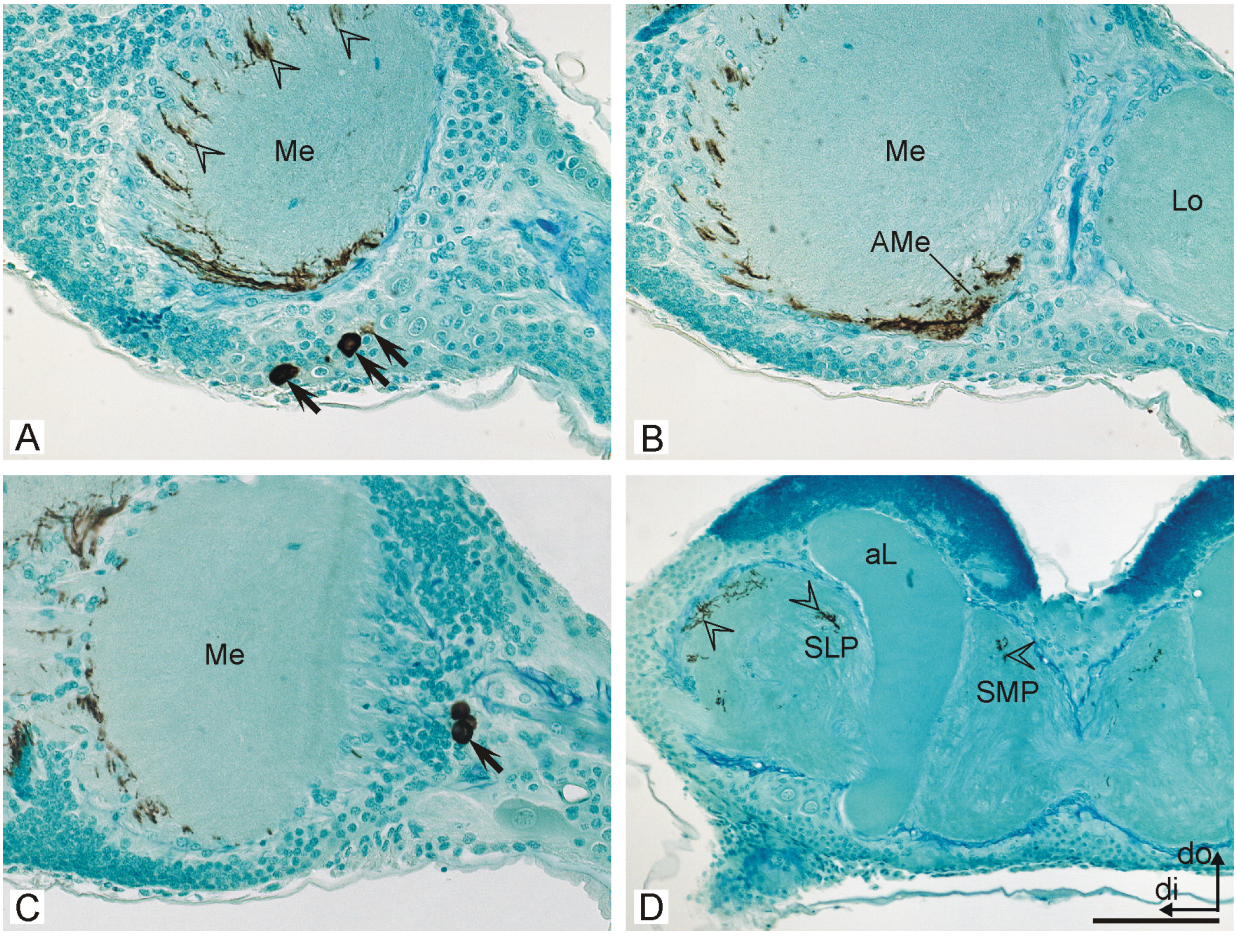

Fig. 4. The histological examination of the brain of the control animal (same as in Fig. 3) showed no abnormalities compared to untreated animals. **A,B,C:** In the sham-operated optic lobe, three of the 12 present anterior PDH-ir medulla neurons are shown (arrows in A). Also, the accessory medulla (B, AMe), and the posterior PDH-ir medulla neurons (arrow in C) are unchanged. Open arrowheads in A: PDH-ir fibres in the distal fibre-fan of the medulla. **D:** In addition, in the central brain, the arborisation pattern of PDH-ir fibres (arrowheads) is normal. SLP, SMP superior lateral and medial protocerebrum, respectively. aL alpha lobe; Lo lobula; Me medulla. Scale bar in D = 100 μm in A, 200 μm in B,C,D. Coordinates in D: di distal, do dorsal for A–D.

for 10 seconds with a 1.1 MΩ electrode. With these settings, six animals were lesioned in the area of the AMe. On an experimental animal which was prepared as described above, the tip of the electrode was put on the surface of the AMe with a micromanipulator. The electrode was pushed forward to penetrate the neurolemma, then retracted until the tip was equal with the surface, and again moved forward for about 100 μm. A chlorided silver wire fixed in the hemolymphe of the head capsule was used as reference electrode. After applying the lesion current, the electrode was retracted, the reference electrode removed, and the cuticle was flapped back and sealed with wax. Then, the animal was returned to its running-wheel.

Since none of the six experiments was successful, a series of 16 test experiments was performed, where animals were electro-cauterised at the site of the AMe as described above. The animals were treated with different power settings of the coagulator up to full power, and currents were applied for up to 20 seconds. In a part of these experiments, electrodes with lower resistance (0.5 MΩ, length of blank tip 55 μm) were used. After seven days, the animals were sacrificed and prepared for PDH-immunocytochemistry.

For controls, three animals were sham operated. This operation covered all steps of the lesion experiments including anaesthesia, opening of the head capsule and rupture of the neurolemma above the AMe. Only the actual lesion was omitted.

Activity analysis

Locomotor activity was monitored in running-wheels in constant darkness at 26 °C as described previously (Stengl and Homberg, 1994). Activity was visualised with double-plot activity histograms; the heights

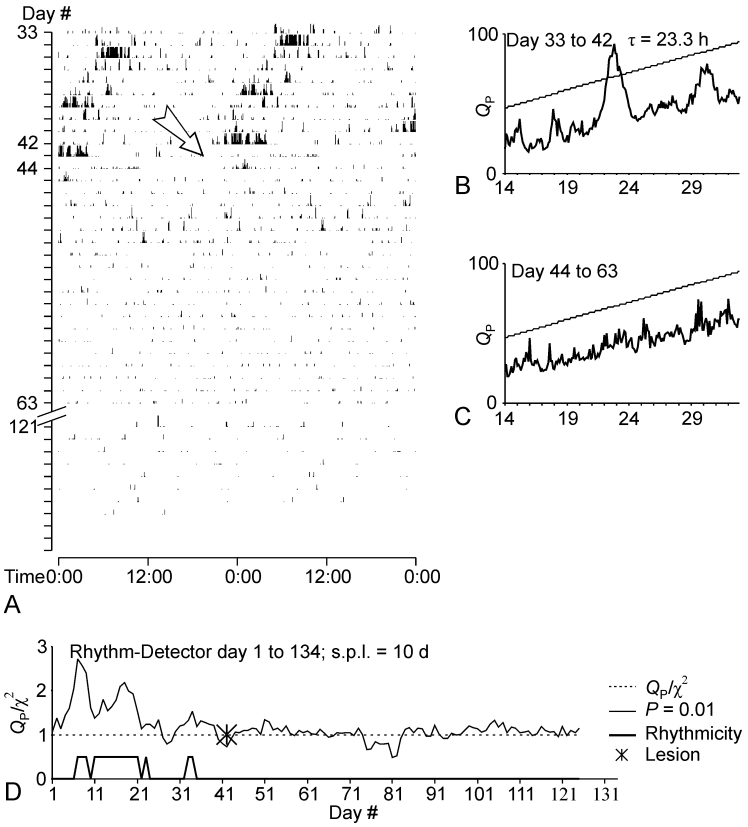

Fig. 5. Locomotor activity of a postoperatively arrhythmic animal with the AMe lesioned with a glass pipette (animal ID 15 in Table 2). **A:** The double-plot activity histogram shows circadian rhythmic wheel-running activity (period length $\tau = 23.3$ h) in constant darkness before the operation (**B:** χ^2-periodogram, day 33–42). After excision of the AMe (arrow in A, day 43) the animal became immediately arrhythmic (**C:** χ^2-periodogram, day 44–63) with a low amount of activity. **D:** The animal never regained rhythmic activity throughout its lifetime as indicated by the activity histogram and the Rhythm Detector. The scan periodogram plot (Q_P/χ^2) over the complete length of the wheel-running recording (day 1–134) detects rhythmic peaks in consecutive 10-day-χ^2-periodograms (solid line, Rhythmicity) only before removing of the AMe. s.p.l. = single periodogram length. For histology, see Fig. 6.

of the bars represent the number of revolutions per 5 min, truncated at 30 revs./min (Stengl and Homberg, 1994). To distinguish rhythmic from arrhythmic locomotor activity, χ^2-periodograms (Sokolove and Bushell, 1978) were used. For a more objective and automated judgment of postoperative rhythmicity, the "scan periodogram analysis with Rhythm Detector" was used, which was programmed in Visual Basic for Applications (VBA 6), and developed for assessing postoperative rhythmicity in AMe transplantation experiments (Chapters IV, V). Briefly, raw data were merged into 30 minute intervals and converted into Excel XP format. Over a defined single periodogram length (s.p.l.) of 8, 10 or 12 days the program calculated a χ^2-periodogram from day 1 to day X, then from day 2 to day X+1, until the last day of the recording. For every periodogram, the software determined maxima (Q_P = peak height), the period τ, the χ^2 for $p = 0.01$ at τ, and the width of the peak (at the intersection with the Sokolove significance line). To normalise Q_P against χ^2, the quotient Q_P/χ^2 was calculated and plotted against the number of the starting day of the respective single periodogram on the data record ("Q_P/χ^2"-curve in Fig. 3D). The according χ^2-value was normalised to 1 and plotted as well ("$p = 0.01$"-curve in Fig. 3D). Only peaks with threshold heights $\geq 20\,\%$ and widths ≥ 0.7 h, well above the values typically occurring in periodogram peaks in arrhythmic data, were chosen to indicate rhythmicity. In this case, an arbitrary value of 0.5 was assigned to the "Rhythmicity"-curve of the rhythm detector plot; otherwise the value was set to zero (Fig. 3D). Hence, a locomotor record was judged as rhythmic, if the post-operative scan periodogram analysis revealed peaks exceeding both thresholds for at least two consecutive days in at least one scan with 8, 10, or 12 days, respectively. Conventional χ^2-periodograms were generated with a respective function of the VBA-program *Tempus* which was used for the scan periodogram analysis.

Immunocytochemistry

Following activity recordings, brains of operated animals were dissected, fixed overnight in a formaldehyde/picric acid solution (aqueous Bouin's solution modified after Hollande; Romeis, 1989), washed in clear water, dehydrated in an ethanol series, and embedded in paraffin (Paraplast plus, Sigma, Germany). Serial frontal 10 μm sections were cut as ribbons, mounted on microscope slides, deparaffinised with xylene, and rehydrated in descending ethanols. The immunostaining was performed using anti-*Uca*-β-PDH-antiserum (# 3B3; Dircksen et al., 1987) at a concentration of 1:10,000, which was detected with the three-step peroxidase-anti-peroxidase method

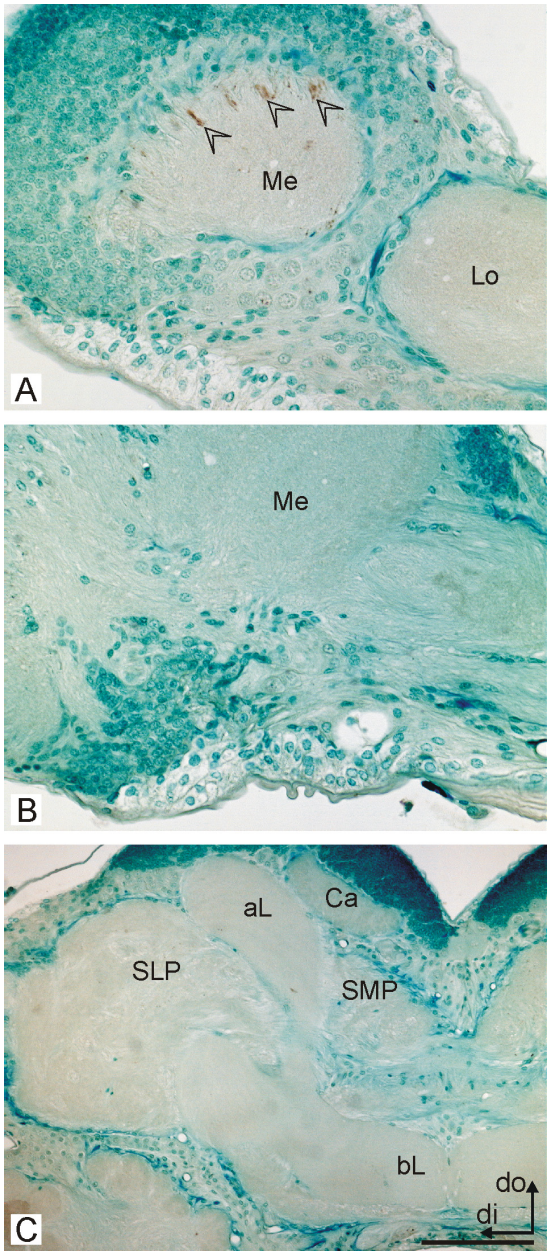

Fig. 6. The histological examination of the arrhythmic lesioned animal (shown in Fig. 5) revealed the complete loss of the anterior (**A**) as well as of the posterior PDH-ir medulla neurons (**B**). Nevertheless, PDH-ir fibres in the distal fibre-fan are present (arrowheads in A), indicating that they originate from the PDH-ir lamina cells, which were not affected by the lesion. The staining intensity of these fibres is weaker than in animals with intact or remnant PDHMe (Figs. 4, 8, 10). **C:** In the usual arborisation areas of PDH-ir fibres in the central brain (shown here is the right hemisphere), no PDH-ir fibres are recognisable. aL alpha lobe; bL beta lobe; Ca calyx of the mushroom body; Lo lobula; Me medulla; SLP, SMP superior lateral and medial protocerebrum, respectively. Scale bar in C = 100 μm in A,B, 200 μm in C. Coordinates in D: di distal, do dorsal for A–C.

according to Sternberger (1979; see also Reischig and Stengl, 1996). Detection of peroxidase was carried out with 3,3'-diaminobenzidine/H_2O_2 as chromogene. To visualise structures of not immunoreactive tissue, the paraffin sections were counterstained in 1 % methylene blue. Parallel to the experimental animals, untreated animals were processed in the same way for control of stainings.

RESULTS

To determine the roles of the PDH-ir medulla neurons (PDHMe) in generating, maintaining, and communicating circadian timing information, lesions of the AMe and adjacent neurons were performed in free-running cockroaches combined with PDH immunocytochemistry. Prior to the actual lesions, the left optic lobe was removed, and the forerun activity was assessed in running-wheels under constant environmental conditions. Of the 45 animals treated in this way, 24 animals were lesioned; the other were excluded due to unstable locomotor activity rhythms. The average period length (τ) was 23.48 ± 0.34 h S.D. ($N = 24$) before the lesion experiments. Altogether 21 of the 24 operated animals survived in running-wheel assays for more than 13 days (average postoperative lifetime was 53 ± 28 days until the animals were sacrificed) and were evaluated further. Except one animal, which died before, all of them could be processed for immunocytochemistry. Three animals were used for controls and only sham-operated (see Materials and Methods). These animals maintained rhythmic activity with about the original period lengths and showed only slight variations in the amounts of activities (Fig. 3; Table 1). The histological reports showed no considerable variations compared to untreated animals in terms of integrity of the AMe and surrounding tissue, and number of anterior and posterior PDHMe (Fig. 4). Also the arborisation patterns of PDH-ir fibres in the treated optic lobe and the central brain was nearly normal, despite the fact that the PDH-ir fibres of the ventrolateral protocerebrum at the side of the sectioned optic lobes were lost, since this area does not receive contralateral PDH-ir input (not shown; compare Chapter VII).

To find an optimal lesion method which is easy to perform, and simultaneously allows for precise ablation of a defined tissue area of about 200–300 μm in diameter together with minimum damaging of the surrounding tissue, three different procedures were tested. All methods were previously tested on normal cockroaches to optimise the handling, before they were applied to the experimental animals. Combining the results of all methods, successful lesions in respect of postoperative arrhythmia were obtained in half of the lesioned animals (Table 1, Fig. 5). Rhythmicity was assessed by inspection

Table 1. *Correlations between postoperative rhythmic activity and remaining and/or regenerated central PDH-ir projections after AMe lesions*

	Rhythmic			Arrhythmic		
Lesions ($N = 18$)	9 (50 %)			9 (50 %)		
Controls ($N = 3$)	3 (100 %)			0 (0 %)		
	+PDH:	–PDH	no histol.	+PDH	–PDH	no histol.
AMe-transplantations	8	0	1	4	5	0
Controls	3	0	0	0	0	0

N represents the numbers of rhythmic and arrhythmic lesioned and control animals according to rhythm detector evaluation (see Material and Methods). The lesions contain 10 lesions by punching out of AMe tissue, two lesions with a small needle, and six lesions performed by electro-coagulation. +PDH and –PDH indicates the number of cockroaches with or without prominent remaining and/or regenerated PDH-ir fibres in the central brain, respectively. no histol.: number of specimen without histological examination.

of the activity histograms and confirmed by evaluation with the "Rhythm Detector" (see Materials and Methods). Since five of these animals showed no remnant or regenerated PDH-ir fibres in the central brain (Fig. 6), four of them showed at least sparse arborisations in some or all typical arborisation areas ipsi- and/or contralaterally to the lesioned side (Table 2). Nevertheless, all of these arborisations showed abnormal patterns and resulted from secondary sprouting of few somata which were left over either in the lesioned optic lobe or in the stump of the sectioned, left optic lobe (not shown). These left-over somata always belonged to the medium sized and/or large type of anterior PDHMe. All of the arrhythmic animals showed profound damages in the region of the AMe, and lost all or most of the anterior PDHMe. However, in most of these animals the posterior PDHMe were left intact (Table 2).

Contrarily, none of the eight animals which showed rhythmicity directly or later after the operation, showed a total lack of PDHMe in the optic lobes, or of PDH-ir fibres in the central brain. Six of them, among them all lesion experiments performed with the coagulator and one by the needle, showed no conspicuous damage of the anterior PDHMe or the AMe at all (Table 2); however, in two of them the posterior PDHMe could not be found. The PDH-ir arborisations in the central brains of these animals were indistinguishable from that of the control animals. Despite normal postoperational fluctuations in the amount of activity, no conspicuous changes in the circadian parameters of their behaviour were detectable. The remaining two animals, however, showed substantial changes in the circadian activity combined with substantial reduction or complete loss of the anterior PDHMe. One animal (# 38 in Table 2) showed only episodic, but still circadian rhythmic locomotor activity after lesion, with a longer period length compared to the forerun activity (Fig. 7). It had only one remaining large PDHMe in the lesioned optic lobe, and showed a largely complete AMe with an undamaged group of posterior PDHMe (Fig. 8). Remaining PDH-ir fibres, which also showed some regeneration activity, could be found in all typical arborisation areas despite the VLP of the side contralaterally to the lesioned optic lobe.

The other animal (# 39 in Table 2) showed only signs of rhythmic behaviour directly after the operation or episodically during the following weeks, but 61 days after lesion it began with clear circadian rhythmic locomotion with a period length equally to the forerun period length (Fig. 9). Surprisingly, this animal lacked all the anterior PDHMe, and showed only sparse remnants of an AMe in the treated optic lobe. On the other hand, it showed two posterior PDHMe. These cells projected into the central brain and innervated the superior lateral and superior medial protocerebrum of the central brain ipsilaterally to the lesioned optic lobe (Fig. 10).

All lesioned animals, even those without any PDHMe, still showed PDH-ir fibres in the distal fibre-fan of the medulla that connects the AMe to the lamina (Fig. 6). Since the staining intensity was rather week in animals which lacked the anterior as well as the posterior PDHMe, the staining was more conspicuous if the posterior PDHMe were still present (Fig. 10).

The three lesion methods employed showed very different results in achieving arrhythmicity. Most successful were lesions obtained by punching out the AMe with glass pipettes; eight of ten animals were postoperatively arrhythmic, the remaining two showed substantial lesions of the AMe (Table 2). Lesions performed by use of a fine needle were tested in only two animals; one of them was arrhythmic with total loss of anterior and posterior PDHMe and AMe, the other nearly undisturbed in rhythmic behaviour as well as in the histology of the AMe and PDHMe. The lesions by electro-coagulation with the coagulator settings reported (see Mate-

Table 2. *Distribution of remaining and/or regenerated PDH-ir fibres in the central brain of AMe-lesioned animals*

Animal ID	Operation	*n* PDH-ir somata in			Prominent PDH-ir arborisations in right and/or left			
		right aPDHMe	right pPDHMe	left OL stump	SMP	SLP	VLP/ ILP	POTu
Arrhythmic								
1	Punched out	0	3	2	–	–	–	–
2	Punched out	4	3	0	–	+	+	–
3	Punched out	1	4	0	–	–	–	–
5	Punched out	0	4	0	–	–	–	–
15	Punched out	0	0	0	–	–	–	–
16	Punched out	2	4	5	+	+	+	+
40	Punched out	0	5	2	+	+	+	+
42	Punched out	2	3	0	+	+	+	+
21	Needle	0	0	0	–	–	–	–
Rhythmic								
38	Punched out	1	6	0	+	+	+	+
39	Punched out	0	2	0	+	+	–	–
20	Needle	12	0	0	+	+	+	+
26	Coagulation	10	0	0	+	+	+	+
27	Coagulation	12	0	0	+	+	+	+
30	Coagulation	12	4	0	+	+	+	+
31	Coagulation	11	3	0	+	+	+	+
35	Coagulation	13	4	1	+	+	+	+
06	Sham	12	4	2	+	+	+	+
10	Sham	10	2	0	+	+	+	+
11	Sham	12	0	0	+	+	+	+

All animals which remained rhythmic after operation showed remaining and/or regenerated PDH-ir fibres in the superior median and superior lateral protocerebrum (SMP and SLP, respectively), but not necessarily in the ventrolateral and inferior lateral protocerebrum (VLP and ILP, respectively), nor in the posterior optic tubercle (POTu). The PDH-ir arborisations in the arrhythmic animals are fibres regenerated from somata which were left over in one of the optic lobes (OL). aPDHMe: anterior PDH-ir medulla neuron somata; pPDHMe: posterior PDH-ir medulla neuron somata. The right optic lobes (in respect to the animal's body axis) were the lesioned ones, whereas the left optic lobes were removed several weeks prior the actual lesion.

rials and Methods) were not successful. All six animals remained postoperatively rhythmic, five of them showed no conspicuous damages of PDHMe or AMe; the remaining one died prior to histological examination.

Ablation of the AMe by electro-coagulation: finding of the settings

For future use of the coagulator to achive defined microlesions in the AMe of cockroaches, it was attempted to find optimal settings of the coagulator together with the most suitable electrode type. In a series of 16 experiments where the right AMe was tried to lesion by employing the operation procedure already described, different values for current intensity and current duration were tested. One week after lesion, the animals were sacrificed. The brains were stained with anti-PDH-antiserum and histologically examined. Since current intensities were to small to be reliabley read from the ampéremeter of the coagulator, they were not recorded (see Materials and Methods). Therefore, current intensity is expressed as the setting of the power dialer knob of the coagulator. The tested settings together with the results achieved are shown in Table 3. Current values in a range of 8–10 delivered for 15–20 seconds with a 0.5 MΩ tungsten electrode were necessary to achieve significant lesions of the AMe, i.e., detectable damages of tissue, reduction of the AMe, and loss or at least substantial decrease of numbers of anterior PDHMe somata (Fig. 11). With these and yet with lower current intensity settings, bubbles forming at the tip of the electrode could be observed. Additionally, due to heat production noticeable wrinkling of the neurolemma around the electrode penetration site could be observed during current delivery. Nevertheless, the lesions were clearly located in the region of the AMe, and surrounding tissue took no significant damage.

DISCUSSION

To investigate the role of the accessory medulla (AMe) and the PDH-ir medulla neurons (PDHMe) in generating circadian rhythmic locomotor activity

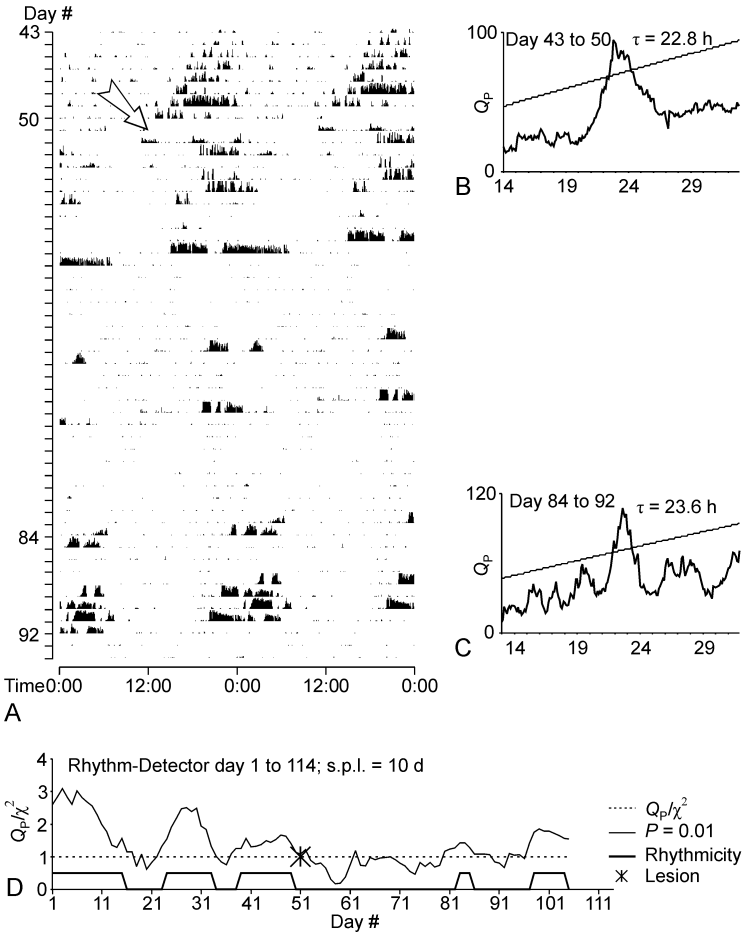

Fig. 7. Locomotor activity of an animal which AMe was lesioned with a glass pipette (animal ID 38 in Table 2). It shows episodic rhythmic behaviour after the operation. **A:** The double-plot activity histogram shows circadian rhythmic wheel-running activity (period length $\tau = 22.8$ h) in constant darkness before the operation (**B:** χ^2-periodogram, day 43-50). After the lesion (arrow in A, day 51) the animal appears to stay rhythmic with altered phase and period (which however is not apparent in the rhythm detector, D). If activity reappears episodically at higher level, the animal behaves rhythmic with a period of 23.6 h (**C:** χ^2-periodogram, day 84–92). **D:** These rhythmic episodes were also found in the Rhythm Detector plot. The scan periodogram curve (Q_P/χ^2) over the complete length of the wheel-running recording (day 1–114) detects rhythmic peaks in consecutive 10-day-χ^2-periodograms (solid line, rhythmicity) before as well as in two activity episodes after the lesion. s.p.l. = single periodogram length. For histology, see Fig. 8.

in the cockroach *L. maderae*, lesions of the AMe and adjacent neuronal somata on free-running animals were performed, and after at least several weeks of activity recording, the brains were examined with PDH-immunocytochemistry. It was shown that successful lesions of the AMe together with substantial reduction of the anterior PDHMe in most cases led to arrhythmic locomotor behaviour; there, the PDH-ir central brain projections were either absent, or, if present, abnormally regenerated. No animal without PDH-ir fibres in the central brain showed postoperative circadian rhythmic locomotor activity, suggesting that the PDHMe, or a subset of them, are responsible for the generation of circadian rhythms and/or transmitting timing information from the optic lobe pacemaker to the central brain. The results of two animals indicate that the presence of only one large anterior PDHMe or only the posterior PDHMe alone may be sufficient to maintain rhythmic behaviour, respectively. Test experiments engaging an electro-cauterisation device achieved precise and locally confined lesions and suggest the coagulator the instrument of choice for further lesion experiments.

Comparison of the lesion methods

The most successful method in the experimental series was to punch out AMe-tissue with a specially prepared glass pipette. After lesion, 8 animals behaved arrhythmic with partially or complete loss of anterior PDH-ir neurons, while another 2 animals stayed rhythmic but with partial destruction of the PDHMe. Nevertheless, this method offers some difficulties in handling, because the pipette has to be conducted by hand. Therefore, the process of punching out leads to deformation of the brain, and includes the great risk of unintentional destruction of surrounding brain structures. Hence, it is quite difficult to confine the lesion to the desired area. Lesions by use of a fine needle are similarly uncomfortable for the same reasons, and were given up after application to two animals, although it was successful in one case.

The application of the coagulator appeared more promising, because invasive rupturing of the neurolemma prior lesion was dispensable. Further, lesions should occur in defined areas around the tip of the electrode, which can be accurately placed inside the tissue. Nevertheless, the first six trials on experi-

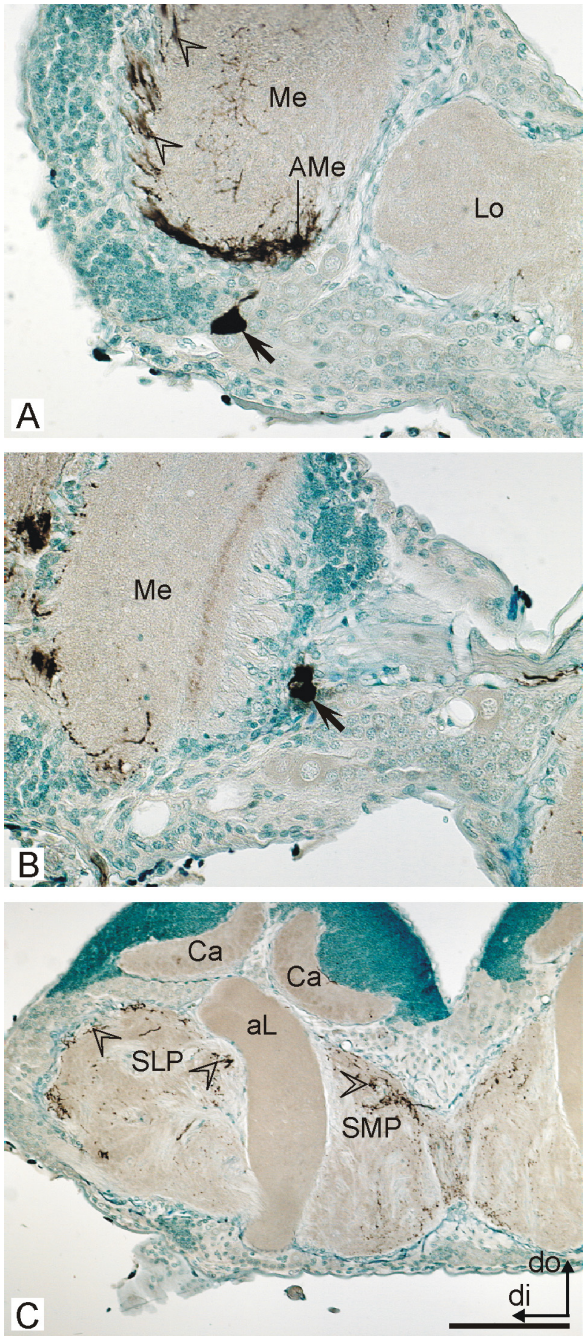

Fig. 8. The histological examination of the animal shown in Fig. 7 revealed one remaining large anterior PDH-ir medulla neuron (**A:** arrow), parts of the accessory medulla (AMe), and all posterior PDHMe (**B:** arrow) in the lesioned optic lobe. PDH-ir fibres are also present in the distal fibre-fan (arrowheads in A) and in the midbrain. **C:** PDH-ir fibres in the midbrain (arrowheads) appeared to be regenerated into their original projection areas, the superior lateral and medial protocerebrum (SLP and SMP, respectively). Spotted PDH-ir staining originate from neurons of the *pars intercerebralis*. aL alpha lobe; Ca calyces of the mushroom body; Lo lobula; Me medulla. Scale bar in C = 100 μm in A, B, 200 μm in C. Coordinates in C: di distal, do dorsal for A–C.

mental animals after adjusting apparently reasonable settings of the coagulator on test animals were rather disappointing; none of the animals showed considerable irregularities in behaviour, and showed no conspicuous damages of the AMe or anterior PDHMe somata; only two animals lacked posterior PDHMe. Therefore, a series of test experiments was performed where animals were lesioned with longer current application times and increased power of the coagulator, and, after one week, histologically analysed. Those higher coagulator settings were avoided in the first experiments, since it was known from previous test experiments, that they result in wrinkling of the neurolemma and formation of steam bubbles at the lesion site due to extensive heat production. The manual of the coagulator explicitly advised to avoid such incidents. Surprisingly, defined coagulations of a tissue area of about 200–300 μm were achieved not until the power knob was set to 8–10 (according to a source voltage of 250–280 V; calculated current up to 0.56 mA with 0.5 MΩ electrode) and current was delivered for 15–20 seconds through a 0.5 MΩ tungsten electrode. Since coagulation depends on current strength and resulting heat production in the tissue around the tip of the electrode, it is assumed that it may be now possible to achieve even smaller but defined lesions with use of 1 MΩ electrodes, but with those high power settings reported here. This will in future allow to achieve targeted lesions of subsets of the PDHMe, and the coagulator will constitute a precise instrument to unreveal the role of subcompartments of the AMe or subpopulations of the AMe neurons in generating, transmitting and entrainment of circadian rhythms in the cockroach.

The role of the PDH-ir medulla neurons in the circadian clock

Roberts (1974) and Sokolove (1975) reported that lesions in the optic lobes in an area between medulla and lobula consistently abolishes circadian rhythmic locomotor activity in free-running cockroaches. However, the absence of rhythmic activity is not a compelling evidence that the pacemaker itself, and not only auxiliary structures were deleted by the lesion. However, it was convincingly shown by transplantation experiments that indeed the pacemaker controlling phase and period of the circadian locomotor rhythm is situated in the optic lobes (Page, 1982) and there, in the region of the AMe (Chapter IV). Nevertheless, lesion experiments are still an appropriate instrument to uncover properties of the function of the clock and its components. Now, much more is known about the elements which obviously form the clock: the AMe as integration and processing centre for timing information, together

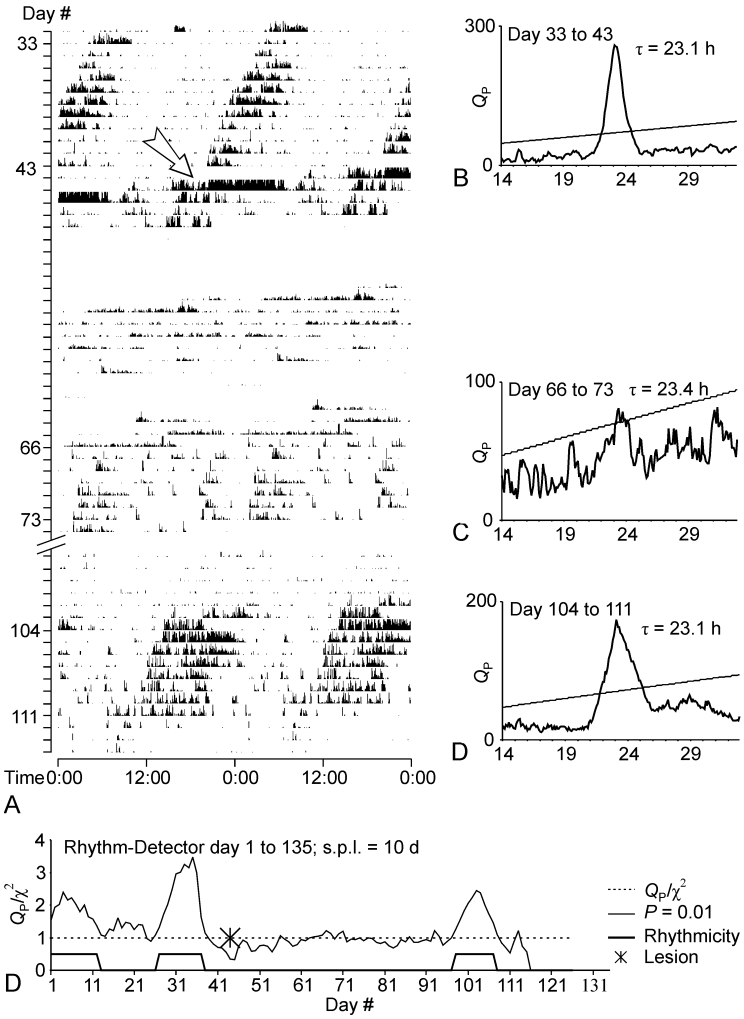

Fig. 9. Locomotor activity of an animal lesioned with a glass pipette (animal ID 39 in Table 2), which shows fluctuating rhythmic activity during two months after the operation. It regained clear rhythmic activity after 58 days postoperatively. **A:** The double-plot activity histogram shows circadian rhythmic wheel-running activity (period $\tau = 23.1$ h) in constant darkness before the operation (**B:** χ^2-periodogram, day 33–43). After the lesion (arrow in A, day 44) the animal appears to stay rhythmic for four days, before it became inactive. Episodic activity with a low rhythmicity reappears (**C:** χ^2-periodogram, day 66–73), which but is not detectable in the Rhythm Detector plot (**E**). Beginning with day 104, clear circadian rhythmic activity reappears with a period of 23.1 h (**D:** χ^2-periodogram, day 104–111), which is also detected in the Rhythm Detector plot (E). s.p.l. = single periodogram length. For histology, see Fig. 10.

with the adjacent neurons which are arranged in morphologically distinguishable groups (Petri et al., 1995; Chapters I, II, VI, VII). Precise lesions aimed to selectively delete certain neuronal groups should largely contribute to solve the questions which of these elements are involved in peculiar clock functions like rhythm generating, entrainment or clock output. In the present work, appropriate methods for AMe lesions were developed, and already some interesting preliminary results were obtained. It could be confirmed that expression of rhythmic behaviour depends on the presence of PDH-ir fibres in the central brain, first of all in the superior lateral and medial protocerebra (compare Stengl and Homberg, 1994; Chapter IV). No animals, which were postoperatively rhythmic, lacked PDH-ir processes in these areas, contrarily to many arrhythmic animals, which showed no PDH-ir fibres in the superior lateral and medial protocerebrum. Therefore, in the cockroach brain these areas are probably the most important relay stations for transmitting timing information of the clock into rhythmic behaviour. A homology of the superior lateral and medial protocerebra of the cockroach to the output sites of fibres originating from the PDH-ir small lateral neurons in *Drosophila* (Helfrich-Förster, 1995) in the dorsal protocerebrum is very likely. Nevertheless, three postoperatively arrhythmic animals still showed PDH-ir fibres in both the superior lateral and medial protocerebra, as well as in other areas in the central brain. They emerged from PDHMe somata which were left over in the stump of the severed left optic lobe and/or at the site of the AMe-lesion of the right optic lobe. These fibres were sparse and apparently resulted from secondary regeneration processes, since they showed a conspicuous sprouted appearance rather than the well-organised arborisation pattern of PDH-ir fibres known from normal animals. Probably, these fibres failed to reestablish circadian rhythmic activity until the animals were sacrificed; such a reestablishing process can last up to several months (Stengl and Homberg, 1994; Chapter IV). Another explanation would be that these fibres originate from a population of PDHMe, which may

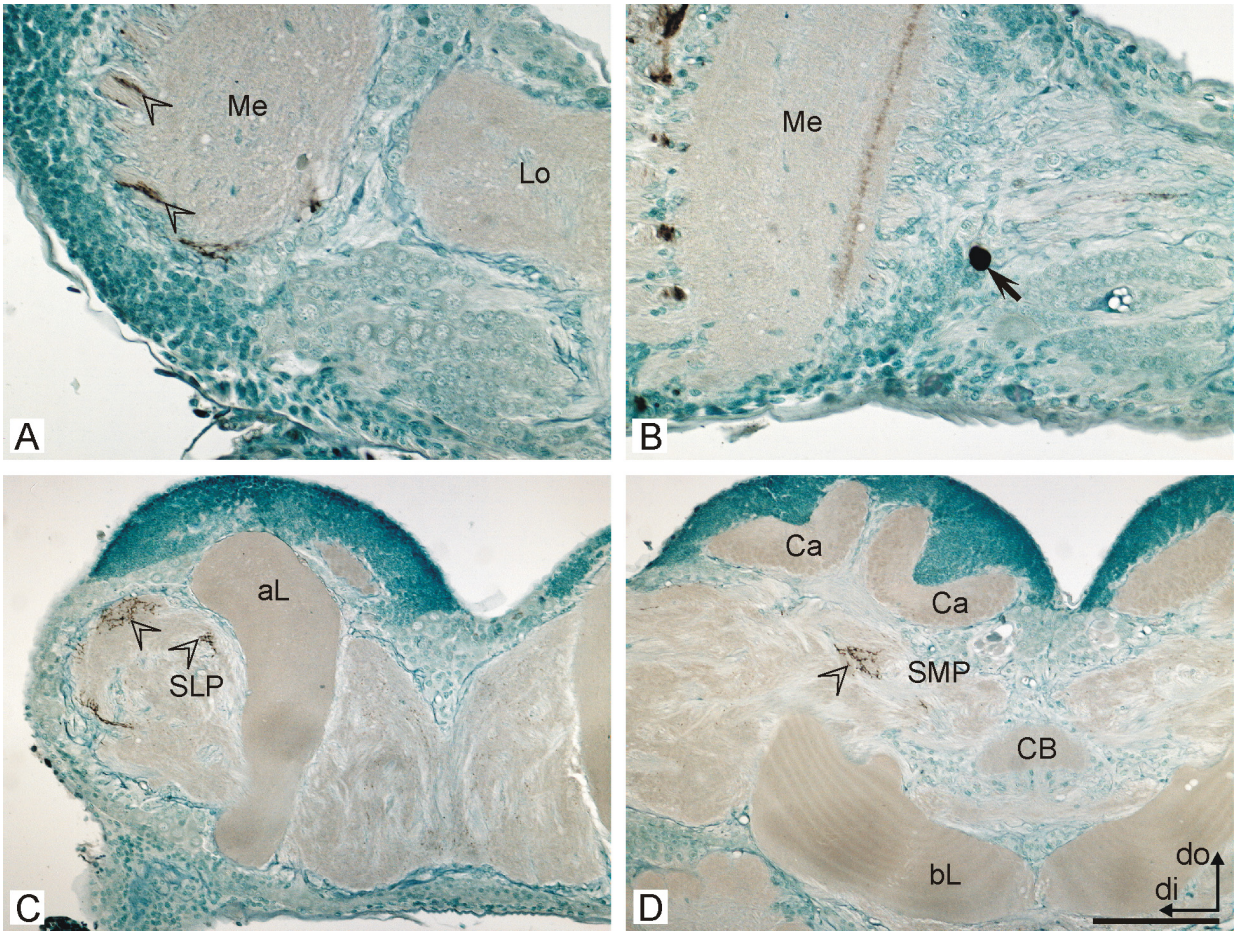

Fig. 10. The histological examination of the animal which activity is presented in Fig. 9 shows no anterior PDH-ir medulla neurons (**A**), no accessory medulla, and the animal retained only two posterior PDH-ir medulla neurons (**B:** arrow) in the treated optic lobe, which arborised in the central brain. Arrowheads in A: PDH-ir fibres in the distal fibre-fan of the medulla are more intensely stained than in animals without PDHMe (Fig. 8); this suggests a participation of the posterior PDHMe to this structure. **C,D:** In the central brain, PDH-ir fibres originating from the posterior PDHMe (arrowheads) ramify exclusively in the superior lateral protocerebrum (SLP) and in a more posterior part of the superior medial protocerebrum (SMP). aL alpha lobe; bL beta lobe; Ca calyces of the mushroom body; CB central body; Lo lobula; Me medulla. Scale bar in D = 100 μm in A,B,D, 200 μm in C. Coordinates: di distal, do dorsal for A–D.

not be able to generate pacemaker activity by itself. However, the presence of these PDH-ir fibres in the midbrains of arrhythmic cockroaches does not argue against their probable role in the timing system of *L. maderae*.

On the other hand, animal # 38 showed postoperative rhythmic activity even with one single large anterior PDHMe left; the posterior PDHMe, however, were intact. This neuron arborised in all central brain areas typical for PDH-ir neurons, except the contralateral ventrolateral protocerebrum. It projected *via* the anterior optic commissure to contralateral brain areas; contralateral connections found in the posterior brain, however, obviously originated from secondary regeneration processes. The postoperative activity of this animal showed an altered circadian period length and an episodic pattern, with few days of pronounced activity followed by phases with no or low activity. This activity pattern was already observed in AMe-transplanted animals which secondary rhythmic activity after transplantation (Chapter IV). Presumably, single PDHMe may be able to maintain rhythmic activity, but for supporting a stable activity pattern and producing the normal period length, a complete set of mutually coupled pacemaker neurons appears to be necessary.

Until now, only indications for the anterior PDHMe to be involved in clock function were present. Animal # 39 however, provides the first evidence that also the posterior PDHMe might be able to sustain circadian rhythmic behaviour. Processes obviously originating from these cells arborise ipsilaterally in the superior lateral and medial protocerebrum. Nevertheless, this is the only animal showing these attributes. Three other animals (# 1,

Table 3. *Test series for evaluation of optimal coagulator settings for AMe-lesions*

Animal ID	Current dialer setting	Current duration (sec)	Electrode resistance (MΩ)	Forming of bubbles	Significant lesion achieved
1	2	10	1.1	–	–
2	2.25	10	1.1	–	–
3	2.25	10	1.1	+	–
4	2.5	10	1.1	–	–
5	2.75	10	1.1	–	–
6	3	10	1.1	+	–
7	3.5	10	1.1	+	–
8	3.75	10	1.1	+	–
9	4	10	1.1	+	–
10	4	15	0.5	+	–
11	5	10	1.1	+	–
12	5	15	0.5	+	–
13	6	15	0.5	+	–
14	8	15	0.5	+	+
15	8	20	0.5	+	+
16	10	15	0.5	+	+

Animals were subjected to AMe lesions with different settings of the coagulator (coagulation current power expressed in dialer settings, current duration expressed in seconds). While lesioning, the formation of steam bubbles could be already observed with power settings of 2.25. Nevertheless, substantial lesion effects could only be observed with a power setting of 8, and current applied for 15 seconds with a 0.5 MΩ tungsten electrode.

5, and # 40) without anterior but intact posterior PDHMe were arrhythmic, and two of them showed no PDH-ir fibres in the central brain. The remaining one with PDH-ir midbrain arborisations additionally had two somata left in the stump of the sectioned optic lobe, from which regenerated fibres sprouted into the midbrain. At least the posterior PDHMe are not mandatory for sustaining circadian rhythmicity, since in four rhythmic animals they were not detectable at all. This may even occur in normal animals, because among the animals without posterior PDHMe is one sham operated control animal. Noticeably, robust rhythmic activity in animal # 39 reappeared only two months after lesion. Therefore, the processes in the midbrain could have been ectopically regenerated and may not occur in normal animals. Moreover, these processes might originate from anterior PDHMe which might have been lost during the preparation. Nevertheless, animal # 39 posed some new and interesting questions about the composition of the circadian clock of the cockroach. More lesion experiments will be necessary to find out whether indeed the posterior PDHMe alone are able to maintain circadian rhythmic behaviour and/or branch in the midbrain also in other cockroaches.

The lesion experiments provided some additional insights into the anatomy of the PDH-ir neuron system of the cockroach. Until now it was not known whether the ramifications of the PDH-ir lamina neurons (PDHLa) are restricted to the lamina or whether they invade additional areas of the optic lobe. The two animals without any anterior or posterior PDHMe still showed PDH-immunoreactivity in the distal PDH-ir fibre-fan of the medulla reaching into the remnants of the AMe. Therefore, these fibres definitely originate from the PDHLa.

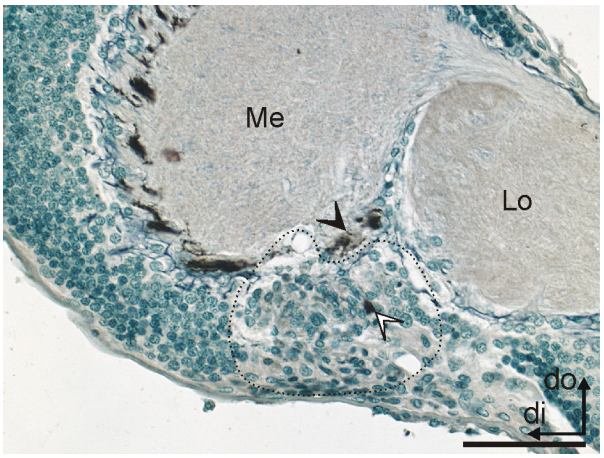

Fig. 11. Paraffin section with PDH immunostaining of the right optic lobe of a cockroach, which was AMe-lesioned by electro-coagulation. This animal participated in an experimental series performed to assess the optimum settings of the coagulator to obtain a complete lesion of the AMe and the anterior PDHMe. Here, the AMe was almost completely destroyed (filled arrowhead). Only one anterior PDH soma survived the treatment (open arrowhead). In the affected area (encircled by the dotted line) all large neuronal somata are destroyed (compare Fig. 4A). Glia cells with small and/or flattened dark nuclei have taken over the area, and caverns in the neuropil and soma region can be recognised. Scale bar = 100 μm. Coordinates: di distal, do dorsal.

In cases were only the anterior PDHMe were lesioned but the posterior PDHMe were still present, the PDH-ir staining of the AMe (or its remnants) and of the fibre-fan was much more intense. This indicates that the posterior PDHMe ramify in the AMe and project further *via* the distal fibre fan to the lamina, since the posterior PDHMe stain conspiciously darker than the PDHLa. The question whether a population of the posterior PDHMe indeed forms midbrain projections, or if all of them restrict their arborisations to the optic lobe, remains to be examined further.

ACKNOWLEDGEMENTS

We are very grateful to Heinrich Dircksen (University of Bonn, Germany) for providing the anti-β-PDH antiserum. This work was supported by the Deutsche Forschungsgemeinschaft (DFG) grants STE 531/7-1, 2, 3, and Human Science Frontier.

LITERATURE CITED

Dircksen H, Zahnow CA, Gaus G, Keller R, Rao KR, and Riem JP. 1987. The ultrastructure of nerve endings containing pigment-dispersing hormone (PDH) in crustacean glands: identification by an antiserum against a synthetic PDH. Cell Tissue Res 250:377–387.

Helfrich-Förster C. 1995. The period clock gene is expressed in central nervous system neurons which also produce a neuropeptide that reveals the projections of circadian pacemaker cells within the brain of *Drosophila melanogaster*. Proc Natl Acad Sci USA 92:612–616.

Helfrich-Förster C, Stengl M, and Homberg U. 1998. Organisation of the circadian system in insects. Chronobiol Int 15:567–594.

Homberg U, Reischig T, and Stengl M. 2003. Neural organisation of the circadian system of the cockroach *Leucophaea maderae*. Chronobiol Int, in press.

Homberg U, Würden S, Dircksen H, and Rao KR. 1991. Comparative anatomy of pigment-dispersing hormone- immunoreactive neurons in the brain of orthopteroid insects. Cell Tissue Res 266:343–357.

Nishiitsutsuji-Uwo J and Pittendrigh CS. 1968. Central nervous system control of circadian rhytmicity in the cockroach. II. The optic lobes, locus of the driving oscillator? Z vergl Physiol 58:14–46.

Page TL. 1982. Transplantation of the cockroach circadian pacemaker. Science 216:73-75.

Page TL and Block GD. 1980. Circadian rhythmicity in cockroaches: effects of early post-embryonic development and ageing. Physiological Entomology 5:271–281.

Petri B and Stengl M. 1997. Pigment-dispersing hormone shifts the phase of the circadian pacemaker of the cockroach *Leucophaea maderae*. J Neurosci 17:4087–4093.

Petri B, Stengl M, Würden S, and Homberg U. 1995. Immunocytochemical characterisation of the accessory medulla in the cockroach *Leucophaea maderae*. Cell Tissue Res 282:3–19.

Reischig T and Stengl M. 1996. Morphology and pigment-dispersing hormone immunocytochemistry of the accessory medulla, the presumptive circadian pacemaker of the cockroach *Leucophaea maderae*: a light- and electron- microscopic study. Cell Tissue Res 285:305–319.

Reischig T and Stengl M. 2002. Optic lobe commissures in a three-dimensional brain model of the cockroach *Leucophaea maderae*: a search for the circadian coupling pathways. J Comp Neurol 443:388–400.

Roberts SK. 1974. Circadian rhythms in cockroaches: effects of optic lobe lesions. J Comp Physiol 88:21–30.

Romeis B. 1989. Mikroskopische Technik. Munich: Verlag Urban und Schwarzenberg.

Sokolove PG. 1975. Localisation of the cockroach optic lobe circadian pacemaker with microlesions. Brain Res 87:13–21.

Sokolove PG and Bushell WN. 1978. The chi square periodogram: its utility for analysis of circadian rhythms. J Theor Biol 72:131–160.

Stanewsky R. 2002. Clock mechanisms in *Drosophila*. Cell Tissue Res 309:11–26.

Stengl M and Homberg U. 1994. Pigment-dispersing hormone-immunoreactive neurons in the cockroach *Leucophaea maderae* share properties with circadian pacemaker neurons. J Comp Physiol A 175:203–213.

Sternberger LA. 1979. Immunocytochemistry. New York: Wiley & Sons.

IV. Ectopic transplantation of the accessory medulla restores circadian rhythmic behaviour in arrhythmic cockroaches (*Leucophaea maderae*).

Reischig T and Stengl M. 2003. J Exp Biol 206:1877-1886

Ectopic Transplantation of the Accessory Medulla Restores Circadian Locomotor Rhythms in Arrhythmic Cockroaches (*Leucophaea maderae*)

Thomas Reischig and Monika Stengl

ABSTRACT

The presence of an endogenous circadian clock in the brain of an animal was first demonstrated in the cockroach *Leucophaea maderae*. However, the clock's cellular basis remained elusive, until pigment-dispersing hormone immunoreactive neurons, which express the clock genes *period* and *timeless* in *Drosophila,* were proposed as pacemaker candidates. In several insect species, pigment-dispersing hormone immunoreactive neurons are closely associated with the accessory medulla, a small neuropil in the optic lobe, which was suggested to be a circadian clock neuropil. Here we demonstrate that ectopic transplantation of adult accessory medullae into optic lobeless cockroaches restores circadian locomotor activity rhythms in *L. maderae*. All histologically examined cockroaches that regained circadian activity regenerated pigment-dispersing hormone-immunoreactive fibres from the grafts to original targets in the protocerebrum. The data show that the accessory medulla is the circadian pacemaker controlling locomotor activity rhythms in the cockroach. Whether pigment-dispersing hormone-immunoreactive neurons are the only circadian pacemaker cells controlling locomotor activity rhythms remains to be examined.

Indexing terms: Circadian Rhythms, accessory medulla, locomotor activity rhythms, pigment-dispersing hormone, pacemakers, cockroaches, *Leucophaea maderae*

Lesion experiments demonstrated for the first time that the locomotor activity rhythm of the cockroach *Leucophaea maderae* is controlled by two bilaterally paired and mutually coupled endogenous circadian pacemakers, which reside in the brains optic lobes (Nishiitsutsuji-Uwo and Pittendrigh, 1968; Roberts, 1974; Sokolove, 1975; reviewed by Helfrich-Förster et al., 1998). It was convincingly shown in lesion experiments that cockroaches without optic lobes remained arrhythmic throughout their lifetime. But, because arrhythmic locomotion does not indicate the absence of an intact circadian clock, the most compelling evidence for the location of the circadian clock in the optic lobes of the cockroach was provided by transplantation experiments (Page, 1982). After exchange of whole optic lobes between animals with different circadian periods, the cockroaches regained circadian locomotor activity several weeks after the transplantation. Interestingly, the regained circadian period was controlled by the transplanted optic lobe (Page, 1982; 1983). The next step in localising the oscillator in the cockroach was the discovery of the PDH-immunoreactive (PDH-ir) neurons, which share properties predicted for circadian pacemaker neurons (Homberg et al., 1991; Stengl and Homberg, 1994; Petri et al., 1995; reviewed by Helfrich-Förster et al., 1998). The PDH-ir neurons are associated with the accessory medulla (AMe), a small neuropil situated at the ventromedial edge of the medulla of the optic lobe (Homberg et al., 1991; Petri et al., 1995; Reischig and Stengl, 1996). Although lesion and transplantation experiments demonstrated that

the suprachiasmatic nucleus (SCN) is necessary and sufficient for the control of circadian locomotor activity rhythms in mammals (Stephan and Zucker, 1972; Inouye and Kawamura, 1979; Sawaki et al., 1984; Ralph et al., 1990; Silver et al., 1996), conclusive evidence for the localisation of the circadian clock in insects is still missing. In *Drosophila melanogaster* PDH-ir lateral neurons contain the clock proteins PERIOD and TIMELESS, and these neurons have been suggested to be circadian pacemaker neurons in fruitflies and cockroaches (Zerr et al., 1990; Ewer et al., 1992; Helfrich-Förster and Homberg, 1993; Stengl and Homberg, 1994; Frisch et al., 1994; Helfrich-Förster, 1995; 1998; 2001; reviewed by Helfrich-Förster et al., 1998). In the absence of the lateral neurons, however, weak rhythmic activity still remains (Helfrich-Förster, 1998), and in the absence of the peptide pigment-dispersing factor, fruitflies remain rhythmic with a shorter period for a few days in constant darkness before becoming arrhythmic (Renn et al., 1999). Thus, to clearly identify the insect circadian pacemaker it has to be shown that transplantation of the pacemaker candidate suffices for rhythm generation in arrhythmic animals. Here we show that ectopic transplantation of fully differentiated AMe tissue grafts to optic lobeless cockroaches restores circadian locomotor activity. Furthermore, we demonstrate histologically that transplanted PDH-ir neurons regenerated to their original targets in the midbrain. The data show that the AMe is the circadian pacemaker controlling locomotor activity rhythms in the cockroach. Because only a small number of animals with regained rhythmicity could be examined histologically, it cannot be excluded that, adjacent to PDH-ir neurons, there are also other circadian pacemaker candidates.

MATERIALS AND METHODS

Animals

To obtain cockroaches (*Leucophaea maderae* Fabricius) with different endogenous circadian periods, two populations were reared in different light regimens (11 h: 11h light:dark (L:D) and 13 h:13 h L:D; 25 °C and 30 % relative humidity) according to Page and Block (1980). The animals were fed with dried dog food, potatoes, and water *ad libidum*.

Surgery

All operations were performed on male cockroaches under steady CO_2 anaesthesia. Cell culture medium

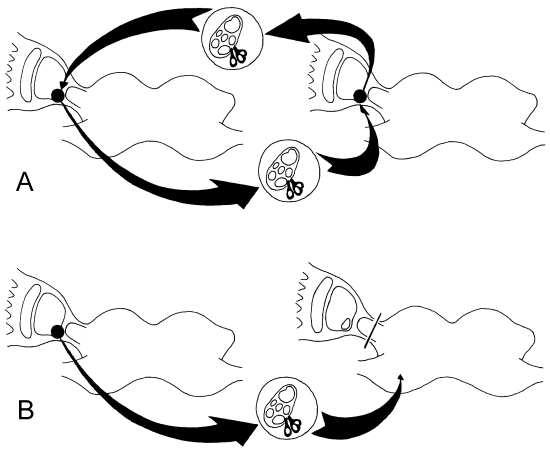

Fig. 1. Illustration of the two transplantation methods used in this study. **A:** Accessory medulla (AMe)-grafts were exchanged between animals raised in 11 h:11 h L:D and 13 h:13 h L:D cycles. The left (in respect to the body axis) optic lobes were sectioned at least three weeks before the transplantations. **B:** The AMe-grafts (in control experiments: medulla-grafts) were transplanted into the right antennal lobe of host animals. The remaining right optic lobes were subsequently removed. See Materials and Methods for further details.

(L 15, Gibco, Eggenstein, Germany) containing penicillin and streptomycin was used to rinse the wounds. For the initial left optic lobe (OL) section, a triangular cuticular flap was cut into the head capsule to expose the OL. With an iridectomy scissor, the optic nerves and the optic stalks were cut, and the OL was removed; the cuticle was flapped back in place and sealed with wax.

For transplantation of AMe tissue into the right antennal lobe (AL) of a host cockroach (Fig. 1B), its right brain hemisphere was exposed. With a razorblade fragment, a pocket was cut into the right AL. Then, the donor animal was decapitated, its brain exposed, and the perineurium of one OL was removed. According to external markers, tissue containing the AMe with its adjacent PDH-ir cells (in controls: tissue out of the adjacent medulla) was excised from the donors brain with a fine glass pipette (tip-∅ 150–250 μm). The tip of the pipette was stuck into the AL of the host animal, the graft tissue was carefully blown out, and occasionally its position was corrected with an eyebrow hair. Then, the right optic lobe was removed; the cuticle was flapped back in place and sealed with wax. In the OL-to-OL transplantations, animals were donors and host at the same time (Fig. 1A) and the AMe graft was implanted into the location of the host's removed AMe.

Activity analysis

Locomotor activity was monitored in running-wheels in constant darkness at 26 °C as described previously (Stengl and Homberg, 1994). Activity was visualised with double-plot activity histograms; the heights of the bars represent the numbers of revolutions per 5 min, truncated at 30 revs./min (Stengl and Homberg, 1994). To distinguish rhythmic from arrhythmic locomotor activity (Figs. 2, 3) we used χ^2-periodograms and MESA (mass entropy spectral analysis; Dowse and Ringo, 1989), and averaged locomotor activity plots per circadian day, to scrutinise rhythmic data obtained. For a more objective, automated judgement of rhythmicity, we developed a new software in Visual Basic for Applications (VBA): the "scan periodogram analysis with Rhythm-Detector" allows distinction between rhythmic and arrhythmic episodes in long data sets. Raw data were merged into 30-minute intervals and converted into Excel 97 format. χ^2-periodograms were calculated with VBA according to the algorithms of Sokolove and Bushell (1978). The "scan periodogram analysis" was performed as follows: Over a defined single periodogram length (s.p.l.) of at least $X = 8$ days the program calculated a periodogram from day 1 to day X, then from day 2 to day X+1, until the last day of the recording. For every periodogram, the software determined the maximum (Q_P = peak height), the period τ, the χ^2 for $p = 0.01$ at τ, and the width of the peak at the intersections with the Sokolove significance line (SSL, $= \chi^2$ for $p = 0.01$). To normalise Q_P against χ^2, the quotient Q_P/χ^2 was calculated and plotted against the number of the starting day of the respective periodogram on the data record (Q_P/χ^2 curve in Fig. 3C). The according normalised χ^2 value is 1 and was plotted as well (χ^2 for $p = 0.01$ in Fig. 3C).

To distinguish "rhythmic" from "arrhythmic" periodogram peaks we averaged peak values from optic lobe-less cockroaches with no recognisable periodicities (see next paragraph). This analysis revealed 26.6 % of "arrhythmic" periodogram peaks exceeding the SSL. These peaks had low peak heights (9.2 ± 7.8 %; mean ± mean S.D., with $0\,\% = \chi^2$ and $100\,\% = 2 \times \chi^2$), and narrow widths ($0.3 \pm 0.1$ h), as compared with periodogram peaks calculated over rhythmic activity phases. Therefore, only peaks with heights $\geq 20\,\%$ and widths ≥ 0.7 h, well above the values of arrhythmic periodogram peaks, were chosen to indicate rhythmicity. In this case an arbitrary value of 0.5 was assigned to the "Rhythmicity"-curve of the Rhythm Detector plot; otherwise the value was set to zero (Fig. 3C). Hence, a locomotor record was judged as rhythmic, if the postoperative scan periodogram analysis revealed at least one peak with a peak height $\geq 20\,\%$ together with a peak width ≥ 0.7 h for at least 2 consecutive days (Fig. 3C). With MESA (Dowse and Ringo, 1989; with use of a demo version of El Temps 1.172, a chronobiological evaluation program written by Antoni Díez-Noguera, Barcelona, Spain) and averaged locomotor activity plots per circadian day, we confirmed rhythmicity in data sets obtained with our new evaluation software. Thus, we obtained a reliable, new, automated analysis-method for long data records with objective measures of short episodes of rhythmicity, which avoided subjective selection of data sets and misjudgement of randomly generated activity peaks.

For the averaged activity plots, the circadian period lengths of the activity episodes in question were determined. The activity values were processed into a matrix using the same algorithms as for periodogram analysis (Sokolove and Bushell, 1978), with the determined period lengths as the test period. The means ± S.D. of activity amounts for every 30 min bin representing the same circadian time were calculated. The circadian day was normalised to 24 hours. The activity onset of the first day of the examined activity episode was used as phase reference point and set to CT 12.

Analysis of "arrhythmic" periodogram peaks

To analyse height and width of periodogram peaks in actual arrhythmic data records, we selected 30 bilobectomised, arrhythmic animals (as judged by eye on activity histograms and selective χ^2-periodogram analysis). Using the "scan periodogram analysis", we calculated consecutive 10-day χ^2-periodograms (day 1 to 10, day 2 to 11 etc.; $n = 3445$ for all animals) over the whole postoperative data records. The means ± S.D. of the heights and widths of all periodogram peaks that exceeded the SSL were calculated for every animal. Then, the total mean, as well as the mean of the standard deviations for all 30 animals was calculated.

Moreover, we performed the periodogram peak analysis described above on randomly permutated activity data records (with Monte Carlo simulations) of 10 untreated, freerunning cockroaches with prominent circadian rhythmic locomotor activity. The data records were about 10 weeks long, and every record was randomised and subsequently analysed 10 times. This resulted in a total of 7020 single periodograms, of which 88.1 % showed peaks exceeding the SSL. The mean height of these peaks was 10.2 ± 9.8 %, and the mean width 0.2 ± 0.1 h; these values are within the range obtained by the respective evaluation of the generically arrhythmic animals and therefore, further support the rhythmicity-

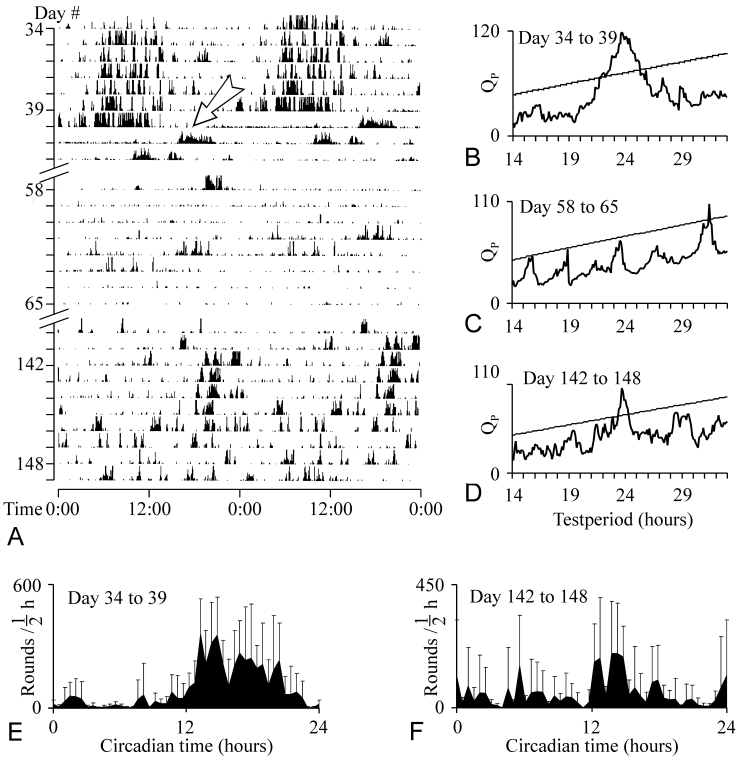

Fig. 2. Regained circadian rhythmic locomotor activity in an optic lobe-less cockroach after transplantation of one accessory medulla into the antennal lobe (animal ID 13/84, Table 2). **A:** Double-plot activity histograms show circadian wheel-running activity ($\tau = 24.2$ h) in constant darkness before the operation (**B:** day 34–39, χ^2-periodogram). The operated cockroach is arrhythmic for 101 days after the operation, as shown in the χ^2-periodogram (**C:** day 58–65). Then, the cockroach regains rhythmic activity with $\tau = 23.7$ h, as shown in the χ^2-periodogram analysis (**D:** day 142–148; periodogram peak height = 40.7 %, width = 1 h). Additionally, two activity plots show the mean locomotor activity ± S.D. of the animal during the course of a circadian day before (**E:** day 34–39) and after the transplantation (**F:** day 142–148). Histological data of this animal are shown in Fig. 4C,D.

threshold selected for the Rhythm-Detector. Interestingly, the number of periodogram peaks exceeding the SSL obtained with the randomly permutated data was much higher than in the arrhythmic animals. This is apparently due to a more even distribution of activity over the whole data records after the randomisation, compared with generically arrhythmic animals. This results in a more even distribution of the Q_P values just below the SSL in the periodograms and therefore, leads to a higher probability of single Q_P values to slightly exceed the SSL.

We further analysed permutated activity records of the mentioned rhythmic animals with our Rhythm-Detector analysis. Automated evaluation allowed us to perform 1000 permutations and subsequent analyses for every data record, with single periodogram lengths of 10 days. This resulted in a total number of 10,000 Rhythm-Detector analyses, of which 9 (0.09 %) indicated rhythmicity applying to the rhythmicity criteria stated above. Thus, the Rhythm-Detector judges 99.91 % of randomly permutated data records as arrhythmic and, thus, has a negligible error rate.

Immunocytochemistry

Following activity recordings, brains of operated animals were dissected, fixed in a formaldehyde solution (together with those of untreated animals to act as a control for staining), and either embedded in gelatine/albumin, or in paraffin. Serial sections (gelatine: 30 μm; paraffin: 10 μm) were cut and stained using anti-β-PDH-antiserum (Dircksen et al., 1987) with the three-step peroxidase-anti-peroxidase method according to Sternberger (1979; see also Reischig and Stengl, 1996); detection of peroxidase was carried out with 3,3'-diaminobenzidine/H_2O_2. The paraffin sections were counterstained in 1 % methylene blue.

To determine whether control or test animals regain rhythmicity in the locomotor assays cockroaches were left in the running-wheels for long as possible. Once the cockroach appeared to approach its natural death (when it became weak and showed either decreased or strongly increased activity) it was sacrificed and its brain was removed for immunocytochemistry. This focus on the long-term analysis of locomotor activity records of transplanted and control animals necessarily takes into account that several of the operated animals will die unexpectedly before they can be examined immunocytochemically.

RESULTS

To determine, whether the AMe with PDH-ir output neurons is sufficient for controlling locomotor activity rhythms in insects, we performed transplantation experiments in a large insect, the cockroach *L. maderae* (Figs. 1–4). Grafts containing the AMe with PDH-ir cells (Fig. 4A) were selectively excised

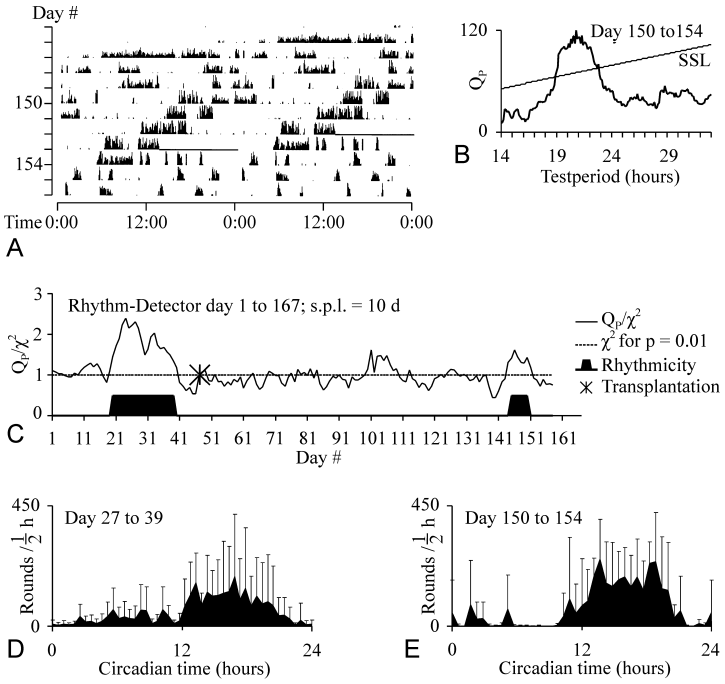

Fig. 3. Double-plot activity histogram (**A:** day 145–156) and χ^2-periodogram analysis (**B:** day 150–154; SSL = Sokolove significance line = χ^2 for $p = 0.01$) of another optic lobe-less cockroach (animal ID 13/21, Table 2) shows circadian wheel-running activity ($\tau = 20.8$ h) in constant darkness 148 days after the transplantation. The solid line at day 153 indicates computer failure. **C:** The rhythm scan periodogram plot (Q_P/χ^2) over the complete length of the wheel-running recording (day 1–167) detects rhythmic peaks in consecutive 10-day-χ^2-periodograms (Rhythmicity), before removal of the remaining optic lobe (day 19–39), and after the transplantation (day 143–151). s.p.l. = single periodogram length. Additionally, rhythmic activity can be seen in the two activity plots, which show the averaged locomotor activity ± S.D. of the animal during the course of a circadian day before (**D:** day 27–39) and after the transplantation (**E:** day 150–154).

from optic lobes of adult cockroaches using glass micropipettes, and transplanted into the brains of adult host cockroaches. Then, the host animals were set back into running-wheels to search for regained circadian locomotor activity. Because many wildtype cockroaches with intact circadian pacemakers do not show circadian locomotor activity in running-wheel assays, the absence of rhythmicity does not necessarily indicate the absence of an intact clock. Only positive behavioural evidence indicates the presence of an intact circadian clock (Stengl and Homberg, 1994). Thus, we wanted to know whether transplantation of the AMe alone, but not transplantation of adjacent medulla tissue allows recovery of circadian locomotor activity. In addition, we wanted to examine whether all cockroaches with regained circadian activity also show regeneration of ectopic PDH-ir neurons into original target areas in the protocerebrum. This would suggest that PDH-ir neuronal connections to the central brain are necessary for expression of circadian locomotor rhythms, especially since the PDH-ir somata only comprise 1 % of all grafted somata.

AMe-grafts measured about 150–250 μm in diameter, and included the neuropil of the AMe with about 1,000 associated cells (970 ± 258 (mean ± S.D., $N = 7$), among them 12 ± 4 (≈ 1 %) PDH-ir somata. By raising one group of cockroaches in an 11 h:11 h L:D cycle and another group in a 13 h:13 h L:D cycle, we obtained two populations of animals with significantly different endogenous periods in free-running activity rhythms (Page and Block, 1980; Page, 1982). In a total of 179 individuals ($N = 91$ for the 11 h:11 h L:D cycle, and $N = 88$ for the 13 h:13 h L:D cycle) the left optic lobe was removed. Then, the periods of the free-running locomotor activity rhythms of the one-lobed cockroaches were assessed in running-wheel assays (see Materials and Methods). Period lengths of these operated cockroaches were (mean ± S.D.) 22.56 ± 0.41 h ($N = 70$, 11 h:11 h L:D cycle), and 23.79 ± 0.33 h ($N = 58$, 13 h:13 h L:D cycle), respectively. Of the 179 animals 106 (54 in the 11 h:11 h L:D cycle, 52 in the 13 h:13 h L:D cycle) were selected for further experiments, while 73 cockroaches (41 %) were excluded because of a lack of stable rhythmic locomotor activity rhythms. Altogether 87 (82 %) of the 106 operated animals, which survived in running-wheel assays for more than 14 days (3.0 ± 1.5 months), were evaluated further, and, if they did not die before, were processed for immunocytochemistry. We focused on long-term analysis of locomotor activity records of transplanted and control animals to search for recovery of rhythmic activity. Thus, we favoured long-term survival at the expense of fast and frequent immunocytochemical analysis.

In a first set of transplantation experiments we exchanged the remaining AMe between cockroaches of different endogenous periods ($N = 7$). Animals were donors and hosts at the same time, thus, the graft was implanted into the space of the host's removed AMe (Fig. 1A). Two of the seven animals regained circadian locomotor activity (Tables 1, 2) four weeks after the transplantations. Immunocytochemistry in one of these specimens revealed PDH-ir somata ($n = 2$) at the transplantation site as well

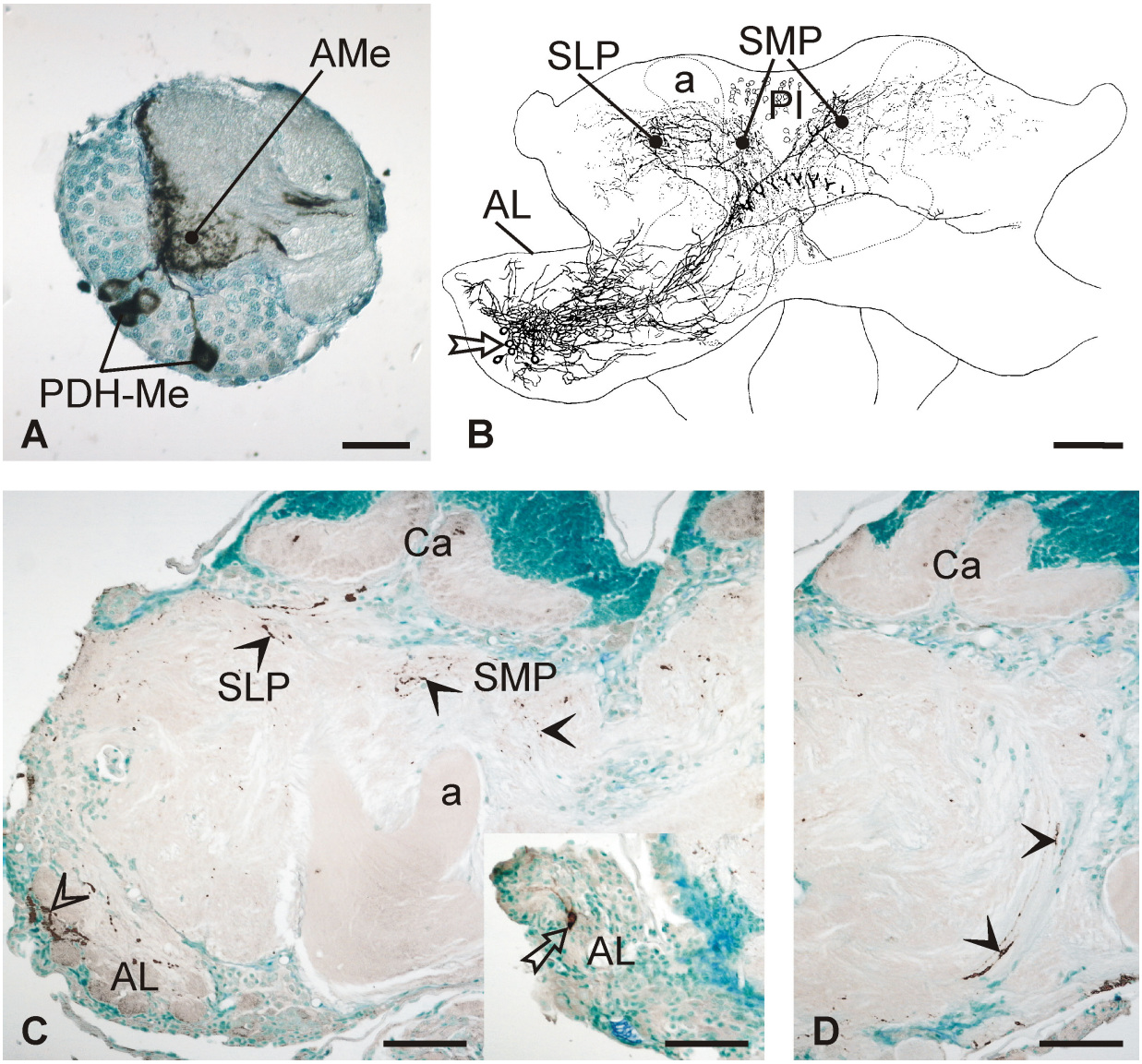

Fig. 4. PDH-immunoreactivity in an accessory medulla (AMe)-explant as used for transplantations (A), and in the central brains of two postoperatively rhythmic cockroaches (B–D). **A:** In the 10 μm paraffin section of an excised AMe-graft two large and two medium-sized PDH-ir medulla neurons (PDH-Me) send processes into the AMe. Counterstaining with methylene blue shows unstained somata next to the PDH-Me. **B:** Reconstruction of PDH-immunoreactivity in the brain of a postoperatively rhythmic cockroach (animal ID 11/16, Tables 2, 3). Three large and two medium-sized grafted PDH-ir cells in the antennal lobe (AL, arrow) project *via* new routes to original arborisation sites in the superior medial and superior lateral protocerebra (SMP and SLP, respectively). Faintly stained PDH-ir neurons in the *pars intercerebralis* (PI) give rise to spotted staining in the protocerebrum, which can be clearly distinguished from regenerated fibres. a, alpha lobe. **C:** Frontal brain section of the animal (animal ID 13/84, Tables 2, 3) in Fig. 2 with regenerated PDH-ir arborisations in the superior median and lateral protocerebra (SMP and SLP, respectively; arrowheads), and antennal lobe (AL, open arrowhead). Inset: Grafted large PDH-ir soma in the anterior AL (arrow). a, alpha lobe; Ca, calyces of the mushroom bodies. **D:** A more posterior slice of the same brain shows regenerated fibres invading the protocerebrum *via* the antenno-glomerular tract (arrowheads). Scale bars = 50 μm in A, 200 μm in B, 100 μm in C,D.

Table 1. *Correlation between regained rhythmic activity and regenerated central PDH-ir projections*

	Rhythmic			Arrhythmic		
AMe-transplantations ($N = 45$)	13 (29 %)			32 (71 %)		
Controls ($N = 42$)	5 (12 %)			37 (88 %)		
	+PDH:	–PDH	no histol.	+PDH	–PDH	no histol.
AMe-transplantations	4	0	9	10	8	14
Controls	1	0	4	2	19	16

N represents the number of rhythmic and arrhythmic operated and control animals according to Rhythm Detector evaluation (see Materials and Methods). The number of AMe transplantations comprises 7 transplantations into the optic lobe and 38 into the antennal lobe. +PDH and –PDH indicate the number of cockroaches with or without PDH-ir somata and regenerated PDH-ir fibres in the central brain, respectively. No histol. represents the number of specimens without histological examination.

as regenerated PDH-ir fibres in the midbrain (data not shown). Because it was difficult to unequivocally distinguish implanted PDH-ir neurons from remaining host PDH-ir cells, we continued with ectopic transplantations. In 45 experiments the AMe-graft was inserted into the right antennal lobe of arrhythmic cockroaches, which had both optic lobes removed (Fig. 1B). In one control group ($N = 22$) the remaining optic lobe was removed without further transplantations. In another control group ($N = 20$) the remaining optic lobe was removed and grafts of medulla tissue next to the AMe were transplanted into the host's antennal lobe.

After transplantation or control surgery, in most cases the locomotor activity was disrupted for several days, and then became arrhythmic. The amounts and patterns of arrhythmic locomotor activity largely varied between individuals as well as within the postoperative lifespan of a single individual. Rhythmic locomotor activity returned in several animals, but often became arrhythmic again. Based on these observations, we developed a new method for an automated search of shorter rhythmic episodes in long data records with rather strict standards for rhythmicity, to avoid biased judgement of periodicity (see Materials and Methods).

Applying this analysis, a total of 18 (21 %) out of the 87 animals examined, regained rhythmic locomotor behaviour (Tables 1, 2). Among the rhythmic animals were 13 cockroaches with AMe transplants and 5 controls (Tables 1, 2; Figs. 2, 3). Significantly more animals regained rhythmicity in the transplantation group (29 %) versus the control group (12 %), as tested with a single-tailed two-by-two frequency table, which involves a χ^2 test with one degree of freedom (df) ($\chi^2 = 3.82$, $p \geq 0.05$, $\mathrm{df} = 1$). As a second test, we applied a G-test of association, which compared the distributions of values between the AMe-transplanted and the control groups. We assumed the results of the control operations as the predicted values for the AMe-transplantations, if the transplantations would have no effect. Therefore, we would expect 6 rhythmic animals in the 45 AMe-transplantations. However, the frequency of rhythmic animals differed significantly from those predicted by the control operations ($\mathrm{G} = 7.44$, $p \geq 0.05$, $\mathrm{df} = 1$).

The regenerated rhythmic behaviour of all these animals differed in at least one of the following criteria from rhythmic behaviour of normal animals: (i) rhythmicity was only transiently maintained (Table 2), (ii) the onsets of locomotor activity were more variable, (iii) phases of rhythmic activity were sometimes interrupted by bursts of continuing activity, (iv) the amount of activity often fluctuated from one circadian day to the next, (v) sometimes unusual period lengths occurred (Table 2), (vi) rhythmic activity phases were often introduced by long bursts of activity (Fig. 3A). No correlation was detectable between the periods of donors and hosts (Table 2).

Of the 45 AMe-transplantations 22 (49 %) animals could be examined histologically before they died. Of these, PDH-ir somata ($n = 1$–5) in the antennal lobe and PDH-ir midbrain arborisations were observed in all of the cockroaches that regained rhythmicity after transplantation of the AMe ($N = 4$; Tables 1, 2; Fig. 4B–D). Among the transplanted PDH-ir neurons, mostly two of their three size classes, the medium-sized (12–16 μm) and large ($> 16\,\mu$m), but only one of the small ($< 12\,\mu$m) PDH-ir somata were found (Table 3). Additionally, 10 (31 %) of the 32 arrhythmic AMe-transplanted animals expressed PDH-ir terminals in the midbrain (Table 4). In all rhythmic animals examined (including one rhythmic control animal) regenerated PDH-ir fibres arborised in the superior medial and superior lateral protocerebra (SMP and SLP, respectively; $N = 5$), but PDH-immunoreactivity in the ventro- or inferior lateral protocerebra or in the posterior optic tubercles was not found in all rhythmic animals (Table 4). In the AMe-implanted antennal lobes, we did not found any AMe-like neuropil structure retained from the im-

Table 2. *Correlations between pre- and postoperative rhythmicity*

Animal ID	Initial light condition (h:h)	τ forerun (h)	τ donor (h)	τ post-op. (h)	Duration of rhythmic activity (days)	Onset of rhythmic activity (days)
AMe-transplantations						
11/16	LD11:11	22.4	23.9	23.2	14	44
11/18	LD11:11	22.6	23.8	20.4	7	54
11/23	LD11:11	22.4	23.8	23.9	5	99
11/47	LD11:11	22.2	23.8	23.6	6	16
11/49	LD11:11	23.0	23.8	27.8	5	19
11/68	LD11:11	22.7	23.8	23.2	9	25
11/79	LD11:11	23.1	23.8	27.9	9	15
13/01*	LD13:13	23.8	22.6	23.4	12	29
13/06*	LD13:13	23.8	22.6	23.4	11	25
13/05	LD13:13	23.9	22.6	23.2	12	17
13/21	LD13:13	23.5	22.6	20.8	5	148
13/84	LD13:13	24.2	22.6	23.7	7	102
13/87	LD13:13	23.3	22.6	28.2	5	10
Controls						
11/59	LD11:11	22.6	23.8	22.1	6	106
11/64	LD11:11	22.9	23.8	20.9	7	57
13/39	LD13:13	23.8	22.6	24.1	13	56
13/46	LD13:13	22.2	22.6	28.5	7	47
13/58	LD13:13	23.7	22.6	20.6	6	46

List of all animals which regained circadian rhythmic locomotor activity, as revealed by Rhythm Detector analysis (see Materials and Methods). Animals were raised in 11 h:11 h L:D or 13 h:13 h L:D, and received accessory medulla (AMe)-grafts from donor animals of the opposite L:D cycle. τ forerun: freerunning circadian period lengths (τ) in hours for mono-lobectomised animals assessed before the transplantation/control experiment. τ donor: τ of donor animals. τ post-op: τ after transplantation/control experiment. The duration of the free-running rhythmic activity episode was determined on the activity histogram plots. Onset of rhythmic activity was counted from the day of the operation until the first day of rhythmic activity. *Animals received AMe-graft into the right optic lobe; all other animals received AMe-graft into the right antennal lobe.

planted tissue, but regenerated PDH-ir fibres in the antennal lobe showed varicosities.

Regained rhythmicity in the one control animal, which could be histologically examined, also correlated with the presence of regenerated PDH-ir arborisations in the midbrain (Tables 2, 3, 4). The PDH-ir somata were found in the antennal lobe, which was implanted with medulla tissue, as well as in the stump of one sectioned optic lobe. Moreover, two other arrhythmic control animals each head one PDH-ir soma in an optic lobe stump. Because 3 of the 22 histologically examined controls exhibited PDH-ir neurons, the expected error rate for these difficult control surgeries was 14 %.

DISCUSSION

To examine whether the AMe is the circadian pacemaker of the cockroach *L. maderae*, we transplanted AMe grafts into optic lobe-less arrhythmic hosts. Here we show that the ectopically transplanted AMe-grafts restore transient circadian rhythmic activity in optic lobe-less cockroaches. In addition, all of the histologically examined rhythmic animals showed PDH-ir regeneration into original target areas in the superior protocerebrum. Thus, our study demonstrates for the first time that the AMe contains the circadian pacemaker of the cockroach *L. maderae*. Future studies have to test whether other additional neurons, neighbouring the PDH-ir neurons, are responsible for the control of circadian locomotor rhythms.

Complete arrhythmicity after removal of both optic lobes was repeatedly demonstrated in *L. maderae* as in other cockroaches (Roberts, 1974; Sokolove, 1975; Lukat and Weber, 1978; Page, 1982; Stengl and Homberg, 1994), crickets (Loher, 1972; Tomioka and Chiba, 1984; Abe et al., 1997), and wetas (Waddell et al., 1990). Thus, re-established rhythmicity after AMe-transplantation in cockroaches without optic lobes strongly suggests that the transplanted AMe-grafts indeed contained the circadian pacemaker. This is supported by the significant difference in the number of rhythmic animals in the transplantation group versus the control group. Furthermore, only the presence of circadian rhythmicity argues for the presence of an intact circadian clock, but the absence of circadian locomotor rhythms does not prove the lack of an intact circadian clock (Stengl and Homberg, 1994; Stengl, 1995). This is also shown by the occurrence of 41 % apparently arrhythmic cockroaches with one intact circadian clock in the foreruns of the locomotor activity assays of

Table 3. *Distribution of soma sizes of transplanted PDH-ir neurons in postoperatively rhythmic animals*

Animal ID	Soma sizes (μm)
11/16	13, 15, 20, 20, 23
11/18	20
13/01	16, 22
13/39	11
13/84	18, 19

Most transplanted PDH-ir somata in postoperatively rhythmic animals belong to the medium-sized (diameter, 12–16 μm) and large (diameter, $>16\,\mu$m) PDH-ir medulla somata. The control animal 13/39 also has four leftover PDH-ir medulla somata in the left optic lobe stump belonging to the larger somata. *Animal received graft into the right optic lobe.

the current study. Thus, the presence of successfully transplanted PDH-ir neurons in arrhythmic animals does not weaken the conclusion that the transplanted tissue contains the circadian clock. In addition, the selective transplantation of medulla control tissue next to the AMe, but within the predicted pacemaker location according to Sokolove (1975), restored rhythmicity in arrhythmic animals significantly less often than did AMe transplants. With an error rate of 14 %, we also transferred PDH-ir neurons during our control transplantations, or single PDH-ir medulla neurons were accidentally left in the remaining stump after optic lobe excision. This is not surprising, because PDH-ir somata (and possibly other neurons of the AMe) are sometimes not directly beneath the AMe, but slightly dislocated towards the medulla or lobula, where we set our cut. Thus, it is likely that in all of the 12 % rhythmic controls rhythmicity was generated by accidentally transferred or left over AMe neurons, as shown by immunocytochemistry in three control animals (Table 4).

Thus, because cockroaches with intact circadian pacemakers sometimes show only short or no periods of rhythmicity, any episode of clear rhythmicity indicates that these animals contain circadian pacemakers, while arrhythmicity allows no final conclusion about the presence of an intact clock. Since no clear, objective measures for transient rhythmicity in long data sets have been published before, we took great care to develop new software and standards to distinguish rhythmic from arrhythmic episodes in long data sets. Because different analysis methods such as MESA and χ^2-periodogram analysis, as well as a subjective judgement by eye, confirmed our observations, we consider our analysis program to be very reliable. In addition, because rather strict criteria were used for distinction of rhythmicity versus arrhythmicity, we very likely underestimate the number of rhythmic animals in the transplantation group.

Because the lack of circadian rhythmicity in cockroaches without optic lobes is well established by lesion experiments from different laboratories (Roberts, 1974; Sokolove, 1975; Lukat and Weber, 1978; Page, 1982; Stengl and Homberg, 1994), return of rhythmicity in transplanted animals demonstrated in the present study shows that the transplanted tissue contains circadian pacemaker neurons. However, it does not distinguish which of the transplanted cells are circadian pacemaker cells. The correlation between the presence of regenerated PDH-ir processes in original target areas in all histologically examined rhythmic animals suggests a role for PDH-ir neurons as circadian pacemaker candidates. However, because we focused on long-term behavioural analysis at the expense of histological examination, only five of the cockroaches with regained rhythmicity could be examined histologically. Thus, we cannot draw a statistically significant conclusion about the cellular nature of circadian pacemaker neurons within the AMe transplants. But it is likely that at least a subgroup of PDH-ir neurons relays the circadian information to the midbrain, because regeneration of PDH-ir neurons to original midbrain targets also correlated with regained circadian activity rhythms after transection of the optic stalk (Stengl and Homberg, 1994).

That the circadian pacemaker is at least partly composed of the PDH-ir neurons is further supported by findings in the fruitfly *Drosophila melanogaster*. In the fruitfly, pigment-dispersing factor is colocalised with the clock proteins PERIOD and TIMELESS in the same circadian pacemaker candidates, the lateral neurons (Helfrich-Förster 1995, 1998). In addition, PDH is thought to be the crucial circadian output- and coupling neuropeptide in insects (Renn et al., 1999; Blanchardon et al., 2001; Taghert, 2001; Reischig and Stengl, 2002). The importance of PDH-ir neurons for circadian activity is further supported by our observation that regained rhythmic activity strictly correlated with regeneration of transplanted PDH-ir neurons into the SMP and SLP, which are the clock's presumed output regions to locomotor centre pathways in wildtype cockroaches as well as in *Drosophila*

Table 4. *Distribution of regenerated PDH-ir fibres in the central brain of postoperatively rhythmic and arrhythmic animals*

	Number of PDH-ir Somata			Regenerated PDH-ir fibres in			
Animal ID	Total	Implantation site	left OL stump	SMP	SLP	VLP & ILP	POTu
Rhythmic animals							
11/16	5	5	0	+	+	−	+
11/18	1	1	0	+	+	+	−
13/01	2	2*	0	+	+	−	−
13/84	3	3	0	+	+	−	+
13/39†	5	1	4	+	+	+	+
Arrhythmic animals							
11/02	8	6*	2	+	+	+	+
11/04	4	3*	1	+	+	−	+
11/06	3	0*	3	+	+	+	+
11/19	4	4	0	+	+	+	−
11/24	?	?	?	−	−	+	−
11/75	?	?	?	+	+	+	−
13/14	2	2	0	+	+	−	+
13/71	?	?	?	+	+	+	−
13/72	3	2	1	+	+	+	+
13/86	?	?	?	+	+	+	+
13/62†	1	0	1	+	+	+	+
13/80†	1	0	1	+	+	+	−

All of the 5 animals that regained circadian locomotor activity, and which could be histologically examined, showed regenerated PDH-ir fibres in the superior median and superior lateral protocerebrum (SMP and SLP, respectively), but not necessarily in the ventrolateral and inferior lateral protocerebrum (VLP and ILP, respectively), nor in the posterior optic tubercle (POTu). As it is known from behavioural assays in normal wild type animals, apparent arrhythmicity in running-wheel assays is common and thus, does not indicate the lack of an intact circadian pacemaker. Thus, it is to be expected that also arrhythmic animals also show PDH-immunoreactivity. Additionally, because leftover PDH-ir neurons were found in the optic lobe (OL) stump in at least 7 of 44 histologically examined animals, approximately 16 % of optic lobe excisions are expected to be incomplete. The control animals are marked with a dagger. *Animals received AMe-graft into the right OL; all other animals received AMe-graft into the right antennal lobe. Question marks represent somata that could not be localised and were apparently lost during the histological procedures.

(Homberg et al., 1991; Renn et al., 1999). Arborisations in the ventrolateral and inferior lateral protocerebrum, or posterior optic tubercle, which are also arborisation sites for PDH-ir terminals in wild-type cockroaches (Homberg et al., 1991), were not necessary for regained locomotor activity. Because rhythmicity resumed within ≥ 10 days of the operation (Table 2), circadian outputs to locomotor centre pathways appear to rely on regenerated neuronal connections, but not on diffusible factors as shown in vertebrates (see Silver et al., 1996).

In both the fruitfly and the cockroach, there are different size groups of PDH-ir neurons next to the AMe. In *Drosophila*, small PDH-ir lateral neurons project to the superior lateral protocerebrum and large PDH-ir lateral neurons appear to connect both optic lobes. In the cockroach, only subgroups of the large and medium-sized PDH-ir neurons project to the protocerebrum, and appear to connect both accessory medullae (Reischig and Stengl, 2002). Because in the current study large and medium-sized transplanted PDH-ir neurons (Table 3) were found to regenerate to the superior lateral protocerebrum, it is likely that at least these two subgroups of the PDH-ir neurons are circadian pacemaker neurons that can drive circadian locomotor behaviour. This is in contrast to some findings in *Drosophila* indicating that only the small lateral neurons have pacemaker function (Park et al., 2000). However, since in *disco* mutants a single large PDH-ir neuron with aberrant connections to the superior lateral protocerebrum correlates with rhythmic locomotor behaviour (Helfrich-Förster, 1998), also in the fruitfly, as in the cockroach, all PDH-ir neurons might be circadian pacemakers.

In contrast to the transplantation studies of Page (1982), our experiments could restore rhythmic behaviour but not period length. The regained period lengths were dissimilar to the donors' periods, and ranged from 20.4 to 28.5 hours, closely reflecting the range of periods of non-coupled vertebrate SCN pacemaker neurons in vitro (Honma et al., 1998). Our immunocytochemical results indicate that only a few of the transplanted AMe neurons survived in the host's antennal lobe, and that the neuropil of the AMe is lost in the host. Apparently, coupling interactions between transplanted AMe neurons, which might generate the characteristic period

of the wildtype cockroach, are strongly reduced or missing. Thus, it is likely that an insect as well as a vertebrate circadian pacemaker constitutes its period *via* coupling in an interconnected neuronal network rather than *via* single independent pacemaker neurons (Honma et al., 1998). In addition, we assume that adjacent the PDH-ir neurons, also other neurons of the AMe are circadian pacemakers, because no correlation between the number of surviving PDH-ir somata and overt period lengths was observed (Table 2). The different period lengths might possibly indicate varying amount of coupling between different pacemaker cells in the transplanted grafts (Michel and Colwell, 2001). This further adds to the assumption that the period of the circadian system depends on the period of single pacemaker cells as well as on the coupling between the pacemakers. Furthermore, in hamsters (*Mesocricetus auratus*) it was shown that quality and period lengths of rhythmicity after SCN-transplantation was influenced by the number of re-established neuronal connections, the graft volume, and the attachment site of grafts (Davis and Viswanathan, 1996; LeSauter et al., 1997). Therefore, the lack of the normal AMe neuropil might explain why regenerated rhythmicity occurred only transiently, and why some animals did not regain rhythmic locomotor activity, even in the presence of successfully transplanted PDH-ir neurons. However, it cannot be determined whether these arrhythmic animals lacked a functional clock, since also about 1/3 of non-operated cockroaches with intact circadian clocks did not express circadian locomotor activity in running-wheel assays.

With the exceptions of the transplantations of whole optic lobes by Page (1982), transplantation of small, defined brain regions containing circadian oscillators succeeded only in vertebrate species (Sawaki et al., 1984; Lehman et al., 1987; Ralph et al., 1990; Grosse and Davis, 1998), thus, identifying the suprachiasmatic nucleus as the circadian pacemaker centre controlling locomotor activity in mammals. Only transplantations of embryonic or developing tissue within a narrow time window after birth of the donors succeeded (Romero et al., 1993; Kaufman and Menaker, 1993). Reorganisation of identifiable, fully differentiated central nervous system (CNS) neurons after ectopic transplantation from and into adult animals has not been reported before. Thus, the cockroach is not only an excellent model organism to study the neurophysiology of circadian timing, but also an interesting system for studies of neuronal regeneration after CNS damage or transplantation, because of its dramatic power in repairing severed neuronal connections.

ACKNOWLEDGEMENTS

We thank Rita Zintl for excellent technical assistance. We are very grateful to Dr. H. Dircksen (University of Bonn, Germany) for providing the anti-β-PDH antiserum, and to Dr. R. Brandl and an unknown referee for advice with statistics. This work was supported by the Deutsche Forschungsgemeinschaft (DFG) grants STE 531/7-1, 2, 3, and Human Science Frontier.

LITERATURE CITED

Abe Y, Ushirogawa H, and Tomioka K. 1997. Circadian locomotor rhythms in the cricket, *Gryllodes sigillatus*. I. Localisation of the pacemaker and the photoreceptor. Zoolog Sci 14:719–727.

Blanchardon E, Grima B, Klarsfeld A, Chelot E, Hardin PE, Preat T, and Rouyer F. 2001. Defining the role of *Drosophila* lateral neurons in the control of circadian rhythms in motor activity and eclosion by targeted genetic ablation and PERIOD protein overexpression. Eur J Neurosci 13:871–888.

Davis FC and Viswanathan N. 1996. The effect of transplanting one or two suprachiasmatic nuclei on the period of the restored rhythm. J Biol Rhythms 11:291–301.

Dircksen H, Zahnow CA, Gaus G, Keller R, Rao KR, and Riem JP. 1987. The ultrastructure of nerve endings containing pigment-dispersing hormone (PDH) in crustacean glands: identification by an antiserum against a synthetic PDH. Cell Tissue Res 250:377–387.

Dowse HB and Ringo J. 1989. The search for hidden periodocities in biological time series revisted. J Theor Biol 139:487–515.

Ewer J, Frisch B, Hamblen-Coyle MJ, Rosbash M, and Hall JC. 1992. Expression of the period clock gene within different cell types in the brain of *Drosophila* adults and mosaic analysis of these cells' influence on circadian behavioural rhythms. J Neurosci 12:3321–3349.

Frisch B, Hardin PE, Hamblen-Coyle MJ, Rosbash M, and Hall JC. 1994. A promoterless period gene mediates behavioural rhythmicity and cyclical per expression in a restricted subset of the *Drosophila* nervous system. Neuron 12:555–570.

Grosse J and Davis FC. 1998. Melatonin entrains the restored circadian activity rhythms of syrian hamsters bearing fetal suprachiasmatic nucleus grafts. J Neurosci 18:8032–807.

Helfrich-Förster C. 1995. The period clock gene is expressed in central nervous system neurons which also produce a neuropeptide that reveals the projections of circadian pacemaker cells within the brain of *Drosophila melanogaster*. Proc Natl Acad Sci USA 92:612–616.

Helfrich-Förster C. 1998. Robust circadian rhythmicity of *Drosophila melanogaster* requires the presence of lateral neurons: a brain-behavioural study of disconnected mutants. J Comp Physiol A 182:435–453.

Helfrich-Förster C. 2001. The locomotor activity rhythm of *Drosophila melanogaster* is controlled by a dual oscillator system. J Insect Physiol 47:877–887.

Helfrich-Förster C and Homberg U. 1993. Pigment-dispersing hormone-immunoreactive neurons in the nervous system

of wild-type *Drosophila melanogaster* and of several mutants with altered circadian rhythmicity. J Comp Neurol 337:177–190.

Helfrich-Förster C, Stengl M, and Homberg U. 1998. Organisation of the circadian system in insects. Chronobiol Int 15:567–594.

Homberg U, Würden S, Dircksen H, and Rao KR. 1991. Comparative anatomy of pigment-dispersing hormone-immunoreactive neurons in the brain of orthopteroid insects. Cell Tissue Res 266:343–357.

Honma S, Shirakawa T, Katsuno Y, Namihira M, and Honma K. 1998. Circadian periods of single suprachiasmatic neurons in rats. Neurosci Lett 250:157–160.

Inouye ST and Kawamura H. 1979. Persistence of circadian rhythmicity in a mammalian hypothalamic "island" containing the suprachiasmatic nucleus. Proc Natl Acad Sci USA 76:5962–5966.

Kaufman CM and Menaker M. 1993. Effect of transplanting suprachiasmatic nuclei from donors of different ages into completely SCN lesioned hamsters. J Neural Transplant Plast 4:257–65.

Lehman MN, Silver R, Gladstone WR, Kahn RM, Gibson M, and Bittman EL. 1987. Circadian rhythmicity restored by neural transplant. Immunocytochemical characterisation of the graft and its integration within the host brain. J Neurosci 7:1626–1638.

LeSauter J, Romero P, Cascio M, and Silver R. 1997. Attachment site of grafted SCN influences precision of restored circadian rhythm. J Biol Rhythms 12:327–38.

Loher W. 1972. Circadian control of stridulation in the cricket *Teleogryllus commodus* Walker. J Comp Physiol 79:173–190.

Lukat R and Weber F. 1978. The structure of locomotor activity in bilobectomised cockroaches (*Blaberus fuscus*). Experientia 35:38–39.

Michel S and Colwell CS. 2001. Cellular communication and coupling within the suprachiasmatic nucleus. Chronobiol Int 18:579–600.

Nishiitsutsuji-Uwo J and Pittendrigh CS. 1968. Central nervous system control of circadian rhytmicity in the cockroach. II. The optic lobes, locus of the driving oscillator? Z vergl Physiol 58:14–46.

Page TL. 1982. Transplantation of the cockroach circadian pacemaker. Science 216:73–75.

Page TL. 1983. Regeneration of the optic tracts and circadian pacemaker activity in the cockroach *Leucophaea maderae*. J Comp Physiol A 152:231–240.

Page TL and Block GD. 1980. Circadian rhythmicity in cockroaches: effects of early post-embryonic development and ageing. Physiological Entomology 5:271–281.

Park JH, Helfrich-Förster C, Lee G, Liu L, Rosbash M, and Hall JC. 2000. Differential regulation of circadian pacemaker output by separate clock genes in *Drosophila*. Proc Natl Acad Sci USA 97:3608–3613.

Petri B, Stengl M, Würden S, and Homberg U. 1995. Immunocytochemical characterisation of the accessory medulla in the cockroach *Leucophaea maderae*. Cell Tissue Res 282:3–19.

Ralph MR, Foster RG, Davis FC, and Menaker M. 1990. Transplanted suprachiasmatic nucleus determines circadian period. Science 247:975–98.

Reischig T and Stengl M. 1996. Morphology and pigment-dispersing hormone immunocytochemistry of the accessory medulla, the presumptive circadian pacemaker of the cockroach *Leucophaea maderae*: a light- and electron-microscopic study. Cell Tissue Res 285:305–319.

Reischig T and Stengl M. 2002. Optic lobe commissures in a three-dimensional brain model of the cockroach *Leucophaea maderae*: a search for the circadian coupling pathways. J Comp Neurol 443:388–400.

Renn SC, Park JH, Rosbash M, Hall JC, and Taghert PH. 1999. A *pdf* neuropeptide gene mutation and ablation of PDF neurons each cause severe abnormalities of behavioural circadian rhythms in *Drosophila*. Cell 99:791-802.

Roberts SK. 1974. Circadian rhythms in cockroaches: Effects of optic lobe lesions. J Comp Physiol 88:21–30.

Romero MT, Lehman MN, and Silver R. 1993. Age of donor influences ability of suprachiasmatic nucleus grafts to restore circadian rhythmicity. Brain Res Dev Brain Res 71:45–52.

Sawaki Y, Nihonmatsu I, and Kawamura H. 1984. Transplantation of the neonatal suprachiasmatic nuclei into rats with complete bilateral suprachiasmatic lesions. Neurosci Res 1:67–72.

Silver R, LeSauter J, Tresco PA, and Lehman MN. 1996. A diffusible coupling signal from the transplanted suprachiasmatic nucleus controlling circadian locomotor rhythms. Nature 382:810–83.

Sokolove PG. 1975. Localisation of the cockroach optic lobe circadian pacemaker with microlesions. Brain Res 87:13–21.

Sokolove PG and Bushell WN. 1978. The chi square periodogram: its utility for analysis of circadian rhythms. J Theor Biol 72:131–160.

Stengl M. 1995. Pigment-dispersing hormone-immunoreactive fibres persist in crickets which remain rhythmic after bilateral transection of the optic stalks. J Comp Physiol A 176:217–228.

Stengl M and Homberg U. 1994. Pigment-dispersing hormone-immunoreactive neurons in the cockroach *Leucophaea maderae* share properties with circadian pacemaker neurons. J Comp Physiol A 175:203–213.

Stephan FK and Zucker I. 1972. Circadian rhythms in drinking behaviour and locomotor activity of rats are eliminated by hypothalamic lesions. Proc Natl Acad Sci USA 69:1583–1586.

Sternberger LA. 1979. Immunocytochemistry. New York: Wiley & Sons.

Taghert PH. 2001. How does the circadian clock send timing information to the brain? Semin Cell Dev Biol 12:329–341.

Tomioka K and Chiba Y. 1984. Effects of nymphal stage optic nerve severance or optic lobe removal on the locomotor rhythm of the cricket, *Gryllus bimaculatus*. Zool Sci 1:385–394.

Waddell B, Lewis RD, and Engelmann W. 1990. Localisation of the circadian pacemakers of *Hemideina thoracica* (Orthoptera; Stenopelmatidae). J Biol Rhythms 5:131–19.

Zerr DM, Hall JC, Rosbash M, and Siwicki KK. 1990. Circadian fluctuations of period protein immunoreactivity in the CNS and the visual system of *Drosophila*. J Neurosci 10:2749–2762.

V. Scan periodogram analysis: a new method for automated detection of short circadian rhythmic activity phases in long data records.

Scan periodogram analysis: a new method for automated detection of short circadian rhythmic activity phases in long data records

Thomas Reischig

ABSTRACT

A new method is presented which allows for an automated and more objective detection of short circadian rhythmic episodes in long activity data records performed for up to several months, which contain arrhythmic behaviour. The analysis is performed by a software, which is designed as an add-in for the spreadsheet program Microsoft Excel, and written in the programming language Visual Basic for Applications. The program, called *Tempus*, performs progressing χ^2-periodogram analyses over the whole data records. The intervals analysed by the single periodograms are much smaller than the complete data record. With application of this "periodogram scan analysis" on generically arrhythmic as well as on randomised data, thresholds for peak-analysis of the single periodograms were determined to recognise rhythmicity in activity records. Thus, it was possible to separate circadian rhythmic from arrhythmic cockroaches (*Leucophaea maderae*) in transplantation experiments. Hence, the scan periodogram analysis allowed to identify the AMe as circadian clock controlling locomotor activity in cockroaches. Now, *Tempus* was further developed into a chronobiology analysis program, which might be expanded to any desired functionality due to its modular construction. The software can easily be applied to any circadian time series data recorded as ASCII (pure text) files.

A common task in chronobiology is to detect and to analyse circadian rhythmicity among data collected as time series records. Such data may include all kinds of behavioural or physiological data, e.g., wheel-running activity of cockroaches. Cockroaches that were lesioned at the site of their circadian pacemaker, the accessory medulla (AMe), or which were ectopically transplanted with tissue containing the AMe after their optic lobes were removed, commonly became arrhythmic afterwards (Homberg et al., 2003; Chapters III, IV). Nevertheless, in some AMe-transplanted subjects circadian rhythmic activity seemed to resume for small activity episodes of up to 14 days, while the data records lasted up to 9 months. However, these episodes were embedded in an arrhythmic and inconsistent activity background and hence, often difficult to be recognised and evaluated. The problem was to examine, whether such rhythmic episodes in a population of AMe-transplanted cockroaches occurred significantly more often compared to a control group with no implantations, or which received grafts not containing the AMe. Arrhythmic cockroaches often behave fairly irregular. With a low probability, groups of activity data samples might be arranged in an "apparently circadian pattern" by chance and thus, support biased interpretation of the data. Thus, it was necessary to develop a method which allows for an automated detection of small circadian rhythmic episodes in longer datasets, and distinguish these from arrhythmic data.

One of the most important methods to detect and to analyse circadian rhythmicity, is still the χ^2-periodogram (chi-square-periodogram) analysis (Sokolove and Bushell, 1978). Other methods, such as fourier analysis, autocorrelation and mass entropy spectral analysis (MESA) are popular for some advantages, but lack a statistical test to valuate the

occurrence of circadian rhythmicity within the data (De Prins and Hecquet, 1992; Klemfuss and Clopton, 1993; Levine et al., 2002). A statistical test present in the χ^2-periodogram analysis allows for determining adequate and revisable criteria to indicate rhythmicity.

The concept for a "scan periodogram analysis" is to detect small rhythmic data stretches by performing a sequence of single χ^2-periodogram analyses over a whole data record. The intervals analysed by every single periodogram are a multiple smaller than the whole data record. The single periodograms consecutively analyse data segments following a peculiar algorithm: If the length of the single periodogram is, e.g., limited to 10 days, the first periodogram evaluates day 1 to day 10 of the record, the second periodogram day 2 to day 11 and so on, until the end of the record. If a single periodogram detects rhythmicity, i.e., it has a peak exceeding the so-called Sokolove significance line, this event is reported on an XY plot of the data track. If rhythmicity occurs in otherwise arrhythmic data episodes, it should be detected this way.

However, also in arrhythmic data tracks the periodograms frequently report peaks slightly exceeding the Sokolove significance line. These peaks commonly have rather low amplitudes and narrow widths as compared to periodogram peaks occurring in obviously rhythmic data. Thus, a function for measuring peak heights and widths was implemented into the analysis. After determining certain thresholds for peak amplitudes and widths, peaks with values above these thresholds could now be separated from smaller peaks. For an objective definition of thresholds for the recognition of rhythmicity, scan periodograms of rhythmic and arrhythmic, as well as of randomly permutated data sets were analysed. These thresholds were used to evaluate transplantation (Chapter IV) and lesion experiments (Chapter III).

For the development of this analysis program, the program language Visual Basic for Applications (VBA 6) was used, since it is already implemented in Excel, and the available data could easily be imported into Excel. The algorithms were further developed into a chronobiological analysis program, called *Tempus*, which is easy to use and open for further improvement to any function requested in chronobiology.

The present report is divided into two main parts. The first part is a manual which describes the functions of *Tempus* and also contains detailed descriptions of the algorithms used[1]. Part II describes the use of the Rhythm Detector analysis in a particular application, the transplantation of pacemaker tissue into arrhythmic cockroaches.

PART 1: PROGRAM DESCRIPTION

General concept

Tempus is an Excel add-in file (currently *Tempus_ V1.6.xla*) written in Visual Basic for Applications 6 (VBA). Once the *Tempus* file is started in Excel, the program is resident in the Excel environment. After simultaneously pressing **Ctrl**+**y**, the central user dialogue for the program control (the "main menu") appears (Fig. 1). From there, ASCII (= pure text) files containing time series data will be imported, i.e., for every ASCII file containing one series of data a new Excel workbook (the experiment workbook) is created. The first worksheet of the experiment workbook receives a data information header and the raw data, while several more worksheets are automatically added in which the evaluation results will be documented and stored.

For evaluation, an experiment workbook is opened *via* the main menu. After choosing a time interval to investigate within the current experiment, an evaluation category will be selected in the registers of the main menu. Then, the appropriate parameters will be entered, and the particular evaluation is started by pressing the respective command button. The results of the evaluation will be written on the dedicated worksheet of the experiment workbook in tabular form, and, if adequate, a diagram is plotted. The diagrams may be printed directly from the main menu by just pressing the **Print chart** button. To store the results permanently, they may be moved to one of the *Archive* worksheets of the experiment workbook. After closing the main menu, the data in the experiment workbook can be accessed and processed in Excel as usual. As long as the *Tempus* add-in is active, the main menu can be immediately reopened by pressing **Ctrl**+**y**, and the investigation of the current experiment may be continued, or another may be selected. If the exploration of an experiment is finished, it may be closed *via* the main menu, and the evaluation results might been saved. For some computing time consuming evaluation methods which do not require individual parameter input, it is possible to select multiple experiment workbook files and run the evaluation automatically on all of them. After the work is finished, *Tempus* may be permanently quitted through its main menu.

[1] Formatting convention: Headlines referred within the text body, names of worksheets, as well as other text emphasisings, are marked by *italics*. Terms that directly refer to program functions of *Tempus* or Excel, such as menu commands, register names, dialogue options, or key combinations, are marked by **bolds**.

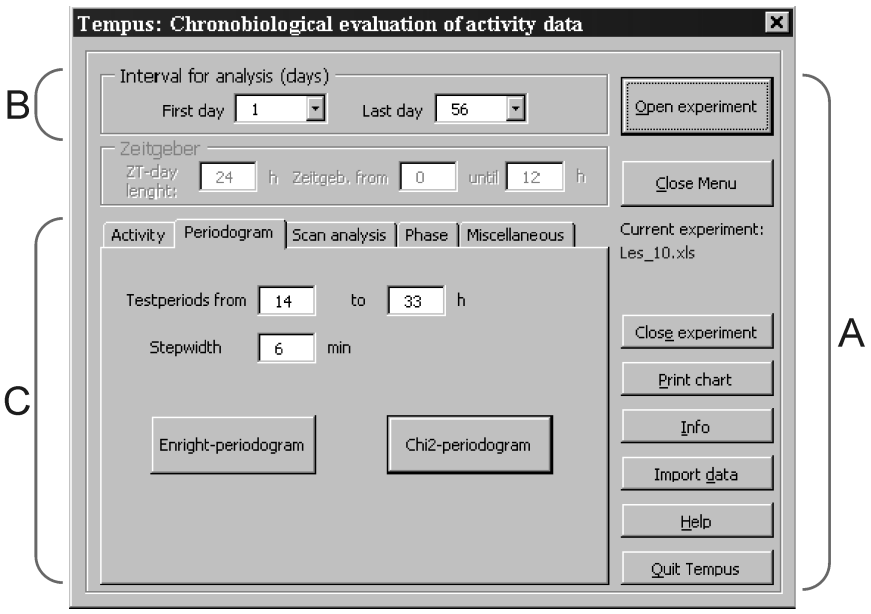

Fig. 1. The main menu is the central control dialogue of *Tempus*. **A:** The **command button section** provides general control elements. **B:** The data interval to be analysed will be determined in the **input section**. **C:** The **evaluation register sections** contain the analysis methods with dedicated commands, options, and input boxes. After opening the main menu, the register **Periodogram** is by default activated.

System requirements and auxiliary software

Tempus was initially programmed in Excel 97 under Windows NT4, than further developed in Excel 2002 under Windows XP Pro. It was successfully tested in Excel 2000 under Windows 2000, and in Excel 97 under Windows 95. Therefore, it is expected to run with all Excel versions from Excel 97 up (VBA must already be installed, what should be the case in most local MS Office installations), and under all Windows versions from 95 up. Nevertheless, the results of the automated chart formatting differ slightly between several Excel versions; formatting was optimised for use in Excel 2002. Since *Tempus* is an Excel add-in, Excel has of course to be already installed on the computer before the program can be run. *Tempus* can be used on all PCs with a CPU speed ≥ 133 MHz. However, evaluations like the Rhythm Detector are fairly computing time intensive and are profiting from a faster CPU.

Currently, *Tempus* works with input data derived with the activity data recording program AAR 1.04 (H. Fink 1992, Konstanz, Germany), which were converted into ASCII files by means of the DOS-program convert.exe (Günther Stöckl 1997, Regensburg, Germany). However, all ASCII files containing evenly recorded time series data that fulfil the requirements described in the section *Main menu→Command Import data* might be suitable.

The use of the printer driver FinePrint (available at http://www.fineprint.com) is strongly recommended. This program allows printing of several print jobs on one sheet. Before final printout, the jobs can be resorted and/or selectively deleted. Furthermore, it is possible to save the printouts to the hard disk without the need of creating hardcopies. If FinePrint is not resident on the computer or it is not configured as standard printer, the "Print chart" function of *Tempus* currently allows printing only if the active printer can be set to 600 dpi print resolution (if it is possible, this will be done automatically by the printer driver). Many ink jet printers allow only 720 instead of 600 dpi, what will cause an error message and the print job to be terminated. However, after closing the *Tempus* main menu the diagrams can be printed directly from Excel on any printers.

Getting started

Excel is a prerequisite for *Tempus*. *Tempus* consists of the *Tempus_1.6.xla* Excel add-in file, and the *TempusDoc* folder containing the *Tempus* description files in HTML format. Both can be copied to any desired folder, but must be kept together in one folder. Then, *Tempus* can be started by double click on the *Tempus_1.6.xla* file in the explorer, or by opening it *via* the Excel **File→Open** menu. It is necessary to allow the execution of macros in Excel; at least set the macro security option to medium, and select **Activate macro** every time you start *Tempus*. Alternatively, *Tempus* can be integrated into Excel *via* the add-in manager. To do that, both the file and the documentation folder have to be copied into the MS Office add-in folder (which for Office 2002 might for example look like [Drive]\[Program folder]\Microsoft Office\Office10\Macro, depending on the individual installation). Then, it can be activated in Excel *via* the menu path **Tools→Add-Ins**. After check-

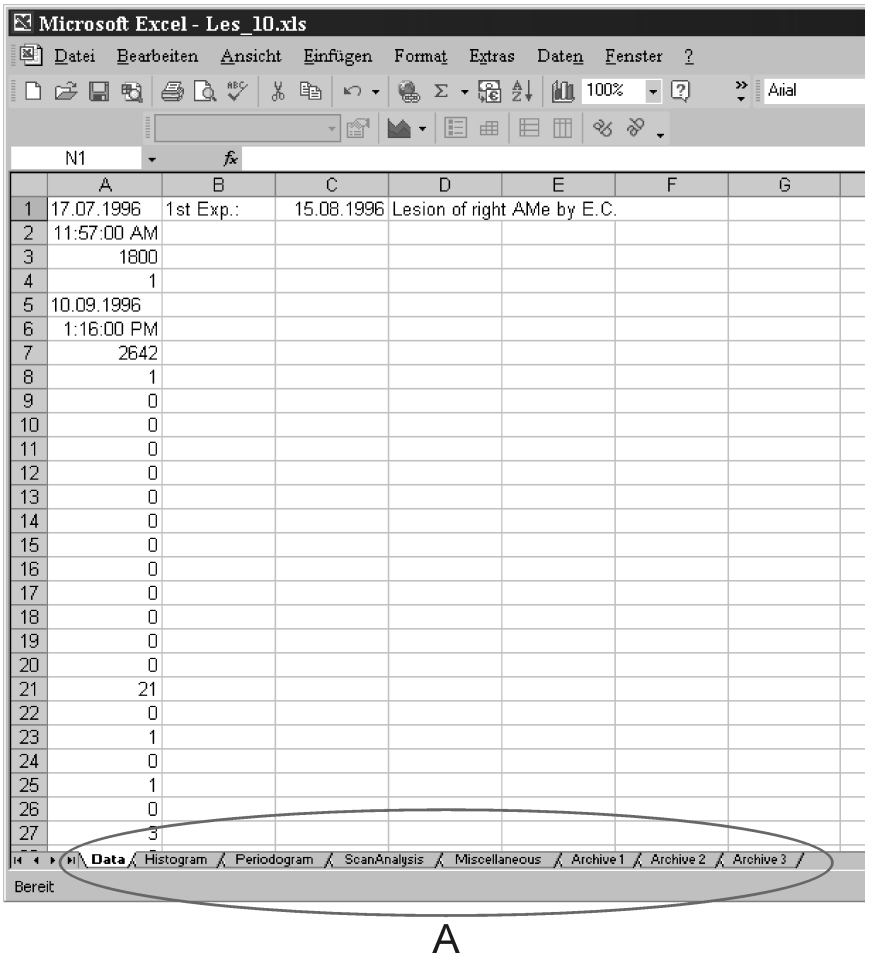

Fig. 2. The experiment workbook contains the raw data and the analysis results of a data record. The ellipse (**A**) indicates the associated worksheets.

ing *Tempus_1.6* in the dialogue offered, *Tempus* is started any time Excel is opened. To deactivate autonomous starting of *Tempus*, uncheck the respective option. If *Tempus* starts for the first time in a given Excel session, a little welcome dialogue appears which remembers that the *Tempus* main menu can be opened by simultaneously pressing **Ctrl**+**y**.

The experiment workbook

An experiment workbook is created after applying the **Import data** command in the main menu of *Tempus* to an appropriate ASCII file; see *Main menu→Command Import data* for more details on the import procedure. The experiment workbook contains seven worksheets named *Data*, *Histogram*, *Periodogram*, *ScanAnalysis*, *Miscellaneous*, *Archive 1*, *Archive 1*, and *Archive 3*, in this order (Fig. 2). It is strictly recommended not to rename or change the order of the worksheets *Data, Histogram*, *Periodogram*, *ScanAnalysis,* and *Miscellaneous*, since *Tempus* will access them both by name and order; if *Tempus* does not find the expected worksheet name in the correct position, an error message will be issued and the work interrupted. For reformatting of damaged workbooks, see *Miscellaneous→Reformat data*. The worksheets *Archive 1–3* serve for permanent storage of evaluation results, and may be renamed or deleted without any effect for the execution of *Tempus*; moreover, additional worksheets may be added as long as they do not intercalate anywhere between the sheets *Data* and *Miscellaneous*.

The worksheet *Data* contains a data information header in Cells *A1–A8*, followed by the belonging track of raw data in column *A*, beginning at *A9* (Fig. 2). Every number in the data track represents the number of events (e.g., rounds of a running-wheel) in a certain time interval, which is documented in cell *A3* in number of seconds (= sample length). The date of the beginning of the recording is documented in cell *A1* (format: dd.mm.yyyy), the respective time of day in cell *A2* (format: h:mm:ss AM/PM. The date and daytime of the end of the recording are in cells *A5* and *A6*, respectively, and are formatted accordingly. Cell *A7* contains the number of samples present in the whole data record. Cells *A4* and *A8* are currently not relevant for data description and contain a "1" as place-marker. Cell *B1* shows

the description "1^{st} Exp.:" and refers to cells *C1* and *D1*. These cells are empty after an experiment workbook is newly created, but will contain the date (*C1*) and kind (*D1*) of a given experimental manipulation, after they have been inserted manually (see *Miscellaneous→Insert experiment date and description*). However, adding these data is not crucial for the execution of *Tempus*.

The header is read out every time the data are loaded into *Tempus*, and serves for correct interpretation of the data. It should therefore not be edited. In addition, the correct cell formats in the header are necessary for *Tempus* to recognise the data and read them. Alterations herein will cause *Tempus* to refuse reading the data; if this nevertheless happens, reformatting the workbook (*Miscellaneous→Reformat data*) should recover the original state.

The worksheets *Histogram*, *Periodogram*, *ScanAnalysis*, and *Miscellaneous* are the scratch book of *Tempus*, were the evaluation results will be documented. These results were deleted and replaced every time a new evaluation is started that will write onto the particular worksheet. If an evaluation process is finished, the results were documented as a table on the respective worksheet, and, if appropriate, a diagram is plotted. To prevent the results from being overwritten at the next round of evaluation, the whole table *together* with the respective diagram has to be moved to one of the *Archive* sheets or to a newly added sheet; moving the diagram alone will cause it to loose its link to its source data, as soon as these are deleted or overwritten. Then, the diagram will show either nothing or false results.

The sheet *Histogram* serves for plotting of double plot activity histograms. The sheet *Periodogram* is used for plotting Enright- and χ^2-periodograms. On sheet *ScanAnalysis* both the results of the Rhythm Detector and the periodogram peak analysis are documented. The sheet *Miscellaneous* serves for all other evaluations, which currently cover tabular outputs of raw data, XY-plots of activity, and calculations of average days.

Main menu

The main menu is the central command interface for the control of *Tempus*. As long as *Tempus* is resident in Excel, it can always be called by simultaneously pressing **Ctrl+y**. If a valid experiment workbook is already open and active, the data will be automatically read into the program and it can be worked on. If any other Excel file is open or if the experiment workbook does not comply with the requirements of *Tempus* for any reason, a warning message will be issued.

The main menu consists of three sections (Fig. 1):

- The **command button section** (Fig. 1A) contains options for the general control of *Tempus*. The respective functions are described below. Between the commands **Close menu** and **Close experiment,** the file name of the active experiment is displayed. Here, also a warning message appears if one works on randomly permutated data (see *Miscellaneous→Permutate data*).
- The input section **Interval for analysis** (Fig. 1B) allows for determining the time interval in the data record in which an evaluation will be performed. The inputs apply for all evaluations to be selected in the registers. The selected days of the analysis interval borders are fully included in the evaluations, i.e., if days 1–3 are selected, the evaluation will cover indeed 72 hours. After an experiment is loaded or the main menu is recalled onto an active experiment, the first and last day of the whole data record are preselected. Inputs may be performed numerically as numbers of days, or may be selected by means of the dropdown controls in the input boxes. There, the available numbers of days together with the respective calendrical dates are displayed.
- The input section **Zeitgeber** currently implies no functionality.
- The **evaluation register section** (Fig. 1C) contains commands, options, and input boxes for the available evaluations. It consists of the registers **Activity**, **Periodogram**, **Scan analysis**, **Phase**, and **Miscellaneous**. The respective functions are described below. In the appendix, details for the inputs for particular registers and commands are specified. At main menu start-up, the register **Periodogram** is set to the front, since probably it will be that one mostly in use.

Command *Open experiment*. This command opens a dialogue which allows for selecting a drive, a directory and there, an Excel file (*.xls) to be opened. If the selected file is already open, it will not be reopened, but moved to the foreground and activated. Activation means that the data are read into *Tempus* and default values are set appropriatly. The file name of the currently active experiment appears below the **Close Menu** command button of the main menu. If the Excel file selected is no valid *Tempus* experiment workbook, it will be opened but a warning message appears.

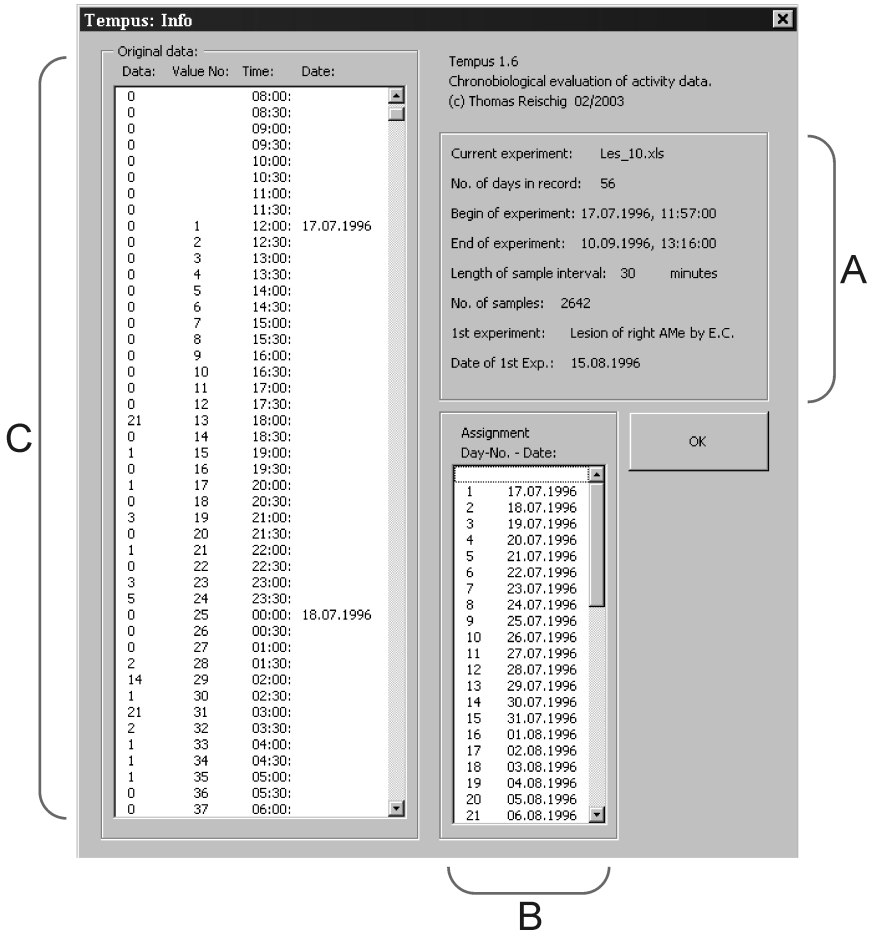

Fig. 3. Info dialogue. **A:** Header information section. **B:** Assignment section. **C:** Original data section.

Command *Close menu*. With **Close menu** the main menu is temporarily closed, but *Tempus* remains resident in Excel and can be immediately recalled by pressing **Ctrl**+**y**. Closing the main menu is necessary to directly access the experiment workbook, e.g., to change the active worksheet for reviewing earlier evaluations, to move evaluation results to *Archive* worksheets, or to format diagrams.

Command *Close experiment*. This closes the active experiment and offers a dialogue to choose for saving it, if any alterations to the experiment workbook occurred. Excel files that are not valid experiment workbooks cannot be closed with this option.

Command *Print chart*. This sends a selected diagram to the active printer, which will be your standard printer, if not previously selected otherwise in the Excel **File→Print** menu. If you use FinePrint but this is not your standard printer, select FinePrint manually if intended. If an evaluation is just finished, the diagram is already selected afterwards, and one needs only to press the **Print chart** button to get a printout. Otherwise, the diagram has to be explicitly selected between closing and reopening of the main menu. For more details to printer requirements, see *System requirements and auxiliary software*.

Command *Info*. After pressing the **Info** command button a dialogue appears which provides detailed information about the active experiment. It consists of three sections (Fig. 3):

- The **header information section** (Fig. 3A) displays the file name of the current experiment together with all information that can be derived from of the data header in worksheet *Data*. The **No. of days in record** includes all *calendrical* days which are covered by the activity record; e.g., if one record covers 49 hours, the number of days will be 3; if the record is 48 hours or less, but larger than 24 hours, the number of days will be 2. **Begin of experiment** tells the date and time of day of the actual beginning of the recording, **End of experiment** the respective items for the end of the recording. The **Length of the sample interval** is given in minutes. The **No. of samples** tells the number of record-

ing intervals which are present in the recording. The product (length of sample interval x number of samples) might be a few minutes smaller than the interval between begin and end of recording due to down-rounding if the data *Tempus* works with are binned from original data. The **1st experiment** and **Date of first experiment** statements will tell the kind and the date of a manipulation within the data record, respectively, if any were declared (see *Miscellaneous→Insert experiment date and description*).

- The **assignment** section (Fig. 3B) tells the allocations of day numbers and calendrical dates for the whole record, if an experiment is loaded.

- The **original data** section (Fig. 3C) shows the actual raw data samples in the left column. The next two columns indicate the respective sample numbers and the time of day of the beginning of the recording of the indicated sample. The rightmost column presents the respective calendrical dates, which generally are displayed only for the 00:00 h values of every day, but additionally also for the actual first and the last sample of the recording. If a recording did not start exactly at 00:00 h, "0"-values are introduced during data import to artificially set the begin of the recording to 00:00 h. These artificial values precede the actual data, but can be recognised since no sample numbers are assigned to them. See *Command Import data* for more details.

Command *Import data*. This option facilitate the import of ASCII data files containing uniformly recorded activity or physiological data into *Tempus* through creating an experiment workbook out of them; the original text file itself will remain unaffected. After pressing this button, a dialogue opens which allows to choose a text file which must be of the form *.txt. After selecting a file, press **Open**. A workbook will be created in the form described in *The experiment workbook*, formatted accordingly, and the header (Fig. 4) together with the raw data will be copied to the *Data* worksheet. Then, the workbook will be automatically saved to the directory of the according text file in the form *.xls (where * is the name of the source file), and closed. After that, a dialogue appears which offers the options to import another file, or to terminate the importing process.

Source text files to be imported this way must comply with the following format:

```
06.08.2002
14:13:00
1800
1
15.10.2002
11:23:00
3360
1
27
12
53
...
```

Fig. 4. Data header.

Lines 1–2 determine the date and time of day of the begin of the recording (required time format: date: dd.mm.yyyy, time: hh:mm:ss; *not* AM/PM). Line 3 determines the sample lengths in seconds. Line 4 is an arbitrary value without meaning so far. Lines 5–6 determine the end of the recording (formatted as above), line 7 the number of samples in the record, line 8 is again an arbitrary value. The actual data track starts with line 9 ("27" in the given example).

The value of a single sample should never exceed 2,147,483,647 (= double integer limit), and the number of samples should not exceed 65,526, the latter due to limitations of Excel. This restriction nevertheless allows for continuous recording of 455 days with a sample length of 10 minutes. If needed, the recording time may be extended to the threefold length by binning the samples to 30 minutes, what should be sufficient for most circadian analyses.

If a recording did not start exactly at 00:00 h, "0"-values are introduced during data import to artificially set the begin of the recording to 00:00 h.

A manual conversion of text data to an experiment workbook might be performed as follows: Create an empty Excel workbook, than format it (*see Miscellaneous→Reformat data*). Determine the time difference between the actual time of the beginning of the recording, and the beginning of the same day (00:00 h). Calculate the number of samples which would fit into this interval (down-round if necessary), then type this many "0" into column *A*, beginning with cell *A9*, one "0" into every following cell. Paste the ASCII data row into column *A* of the *Data* worksheet, beginning with the cell following the last "0" entrance. Eventually, remove delimiters with the **Search and Replace**-function of Excel. Type the header information as required into Cells *A1–A8*. The number of samples is determined by the row number of the last data value minus 8 (= header space); add the number of the additional "0" values. All other information you should know from your recording procedure. Reformat the workbook by engaging the reformatting function again if necessary.

Command *Help*. Here you find this program description in HTML-format. Pressing the **Help-**

button will evoke your web browser and display this documentation. To do this, the folder *TempusDoc* must reside in the same folder as the *Tempus_ 1.6.xla* file.

Command *Quit Tempus*. This quits *Tempus* permanently by removing it from the Excel environment. One might restart it *via* the Excel **File→Open** menu, with the Add-In manager, or by double-click onto the *Tempus_ 1.6.xla* file in the explorer.

Register Activity

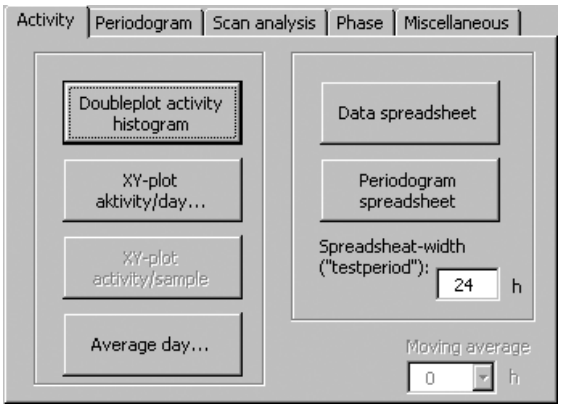

Fig. 5. Contents of the register **Activity**.

In this register, one will find the options to visualise directly the activity present in the active experiment (Fig. 5). The data are evaluated in the range determined in the **Interval for analysis** input section of the main menu. The button **XY-plot activity/sample** and the input field **Moving average** are currently not active.

Command *Double plot activity histogram*. After pressing this button, a double plot activity histogram or actogram (called so although here it is actually a line plot) of the specified data interval is produced onto the *Histogram* worksheet of the experiment workbook (Fig. 6). Unfortunately, due to the limited graphing capabilities of Excel it rather resembles an ancient event recorder output and cannot be improved much, as long Excel does not support diagrams with multiple y-axes. Nevertheless, performing the activity histogram will at most be the first step to obtain information about the data.

The upper scale of the activity plot shows the time of day in full hours, the scale on the right shows the day numbers. The activity record of day 1 starts at the upper left corner below the "hours" scale and reaches to the middle of the scale (0 h); then, day 2 begins. Day 2 is again plotted below day 1 in the left half of the actogram, followed at the right by day 3, etc. Note, that the scale at the right indicates the day numbers for the left half of the actogram; for the right half, read the adjacent day number and add 1. Since the *Histogram* worksheet is reserved for the histogram plot only, it will generally be performed once for the whole data record, and then might remain on the sheet. Stretch the actogram plot if the number of days is very high and the plot is difficult to read.

Command *XY-plot activity/day*. The XY-plot of activity amount versus time will be plotted to the *Miscellaneous* worksheet (Fig. 7). The x-axis represents the time in numbers of experimental days, the y-axis the activity amounts. The activity of every single day is summarised and plotted to the respective day. Although this does not give information about circadian behaviour, the fluctuation of activity over the whole data record can easily be visualised, and, e.g., relations between activity amount and overt period length may be investigated.

After pressing the respective XY-plot command button, a dialogue appears which allows for choosing between a linear or a decadic logarithmic plot of the activity amount on the y-axis (Fig. 8). The checkbox **Serial evaluation** on the top of the dialogue let choose for an automatic, sequential evaluation of multiple experiment files. After checking this option and pressing **OK**, the experiment workbooks to evaluate can be selected in the appearing dialogue. After pressing **Open**, every selected workbook is automatically opened, the analysis is executed for the *whole* length of the data record, the diagram is plotted, and send to the active printer. Then the workbook is closed. The results will *not* be saved to the experiment workbooks; the serial evaluation function is designed to quickly get an overview over a large set of data without altering the workbook contents. It is strongly recommended to close all respective workbooks before serial evaluation is started over them, because the attempt of *Tempus* to reopen a workbook will interrupt the working process until reopening is confirmed or refused in the appearing dialogue.

Command *Average day*. This function allows to plot the mean activity over the course of an average day in a given data record, calculated over the number of days specified in the input section of the main menu (Fig. 9). The diagram will be issued to the *Miscellaneous* worksheet. The average day calculation can be performed for both *Zeitgeber* day and

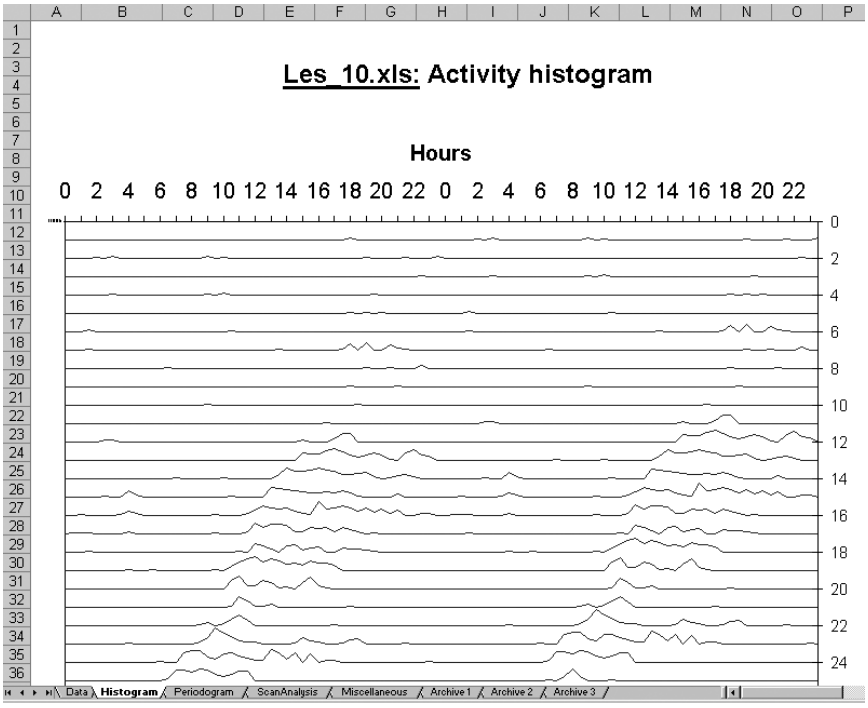

Fig. 6. Double plot activity histogram of an animal, which participated in AMe lesion experiments.

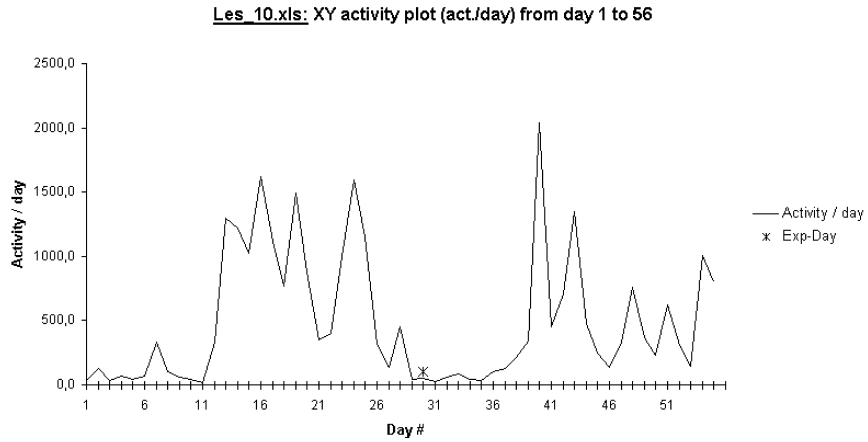

Fig. 7. XY activity plot with linear scale of activity amounts per day. The first 26 days of this animal are also shown in the double plot activity histogram in Fig. 6.

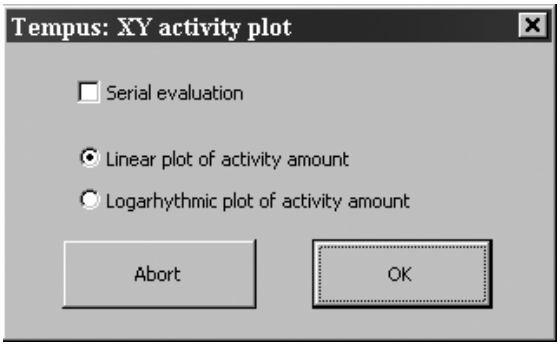

Fig. 8. Option dialogue for the XY activity plot.

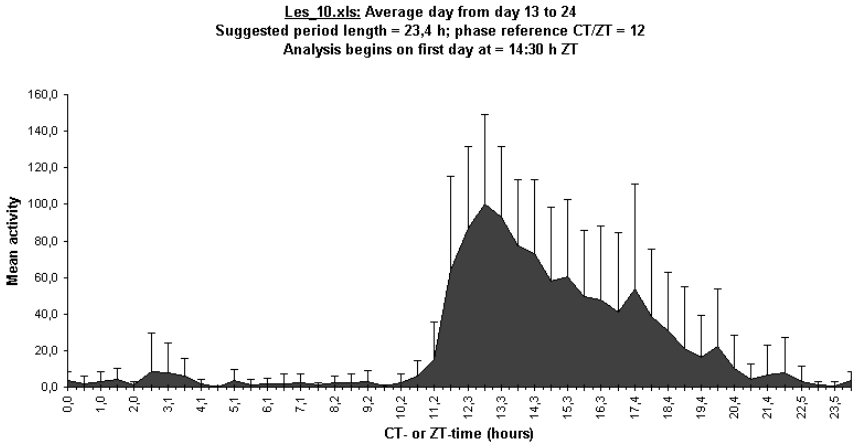

Fig. 9. Average day plot. The average circadian day of this cockroach shows the typical rapid increase of activity around CT 12, and a sloping decrease of activity later in the activity phase. The corresponding double plot activity histogram of this animal is shown in Fig. 6, a periodogram over the days evaluated here in Fig. 11.

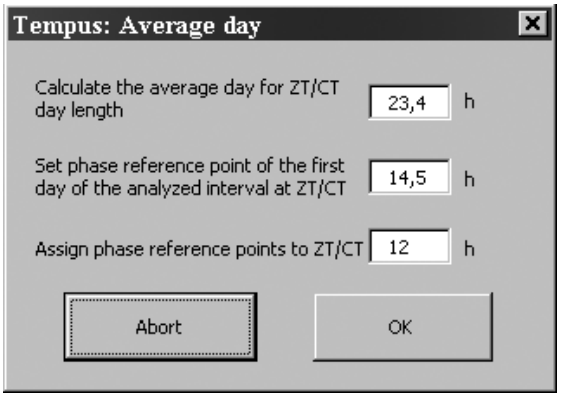

Fig. 10. Input dialogue for the average day plot. The inputs shown here were used to obtain the plot shown in Fig. 9. The periodogram in Fig. 11 delivered the CT day length, which is set in the first input box. The phase reference point of the second input box was obtained by determining the activity onset in day 13 with the actogram in Fig. 6. The third input box contains the definition of CT 12 as activity onset for the night active cockroach.

circadian day. For the average day plot, the activity of every sample record that belongs to the same daytime (*Zeitgeber* time or circadian time, as specified) of every selected day is summarised, and their mean values and standard deviations over the days are calculated. This is particularly valuable to characterise the typical activity pattern of an animal, e.g., the morning and evening peaks in *Drosophila*. The x-axis of the plot shows the time of day in hours, the y-axis the mean activity per sample. If the plot is calculated for a circadian day unequally to 24 real-time hours in freerunning condition, the circadian day length on the x-axis will be normalised to 24 hours. In this case, the average day will be calculated for the specified period after setting the raw data into a matrix employing the same algorithm as used for periodogram analysis. The row wide of this matrix is determined by the number of data samples occuring in the period.

After selecting the interval of days to be analysed, pressing the **Average day** command button evokes a dialogue for the input of three parameters required for the analysis (Fig. 10).

The input **Calculate the average day for ZT/CT day length** determines the length of the animal's day. This day length might be determined by the length of a *Zeitgeber* period (in most cases, 24 hours), or, in freerunning condition, by the length of the circadian day of the time interval to be analysed. The latter is characterised by the period length, which must be assessed prior to the average day calculation with the periodogram analysis (see *Register Periodogram*).

The input **Set phase reference point...** specifies the phase reference points. This might be the beginning, the maximum, or the end of an activity phase either in a *Zeitgeber* day or in a circadian day of a data record. If the day length is controlled by a *Zeitgeber*, just take the according *Zeitgeber* time (e.g., time of switching light on or off, respectively). In freerunning condition, determine the daytime when the phase reference point occur on the 1^{st} *day* of the interval to be analysed on the activity histogram (see *Command Histogram*); this might result to any value between 0 h and 24 h. In case the phase reference point is difficult to determine on the first day selected, it is recommended

to choose another day as first day where the phase reference point is better to assess. The appropriate selection of the phase reference point largely influences the accuracy of the plot.

The input **Assign phase reference points to ZT/CT** specifies onto which *Zeitgeber* or circadian time of day on the x-axis the activity occuring at the phase reference points have to be plotted. In an entrained condition, this value is usually equal to the phase reference points determined above, but may vary with special definitions for the experimental specimen in question. For a general example, in a night active cockroach entrained by a light/dark cycle, the time of light off is regularly set to ZT 12:00 h. Then, type 12 h into both the second and the third input box. Note, that if *Zeitgeber* time is unequal to 24 hours, the x-axis will nevertheless be normalised to 24 hours. In freerunning condition, the time of day for the phase reference point is fully dependent from the respective definitions. For example, in cockroaches, which are active at nighttime, the phase reference for activity onset is defined as 12:00 h; in animals active at daytime, the onset of activity is generally defined as 00:00 h. Press **OK**, if the inputs are finished.

Command *Data spreadsheet*. This function returns the raw data of the specified analysis interval as a pure table, which width corresponds to the number of values per day; i.e., each row contains all samples of the respective day. The data spreadsheet will be issued to the *Miscellaneous* worksheet.

Command *Periodogram spreadsheet*. This is similar to the function **Data spreadsheet** and writes a pure table of the raw data onto the *Miscellaneous* worksheet. However, the data were set up into a matrix by the same algorithm as used for periodogram analysis (see *Register periodogram*), and exactly this matrix will be returned. The row width of the table is to be determined in the respective input box. This value corresponds to a particular testperiod in the periodogram analysis, and the matrix is calculated accordingly. This function is interesting for error analysis, if the VBA code will be modified for further improvement of the periodogram algorithms.

Register Periodogram

In this register (see the main menu on Fig. 1), the functions for the periodogram analyses are located. The data are evaluated in the range determined in the **Interval for analysis** input section of the main menu. Currently, χ^2-periodogram and Enright periodogram calculations are available. Both periodograms are issued onto the *Periodogram* worksheet. The input boxes **Testperiods** determine the interval for the testperiods in both periodogram analyses, the input box **Stepwidth** specifies the intervals between the single testperiods.

Both kinds of periodograms base on the same type of matrix analysis to assess rhythmicity in time series data (Enright 1965). The χ^2-periodogram is further extended by a statistical test based on the χ^2 distribution of the single data, to test the probability of rhythmicity for a given testperiod (Sokolove and Bushell, 1978).

Briefly, for every testperiod within the specified testperiod interval, the raw data are set up into a matrix with a row width equally to the number of data samples occurring in the time interval determined by the respective testperiod. Since the number of all data samples in a row will mostly not exactly fit into the given testperiod, some data values were omitted following a peculiar algorithm, to provide the best fit into the matrix. The values of every column of the matrix are averaged (= mean of column values). Then, all means of column values were again averaged, leading to mean of all data in the matrix. The mean of all data will be subtracted from every mean of column values, and the results were squared to avoid negative numbers. These results will then be summarised, and the square root of the sum is calculated. The resulting number is now termed the A_P of a given testperiod, were P represents this testperiod. In other words, the A_P is the sum of the variances of all means of the column values. The A_P is highest if the testperiod is equal to a period length of any rhythmicity in the data. In this case, the highest and the lowest data values, respectively, stand one below the other in the matrix. Then, high values for the variances of the column means occur, which sum is this high A_P. In an Enright periodogram analysis, the A_P for every testperiod is plotted against the respective testperiod.

In the χ^2-periodogram, for every testperiod a so-called Q_P value is determined. For this, the respective A_P value is calculated, squared and multiplied with the number of columns in the matrix. Then, this product is divided by the variance of all values in the matrix. Hence, if the matrix values would be normally distributed (what is not the case, if any clear rhythmicity occurs in the data), the Q_P would approximately correspond to a χ^2 distribution with (column number – 1) degrees of freedom. The Q_P value (often termed the "power" of the periodogram) is higher, the more the data distribution contains any rhythmicity in the given testperiod, and is plotted against its testperiod. The highest Q_P in the periodogram states, that its respective testperiod is the period length τ (tau) of a circadian rhythm in the data interval evaluated. Additionally, the χ^2 distribution for every testperiod is determined for the probability p, and the respective degree of freedom. The latter is the number of values in a matrix row, minus 1. In *Tempus*, p is fixed to 0.01, without Bonferroni correction; i.e., the probability for any Q_P values in a presumed χ^2 data distribution not to reside within this distribution is less than 0.01 %. Plotting of the χ^2 values against the respective testperiods results into a sloping line, which herein is termed the Sokolove significance line (SSL). This means that if a Q_P exceeds the SSL, the probability that rhythmicity occurs with a τ equally to the respective testperiod is higher than 99 %. For more details, refer to Sokolove and Bushell (1978).

Command *Enright periodogram*. The command **Enright periodogram** issues a periodogram cal-

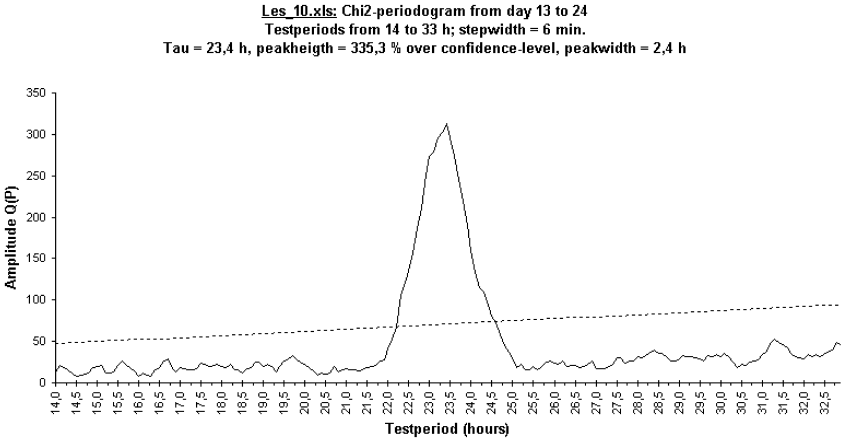

Fig. 11. A χ^2-periodogram covering day 13 to 24 of the animal which actogram is shown in Fig. 5. It shows highly significant rhythmicity with a period length of 23.4 hours.

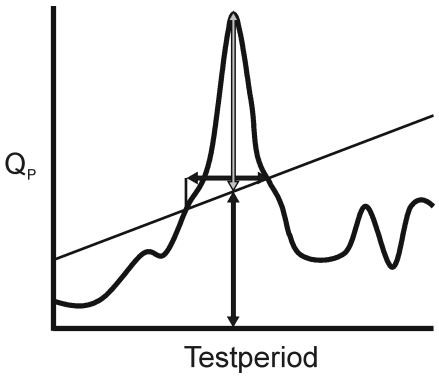

Fig. 12. Method for measurement of the periodogram peak values demonstrated in a fictive χ^2-periodogram. The height of the periodogram peak over the Sokolove significance line (grey vertical arrow) is expressed in percent of the height of the respective χ^2-value for $p = 0.01$ (black vertical arrow), which is here about 120 %. The width of the peak is measured between the intersections of the peak with the Sokolove significance line (horizontal arrow) and is expressed in testperiod hours.

culated after the algorithm published by Enright (1965) onto the *Periodogram* worksheet. The x-axis of the diagram indicates the testperiods; the y-axis indicates the A_P values calculated for the respective testperiods. The headline of the diagram shows the evaluated data interval in number of days, further the testperiod interval together with the respective stepwidth, and the determined period length τ (indicated as the testperiod where the highest A_P value in the periodogram occurred). Press the **Enright-Periodogram** button after you have finished your settings.

Command *Chi2-periodogram.* The command **Chi2-periodogram** issues a χ^2-periodogram calculated after the algorithm published by Sokolove and Bushell (1978) onto the *Periodogram* worksheet (Fig. 11). The x-axis of the diagram indicates the testperiods; the y-axis indicates the Q_P values calculated for the respective testperiods. The sloping line (herein called Sokolove significance line, SSL) marks the χ^2 values for $p = 0.01$ for the respective testperiods; therefore, periodogram peaks exceeding the line indicate a probability for rhythmicity of 99 %. The headline of the diagram shows the evaluated data interval in number of days, further the testperiod interval together with the selected stepwidth, and the determined period length τ (indicated as the testperiod where the highest Q_P value in the periodogram occurred). The height of the largest peak is indicated as a relative value, determined by how much the highest Q_P value exceeds the respective χ^2 value. The height is expressed in %, with 100 % being the distance of the height of the respective χ^2 over the x-axis (Fig. 12). Thus, a peak height of 0 % indicates that the peak lies exactly on the SSL; 100 % indicates that the peak height value is twice the time of the respective χ^2 value. The width of the largest peak is expressed in hours on the x-axis and is determined by the distance between the two intersections of the periodogram peak with the SSL (Fig. 12).

Press the **Chi2-Periodogram** button after you have finished your settings. The default values for the testperiod interval and the stepwidth are within a common range and should suit for most evaluations. However, if one peak is higher than the actual peak of interest, the data for this highest peak will be displayed. This is especially common if e.g., a peak

around 24 h is quite small, and another peak on the right side of the periodogram exceeds the SSL by an amount which might be lower than the 24 h peak, but is higher in terms of absolute Q_P values. In this case, one might narrow the testperiod interval borders to exclude the disturbing peak to get the result values for the peak of interest. *Tempus* automatically recognises peaks which exceed the SSL and excludes peaks which might have a higher Q_P value, but do not exceed the SSL. Increasing the testperiod stepwidth will speed up the calculation time, but will negatively affect the accuracy of the periodogram. Reducing the stepwidth might be of interest if two peaks, i.e., two rhythms that lie close together, should be separated. This might enhance accuracy, but is only reasonable if the raw data sample interval is smaller than 15 minutes.

Register Scan Analysis

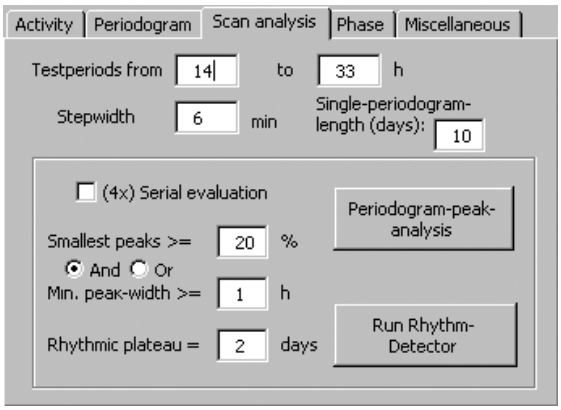

Fig. 13. Contents of the register **ScanAnalysis**.

This register (Fig. 13) provides the options and commands for the data scan analyses, i.e., the periodogram peak analysis and the Rhythm Detector analysis. These analyses work on the analysis interval specified in the input section of the main menu. Both analyses base on the following procedure: For a number of days X (to be specified in the **Single periodogram length** input box), the program calculates a χ^2-periodogram from day 1 of the specified analysis interval to day X, then from day 2 to day X+1 and so on, until the end of the interval ("periodogram scan"). There, the analysis stops at day (last day of the analysis interval – X + 1). In both analysis methods, the single periodograms obtained will be differentially evaluated (see below). The values for testperiod interval borders and stepwidth determine parameters of the single periodograms and have the same meanings as described in *Register Periodogram*; generally, it may not be necessary to change them.

The checkbox **(4x) Serial evaluation** allows for an automated sequential evaluation of multiple experiment files. After checking this option and pressing **OK**, a new dialogue appears which allows for the selection of several experiment workbooks. As in all other options applying to multiple files, all files have to reside in one directory. After pressing **Open**, every selected workbook is automatically opened, the analysis is executed for the *whole* length of the data record using the parameters specified, the diagram is issued, and send to the active printer. Then the workbook is closed. The results are *not* saved to the workbooks; the serial evaluation function is designed to automate the evaluation of larger sets of data while simultaneously getting printouts, without altering the workbook contents. The serial evaluation is carried out differentially in one aspect for peak analysis and Rhythm Detector: Since in the periodogram peak analysis only one analysis is performed for every experiment file, the evaluation for the Rhythm Detector is carried out four times for every data record, with single periodogram lengths of 6, 8, 10, and 12 days, respectively. Here, the use of FinePrint is of particular value. Furthermore, since the computation of the scan analyses is quite consuming, it is possible to perform it overnight. It is strongly recommended to close all respective workbooks before the serial evaluation is started, because the attempt of *Tempus* to reopen a workbook will interrupt the working progress until the appearing dialogue is quitted. This is particularly annoying during overnight evaluations.

Command *Periodogram peak analysis*. This function produces a periodogram peak analysis diagram to the *ScanAnalysis* worksheet. The analysis determines the mean height and width of the highest peak of every single periodogram of a periodogram scan (compare Fig. 12) including standard deviations together with the respective maximum/minimum values. The periodogram peak analysis is particularly useful to assess reasonable threshold parameters for the Rhythm Detector evaluation. Either arrhythmic and/or randomly permutated data records may be used to determine mean heights and widths together with standard deviations of periodogram peaks exceeding the SSL, which occur in arrhythmic data sets (Fig. 14).

The x-axis of the periodogram peak plot indicates the numbers of days of the analysis interval. The left y-axis indicates the quotient Q_P/χ^2 (continuous blue curve), where Q_P is the highest Q_P value which occurred in a single periodogram (the periodogram

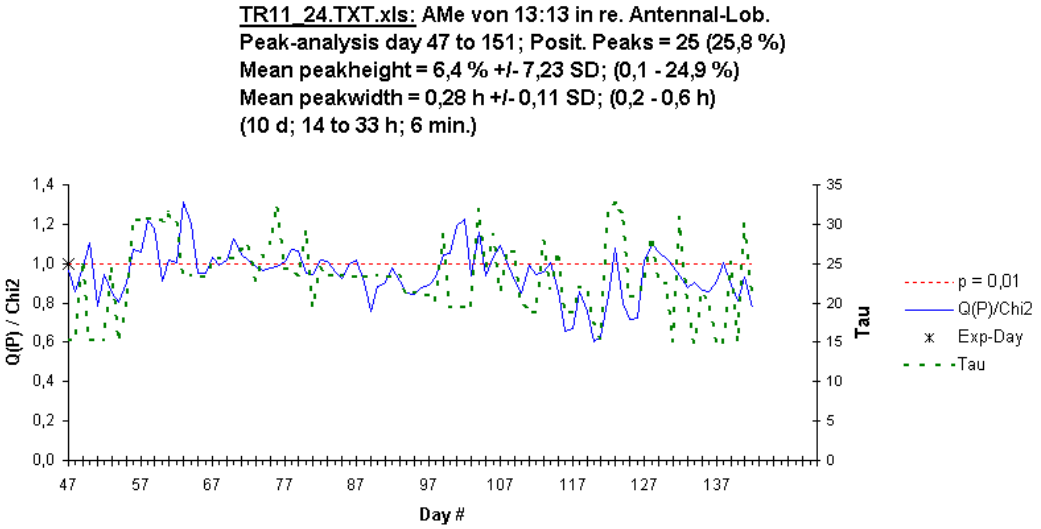

Fig. 14. A plot of a periodogram peak analysis of an animal, which remained arrhythmic after transplantation of an AMe into the right antennal lobe. The plot covers the interval from the day of the operation (marked with an asterisk visible here on the left y-axis) until the end of the recording. The $p = 0.01$ and Q_P/χ^2 curves are identical to the curves presented in the Rhythm Detector plot (Fig. 15). Additionally, the course of the respective period length (τ) values is displayed by the dotted green line. This curve appears very ragged, since these τ values do not correspond to any established rhythmicity. The main information about the periodogram peak values are to be read from the chart headlines.

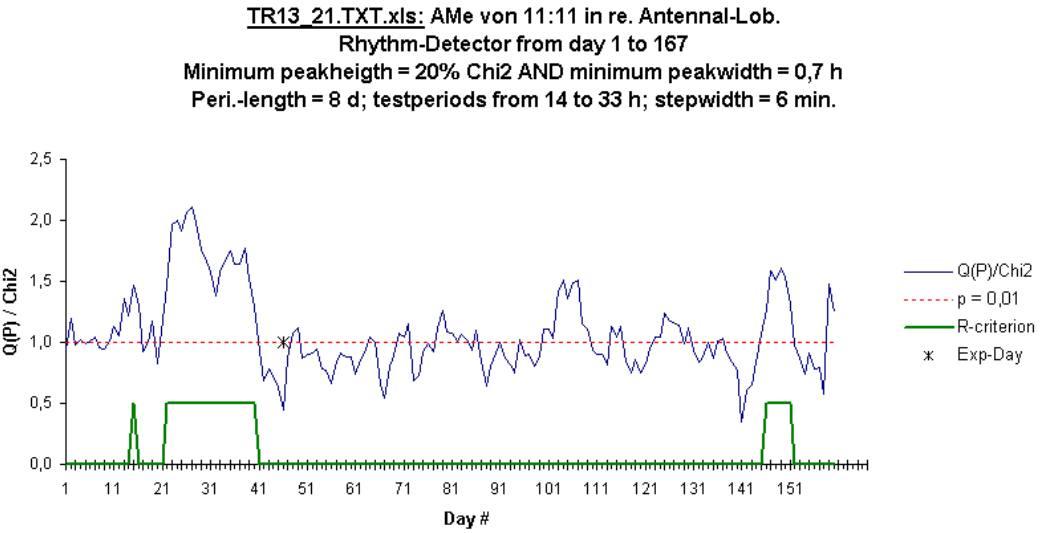

Fig. 15. Rhythm Detector plot of an AMe-transplanted cockroach, which regained circadian rhythmic activity several months after the transplantation. The single periodogram length was here determined to 8 days. The threshold values that determine rhythmicity were 20 % for peak height and 0.7 h for peak width, while both values had to be simultaneously reached or exceeded (AND-condition). The blue curve marks the Q_P/χ^2 values of the respective highest periodogram peaks of every single periodogram. In the time before the operation (day marked by an asterisk) this curve is mostly elevated over the normalised χ^2-values (straight red dotted line), and then rather oscillates around the normalised χ^2-values. The green curve (R-criterion) is elevated to an arbitrary value of 0.5 where the periodogram's peak threshold values are reached or exceeded. This is the case in a large part of the activity before operation, and after the operation between days 146 and 151.

peak), and χ^2 is the respective χ^2 value (see *Register Periodogram*). While calculating the quotient Q_P/χ^2, Q_P is normalised relative to its χ^2; hence, the χ^2 is normalised to 1, and is plotted as well (the straight dotted line). Note, that if a given single periodogram was calculated from day x_1 to day x_2, its Q_P/χ^2 value is plotted to day x_1. The right y-axis indicates the period length τ determined by the respective single periodograms, which is represented by the dotted green curve. Thus, the fluctuation of τ over the analysed time interval is reported. This curve remains relatively smooth if a stable circadian rhythm occurred, but ragged, if this was not the case. If an experimental manipulation was specified, its day number is indicated by a little star on the χ^2-line.

The most important information delivered by this analysis however appear in the headline of the diagram. The first line indicates the filename of the experiment workbook and a short description of the experimental manipulation, if any was specified. The second line shows the analysis interval, and the number and percentage of single periodograms with peaks exceeding the SSL. "Mean peak height" indicates the mean heights of all periodogram peaks exceeding the SSL, and the respective standard deviation (S.D.). In brackets, the minimum and maximum values that were reached in this trial are shown. "Mean peak width" indicates the mean width of all periodogram peaks exceeding the SSL with the respective S.D., and minimum/maximum values in brackets. For definition of peak height and width, refer to Fig. 12. The last line of the chart shows in brackets the specifications of the single periodogram used (single periodogram length, first and last value of testperiod interval, and testperiod stepwidth).

Command *Run Rhythm Detector.* This function issues the Rhythm Detector plot to the *ScanAnalysis* worksheet (Fig. 15). The generation of a Rhythm Detector plot is explained in Fig. 16 in more detail. The Rhythm Detector is designed to recognise short rhythmic activity phases in longer data sets containing arrhythmic episodes, especially after experimental manipulations that directly influence the circadian pacemaker (see *Part II*). Single periodograms of the specified lengths are calculated while scanning the data record as described above. Rhythmicity is assessed by determining the occurrence of periodogram peaks exceeding the SSL, by measuring the heights and the widths of this peaks (compare Fig. 12), and by finally determining whether these peaks exceed specified thresholds. These thresholds will be determined in the input boxes **Smallest peaks** and **Min. peak-width**. With the **And** and **Or** options, it can be selected if either simultaneously both, or only one threshold criterion allone has to be fulfilled to indicate rhythmicity. Filtering for one specific criterion can be achieved by selecting the **Or** option, and setting the respective other criterion to a very high value that will definitely not occur.

The input **Rhythmic plateau** allows further to determine how many "rhythmic" days have to follow in sequence (thus, forming a plateau of the rhythm detector curve) to judge a Rhythm Detector analysis as "rhythmic". This function currently applies for evaluation series with randomly permutated data only (see *Register Miscellaneous→Permutate data*).

If the selected criteria were fulfilled for any single periodogram, the day in the Rhythm Detector plot corresponding to the first day of the respective single periodogram will be marked as "rhythmic", and an arbitrary value of 0.5 will be assigned to it. Otherwise, this value will be set to zero. This leads to the Rhythm Detector curve (= *R-criterion* curve in the plot in Fig. 15). For reasons mentioned in Fig. 16D, the periodogram peaks are highest if a single periodogram lies well upon the rhythmic data episode, and decline if they contain additionally arrhythmic data portions while the scan is entering or leaving the rhythmic data stretch. Thus, the Rhythm Detector cannot deliver exact information about the locations of the transients of rhythmic to arrhythmic behaviour (and *vice versa*). It rather marks the centre of the data interval where rhythmicity occurs, with a certain shift backwards. If incidences for rhythmicity are recognised by the Rhythm Detector-analysis in a certain partition of any data, the actual dimensions of this activity episodes have always to be determined by careful judgement of the respective actogram.

In the Rhythm Detector plot, the x-axis indicates the day numbers in the recording. The y-axis indicates the quotient Q_P/χ^2 (scan periodogram curve; continuous blue curve in Fig. 15), where Q_P is the highest Q_P value which occurred in a single periodogram (the periodogram peak), and χ^2 is the respective χ^2 value. While calculating the quotient Q_P/χ^2, the Q_P is normalised relative to its χ^2, which has now the value 1. These normalised χ^2 are drawn as dotted red line into the Rhythm Detector plot (χ^2-line for $p = 0.01$ in Fig. 15). Note, that if a single periodogram was calculated from day x_1 to day x_2, its Q_P/χ^2 value is plotted to day x_1 (i.e., the number of the first day of the single periodogram). If an experimental manipulation was specified, its day number is indicated by a little star on the χ^2-line.

The first headline of the chart indicates the filename of the experiment workbook and a short description of the experimental manipulation, if any is specified. The second line shows the time interval

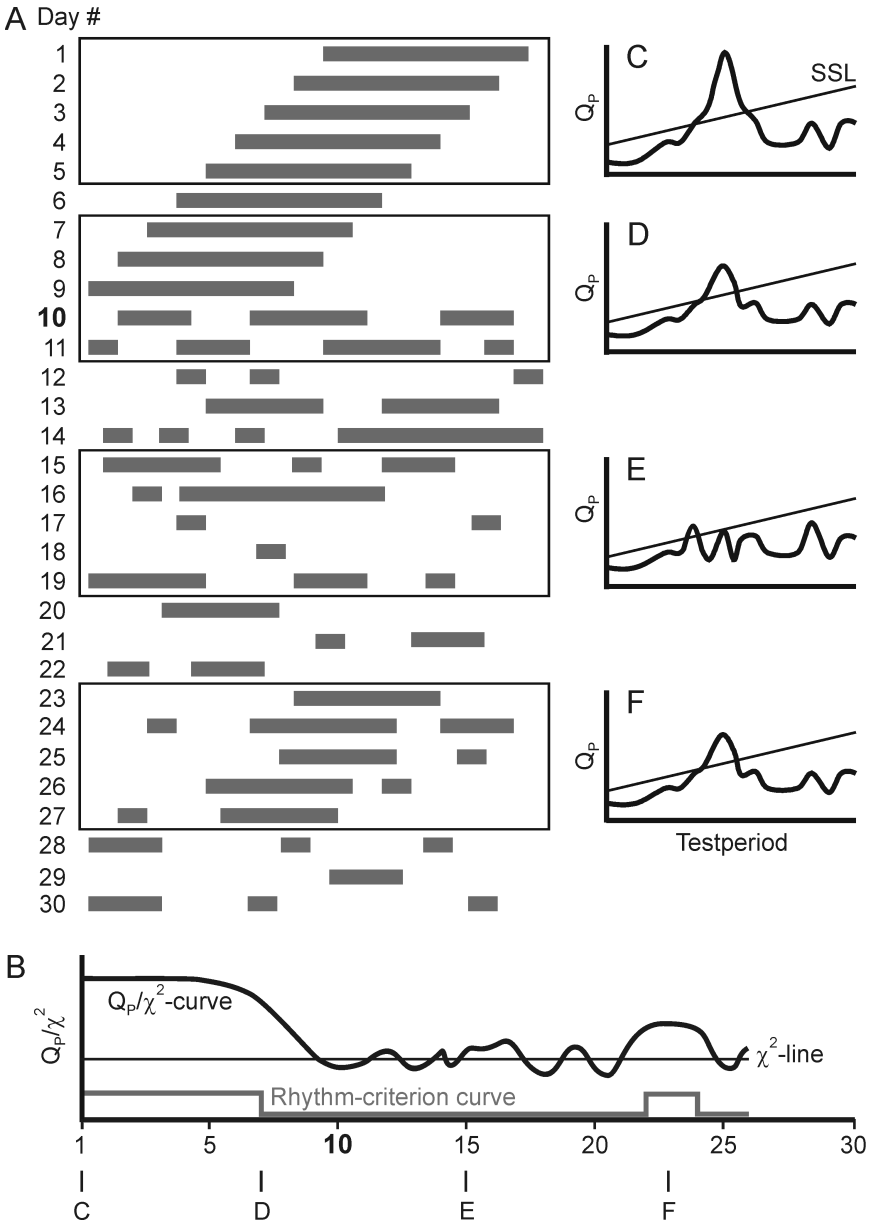

Fig. 16. Generation of a Rhythm Detector plot demonstrated in a fictive transplantation experiment. **A:** The single plot actogram shows circadian rhythmic activity from day 1 to day 9. At the beginning of day 10, the circadian pacemaker is assumed to be destroyed and replaced by a grafted pacemaker, and initially, the animal behaves arrhythmic. From days 23 to 27, rhythmic behaviour is reestablished. This data track is assumed to be scanned by the Rhythm Detector (RD) with a single periodogram length of 5 days. The rectangles in the actogram mark the intervals from which the exemplary single periodograms (C-F) were calculated. **B:** Here, the resulting RD plot is shown. C–F indicate where the results of the respective exemplary periodograms are plotted to. **C:** The first periodogram is calculated from days 1–5 and shows a prominent peak exceeding the Sokolove significance line (SSL). The respective Q_P/χ^2 value, which largely exceeds the χ^2-line, is plotted to day 1 in the RD plot (Q_P/χ^2-curve). The rhythm-criterion curve of the RD plot is elevated to an arbitrary value above the x-axis. Thus, it indicates rhythmicity according to presetted periodogram peak dimension thresholds. **D:** This periodogram is calculated from days 7–11; its results are plotted to day 7 in the RD plot. Note, that the periodogram already contains an arrhythmic portion of the activity data, and therefore, this periodogram peak is lower than that of the first days of the recording. Hence, the Q_P/χ^2-curve in the RD plot already decreases to lower values, before the actual operation day (day 10) is reached in the RD-plot. **E:** This periodogram is calculated from days 15–19. It indicates arrhythmicity due to the small periodogram peak that does not reach the determined threshold values. Therefore, the rhythm-criterion curve is set to zero. Other periodograms performed in the arrhythmic data stretch may not even have peaks exceeding the SSL and therefore, deliver Q_P/χ^2-values below 1. This results in a Q_P/χ^2-curve oscillating around the χ^2-line while scanning arrhythmic data stretches. **F:** This periodogram is calculated from days 23–27, and includes a data portion with regained rhythmicity. This leads to a peak with dimensions exceeding the determined threshold values; thus, the rhythm-criterion curve indicates rhythmicity. Since regained rhythmicity is generally less continuous than generic rhythmicity, the periodogram peak is correspondingly lower.

analysed in numbers of days. Then, the rhythmicity criteria which applied for this analysis are indicated as well as their logical connection by the AND/OR operands. The last line contains the parameters of the single periodograms.

Register Phase

The register **Phase** implies currently no functionality. It is prepared for future projects, which will cope with the evaluation of experimentally induced phase shifts and the creation of phase response curves.

Register Miscellaneous

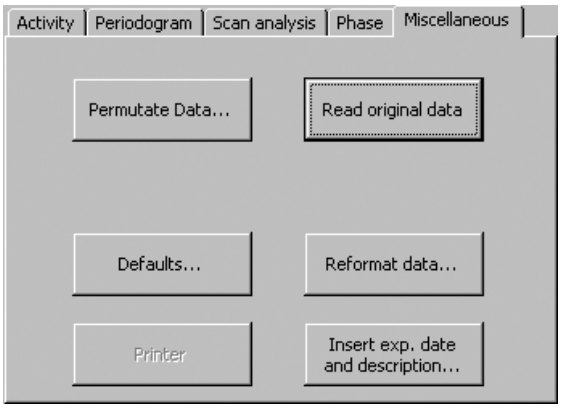

Fig. 17. Contents of the register **Miscellaneous**.

Here, some auxiliary functions are situated which allow for randomised permutation of data, viewing the default values used throughout *Tempus*, reformatting damaged workbooks, and assigning dates and descriptions of manipulations to experiment workbooks (Fig. 17).

Command *Permutate data.* This function activates a dialogue, which offers options to perform randomised data permutations (Fig. 18). Data values will change their places within the data series as determined by the random generator of the computer. This simulates a data series with no time-dependent correlations between the data. Data permutation is useful to assess reasonable parameter thresholds for the Rhythm Detector by means of the periodogram peak analysis (see *Register Scan Analysis*). Furthermore, the parameters for the Rhythm Detector can be tested on permutated data sets. Since permutation and subsequent rhythm detector analysis can be automatically iterated thousands of times, the adequacy of selected parameters can be statistically tested.

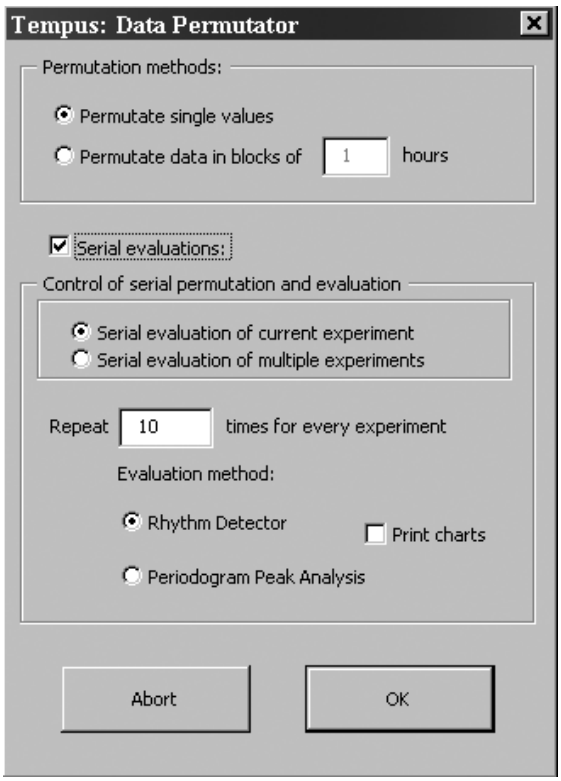

Fig. 18. The input- and option dialogue for the data permutator. This setting would perform 10 series of randomised permutations of single samples with subsequent Rhythm Detector evaluations to the active experiment. No diagrams would be printed, but the results would be stored to a separate text file.

The first box of the data permutator dialogue offers options for two different methods of permutation. The first method is the permutation of single values, i.e., all samples of a data record will be randomly scattered throughout the whole record. This is the most applicable method to get fully randomised permutation of the data. The second option provides a method that permutates connected blocks of data samples, which lengths will be specified in the adjacent input box.

After clicking the **OK** button, the data of the active experiment are permutated and can be evaluated as usual. The message "Permutated data!" appears above the **Close experiment** button of the main menu to inform you that you are now working on permutated data. Permutation of the data takes place only in the memory of the computer; the original data on the *Data* worksheet will not be affected. To restore the original state, refer to *Command Read original data*, or just close and reopen the main menu.

The checkbox **Serial evaluations** offers the opportunity to perform iterative permutations and subsequent evaluations of the active experiment (option **Serial evaluation of current experiment**),

or to perform this iterations and evaluations automatically onto multiple experiment files to be selected (option **Serial evaluation of multiple experiments**). The input box **Repeat X times for every experiment** allows to specify how many times these iterative evaluations should be performed, either with the current experiment, or with each of several selected experiments. Again, it is recommended to keep all respective workbooks closed before the serial evaluation is started. One of two evaluation methods can be selected for iterative permutations and evaluations: the Rhythm Detector or the periodogram peak analysis. Both analyses will be performed on the whole data record. Appropriate settings for these evaluations (i.e., testperiod interval and stepwidth for both periodogram peak and Rhythm Detector analysis, or periodogram peak thresholds and plateau length for the Rhythm Detector) should be finished before the permutation is started. During evaluations, for both methods text files are created which show the results achieved. These files are stored in the folder of the evaluated experiments and will be named **PermRhytDet.txt* or **PermPeriPeak.txt*, respectively, where * is the name of the respective experiment workbook file. Contrarily to the **PermPeriPeak.txt* file, which is created after all iterations are finished, the **PermRhytDet.txt* file will be renewed after every single Rhythm Detector run; thus, preliminary results can be checked while the evaluation is still running. Note, that a 1,600 MHz computer will work about 7–8 hours for 1,000 serial Rhythm Detector analyses of one 100-day data record (using default values for the single periodograms). After evaluation, move or rename the *.txt-files, since they will be overwritten, if a serial analysis is started again with the respective experiment workbooks. The checkbox **Print charts** allows to print the resulting diagrams, what however is only reasonable if either FinePrint is the active printer, or if only few evaluation iterations are performed.

Command *Read orig. data*. This function restores the original state after randomised data permutation. After presssing the **Read orig. data button** the original data will be read in the correct sequence from the worksheet *Data* of the active experiment, and the warning "Permutated data!" will disappear from the main menu.

Command *Defaults*. The function **Defaults** shows the default parameter values for periodogram and scan periodogram analyses, average day calculation, and the periodogram spreadsheet function. Changing of the default values is currently not possible.

Command *Reformat data*. The function **Reformat data** allows to reformat damaged experiment workbooks, or to initially format manually created workbooks, to make them accessible by *Tempus*. Pressing the button evokes a dialogue, which allows for selecting one or several workbooks to reformat. Then, after clicking **Open**, the selected workbooks are automatically opened, and number and names of the worksheets in every workbook are checked and corrected according to the specifications stated in *The experiment workbook*. Then, the appropriate spreadsheet cell formats for the data header in the *Data* worksheet are created restored; the workbook will be safed, and closed. The contents of the workbooks will not be altered by this process. It is recommended to keep all workbooks closed that should be processed.

Command *Insert experiment date and description*.

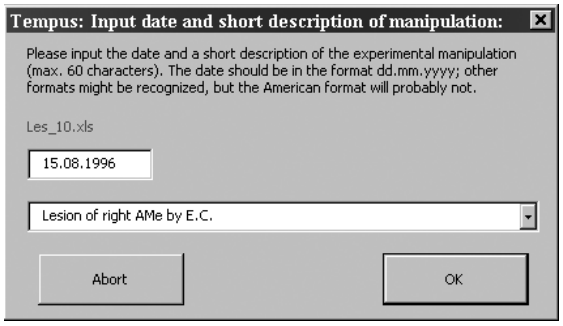

Fig. 19. Input dialogue for assigning a date and a short description for an experimental manipulation to an experiment workbook.

The command **Insert experiment date and description** allows to add the date and a short description of an experimental manipulation, which may be applied to an experimental animal. This command evokes a dialogue that which allows to select one or more workbooks to process. Then, after clicking **Open**, the first of the selected workbooks is opened. A dialogue appears which shows the filename of the workbook and two input boxes (Fig. 19), eventually displaying date and experiment descriptions, if any were already specified. Fill in the date in the first box (format: dd.mm.yy or dd.mm.yyyy). Then, fill in the experiment description (e.g., "Lesion of pacemaker site") in the second box. It is also possible to select 10 prepared descriptions in this box, which are named "Experiment type 1", "Experiment type 2" etc; these descriptions might eventually be changed within the VBA code (module "Format_Data"). After finishing the inputs, pressing **OK** will save and

close the workbook, and the next workbook will be opened, until all selected workbooks are processed. It is recommended to eventually close all workbooks, which should be processed.

Errors

While executing *Tempus*, two main categories of errors may be encountered. The first type of errors are caused by inappropriate parameter inputs, e.g., analysis intervals which do not fit into the possible interval determined by the length of the active experiment, parameters exceeding the specified range, floating point inputs where integers are required, non numerical inputs where numbers are required, etc. The user will be limited to create erratic inputs by an error message, which displays the kind of the input error, and the last appropriate input (or the respective default value) will be restored in the respective input box. This should prevent mistakes in the data evaluation as well as runtime errors, which occur if the program runs into an unexpected situation.

Runtime errors constitute the second category of errors. If any occurs, the execution of *Tempus* will halt in the respective location of the code, the VBA editor appears, and the code together with an error description will be displayed. If one is not familiar with VBA to fix the error, it is recommended to stop the debugging process in the VBA window (menu **Execute**), then to close the VBA window, and to restart *Tempus* by pressing **Ctrl**+**y**. Since the runtime error might be caused by erratic inputs that were not expected by the programmer, try to resume the evaluation.

The most frequent cause of runtime errors, however, are experiment workbooks, which do not fit the structure expected by *Tempus*. Since this incidence is largely covered by error handlers, it might occur that e.g., worksheet names or their correct order in the workbook are accidentally changed during evaluation. This could happen if a previous evaluation is interrupted for any reason, and a newly created diagram worksheet remains intercalated between the first five worksheets of the experiment workbook. The first way to overcome this situation is to check the worksheet integrity, and to restore it manually, if required (see *The experiment workbook*). If this does not help, reformat the workbook (see Register *Miscellaneous→Reformate data*).

A quite inconvenient runtime error is caused by so-called "automation errors" in Excel. If one occurs, Excel runs into an instable condition and probably can only be closed by means of the *Task manager* in Windows. Fortunately, these errors are rare, and in most cases, it is possible to save all open workbooks prior Excel shutdown. The automation error occurs if e.g., Excel looses its internal link to any user dialogue and seems to be caused by a bug in Excel.

PART 2: DATA ANALYSIS

Tempus was successfully used to compare the occurrence of rhythmicity in accessory medulla (AMe)-transplanted cockroaches *versus* control animals. For experimental details, refer to Chapter IV. This section describes additional details for the data evaluation which were not mentioned there, and shows some aspects for correct application and valuation of the results which could be derived with the Rhythm Detector analysis. The report might be used as a guideline for how to analyse similar problems with the aid of *Tempus*. For special details concerning program handling to perform a task, refer to the respective chapters in *Part I*.

After finishing the transplantation experiments, recordings of 87 animals remained which were suitable for further analysis. These animals survived the operation for up to 6.2 months (mean 3.0 ± 1.5 months, mean $\pm$ S.D.). A total of 45 of these animals received AMe-tissue, while 42 control animals received either no implant or grafts, which did not contain an AMe. The goal was to find out whether animals receiving AMe-grafts would restore rhythmic activity; this would demonstrate that the AMe contains a circadian pacemaker.

Indeed, a couple of AMe-transplanted animals displayed clearly recognisable circadian activity weeks or months after the operation. The problem was, that these rhythmic activity occurred only episodically, and lasted maximally 14 days, but often less. This postoperative rhythmic activity was situated into an arrhythmic activity background with fluctuating activity patterns and amounts, and, therefore, often difficult to be recognised within. Moreover, rhythmic episodes appeared to occur also in some of the control animals. Postoperatively rhythmic and arrhythmic animals had to be separated without bias.

First evaluations with the Rhythm Detector

To objectively separate rhythmic from arrhythmic data records, the Rhythm Detector was applied to these 87 recordings. To accelerate the task, the **(4x) serial evaluation** function was used, which automatically processed all files sequentially. With this function, for every workbook (= single experiment) four Rhythm Detector scans were sequentially executed, with 6, 8, 10, and 12 days single periodogram

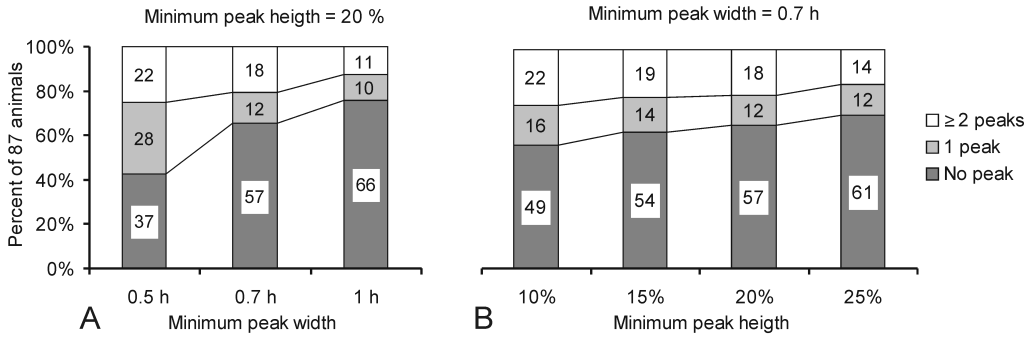

Fig. 20. Results of six different Rhythm Detector analyses of the 87 AMe-transplanted and control cockroaches after combining several threshold values, which both had to be reached or exceeded to indicate rhythmicity. The threshold combination 20 % peak height and 0.7 % peak width is present in both A and B. Rhythm Detector analyses with no, one, or more than one and connected postoperative Rhythm Detector peaks are counted. **A:** Results with minimum peak width thresholds of 0.5, 0.7, and 1 hours, with minimum peak height fixed to 20 %. Note the steep decrease of numbers of animals in the "one peak" category after changing the threshold from 0.5 to 0.7 peak width. **B:** Results with minimum peak height thresholds of 10, 15, 20, and 25 %, with minimum peak width fixed to 0.7 hours. The numbers of animals in the "one peak" and "two or more peaks" categories decrease rather linearly while increasing the minimum peak height threshold.

lengths, respectively[2]. The periodogram parameters were left to the defaults. The result diagrams were automatically sent to the FinePrint printer driver. The diagrams were generally not printed as hardcopy but stored as FinePrint files, with all four Rhythm Detector scans of one workbook collected onto one sheet. Then, on these FinePrint files, the Rhythm Detector charts were examined with respect to postoperative occurrence of Rhythm Detector peaks (the R-criterion curve in the charts; Fig. 15).

In the foreruns, rhythmicity was clearly detectable by elevated R-criterion curves and high Q_P/χ^2 values above the χ^2-line. The Q_P/χ^2 values began already to decline before the operation day; this phenomenon is explained in Fig. 16. After the operation, which included the removal of the remaining optic lobe, the Q_P/χ^2 curves oscillated around the χ^2-lines, and the R-criterion curve was mostly set to zero. Occasionally, the R-criterion curves were elevated to the 0.5-value, thus indicating rhythmicity according to the preselected thresholds. According to the postoperative R-criterion results, three categories were defined: no peak, one peak, or two or more peaks, respectively. The "two or more peaks" category applies if two or more peaks are connected, i.e., they occur in subsequent days; more than one, but isolated peaks were designated to the "one peak" category. For every single experiment file it was determined, whether one of these categories applied to any of the Rhythm Detector scans with 8, 10, or 12 day single periodogram length, respectively. The scans with 6-day single periodogram lengths were disregarded because it soon turned out, that this interval is too short to detect rhythmicity reliably. If more than one category applies for one single experiment, the "highest" category was chosen to characterise the respective experiment; e.g., if the respective 8-day periodogram scan revealed one peak, and the 10-day periodogram revealed two, the record was moved into the "two or more peak" category. Then, the records in each category were counted.

This complete evaluation of all 87 experiment records was performed for several Rhythm Detector thresholds: peak heights of 10, 15, 20, and 25 %, respectively, and peak widths of 0.5, 0.7, and 1.0 hours, respectively. All categories were tested in every possible combination, and connected by the AND condition, what means that both thresholds must be reached or exceeded to indicate rhythmicity[3]. This resulted in 12 complete evaluations of the 87 transplantation experiments. The results for six combinations are shown in Fig. 20. Briefly, it turned out that the more restrictive the thresholds were set, the less experiments belonged to the "one peak" and "two or more peaks" category. The number of these "rhythmic" experiments decreased rather linearly while increasing the peak height threshold. Contrarily, a quite large decrease in the number of the "one peak" category was observed while turning from the 0.5 h to the 0.7 h peak width threshold.

[2]One complete scan of 87 animals lasted about 18 hours on a 400 MHz PC; a 2 GHz PC should accomplish it now in about 3 hours.

[3]The OR condition, i.e., only one criterion has to be fulfilled to indicate rhythmicity, was additionally tested for several thresholds, but the results were discarded because unreasonable high amounts of "rhythmic" experiments occurred. Several different values for periodogram parameters were additionally tested, but the results were not taken into further account, since they revealed no additional information.

This was consistent with the observation that periodogram peaks derived from obviously arrhythmic data sets and which exceeded the Sokolove significance line (SSL), could sometimes be fairly high, but are generally not more than 0.5 hours wide.

After careful consideration of these results, it appeared that reliable thresholds for assessing postoperative rhythmicity were 20 % peak height and 0.7 h peak width, while *both* criteria had to be reached or exceeded simultaneously. Further, it seems reasonable to refuse all records, which showed only single Rhythm Detector peaks or several single peaks that are not connected; thus, a "two or more peaks" criterion should apply to assess rhythmicity. Nevertheless, the thresholds applied might appear to be chosen somewhat arbitrarily. Therefore, the periodogram peak analysis was applied to measure heights and widths of periodogram peaks occurring in 10-day-periodograms scanned over arrhythmic data records.

Exploring "arrhythmic" periodogram peaks: the periodogram peak analysis

It was necessary to get a better idea about the frequency and the appearance of those periodogram peaks exceeding the SSL, which repeatedly occur in arrhythmic data tracks. Thirty of the 87 experiments were selected by judgement of the respective activity histograms, which showed no recognisable sign of rhythmicity in the postoperative parts of the data records. They were selected among animals without optic lobes and there, preferably but not exclusively, among animals, which received no additional grafts. The postoperative data tracks were selectively surveyed by periodogram analysis to confirm that they do not contain circadian rhythmic episodes. Then, the periodogram peak analysis (see *Register scan analysis→Periodogram peak analysis*) was applied first to the preoperative, then to the postoperative parts of these 30 records, with single periodogram lengths of 10 days. For every particular scan, the percentage of periodograms with peaks exceeding the SSL among all periodograms calculated was determined, together with the means and SDs of their respective peak heights and widths. Then, the means of these values for all 30 experiments were calculated. It turned out that about 79.7 % of 1565 single periodograms in preoperative data stretches exceeded the SSL[4]. These periodograms had a peak height of 101.4 ± 62.5 % (mean ± mean S.D.), and a peak width of $1.8\,\text{h} \pm 0.8\,\text{h}$ (mean ± mean S.D.). Postoperatively, periodograms with peaks exceeding the SSL were less frequent (26.6 % of 3445 calculated periodograms), with a mean peak height of 9.2 ± 7.8 %, and a mean peak width of 0.3 ± 0.1 h. These values were well inside the thresholds 20 % peak height and 0.7 h peak width, and suggest their application as suitable, since they are considerably higher than the mean values of peaks occuring in arrhythmic data *plus* the respective standard deviations. Nevertheless, maximum values for peak heights and widths were occasionally observed exceeding these threshold values, with a maximum peak height of 60.8 % and a maximum peak width of 1.1 h observed in different generically arrhythmic data records. This observations demonstrate that rhythmicity cannot be judged upon single peaks only. The chance for single peaks exceeding the threshold values is yet given, but decreases rapidly if more than one of such large peaks are required to follow in sequence (thus, forming a plateau in the Rhythm Detector curve) to assess rhythmicity. However, the demand for too many peaks following in sequence to indicate rhythmicity covers the danger for overlooking short, but prominent rhythmic episodes.

The periodogram peak and Rhythm Detector analyses applied to randomised data

The results of the periodogram peak analyses applied to obviously arrhythmic data supported the suitability of the threshold values determined previously to indicate rhythmicity. However, the arrhythmic data were manually selected upon several criteria and hence, still might include some bias. Therefore, randomised data permutations were applied to ten weeks long data recordings of freerunning, untreated cockroaches with stable circadian rhythmicity, which were subsequently evaluated with periodogram peak analysis and with the Rhythm Detector.

Every record was randomised and subsequently analysed with the periodogram peak analysis ten times. This resulted in altogether 7,020 single periodograms, of which 88.1 % showed peaks exceeding the SSL. The mean height of these peaks was 10.2 ± 9.8 %, the mean width 0.2 ± 0.1 h; these values are within the range obtained by the respective evaluation of the generically arrhythmic animals and therefore, further support the rhythmicity thresholds selected for the Rhythm Detector. Interestingly, the number of periodogram peaks exceeding the SSL obtained with the randomly permutated data was considerably higher than in the arrhythmic animals.

[4]It should be considered, that the left optic lobes of these animals were excised at the beginning of the data recording, leading to longer phases with no stable rhythmicity in some animals after this operation; in untreated animals, the percentage of "rhythmic" periodogram peaks should be considerably higher.

This is obviously due to a more even distribution of activity over the whole data records after the randomisation, compared to generically arrhythmic animals. This results in a more even distribution of the Q_P values just below the SSL in the periodograms and therefore, leads to a higher probability of single Q_P values to slightly exceed the SSL.

Moreover, permutated activity records of the mentioned rhythmic animals were evaluated with the Rhythm Detector analysis. With the serial evaluation function of *Tempus*, 1,000 permutations and subsequent analyses for every of the ten rhythmic data records were performed, with single periodogram lengths of 10 days. This resulted in a total number of 10,000 Rhythm Detector analyses, of which 9 (0.09 %) indicated rhythmicity applying to the rhythmicity criteria stated above. Thus, the Rhythm Detector judges 99.91 % of randomly permutated data records as arrhythmic and, thus, has a negligible error rate.

Based on the results of (i) Rhythm Detector scans with different threshold combinations, and (ii) periodogram peak analyses of generically arrhythmic as well as on rhythmic but randomised data, the postoperative rhythmicity of the transplantation experiments was finally assessed by applying threshold criteria of 20 % peak height and 0.7 h peak width. *Both* criteria had to be reached or exceeded on at least two subsequent days. Evaluating the 87 experiments in this way revealed 13 postoperative rhythmic cockroaches in the AMe-transplanted group and 5 animals in the control group. A comparison of these groups with two statistical tests (G-test and two-by-two frequency table) revealed a significant higher amount of postoperatively rhythmic animals in the AMe-transplanted group. Thus, it could be shown, that the AMe is or contains a circadian pacemaker controlling locomotor activity in the cockroach *Leucophaea maderae* (Reischig and Stengl, 2003).

CONCLUSION AND OUTLOOK

The new Rhythm Detector analysis was created to find small stretches of circadian rhythmic activity in longer and mostly arrhythmic activity data recordings in an automated and unbiased manner. In the evaluation of pacemaker transplantation experiments, it proved to be an indispensable tool to confirm the role of the AMe as circadian clock in cockroaches.

The experiences gathered during development and application of the Rhythm Detector showed that great care must be taken to find applicable thresholds for the detection analysis. If the threshold values, first of all that for peak width, are too low, the error rate for falsely detected rhythmicity drastically increases. Too high thresholds might cause the loss of in fact rhythmic incidences, since periodogram peaks of small data stretches covering only few days are rather small, especially if rhythmicity is unstable. It is recommended to apply the periodogram peak analysis to both generically arrhythmic data, if those are available, as well as to generically rhythmic, randomised data, to measure the periodogram peaks occurring in arrhythmic data sets. If both methods reveal different values for the periodogram peaks, the respective higher values should be used for threshold determination. The thresholds for the Rhythm Detector have to be selected above the mean values for "arrhythmic" periodogram peaks *plus* the respective S.D. These thresholds should then be tested by Rhythm Detector scans on generically arrhythmic as well as on randomised data.

It should further be considered that generically arrhythmic behaviour is not the same as randomising of the single samples of rhythmic data, in terms of activity amounts and distributions of activity. Cockroaches, which both optic lobes have been removed, generally show a considerable decrease and fluctuation in activity amount, and sometimes bursting, sometimes more evenly distributed activities. The more even distribution of samples in randomised data compared to generically arrhythmic data is reflected in the increase of small peaks exceeding the SSL. The simulation of a more natural distribution of data samples in arrhythmic animals may be achieved by permutation of data in connected blocks rather than in single samples. This function has been implemented in *Tempus*, but was not yet extensively tested nor systematically applied. However, preliminary trials showed that the error rate of the Rhythm Detector for wrongly detected rhythmicity might slightly increase if the data were permutated in connected blocks of one or more hours; further studies are needed to explore and quantify this phenomenon. However, these observations emphasise the usefulness of additional analysis of generically arrhythmic data records for threshold determination, and not to rely on randomised data only.

If applicable threshold values were found, as last step the Rhythm Detector will be applied to the data. Occasionally, actogram evaluation might not show any plausible rhythmicity in data stretches where the Rhythm Detector found rhythmicity. This occured twice in the transplantation experiments, once in the AMe transplanted and once in the control population. It appears, that the actual error probability of the Rhythm Detector analysis in real data might be a little higher than the results by evaluating randomised data implicate. It is recommended not to reject those "obvious errors", but rather to count

them as well as "rhythmic" in order to maintain the objectivity provided by this analysis. It is to assume that erroneous detection of rhythmicity might occur in experimental and control groups as well, and a statistical comparison of both groups is very important to manifest any statement about the results. Applied in this manner, the Rhythm Detector should be valuable for many more applications similar to the transplantation experiments introduced herein.

While developing the Rhythm Detector analysis, it became a part of a chronobiological analysis program named *Tempus*. The disadvantages of several other computer programs for analysis of chronobiological data sets are, that they require proprietary data formats, that they are expensive, and/or difficult to use. Here, we present a software which works as client application for the very common spreadsheet program MS Excel, and thus, is easy to use for all users who are familiar with Excel. It will work with many evenly recorded time series data which are aimed to be evaluated in the circadian range, and which are presented as pure text (ASCII) files. Special import filters for particular data formats might be realised. Result data are portable to any application, which supports the import of Excel diagrams. This is the case for mostly all actual word processors, vector graphic programs, and presentation applications. Since *Tempus* contains only basic evaluation methods at the time, with VBA it can easily be expanded to any functionality required for chronobiological research, such as data filtering, generation of phase response curves, and elaborated evaluation methods as MESA, autocorrelation, and fourier analysis. In *Tempus*, no programming of special data output functions is required. Even the restrictions of the graphing capabilities of Excel, which mainly concerns the activity histogram plot function, might be overcome by an automated engagement of the vector graphics and presentation program MS PowerPoint, which is commonly distributed parallel with Excel in the MS Office bundle, *via* the common VBA interface.

ACKNOWLEDGEMENTS

I thank Sabine Hofer for the donation of the activity data recordings of the 10 freerunning untreated animals that were used for the randomisation studies.

REFERENCES

De Prins J and Hecquet J. 1992. Data processing in chronobiological studies. In Touitou Y and Haus E, editors. Biological rhythms in clinical and laboratory medicine. Heidelberg: Springer. p 90–113.

Enright JT. 1965. The search for rhythmicity in biological time series. J theor Biol 8:426–468.

Homberg U, Reischig T, and Stengl M. 2003. Neural organisation of the circadian system of the cockroach *Leucophaea maderae*. Chronobiol Int, in press.

Klemfuss H and Clopton PL. 1993. Seeking tau: a comparison of six methods. J interdiscipl Cycle Res 24:1–16.

Levine JD, Funes P, Dowse HB, and Hall JC. 2002. Signal analysis of behavioural and molecular cycles. Biomed Central Neurosci 3:1–25.

Reischig T and Stengl M. 2003. Ectopic transplantation of the accessory medulla restores circadian locomotor rhythms in arrhythmic cockroaches (*Leucophaea maderae*). J Exp Biol. 206:1877–1886

Sokolove PG and Bushell WN. 1978. The chi square periodogram: its utility for analysis of circadian rhythms. J Theor Biol 72:131–160.

APPENDIX: INPUTS FOR PARTICULAR REGISTERS AND COMMANDS

Table 1. *Input field for the register* ***Activity***

Input field	Range	Default	Number type	Applies to
Spreadsheet width ("testperiod")	2-48 h	24 h	Floating point	Periodogram spreadsheet

Table 2. *Input fields for the command* ***Average day***

Input field	Range	Default	Number type
Calculate the average day for ZT/CT day length	5-60 h	24 h	Floating point
Set phase reference point of the first day ...	0-24 h	0 h	Floating point
Assign phase reference points to ZT/CT	0-24 h	12 h	Integer

Table 3. *Input fields for the register* ***Periodogram***

Input field	Range	Default	Number type	Applies to
Testperiods from	1-59 h	14 h	Integer	χ^2-periodogram, Enright-periodogram
Testperiods to	2-60 h	33 h	Integer	χ^2-periodogram, Enright-periodogram
Stepwidth	1-60 min	6 min	Integer	χ^2-periodogram, Enright-periodogram

Table 4. *Input fields for the register* ***Scan analysis***

Input field	Range	Default	Number type	Applies to
Testperiods from	1-59 h	14 h	Integer	Rhythm Detector, Periodogram peak analysis
Testperiods to	2-60 h	33 h	Integer	Rhythm Detector, Periodogram peak analysis
Stepwidth	1-60 min	6 min	Integer	Rhythm Detector, Periodogram peak analysis
Single periodogram length	2-20 h	10 h	Integer	Rhythm Detector
Smallest peaks	1-999 %	20 %	Integer	Rhythm Detector
Minimum peakwidth	0-10 h	1 h	Floating point	Rhythm Detector
Rhythmic plateau	1-10 days	2 days	Integer	Rhythm Detector

Table 5. *Input fields for the command* ***Permutate data***

Input field	Range	Default	Number type	Applies to
Permutate data in blocks of...	1-24 h	1 h	Integer	Permutation methods
Repeat x times for every experiment	2-10000	10	Integer	Serial evaluations

VI. Optic lobe commissures in a three-dimensional brain model of the cockroach *Leucophaea maderae*: a search for the circadian coupling pathways.

Reischig T and Stengl M. 2003. J Comp Neurol. 443:388-400

THE JOURNAL OF COMPARATIVE NEUROLOGY 443:388–400 (2002)

Optic Lobe Commissures in a Three-Dimensional Brain Model of the Cockroach *Leucophaea maderae*: A Search for the Circadian Coupling Pathways

THOMAS REISCHIG AND MONIKA STENGL*
Department of Biology, Animal Physiology, Philipps University Marburg, Marburg, Germany

ABSTRACT

The circadian rhythm of locomotor activity in the cockroach *Leucophaea maderae* is controlled by bilaterally symmetric, apparently directly coupled, circadian pacemakers in the optic lobes. Strong evidence predicts that ventromedial to the medulla, the accessory medulla with associated pigment-dispersing hormone-immunoreactive neurons is this circadian clock. In search for direct coupling pathways between both clocks, we performed horseradish peroxidase backfills from one optic stalk as well as dextran and horseradish peroxidase injections into one accessory medulla. Seven commissures with projections in the contralateral optic lobe were identified and reconstructed. Three of these commissures connected both accessory medullae. Two of these resembled the arborization pattern of the pigment-dispersing hormone-immunoreactive neurons, which are circadian pacemaker candidates in insects. This finding suggests that some of these pacemaker candidates form a direct circadian coupling pathway. For better visualization of reconstructed commissures, we implemented the reconstructions into a three-dimensional model of the cockroach brain. J. Comp. Neurol. 443:388–400, 2002.

Indexing terms: pigment-dispersing hormone; visual system; insects; accessory medulla; neuroanatomy; circadian rhythms

The locomotor activity rhythm of the cockroach *Leucophaea maderae* is controlled by two bilaterally symmetric circadian pacemakers in the optic lobes (Nishiitsutsuji-Uwo and Pittendrigh, 1968; Roberts, 1974; Sokolove, 1975; Page, 1982; reviews by Page, 1984; Chiba and Tomioka, 1987). In contrast to crickets, in the cockroach both pacemakers are strongly coupled (Page et al., 1977; Wiedenmann, 1984; Ushirogawa et al., 1997). There is strong evidence that the accessory medulla (AMe), a small neuropil at the ventromedial edge of the medulla is this circadian pacemaker (Stengl and Homberg, 1994; Reischig and Stengl, 1996; Petri and Stengl, 1997). The AMe is densely innervated by neurites from pigment-dispersing hormone-immunoreactive (PDH-ir) neurons, which are circadian pacemaker candidates in insects (Homberg et al., 1991; Helfrich-Förster, 1995; reviewed by Helfrich-Förster et al., 1998). PDH-ir neurons contain circadian clock proteins, such as PERIOD and TIMELESS in *Drosophila melanogaster* (Helfrich-Förster, 1995; Helfrich-Förster et al., 1998). A comparison of the morphology of PDH-ir neurons in crickets and cockroaches revealed a correlation between the number of PDH-ir commissures, the length of the period, and the strength of coupling (Homberg et al., 1991; Stengl and Homberg, 1994). Therefore, PDH-ir neurons are candidates for a direct neuronal coupling pathway between the strongly coupled pacemakers in the cockroach (Fig. 1A). With PDH immunocytochemistry single PDH-ir neurons cannot be traced; thus, it cannot be discerned whether PDH-ir fibers directly connect both accessory medullae (AMae). Thus, we performed horseradish per-

Grant sponsor: Deutsche Forschungsgemeinschaft (DFG); Grant number: STE 531/7-1; Grant number: STE 531/7-2; Grant number: STE 531/7-3; Grant sponsor: Human Science Frontier.

*Correspondence to: Dr. Monika Stengl, Philipps Universität Marburg, Biology, Animal Physiology, Karl von Frisch Str., 35032 Marburg, Germany. E-mail: stengl@mailer.uni-marburg.de

Received 11 June 2001; Revised 14 November 2001; Accepted 16 November 2001

Published online the week of January 21, 2002

DOI 10.1002/cne.10133

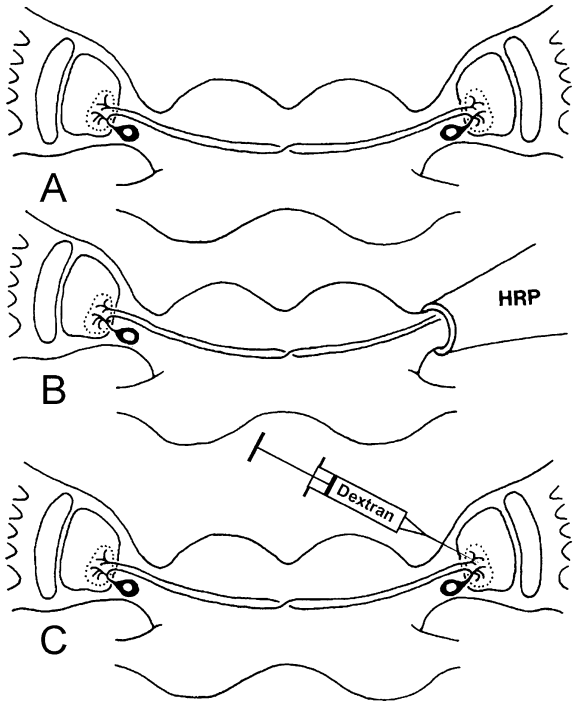

Fig. 1. **A:** Scheme of the cockroach brain with hypothetical direct coupling pathways connecting both accessory medullae. **B:** For horseradish peroxidase (HRP) backfills one of the optic stalks was cut and the HRP-filled suction pipette was slipped over the cut optic stalk. **C:** Dextran or HRP was injected directly into one accessory medulla for further identification of direct coupling pathways.

oxidase (HRP) backfills from one cut optic stalk, to determine all commissures which directly connect both optic lobes. Then, we injected HRP and dextran into one AMe to determine whether any of these commissures directly connect both AMae. We find seven systems of commissures connecting both optic lobes. Three of them connect both AMae. Two of them match the arborization pattern of PDH-ir neurons. Thus, PDH-ir neurons are strong candidates for a direct circadian coupling pathway.

MATERIAL AND METHODS

Animals

Adult male cockroaches (*Leucophaea maderae*) were chosen from laboratory colonies. They were reared at 25°C, 30% relative humidity, and light-dark cycles of 12:12 hours, with lights on at 6:00 AM. The animals were fed dried dog food, potatoes, and water ad libidum.

Abbreviations

AMe(ae)	accessory medulla(e)
AOC	anterior optic commissure
AOTu	anterior optic tubercle
-ir	-immunoreactive
LoVT	lobula valley tract
MC I-III	medulla cell groups I-III
PDH	pigment dispersing hormone
POC	posterior optic commissure
POT	posterior optic tract
POTu	posterior optic tubercle
SLP	superior lateral protocerebrum
SMP	superior median protocerebrum

Suction pipette experiments

For HRP backfills with suction pipettes (n = 23), animals were anesthetized with CO_2 and fixed in a mounting device. A small window was cut into the head capsule above the left optic lobe to expose the brain. The optic stalk and the optic nerves were severed to remove one optic lobe completely. The application pipette with a tip opening of 300–400 μm contained a 1-μl solution of HRP (Serva, Heidelberg, Germany; HRP diluted to 10% in distilled water). The tip was slipped over the stump of the cut optic stalk (Fig. 1B) and fixed with modeling clay to backfill the cut nerve fibers for approximately 24 hours. Then, the animal was decapitated, and the brain was processed for histology.

HRP and dextran injections into one AMe

In addition to HRP injections (n = 30) into one of the two AMae, biotinylated dextran was used as alternative neuronal tracer (n = 36). For the injections, the neurolemma of the optic lobe was penetrated with a glass capillary (Clark, Pangbourne Reading, England), and 0.5–5.0 nl of biotinylated dextran (3,000 molecular weight, lysine fixable, Molecular Probes; 100 mg/ml in 0.1 M sodium phosphate buffer, pH 7.4, containing 10% aqueous blue food dye) was pressure injected with a microinjector (Eppendorf, Microinjector 5242, Hamburg, Germany) under visual control (stereomicroscope, Zeiss, Jena, Germany) into one AMe (Fig. 1C). The region of the AMe could be easily localized with respect to the optic stalk, next to a characteristic trachea (Petri and Stengl, 1997). Before injection into the animal, we injected droplets of solution into mineral oil, to calculate the injected volume by means of the diameter of the droplets. The success of the injection could be visually controlled by observing the spreading of the blue food dye within the neuropil. After the injection, the head capsule was closed with wax to allow intracellular transport of the dye in the surviving animal overnight. The next day, the brain of the injected cockroach was removed.

Histologic procedures

Resolution of details of the branching pattern of weakly stained fibers is greatly improved in conventional light microscopy of stained Vibratome sections of the insect brain, compared with confocal microscopy on whole-mount preparation. Thus, we choose to analyze brain sections. The HRP-treated brains were dissected and fixed for 4 hours or overnight in 4% paraformaldehyde/7.5% saturated picric acid in sodium phosphate buffer (0.1 M, pH 7.4) at room temperature. After embedding in gelatin/albumin (4.8% gelatin and 12% ovalbumin in pure water) and post-fixation in 10% formalin in sodium phosphate buffer (0.1 M, pH 7.4), they were sectioned with a Vibratome in a frontohorizontal plane at 30 μm thickness. The free-floating sections were thoroughly washed in sodium phosphate buffer, stained with 0.03% diaminobenzidine (DAB, Sigma-Aldrich, Deisenhofen, Germany) and 0.025% H_2O_2 in sodium phosphate buffer (0.1 M, pH 7.4) for 20–30 minutes, and then mounted on chromalum/gelatin–coated microscope slides.

The dextran injected brains were dissected, fixed, embedded as described, and sectioned with a Vibratome at 40 μm. The sections were washed in phosphate buffer and incubated in streptavidin horseradish peroxidase conjugate (Amersham, Buckinghamshire, UK) diluted 1:200 in 0.01 M phosphate buffered saline (PBS, pH 7.4) containing 0.5% Triton X-100 (Sigma-Aldrich, Deisenhofen, Germany). After washing in phosphate buffer, the sections were stained by using DAB/H_2O_2 with Ni^{2+} intensification (0.03% DAB, 0.025% H_2O_2, 0.3% nickel ammonium sulfate in 0.05 M Tris-HCl buffer, pH 7.4) for 20–30 minutes.

Evaluation and visualization

Photomicrographs were taken with a Zeiss microscope equipped with a digital Polaroid (Cambridge, MA) 2 M-pixel camera. In Adobe Photoshop 5.0, the contrast of the photomicrographs was optimized. Fiber tracts were reconstructed from series of brain sections with camera lucida equipment on a Leitz microscope. To conserve information about the depth, in camera lucida drawings, we produced a three-dimensional (3D)-computer model of a *L. maderae* brain. Frontal paraffin sections of one brain were photographed with the Polaroid camera and digitally aligned. Contours of brain structures of this image series were segmented, and surface models of prominent neuropils were calculated, processed, and smoothed by using the 3D imaging program Amira 2.1 (Indeed-Visual Concepts GmbH, Berlin, Germany). A multilayer Photoshop image file was created, and the brain and neuropil images, as well as high resolution scans of the tract reconstructions, were exported into the respective layers of this file. The reconstructions and brain structure models were adjusted to match the proportions of the original preparations. Three-dimensionality was achieved by using the transparency functions of the program. With light microscopy of the original sections, the spatial relationships of fibers, somata, and neuropils were controlled.

RESULTS

To identify all commissures connecting both optic lobes and to determine direct connections between both AMae, HRP backfills from the ipsilateral cut optic stalk (n = 23) and injections of dextran (n = 36) or HRP (n = 30) into the ipsilateral AMe were performed. Stained tracts that did not project into the untreated contralateral optic lobe, but ended in different midbrain regions, were excluded, because this study concentrates on the characterization of optic lobe commissures only. We developed a 3D model of the main neuropil structures of the brain to allow embedding of tract reconstructions into the 3D brain model. This method allows to judge at what depth tracts cross in the midbrain with respect to other prominent brain neuropils. Thus, appreciation of branching patterns of presumptive circadian coupling pathways is greatly facilitated.

A comparison of the HRP backfills with the HRP-injections showed that the same fiber tracts and the same contralateral arborization areas were stained. Thus, no artifacts were caused by degeneration of fibers in the cut optic stalk in the backfill experiments and both groups of HRP experiments were pooled in the quantitative analysis. A comparison of the HRP injections and the dextran injections, however, revealed specific differences in the number and type of stained cells. Dextran stainings in the contralateral optic lobe neuropils (Figs. 2B,C,F,G, 3A–F) were much more intense and more consistent compared with the more variable HRP stainings (Fig. 2 A,D,E,H). Detailed evaluation of both types of experiments allowed reconstruction of seven different commissures connecting both optic lobes. In HRP backfills or HRP injections in the ipsilateral optic lobe, the neuropil of the contralateral AMe was never labeled, although stained fibers could be observed in direct vicinity to the contralateral AMe (Fig. 2H). In contrast, staining in the internodular neuropil of the contralateral AMe was regularly observed after injections of biotinylated dextran into the ipsilateral AMe (Figs. 3B,C). Dextran injections confined to the ipsilateral AMe labeled the contralateral AMe and medulla by means of the anterior optic commissure (AOC, tracts 3, 4, Fig. 4C,D) and the posterior optic commissure (POC, tract 7, Fig. 5C) (injection site: Fig. 3F). Thus, apparently maximally three different direct connections exist between the bilaterally paired AMae.

Contralaterally projecting optic tracts

Backfills with HRP and dextran injections revealed seven optic lobe commissures together with corresponding somata (Figs. 4, 5). The commissures were numbered in anterior to posterior order. The experimentally treated optic lobe containing the backfilled optic stalk or the injected AMe was defined as ipsilateral. The opposite, untreated optic lobe was defined as contralateral (contralateral to the injection side). Maximum numbers of stained fibers and contralateral somata per commissure are indicated as n_{max}. The nomenclature of tracts follows the terminology introduced for flies (Strausfeld, 1976) and honeybees (DeVoe et al., 1982; Mobbs, 1984; Hertel et al., 1987).

Tract 1, the intertubercle tract (Figs. 2A, 4A), which becomes the anterior optic tract (thicker, lower fiber tract between lobula and anterior optic tubercle, Fig. 4A), forms the frontalmost commissure in the brain of *L. maderae*. It consists of two fiber bundles: an upper (n_{max} = 13; mean [n_m] ± SD = 7.3 ± 4.2) and a lower bundle (n_{max} = 17; n_m = 10.1 ± 6.4), which connect the contralateral lobula and both anterior optic tubercles (AOTu) (filled arrows in Fig. 4A) to the backfilled optic lobe. Two different soma groups (two arrowheads, lateral group: n_{max} = 5; n_m = 2.7 ± 1.5; arrowhead, medial group: n_{max} = 4; n_m = 2.3 ± 1.2; Fig. 4A) in the anterior cell cortex between the antennal lobe and the lobula contribute to tract 1. The lateral group contributes to the thicker lower nerve fiber bundle. This fiber bundle connects the AOTu to the lobula and is part of the anterior optic tract (Collett, 1972). Tract 1 was never observed in injection experiments.

Tract 2, the serpentine optic commissure (Figs. 2D, 4B), is shaped like a "W." The first "downstroke" (and the second "upstroke") of the bilaterally symmetric "W" run from the lobula to the lateral accessory lobes (LAL, Fig. 4B) the first "upstroke" (and the second "downstroke") connect the lateral accessory lobes with the midbrain anterior to the central body (CB, Fig. 4A,B). The serpentine commissure consists of only few fibers (n_{max} = 4; n_m = 2.7 ± 1.1) passing the midbrain anteriorly to the central body. The serpentine optic commissure, with somata (n_{max} = 2; n_m = 1.6 ± 0.7) above the median edge of the lobula (arrowhead, Fig. 4B), connects the contralateral medulla and lobula, and both lateral accessory lobes to the backfilled optic lobe. In the contralateral optic lobe, tract 2

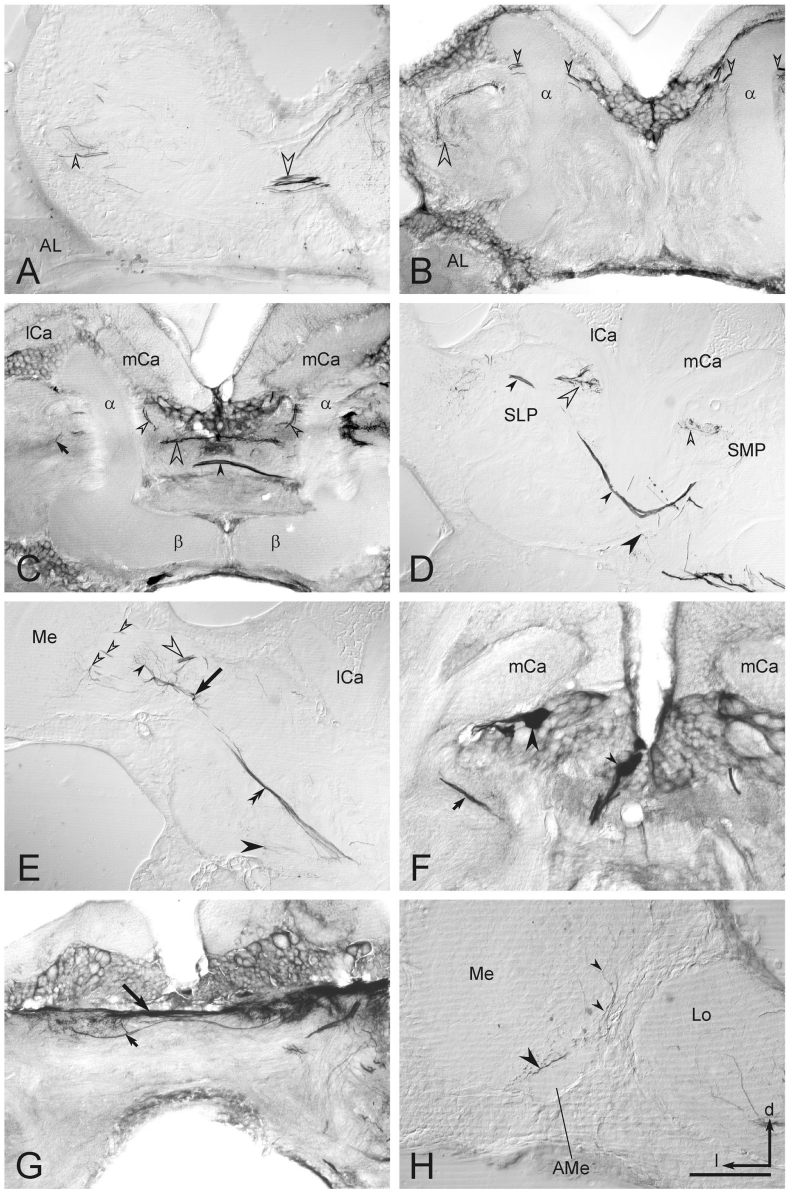

Fig. 2. Positions of commissures and somata stained by horseradish peroxidase (HRP) backfills (A,D,E,H) or dextran injections into the ipsilateral accessory medulla (B,C,F,G) on 30- to 40-μm Vibratome sections. Sections A–G are arranged as they would appear in a preparation from anterior (A) to posterior (G). **A:** Tract 1, the intertubercle tract (large arrowhead) arborizes in the anterior optic tubercle (small arrowhead) in the anterior midbrain. AL, antennal lobe. **B:** Tract 3 loops around the α-lobe (α, small open arrowheads) before it turns to the anterior parts of the superior protocerebrum (large open arrowhead). **C:** Anterior or anteriodorsal to the central body tract 2 (small, filled arrowhead) and tract 4 (the latter as part of the anterior optic commissure: large open arrowhead) are visible. Tract 3 (small open arrowheads) turns up to loop around the α-lobes (α). The arrow points to arborizations of tract 6. β, β-lobe; lCa, lateral calyx; mCa, medial calyces of the mushroom bodies. **D:** Tract 2, the serpentine commissure (small, filled arrowheads), arborizes in the lateral accessory lobe (large, filled arrowhead). Tract 4 branches in the superior median protocerebrum (SMP; small open arrowhead); ramifications of tract 3 and 4 in the superior lateral protocerebrum (SLP) are marked by the large open arrowhead. **E:** Tract 5, the inferior optic tract (double arrowhead), arborizes in the inferior lateral protocerebrum (large, filled arrowhead) and in the lobula (small, filled arrowhead). The arrow shows were the primary neurites of the respective somata join tract 5. Tract 2 (large open arrowhead) sends collateral fibers into the lobula and extends by means of the second optic chiasma to the medulla (Me; small open arrowheads). **F:** In the contralateral pars intercerebralis, the somata of tract 6 (large arrowhead) and tract 7 (small arrowhead) are stained. Short arrow: A segment of tract 6. **G:** The posterior optic commissure (long arrow) consists of approximately 100 fibers and, therefore, is the most prominent optic lobe commissure. Tract 6 (short arrow) connects with three fibers one optic lobe (including the medulla) with the proximal lobula of the contralateral optic lobe. **H:** In HRP backfills, contralateral arborizations (large arrowhead) were observed only distally to the accessory medulla (AMe). Processes from the lobula valley tract (small arrowheads) innervate the medulla (Me). Lo, lobula. Scale bar in H = 200 μm in A–E,G, 100 μm in F,H. d, dorsal; l, lateral.

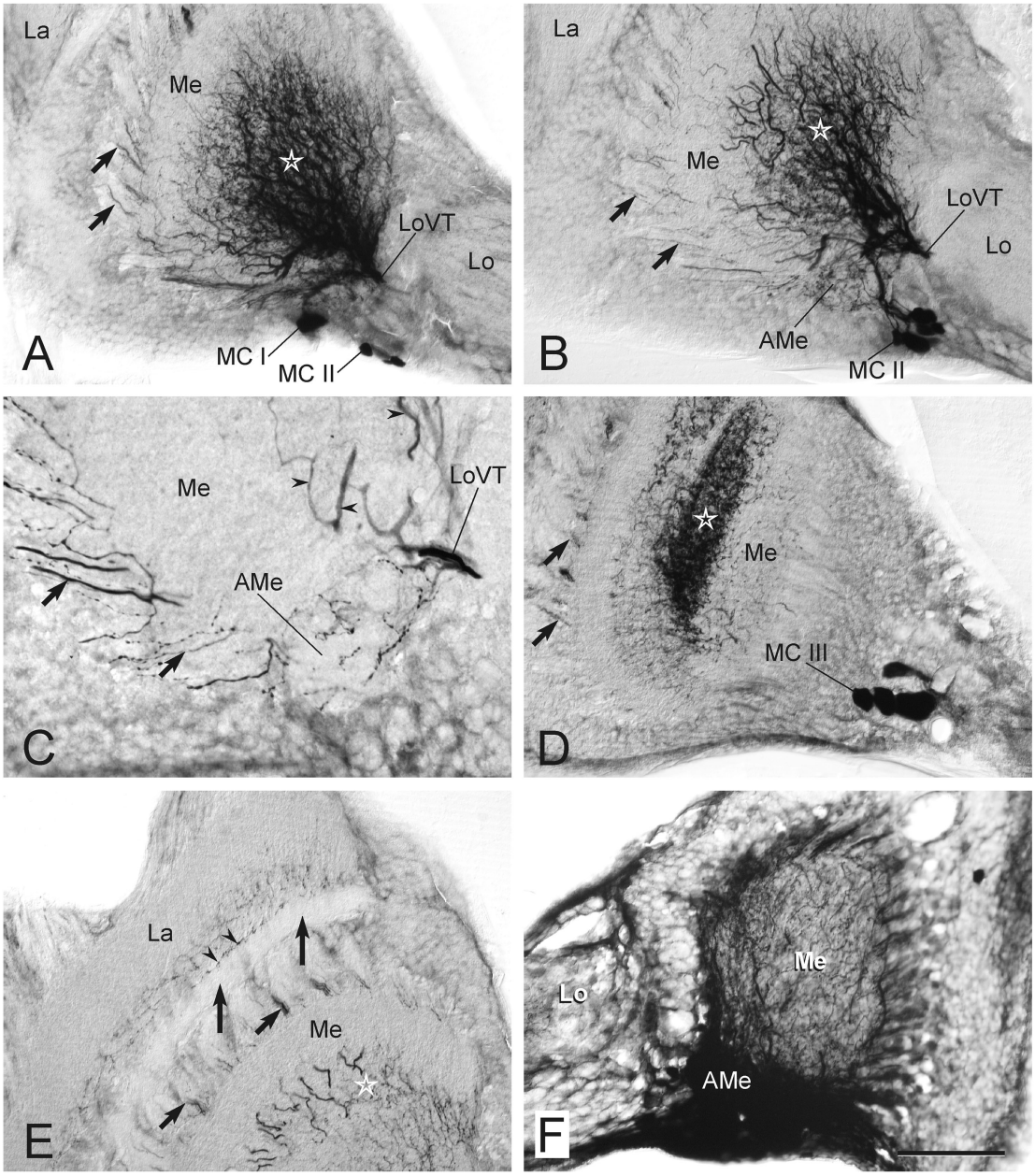

Fig. 3. Stained fibers and somata in the contra- (A–E) and ipsilateral (F) optic lobe after dextran injection into the ipsilateral AMe. **A:** The primary neurites of medulla cells group I (MC I) somata project anteriorly to the AMe to the lobula valley tract (LoVT). They belong to the fibers of the fan-shaped anterior-layer fiber system (arrows) which projects through the anterior layer of the medulla to the proximal lamina (La). Group II (MC II) somata constitute the middle layer fiber system (asterisk), which innervate the medulla (Me) by means of the posterior optic commissure and the LoVT. La, lamina. Lo, lobula. **B:** Two sections deeper (than A) more somata of medulla cells group II (MC II) become visible. Their primary neurites project upward along the posterior dorsal AMe to the lobula valley tract (LoVT). The internodular neuropil of the accessory medulla (AMe) is densely innervated. Arrows point to fibers of the anterior-layer fiber system. The asterisk indicates fibers of the middle-layer fiber system. **C:** Varicose fibers of the fan-shaped anterior-layer fiber system (arrows) innervate the accessory medulla (AMe). Lobula valley tract (LoVT) fibers innervating middle layers of the medulla, possess no varicosities (small arrowheads). **D:** The somata of the medulla cells group III (MC III) lie posterior to the distal lobula and also project into the LoVT. Here, the two-layered arborization pattern of the middle-layer fiber system (asterisk) in the medulla (Me) becomes apparent. Arrows point to fibers of the anterior-layer fiber system in the second optic chiasma. **E:** Fibers emerging from the anterior-layer fiber system (arrowheads) are closely attached to the distal margin of the lamina organ (long arrows). Short arrows: fibers of the anterior-layer fiber system within the second optic chiasma. Asterisk: fibers of the middle-layer fiber system. **F:** In the ipsilateral optic lobe, the injected accessory medulla (AMe) and its respective soma groups are densely stained. The black area below the AMe contains backfilled somata belonging to MC I and II. For other abbreviations, see list. Scale bar in F = 100 μm in A,B,D–F, 50 μm in C.

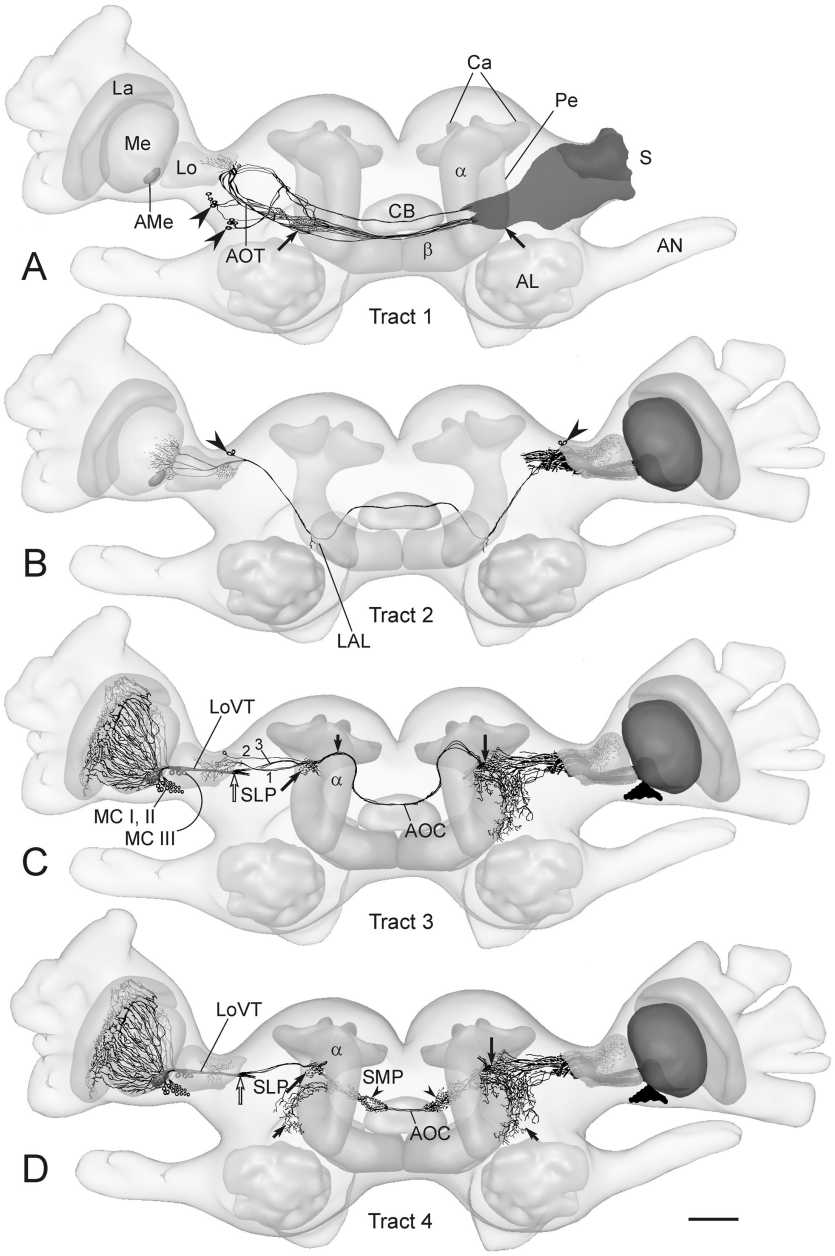

Fig. 4. Frontohorizontal views of the *Leucophaea* brain model with embedded camera lucida reconstructions of optic lobe tracts 1–4. Stained fibers of the ipsilateral optic lobe or medulla at the backfilled or injected side cannot be resolved and, thus, are shaded. Staining of the ipsilateral lamina is not shown. Stained somata of the injected optic lobe are not shown, except for somata of tracts 3 and 4 in the vicinity of the accessory medulla (AMe). **A:** Tract 1. The first, frontalmost commissure is the intertubercle tract, which connects both anterior optic tubercles (filled arrows) to the contralateral lobula (Lo). One group of somata (arrowheads) corresponds to each of the two branches of tract 1. α, α-lobe; β, β-beta lobe; AL, antennal lobe; AN, antennal nerve; AOT, anterior optic tract; Ca, calyces of the mushroom bodies; CB, central body; La, lamina; Me, medulla; Pe, pedunculus of the mushroom body; S, stump of the cut optic lobe. **B:** Tract 2 forms the serpentine commissure and consists of only four fibers. It connects both lateral accessory lobes (LAL) to both lobulae and possibly also to both medullae. Arrowheads point to the respective somata of tract 2. **C:** Tract 3 leads through the upper part of the anterior optic commissure (AOC) and forms characteristic loops (small arrow) frontally around the upper α-lobes (α). It connects the superior lateral protocerebra (SLP; long arrows) to both lobulae by means of three branches (1–3). The branching pattern in the optic lobes consists of two different patterns (Fig. 5D,E) which cannot be distinguished from those of tracts 4 and 7. MC I-III, medulla cells group 1–3; arrows, overlapping arborization fields of tract 3 and 4 in the SLP; open arrow, proximal bifurcation of the lobula valley tract (LoVT). **D:** Tract 4 leads through the anterior optic commissure (AOC), connecting both superior median (SMP; arrowheads), superior lateral (SLP; long arrows: overlapping arborization fields of tract 3 and 4), and anterior superior lateral (SLP; short arrows) protocerebra to optic lobe neuropils. Open arrow, proximal bifurcation of the lobula valley tract (LoVT); α α-lobe. Scale bar = 200 μm in D (applies to A–D).

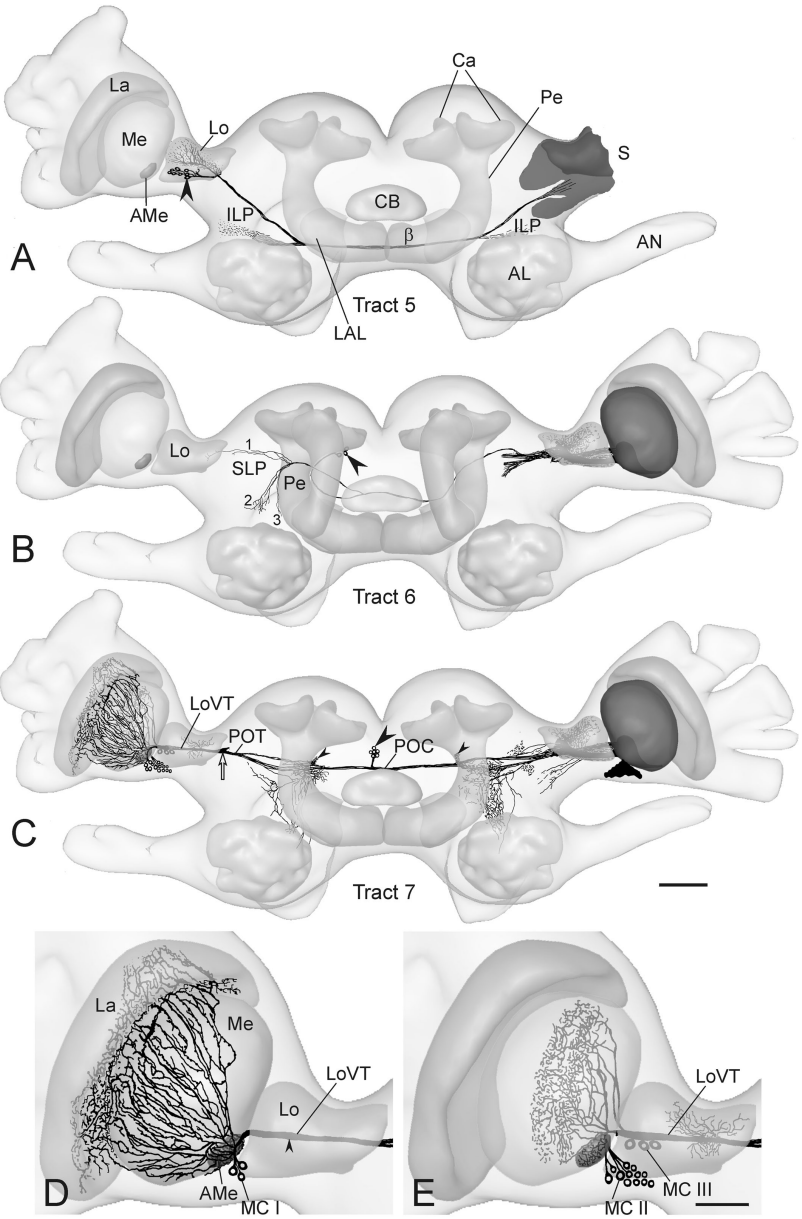

Fig. 5. Frontohorizontal views of the *Leucophaea* brain with embedded camera lucida reconstructions of optic lobe tracts 5–7 (A–C), and reconstruction of the two fiber systems in the optic lobe, which emerge from the lobula valley tract (LoVT) (D,E). **A:** Tract 5, the inferior optic tract, connects the inferior lateral protocerebra (ILP) with both lobulae (Lo). Its somata lie in the cell cortex anteriorly to the lobula (arrowhead). The α-lobes are removed. β, β-beta lobe; AL, antennal lobe; AMe, accessory medulla; AN, antennal nerve; Ca, calyces of the mushroom body; CB, central body; La, lamina; LAL, lateral accessory lobe; Me, medulla; Pe, pedunculus of the mushroom body; S, stump of the cut optic lobe. **B:** Tract 6 connects the backfilled optic lobe to the contralateral lobula (Lo). There, it forms three different branches (1–3). Branch 1 leads to the proximal lobula by means of branches in the superior lateral protocerebrum (SLP), branch 2 turns to the anterior protocerebrum, and branch 3 leads along the Pe. Its respective somata lie in the posterior *pars intercerebralis* (arrowhead). **C:** Tract 7 is part of the posterior optic commissure (POC) and connects the backfilled optic lobe to both posterior optic tubercles (small arrowheads) and to contralateral optic lobe neuropils by means of the posterior optic tract (POT) and the lobula valley tract (LoVT). The bifurcation of the LoVT (open arrow) is shared by neurons of tracts 3 and 4. A soma group associated with the POC lies in the contralateral *pars intercerebralis* (large arrowhead). The α-lobes are removed. **D:** In the contralateral optic lobe, the characteristic fan-shaped anterior-layer fiber system is shown with its respective soma group MC I. It emerges from the LoVT, which contains processes of tracts 3, 4, and 7 and arborizes in the AMe. Varicose fibers extend through the anterior layer of the Me to the proximal lamina (La). **E:** The middle-layer fiber system also originates from the LoVT. It forms arborizations in at least two middle layers of the medulla. The medulla cells group 2 (MC II, and possibly also MC III) belong to this fiber system. The primary neurites of MC II pass the AMe posteriorly, in contrast to MC I primary neurites. They also appear to contribute arborizations to the internodular neuropil of the AMe. Scale bars = 200 μm in C (applies to A–C), 100 μm in E (applies to D,E).

arborizes in proximal, posterior parts of the lobula and sends terminals into an inner layer of the medulla. It does not arborize in the contralateral AMe. In the superior lateral protocerebrum (SLP), tract 2 turns downward posteriorly to the contralateral peduncles of the mushroom bodies. It sends one to three sidebranches into each of the bilaterally symmetric lateral accessory lobes, before it turns up to the posterior, ipsilateral lobula. The serpentine tract was observed in backfills and injection experiments.

Tracts 3, 4, and 7 have a common root: the lobula valley tract (LoVT). The LoVT was defined as the tract that runs in a posterior rim of the lobula from the proximal medulla to the proximal end of the lobula (Strausfeld and Blest, 1970; Milde, 1993). There it bifurcates (open arrow Figs. 4C,D, 5C) into the posterior optic tract (POT, tract 7; Fig. 5C) and to the anterior optic commissure (AOC, tract 3, 4; Fig. 4C,D). The POT participates in the posterior optic commissure (POC, Fig. 5C). Emerging from the LoVT, two distinct fiber systems associated with specific groups of optic lobe somata (MC I-III) could be separated in the contralateral optic lobe (Fig. 5D,E). It was not possible, however, to distinguish which of these two fiber systems belong to the individual tracts 3, 4, and 7 (Figs. 4C,D, 5C). Only in one case a neuron of tract 7 could be unequivocally assigned to the anterior layer fiber system (Fig. 5D). Therefore, in Figures 4C,D and 5C the two distinct optic lobe fiber systems are overlaid. Tracts 3, 4, and 7 were observed in backfills and in injection experiments.

Tract 3 (Figs. 2B–D, 4C) loops around each of the bilaterally symmetric, anterior, upper α-lobes of the mushroom bodies. Its arborizations in both superior lateral protocerebra (SLPs: large, filled arrows, Fig. 4C) could not be separated from arborizations of tract 4. From the ipsilateral SLP, tract 3 sends some prominent fibers (n_{max} = 10; n_m = 5.3 ± 2.1) by means of the anterior optic commissure (AOC), at the upper, anterior edge of the central body and arborizes with fine side-branches in the contralateral SLP. From there, it sends three parallel branches to the contralateral optic lobe neuropils. An anterior branch consists of maximally three fine fibers which ramify in the frontal proximal lobula (branch 1, Fig. 4C). The second branch consists of one fiber emerging from the short neurite of a soma (branch 2, Fig. 4C), which lies superior to the proximal lobula, anterior to the somata of tract 2. Fine fibers emerge from this neurite and ramify within the contralateral anterior proximal lobula. The third branch is the most prominent and joins the bifurcation of the LoVT proximal to the lobula together with tract 7 (branch 3, Fig. 4C). This branch is also shared by two thin fibers of tract 4.

Tract 4 (Figs. 2B–D, 4D) connects parts of both superior median protocerebra (SMPs; arrowheads, Fig. 4D; the neuropil masses of the superior protocerebrum between the mushroom bodies and the central body) and SLPs (large arrows, Fig. 4D; the neuropil masses of the superior protocerebrum between the mushroom bodies and the lobula) with both optic lobes. Tract 4 runs in the AOC ventral to tract 3. It densely innervates both SMPs, turning posteriorly between the α-lobes and peduncles to arborize in proximal and anterior parts of the contralateral SLP. From there, two fibers merge with the third branch of tract 3, which joins the LoVT.

Tract 5 is the inferior optic commissure (Kenyon, 1886) (Figs. 2E, 5A). It forms a commissure ventrally, posteriorly to the lateral edge of the lateral accessory lobes, in the posterior brain. It has somata (n_{max} = 20; n_m = 8.6 ± 6.4) anterior to the lobula and connects the backfilled optic lobe to the contralateral lobula by means of bilaterally symmetric arborizations in the inferior lateral protocerebrum (Fig. 5A). The inferior optic commissure was not observed in injection experiments.

Tract 6 (Figs. 2F,G, 5B) is formed by processes of a group of three somata (n_m = 2.0 ± 0.9), which lie medially to the inner calyx of the mushroom body contralaterally to the injection site. Their primary neurites join a commissure posterior to the central body. From there, the tract extends to the contralateral SLP. In the SLP, it spreads into three separate branches (branch 1–3, Fig. 5B). Branch 1 runs distally and reaches the proximal lobula. Branch 2 turns to the anterior protocerebrum. Branch 3 runs downward along the peduncle. Tract 6 was seen in injection experiments and backfills. It invades the medulla or AMe only unilaterally.

Tract 7 (Figs. 2G, 5C) is part of the posterior optic commissure (POC, Hertel et al., 1987). It consists of several fiber systems (50 to 100 fibers in total), which could not be clearly separated. The fibers connect the backfilled optic lobe to various regions in the ipsi- and contralateral posterior protocerebrum and the tritocerebrum, to the posterior optic tubercles (POTus), and extend into the contralateral optic lobe by means of the LoVT. Associated somata lie not only in the optic lobes (see below) but also in the contralateral pars intercerebralis (n_{max} = 16; n_m = 7.6 ± 6.6; Fig. 2F).

In the backfill experiments, many other fibers crossing the midbrain were visible preferentially in the posterior brain. Because they did not extend to the contralateral optic lobe, they were disregarded. Tracer injections into the AMe revealed only tracts 2–4, and 6–7, whereas backfills showed all tracts 1–7.

Projections in the contralateral optic lobe derived from tracts 3, 4, and 7

In the contralateral optic lobe, two distinct fiber systems emerge from the LoVT (which contains tracts 3, 4, and 7). The first, fan-shaped or anterior-layer fiber system (Figs. 3, 5D) sends varicose fibers in a fan through the anterior layer of the contralateral medulla. These terminate with fine arborizations in the proximal layer of the lamina and in the first optic chiasm. Arborizations are also formed on the distal margin of the lamina organ (Fleissner et al., 2001), a presumptive extraocular photoreceptor organ (Fig. 3E). Stained somata associated with these fibers (medulla cells group 1 = MC I) lie in the cell cortex frontally and medially to the AMe (n_{max} = 4; n_m = 2.4 ± 1.1; Fig. 3A). Their primary neurites form a bundle anterior to the AMe. Before this bundle joins the LoVT, it sends varicose fibers into the internodular neuropil of the AMe. No arborizations are found confined to the noduli of the AMe (Fig. 3B,C). This anterior-layer fiber system was only seen in dextran injections.

The second fiber system, the middle-layer fiber system, was seen in dextran injections and HRP injections and backfills (Figs. 2H, 3, 5E). Most fibers of this system appear to be associated with tract 7. Corresponding somata (MC II, n_{max} = 35; n_m = 12.5 ± 9.7) lie ventromedially to the AMe (Fig. 3A,B). Their primary neurites form one, sometimes two bundles posteriorly to the dorsal neuropil of the AMe. The primary neurites are closely attached with the AMe and join the LoVT. Fibers of this neuron

system were observed in close vicinity to the AMe. But our experiments could not discern whether they also arborize in the AMe. A third group of stained somata (MC III, $n_{max} = 6$; $n_m = 3.8 \pm 2.0$), which cannot be clearly assigned to either of the two fiber systems, lies close to the LoVT posteriorly to the distal lobula (Figs. 3D, 5E).

DISCUSSION

Commissures between both optic lobes were investigated to identify possible direct circadian coupling pathways in the cockroach *L. maderae*. We wanted to know whether neurons with the arborization pattern typical of PDH-ir neurons constitute direct connections between both AMae. Seven commissures were identified that directly interconnect both optic lobes and arborize in various midbrain neuropils. Only three of these commissures, tracts 3, 4, and 7, are candidates for a direct connection between both AMae. Two of them, tracts 4 and 7, resemble the characteristic arborization patterns of PDH-ir neurons (Fig. 6) (Stengl and Homberg, 1994), which are pacemaker candidates in insects. Thus, PDH-ir neurons appear to form a direct circadian coupling pathway.

How complete or how selective are the tracer studies?

Despite that HRP is assumed to be a predominantly retrograde tracer (transport from axonal terminals to soma) and dextran to be a predominantly anterograde tracer (Köbbert et al., 2000), both tracers revealed very similar staining patterns. Thus, we assume that both tracers stain somata (retrogradely) as well as axonal arborizations (anterogradely) of severed neurons. However, both dyes apparently work by means of different uptake mechanisms, because it became obvious that dextran injections resulted in stronger staining and in more stained neurons in the contralateral optic lobe. In addition, neurons with arborizations in the contralateral AMe and the anterior layer of the medulla were only stained with dextran injections but never with HRP injections or HRP backfills. The reason for this selective uptake by specific neurons remains obscure, but indicates that it is advantageous to compare different neuronal tracers. Because we observed all previously described commissures in *L. maderae* (Loesel and Homberg, 2001), in addition to new ones, we assume that our study is rather complete.

To determine whether both AMae are directly connected, we intended to inject tracer selectively into one AMe and looked for staining in the contralateral AMe. Because some tracer usually leaked into medulla cells next to the AMe (see staining of tract 2 in injection studies), it was not always possible to determine whether all stained cells on the contralateral side possess processes in the ipsilateral AMe. Therefore, only a comparison between our tracer studies and single cell stainings (Loesel and Homberg, 1998, 2001; Loesel, 1999), as well as immunocytochemical experiments (Petri et al., 1995; Loesel and Homberg, 1999), allowed the conclusion that tracts 4 and 7 directly connect both AMae.

Structures and functions of the different optic lobe commissures

Optic lobe commissures have been studied in some detail in several insect species, such as in bees (Kenyon, 1896; Mobbs, 1984; Hertel et al., 1987), flies (Strausfeld, 1976; Hausen, 1984), locusts (Boyan et al., 1993; Gewecke and Hou, 1993), crickets (Honegger and Schürmann, 1975; Tomioka et al., 1994; Yukizane and Tomioka, 1995), and moths (Milde, 1993). In cockroaches, visual commissures have been demonstrated by Roth and Sokolove (1975), Mizunami (1995), and Loesel and Homberg (1998, 1999, 2001). A comprehensive analysis of visual commissures in bees (Hertel et al., 1987) combined single cell electrophysiology with morphological analysis by intracellular and extracellular tracers. Thus, we adopted their nomenclature in all cases of apparent homology to commissures in *L. maderae*.

The ipsilateral optic lobe was removed in backfills, and because in the injection experiments overstaining obscured ipsilateral projections, only contralateral optic lobe projections were reconstructed. However, comparison with previously published commissures (Loesel and Homberg, 1998, 2001; Loesel, 1999) allowed us to determine ipsilateral arborization patterns. Thus, we conclude that of the seven fiber tracts, tracts 1 and 5 connect both lobulae; tract 2 connects both medullae and lobulae; tracts 3, 4, and 7 connect the AMe, medulla, lobula, and lamina to the contralateral AMe, medulla, lobula, and lamina; and tract 6 connects the medulla with the contralateral lobula.

Tract 1, the intertubercle tract, is known in different insects as part of a visual pathway carrying movement information from the lobula, by means of the anterior optic tracts and the anterior optic tubercles (AOTu), to other brain areas, such as the lateral accessory lobes (Kenyon, 1886; Jawlowski, 1963; Collett, 1972; Strausfeld, 1976; DeVoe et al., 1982; Fischbach and Lyly-Hünerberg, 1983; Hertel et al., 1987; Boyan et al., 1993; Homberg, 1994). In locusts, the intertubercle tract also contains neurons sensitive to polarized light information (Hofer S, Pfeifer K, Homberg U, unpublished observations), which insects use for sun compass navigation (Wehner, 1984). Because of this response profile and because neurons of this tract do not arborize in the AMe, it is unlikely that tract 1 acts as a direct circadian coupling pathway.

Tract 2, the serpentine tract (named after its arborizations in the serpentine layers of the medullae), has been described in the honeybee (Homberg, 1982; Gronenberg, 1984; Hertel et al., 1987), the cricket (Honegger and Schürmann, 1975; Tomioka et al., 1994; Yukizane and Tomioka, 1995), and in the cockroach (Loesel and Homberg, 2001). In *L. maderae*, neurons of tract 2 respond to small, ipsilateral, moving targets, without being directionally selective (Loesel and Homberg, 2001). Hertel et al. (1987) assume that serpentine tract neurons are involved in the tracking of moving objects. Thus, it is also unlikely that tract 2 is involved in a direct circadian coupling pathway.

Tract 3, to our knowledge, has not been described before. Thus, the arborization pattern of this tract in the optic lobe remains unresolved. It is possible that tract 3 connects both AMae with unknown function. In addition, the single stained neuron (Fig. 4C, branch 2), which could be assigned to tract 3, appears to connect the ipsilateral medulla, and possibly the ipsilateral AMe as well, to the contralateral lobula.

Tract 4 runs through the AOC, which in honeybees contains unidirectional, motion-sensitive neurons connecting both lobulae (Hertel et al., 1987). In bees, the

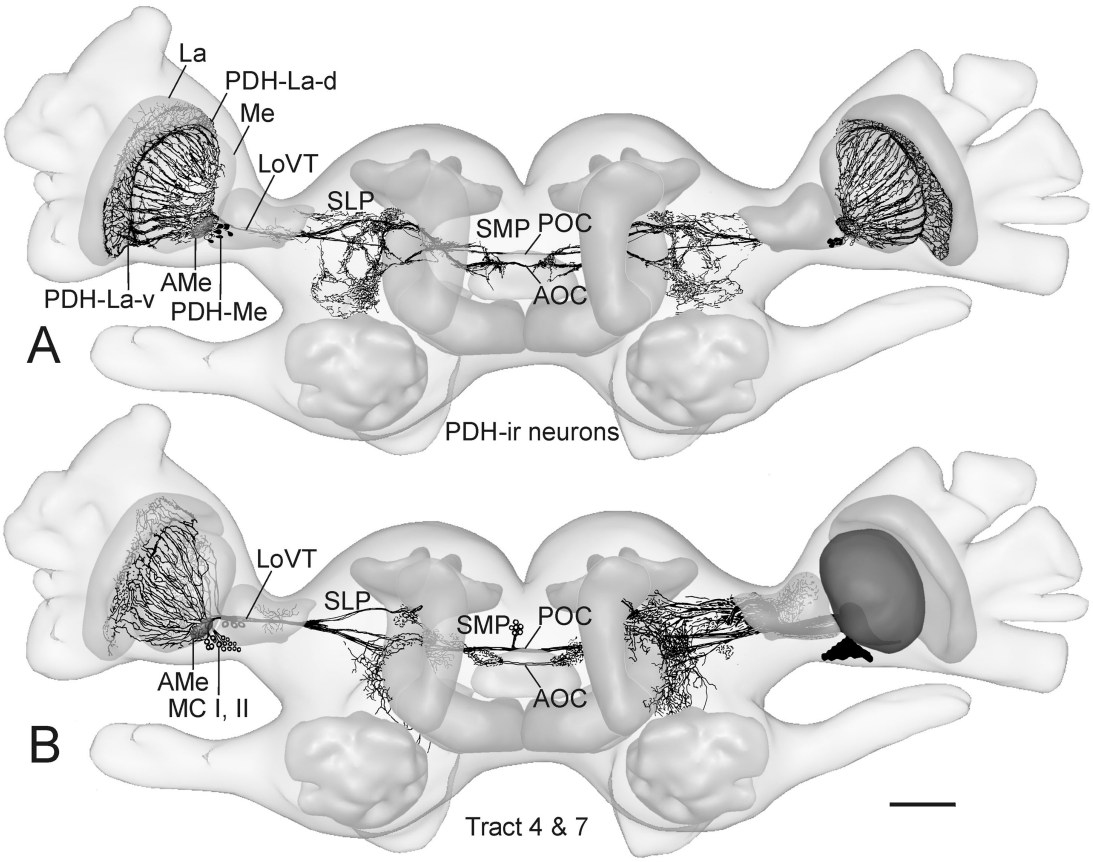

Fig. 6. Reconstructions of tracts 4 and 7 together resemble the arborization pattern of pigment-dispersing hormone-immunoreactive (PDH-ir) neurons. **A:** PDH-ir medulla neurons (PDH-Me) have their somata next to the accessory medulla (AMe). Some of these somata are a subgroup of the medulla cells group 1 (MC I) somata in B. The PDH-ir neurons arborize in the internodular neuropil of the AMe and send fibers by means of the characteristic fan-shaped anterior-layer fiber system over the face of the medulla (Me) to the lamina (La). The PDH-ir medulla cells send processes into the superior lateral- (SLP) and superior median protocerebra (SMP) by means of two commissures, the posterior optic commissure (POC) and the anterior optic commissure (AOC). From the immunocytochemical mass stainings, it cannot be discerned whether any of the PDH-ir cells directly connect both AMae. Dorsal and ventral PDH-ir lamina cells (PDH-La-d, PDH-La-v; Petri et al., 1995) do not project to the contralateral optic lobe. Drawing modified after Stengl and Homberg, 1994. To indicate the depth of arborizations, lamina, medulla, AMe, and lobula of the right side (corresponding to the body axis of the animal) are transparent (see also Figs. 4 and 5), whereas the respective neuropils of the other side are left opaque. LoVT lobula valley tract. **B:** A combination of the reconstructions of tracts 4 and 7 (Fig. 4D, 5C) closely resembles the arborization pattern of PDH-ir neurons in A. MC I cells project by means of the fan-shaped anterior-layer fiber system to the lamina and by means of the lobula valley tract (LoVT) in the POC and, possibly, also in the AOC. In the midbrain, tract 4 neurons arborize in the SLP and SMP, like PDH-ir neurons. Tract 7 neurons outnumber the quantity of posterior PDH-ir neurons. They project by means of the POC into the posterior optic tubercles like PDH-ir neurons, and, additionally, to other arborization areas in the posterior midbrain. Scale bar 200 μm in B (applies to A,B).

three portions of the AOC together contain approximately 3,200 neurons (Fröhlich A, Hertel H, unpublished observations). In *L. maderae* fibers of tract 4 do not respond to light stimuli, are spontaneously active, and connect both SMPs and anterior SLPs with the optic lobes (Loesel, 1999; Loesel and Homberg, 2001). Because tract 4 neurons closely resemble anterior parts of the PDH-ir neuron system (Fig. 6A) (Nässel et al., 1991; Stengl and Homberg, 1994), we assume that they connect the ipsilateral AMe with the contralateral AMe, medulla, and lamina, by means of the first, fan-shaped, or anterior-layer fiber system in the optic lobe. Because they do not respond to ipsilateral light, they possibly form output connections in the ipsilateral optic lobe neuropils, but do not receive ipsilateral optic input.

The inferior optic commissure, tract 5, was described in bees consisting of approximately 210 neurons (DeVoe et al., 1982; Mobbs, 1984; Kenyon, 1886; Hertel et al., 1987) and was also seen in the cricket (Honegger and Schürmann, 1975). In bees and flies, tract 5 neurons are directionally sensitive to movement and might compute binocular optomotor reactions (DeVoe et al., 1982; Hausen, 1984, Hertel et al., 1987; Strausfeld et al., 1995). In *L. maderae* Loesel and Homberg (1999) described a histamine-ir neuron possibly corresponding to tract 5. Like tract 1, tract 5 connects exclusively both lobulae. Thus, tract 5 is apparently not involved in direct circadian coupling.

Tract 6 was regularly stained after injections into the AMe, but its neurons do not reach the contralateral AMe.

Only few terminals reach the contralateral proximal lobula. In bees, Hertel and Maronde (1987) showed neurons with comparable morphology. They responded to light stimuli with spatial opponency in their binocular receptive fields, but did not project into both optic lobes. Thus, tract 6 is apparently not involved in direct circadian coupling.

Tract 7, the POC, is the main tract that connects both medullae and AMae by means of both the anterior- and the middle layer fiber system in the optic lobes. It carries light information and information from the circadian clock and qualifies as direct circadian coupling pathway. In bees, neurons of the POC consist of visual neurons with large arborization fields in the medulla, which also have large receptive fields in response to light stimuli (Hertel et al., 1987). They respond to stationary light with excitations to the ipsilateral and inhibition to the contralateral eye. In hemimetabolous insects, the POC was described after mass backfills in the cricket (Honegger and Schürmann, 1975; Tomioka et al., 1994; Yukizane and Tomioka 1995) and in the cockroach *L. maderae* (Roth and Sokolove, 1975). In all species examined, POC neurons have somata corresponding to MC I and II. Additionally, Roth and Sokolove (1975) described in *L. maderae* a group of neurons posterior to the second optic chiasma, corresponding to MC III. These and other results obtained by single cell stainings in the cockroach (Loesel and Homberg, 1998, 2001; Loesel, 1999) suggest that the POC carries several different types of neurons. Two main groups of neurons can be distinguished by their different soma positions: unilaterally projecting neurons with somata in the pars intercerebralis, contralateral to the optic lobe projection side, and bilaterally projecting neurons (MC I, II) with somata between lobula and medulla. The unilaterally projecting neurons were described as nondirectionally movement-sensitive in locusts (Rind, 1987; Gewecke and Hou, 1993) and as directionally movement-sensitive in hawkmoths (Milde, 1993). Loesel (1999) recorded a neuron of this type with arborizations in the lobula and AMe, as well as in the ocellar nerve contralateral to the soma side. The neuron was inhibited by stationary light to the compound eyes.

At least two types (type 1 with subtypes 1A and 1B) of bilaterally projecting neurons with somata in the optic lobes can be distinguished, according to their arborization pattern in the optic lobes and central brain. Type 1A arborizes in the middle layer fiber system of the medulla (Fig. 5E), in both AMae, and medullae. Neurons of this type react to e-vector rotation of polarized light (cricket: Labhart and Petzold, 1993; cockroach: Loesel and Homberg, 2001). These neurons have little or no arborizations in the median protocerebrum (Labhart and Petzold, 1993; Loesel and Homberg, 2001). Type 1B neurons also arborize in the middle layer fiber system of the medulla, have arborizations in the medulla, perhaps a few sidebranches in the AMe and in addition ramifications in the lobula and posterior protocerebrum (Loesel, 1999; Loesel and Homberg, 2001). These neurons are also polarization sensitive and exhibit oscillatory bursting activity. In bees and hawkmoths, neurons of this type react to light activity changes and are motion insensitive (Hertel et al., 1987; Milde, 1993). Approximately 35 MC II neurons, which contribute to the POC in *L. maderae*, might belong to this subtype.

The second type (type 2) are the fan-shaped, or anterior layer medulla neurons, with primary neurites anterior to the AMe, arborizations in the internodular neuropil of the AMe, fan-shaped arborizations in the anterior layer of the medulla, and arborizations in the proximal lamina. Neurons of this fiber system send branches (Fig. 5D) into the POC. This study showed for the first time that neurons of this type project into the contralateral optic lobe, apparently into the contralateral AMe and lamina. Neurons of the fan-shaped type show PDH-ir and FMRFamid-ir neurons in several orthopteroid insect species, e.g., cockroaches, crickets, locusts, and phasmids (Homberg et al., 1991; Stengl and Homberg, 1994; Würden and Homberg, 1995; Petri et al., 1995). Especially interesting is the association of the fan-shaped medulla fiber system with the contralateral lamina organ, a presumptive extraocular photoreceptor with possible circadian function (Fleissner et al., 2001). These lamina arborizations could serve as light input pathway from the ipsi- or contralateral eye into the circadian clock. Possibly, neurons of the fan-shaped medulla fiber system form the light input pathway from the contralateral eye, which was predicted by the lesion experiments of Page (1983). Also a possibility, this fan-shaped medulla fiber system could be an output pathway from the ipsi-, or contralateral circadian clock to adjust light sensitivity of circadian photoreceptors over the course of the day.

Properties of the neuronal pacemaker coupling pathway

The circadian coupling pathway between the bilaterally symmetric optic lobe pacemakers in the cockroach *L. maderae* has been investigated by neuroanatomic and behavioral experiments (Roth and Sokolove, 1975; Page, 1978, 1983). Page proposed inputs into the ipsilateral pacemaker by ipsi- and contralateral light entrainment pathways, as well as input of phase information by the contralateral pacemaker by means of a coupling pathway. However, he could not distinguish whether these different functional pathways run in the same or in different neuronal tracts. But his experiments allowed him to conclude that the output pathway by which each pacemaker controls locomotor activity is functionally independent of the output pathway that couples both oscillators (Page, 1983). But it remained unresolved whether the light entrainment pathway from the contralateral eye is independent of either the coupling pathway or the output pathway that controls activity.

Page (1978) concluded from his lesion experiments that the coupling pathway is polysynaptic and not directly connecting both pacemaker centers. His lesions attempted to disconnect all monosynaptic optic lobe commissures, which were known at that time (Roth and Sokolove, 1975; discovered only tract 7). However, Page (1978) misjudged the location of the known optic lobe commissures, because the LoVT (as distal extension of tract 7) projects posteriorly to the lobula, in the center of the optic stalk, and not in the dorsal 1/3 of the lobula, as he assumed. Therefore, the LoVT was very likely not affected by his lesions (Page, 1978). Our data suggest that at least two monosynaptic coupling pathways exist between both AMae, one by means of the AOC and one by means of the POC, both of which are at least partly formed by PDH-ir and possibly also by FMRFamide-ir medulla neurons (Stengl and Homberg, 1994; Petri et al., 1995; Fig. 7). We hypothesize that PDH-ir neurons of tract 4 form circadian output pathways that affect locomotor activity rhythms by means

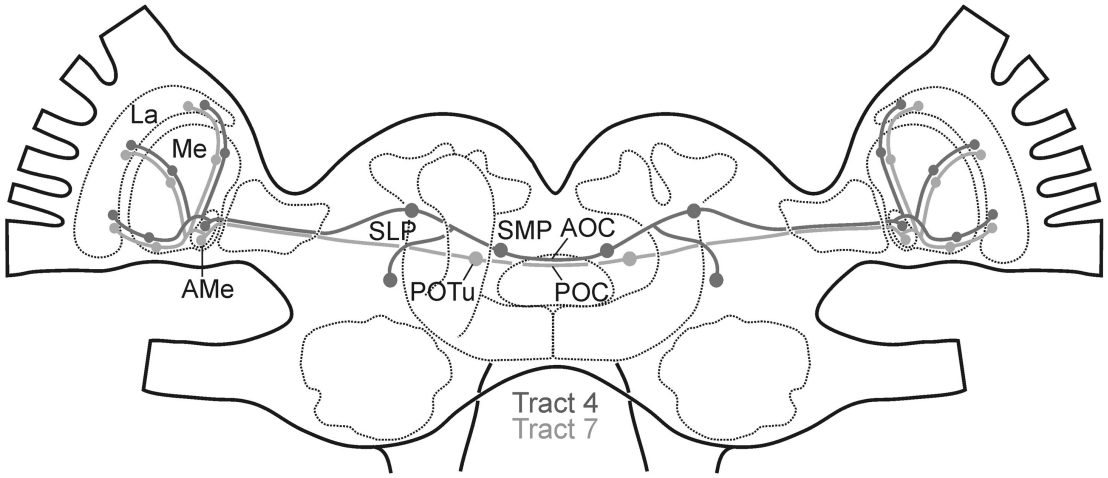

Fig. 7. Scheme of the presumptive circadian coupling pathways in the cockroach brain. The arborization pattern of PDH-like tracts 4 and 7 resemble arborization patterns predicted for circadian output and coupling pathways. The filled circles represent the main sites of synaptic interactions of the two fiber systems. Tract 4 connects both accessory medullae (AMe) by means of the anterior optic commissure (AOC) with arborizations in the anterior and proximal superior lateral protocerebrum (SLP) and superior median protocerebrum (SMP). In both optic lobes, tract 4 appears to arborize in the fan-shaped anterior layer system, connecting the AMae with the medullae (Me) and the laminae (La). Tract 7 connects both AMae by means of the posterior optic commissure (POC) with both posterior optic tubercles (POTu). Tract 7 also arborizes in the fan-shaped anterior layer system of both optic lobes and connects the AMae with the medullae and the laminae. For other abbreviations, see list.

of branches in the SMP. The arborization pattern of tract 4 neurons with branches in the ipsi- and contralateral SMP fits findings by Page (1983), who showed that a pacemaker output pathway can suppress the output of the contralateral pacemaker, apparently by means of branches in the contralateral brain hemisphere. In addition, we hypothesize that PDH- and FMRFamide-ir neurons of tract 7 form monosynaptic coupling pathways between both circadian pacemakers and also receive light input from the ipsi- and contralateral eyes by means of arborizations in the lamina and medulla (Fig. 7). Also in *Drosophila melanogaster*, different experiments suggest that the PDH-ir circadian pacemaker neurons control locomotor activity rhythms by means of branches in the SMP (Helfrich-Förster, 1998; Park et al., 2000), whereas the coupling pathways might project by means of the POC (Helfrich-Förster, unpublished observations).

The role of PDH-ir neurons as a coupling pathway is supported by physiological data combined with computer simulations. A circadian function for PDH has been demonstrated by microinjection of PDH into the optic lobe, resulting in an all-delay type phase response curve (Petri and Stengl, 1997). Computer models showed that a coupling interaction by means of a combination of all-delay and all-advance phase response curves allows for mutual pacemaker coupling and simulates all experimental results from cockroaches (Petri and Stengl, 2001). Thus, we assume that synchronization of both circadian pacemakers could be mediated by a subpopulation of phase-delaying PDH-ir medulla neurons projecting by means of tract 7, together with an unknown parallel neuronal pathway that causes phase-advances. In dextran injections into the ipsilateral AMe combined with PDH and FMRFamide immunocytochemistry, we currently test whether FMRFamide-ir neurons form this second parallel coupling pathway and whether PDH and FMRFamide immunoreactivity is colocalized in cells of tract 7.

ACKNOWLEDGMENTS

We thank Dr. Uwe Homberg for considerable improvement of the manuscript. We also thank Nina Kreissköther for insect rearing.

LITERATURE CITED

Boyan G, Williams L, Meier T. 1993. Organization of the commissural fibers in the adult brain of the locust. J Comp Neurol 332:358–377.

Chiba Y, Tomioka K. 1987. Insect circadian activity with special reference to the localization of the pacemaker. Zool Sci 4:945–954.

Collett T. 1972. Visual neurones in the anterior optic tract of the privet hawk moth. J Comp Physiol 78:396–433.

DeVoe RD, Kaiser W, Ohm J, Stone LS. 1982. Horizontal movement detectors of honeybees: directionally-selective visual neurons in the lobula and brain. J Comp Physiol A 147:155–170.

Fischbach KF, Lyly-Hünerberg I. 1983. Genetic dissection of the anterior optic tract of *Drosophila melanogaster*. Cell Tissue Res 231:551–563.

Fleissner G, Loesel R, Fleissner G, Waterkamp M, Kleiner O, Batschauer A, Homberg U. 2001. Candidates for extraocular photoreceptors in the cockroach suggest homology to the lamina and lobula organs in beetles. J Comp Neurol 433:401–414.

Gewecke M, Hou T. 1993. Visual brain neurons in *Locusta migratoria*. In: Wiese K, Gribakin FG, Popov AV, Renninger G, editors. Sensory systems of arthropods. Basel: Birkhäuser Verlag. p 119–144.

Gronenberg W. 1984. Das Protocerebrum der Honigbiene im Bereich des Pilzkörpers – eine neurophysiologisch-anatomische Charakterisierung. Ph.D. dissertation, Freie Universität Berlin, Germany.

Hausen K. 1984. The lobula complex of the fly: structure, function and significance in visual behaviour. In: Ali MA, editor. Photoperception and vision in invertebrates. New York, London: Plenum Press. p 523–559.

Helfrich-Förster C. 1995. The period clock gene is expressed in central nervous system neurons which also produce a neuropeptide that re-

veals the projections of circadian pacemaker cells within the brain of *Drosophila melanogaster*. Proc Natl Acad Sci U S A 92:612–616.

Helfrich-Förster C. 1998. Robust circadian rhythmicity of *Drosophila melanogaster* requires the presence of lateral neurons: a brain-behavioral study of disconnected mutants. J Comp Physiol [A] 182:435–453.

Helfrich-Förster C, Stengl M, Homberg U. 1998. Organization of the circadian system in insects. Chronobiol Int 15:567–594.

Hertel H, Maronde U. 1987. The physiology and morphology of centrally projecting visual interneurones in the honeybee brain. J Exp Biol 133:301–315.

Hertel H, Schäfer S, Maronde U. 1987. The physiology and morphology of visual commissures in the honeybee brain. J Exp Biol 133:283–300.

Homberg U. 1982. Das mediane Protocerebrum der Honigbiene (*Apis mellifica*) im Bereich des Zentralkörpers: Physiologische und morphologische Charakterisierung. Ph.D. dissertation, Freie Universität Berlin, Germany.

Homberg U. 1994. Flight-correlated activity changes in neurons of lateral accessory lobes in the brain of the locust *Schistocerca gregaria*. J Comp Physiol [A] 175:597–610.

Homberg U, Würden S, Dircksen H, Rao KR. 1991. Comparative anatomy of pigment-dispersing hormone-immunoreactive neurons in the brain of orthopteroid insects. Cell Tissue Res 266:343–357.

Honegger HW, Schürmann FW. 1975. Cobalt sulphide staining of optic fibers in the brain of the cricket, *Gryllus campestris*. Cell Tissue Res 159:213–225.

Jawlowski H. 1963. On the origin of *corpora pedunculata* and the structure of the *tuberculum opticum* (Insecta). Acta Anat 35:346–359.

Kenyon FC. 1896. The brain of the bee. J Comp Neurol 6:133–210.

Köbbert C, Apps R, Bechmann I, Lanciego JL, Mey J, Thanos S. 2000. Current concepts in neuroanatomical tracing. Prog Neurobiol 62:327–351.

Labhart T, Petzold J. 1993. Processing of polarized light information in the visual system of crickets. In: Wiese K, Gribakin FG, Popov AV, Renninger G, editors. Sensory system of arthropods. Basel: Birkhäuser Verlag. p 158–169.

Loesel R. 1999. Neuronale Organisation der Inneren Uhr der Schabe *Leucophaea maderae* unter besonderer Berücksichtigung möglicher Lichtsynchronisationswege. Ph.D. dissertation, Philipps Universität Marburg, Germany.

Loesel R, Homberg U. 1998. Sustained oscillations in an insect visual system. Naturwissenschaften 85:238–240.

Loesel R, Homberg U. 1999. Histamine-immunoreactive neurons in the brain of the cockroach *Leucophaea maderae*. Brain Res 842:408–418.

Loesel R, Homberg U. 2001. Anatomy and physiology of individual neurons of the accessory medulla of the cockroach, *Leucophaea maderae*. J Comp Neurol 439:193–207.

Milde JJ. 1993. Tangential medulla neurons in the moth *Manduca sexta*. Structure and responses to optomotor stimuli. J Comp Physiol [A] 173:783–799.

Mizunami M. 1995. Functional diversity of neural organization in insect ocellar systems. Vision Res 35:443–452.

Mobbs PC. 1984. Neural networks in the mushroom bodies of the honeybee. J Insect Physiol 30:43–58.

Nässel DR, Shiga S, Wikstrand EM, Rao KR. 1991. Pigment-dispersing hormone-immunoreactive neurons and their relation to serotonergic neurons in the blowfly and cockroach visual system. Cell Tissue Res 266:511–523.

Nishiitsutsuji-Uwo J, Pittendrigh CS. 1968. Central nervous system control of circadian rhythmicity in the cockroach. III. The optic lobes, locus of the driving oscillator? Z Vergl Physiol 58:14–46.

Page TL. 1978. Interactions between bilaterally paired components of the cockroach circadian system. J Comp Physiol [A] 124:225–236.

Page TL. 1982. Transplantation of the cockroach circadian pacemaker. Science 216:73–75.

Page TL. 1983. Effects of optic-tract regeneration on internal coupling in the circadian system of the cockroach. J Comp Physiol 153:353–363.

Page TL. 1984. Neuronal organization of a circadian clock in the cockroach *Leucophaea maderae*. In: Porter R, Collins GM, editors. Photoperiodic regulation of insect and molluscan hormones. London: Pitman. p 115–135.

Page TL, Caldarola PC, Pittendrigh CS. 1977. Mutual entrainment of bilaterally distributed circadian pacemakers. Proc Natl Acad Sci U S A 74:1277–1281.

Park JH, Helfrich-Forster C, Lee G, Liu L, Rosbash M, Hall JC. 2000. Differential regulation of circadian pacemaker output by separate clock genes in *Drosophila*. Proc Natl Acad Sci U S A 97:3608–3613.

Petri B, Stengl M. 1997. Pigment-dispersing hormone shifts the phase of the circadian pacemaker of the cockroach *Leucophaea maderae*. J Neurosci 17:4087–4093.

Petri B, Stengl M. 2001. Phase response curves of a molecular model oscillator: implications for mutual coupling of paired oscillators. J Biol Rhythms 16:125–141.

Petri B, Stengl M, Würden S, Homberg U. 1995. Immunocytochemical characterization of the accessory medulla in the cockroach *Leucophaea maderae*. Cell Tissue Res 282:3–19.

Reischig T, Stengl M. 1996. Morphology and pigment-dispersing hormone immunocytochemistry of the accessory medulla, the presumptive circadian pacemaker of the cockroach *Leucophaea maderae*: a light- and electron-microscopic study. Cell Tissue Res 285:305–319.

Rind FC. 1987. Non-directional, movement sensitive neurones of the locust optic lobe. J Comp Physiol [A] 161:477–494.

Roberts SK. 1974. Circadian rhythms in cockroaches: effects of optic lobe lesions. J Comp Physiol 88:21–30.

Roth RL, Sokolove PG. 1975. Histological evidence for direct connections between the optic lobes of the cockroach *Leucophaea maderae*. Brain Res 87:23–39.

Sokolove PG. 1975. Localization of the optic lobe arcadian pacemaker with microlesions. Brain Res 87:13–21.

Stengl M, Homberg U. 1994. Pigment-dispersing hormone-immunoreactive neurons in the cockroach *Leucophaea maderae* share properties with circadian pacemaker neurons. J Comp Physiol [A] 175:203–213.

Strausfeld NJ. 1976. Atlas of an insect brain. Berlin, Heidelberg, New York: Springer.

Strausfeld NJ, Blest AD. 1970. Golgi studies on insects. I. The optic lobes of Lepidoptera. Philos Trans R Soc London B 528:81–134.

Strausfeld NJ, Kong A, Milde JJ, Gilbert C, Ramaiah L. 1995. Oculomotor control in calliphorid flies: GABAergic organization in heterolateral inhibitory pathways. J Comp Neurol 361:298–320.

Tomioka K, Nakamichi M, Yukizane M. 1994. Optic lobe circadian pacemaker sends its information to the contralateral optic lobe in the cricket *Gryllus bimaculatus*. J Comp Physiol A 175:381–388.

Ushirogawa H, Abe Y, Tomioka K. 1997. Circadian locomotor rhythms in the cricket, *Gryllodes sigiilatus*. II. Interactions between bilaterally paired circadian pacemakers. Zool Sci 14:729–736.

Wehner R. 1984. Astronavigation in insects. Annu Rev Enthomol 29:277–298.

Wiedenmann G. 1984. Zeitgeber and circadian activity rhythms of cockroaches: a system of unipolar coupled oscillators. J Interdiscip Cycle Res 15:69–80.

Würden S, Homberg U. 1995. Immunocytochemical mapping of serotonin and neuropeptides in the accessory medulla of the locust, *Schistocerca gregaria*. J Comp Neurol 362:305–319.

Yukizane M, Tomioka K. 1995. Neural pathways involved in mutual interactions between optic lobe circadian pacemakers in the cricket *Gryllus bimaculatus*. J Comp Physiol [A] 176:601–610.

VII. Pigment-dispersing hormone (PDH)-immunoreactive neurons form a direct coupling pathway between the bilaterally symmetric circadian pacemakers of the cockroach *Leucophaea maderae*.

Pigment-Dispersing Hormone (PDH)-Immunoreactive Neurons Form a Direct Coupling Pathway Between the Bilaterally Symmetric Circadian Pacemakers of the Cockroach *Leucophaea maderae*

Thomas Reischig, Bernhard Petri, and Monika Stengl

ABSTRACT

The circadian periodicity of the locomotor behaviour of the cockroach *Leucophaea maderae* is driven by two bilaterally paired and mutually coupled pacemakers, which reside in the brains optic lobes. Transplantation studies showed that this neuronal pacemaker is located in the accessory medulla (AMe), a small neuropil of the optic lobe's medulla. The AMe is densely innervated by a set of a dozen anterior and about four posterior pigment-dispersing hormone immunoreactive (PDH-ir) medulla neurons (PDHMe), which are circadian pacemaker candidates in the fruitfly and in the cockroach. In addition, a subpopulation of these cells appears to connect both optic lobes and is suggested to constitute a circadian coupling pathway. To determine, whether PDHMe directly connect both AMae, we injected rhodamine-labelled dextran as neuronal tracer into one AMe and performed additional PDH-immunocytochemistry. Double-labelled fibres in the anterior, shell, and internodular neuropil of the AMe contralaterally to the injection side showed that indeed PDH-ir fibres directly connect both AMae. This connection is performed by three PDHMe of each optic lobe, which all belong to the anterior PDHMe, but not to the posterior PDHMe. Thus, a subset of anterior PDHMe fulfills the morphological criteria for a circadian coupling pathway. In the central brain, all except one of the typical projection areas are innervated by anterior PDHMe of the ipsi- as well as of the contralateral optic lobe. Hence, most output targets of the clocks are affected by both pacemakers. Our data suggest that anterior PDHMe neurons play multiple roles in generating circadian rhythms, delivering output of timing information, and performing mutual pacemaker coupling in *L. maderae*.

Indexing terms: Pigment-dispersing hormone, optic lobes, insects, cockroaches, accessory medulla, neuroanatomy, circadian rhythms

The locomotor activity rhythm of the cockroach *Leucophaea maderae* is driven by two bilaterally symmetric circadian pacemakers in the optic lobes (Nishiitsutsuji-Uwo and Pittendrigh, 1968; Roberts, 1974; Sokolove, 1975; Page, 1982; reviewed by Page, 1984; Chiba and Tomioka, 1987). Strong evidence suggest that the accessory medulla (AMe; plural accessory medullae, AMae), a small neuropil at the ventromedial edge of the medulla, is the neuronal correlate of this circadian pacemaker (Stengl and Homberg, 1994; Petri et al., 1995; Reischig and Stengl, 1996; Reischig and Stengl, 2003). The AMe is densely innervated by neurites of pigment-dispersing hormone-immunoreactive (PDH-ir) medulla neurons (PDHMe), which are circadian pacemaker candidates in *Drosophila* as well as in the

cockroach. The PDHMe are thought to comprise single oscillator neurons in insects, which timing information is synchronised in the AMe (Homberg et al., 1991; Helfrich-Förster, 1995; reviewed by Helfrich-Förster et al., 1998; Homberg et al., 2003). In *Drosophila melanogaster*, PDH-ir neurons express circadian clock proteins, such as PERIOD, TIMELESS, CLOCK and CYCLE (Helfrich-Förster, 1995; reviewed by Stanewsky, 2002). In contrast to crickets, in the cockroach the bilateral pacemakers are strongly coupled (Page et al., 1977; Wiedenmann and Loher, 1984; Ushirogawa et al., 1997). A comparison of the morphology of PDH-ir neurons in crickets and cockroaches revealed a correlation between the number of PDH-ir commissures, the length of the period, and the strength of coupling (Stengl and Homberg, 1994; Stengl, 1995). We recently demonstrated that seven tracts directly connect both optic lobes in the cockroach; two of them strongly resemble the arborisation pattern of the PDH-ir neurons (Reischig and Stengl, 2002). Therefore, the PDHMe are probably not only proposed circadian pacemaker and output neurons, but additionally appear to form a direct neuronal coupling pathway between the bilaterally symmetric pacemakers in the cockroach. Nevertheless, direct evidence whether these contralateral projections are indeed formed by PDH-ir neurons is still lacking. Thus, we injected the neuronal fluorescent tracer rhodamine-dextran into one AMe and performed subsequent PDH-immunocytochemistry. Confocal laser scan microscopic investigations of this preparations revealed double-labelled fibres in the contralateral AMe, thus showing a direct connection between both AMae performed by PDH-ir fibres. Moreover, most of the termination sites of PDH-ir fibres in the central brain receive input from PDHMe of the opposite optic lobe, thus indicating, that most output targets of the clocks are affected by both pacemakers. Thus, PDH-ir neurons are strong candidates for a direct circadian coupling pathway.

Abbreviations

AMe(ae)	Accessory medulla(e)
AOC	Anterior optic commissure
-ir	-immunoreactive
ILP	inferior lateral protocerebrum
LoVT	Lobula valley tract
MC I-III	Medulla cell groups I-III
PDF	Pigment dispersing factor
PDH	Pigment dispersing hormone
POC	Posterior optic commissure
POT	Posterior optic tract
POTu	Posterior optic tubercle
Rh-D	Rhodamine-dextran
SLP	Superior lateral protocerebrum
SMP	Superior median protocerebrum
VLP	Ventro-lateral protocerebrum

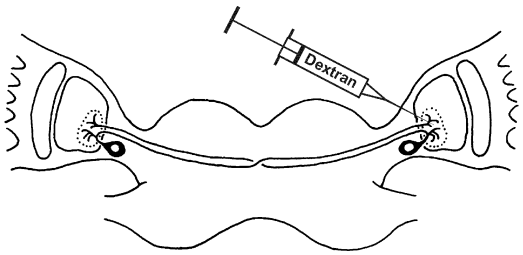

Fig. 1. Scheme of the cockroach brain with hypothetical direct coupling PDH-ir pathways connecting both AMae. Dextran was injected directly into one AMe to identify these coupling pathways. The dye is assumed to stain neurons in antero- and retrograde direction.

MATERIALS AND METHODS

Animals

Adult male cockroaches (*Leucophaea maderae*) were chosen from laboratory colonies. They were reared at 25 °C, 30 % relative humidity, and light-dark cycles of 12:12 h, with lights on at 6 AM. The animals were fed with dried dog food, potatoes, and water *ad libidum*. The nomenclatures for anatomical orientations (left and right, dorsal, ventral etc.) are always quoted according to the longitudinal axis of the animal, except the anterior layer of the medulla, which is here termed, ontogenetically correct, the distal layer (with the distal fibre fan).

Dextran injection

Animals ($N = 50$) were anesthetised with CO_2 and fixed in a mounting device. A small window was cut into the head capsule above the left optic lobe to expose the brain. An amount of 0.5–2 nl rhodamine dextran-solution (dextran conjugated with the fluorescent dye rhodamine, 3,000 MW, lysine fixable, Molecular Probes Inc., USA; 0.1 μg/μl in 0.1 M phosphate buffer (PB), pH 7.4, containing 10 % aqueous blue food dye) was pressure-injected with a microinjector (Microinjector 5242, Eppendorf, Germany) under stereomicroscopic control into one AMe with a glass capillary (Clark, Pangbourne Reading, England). The capillary was pulled to a pipette as used for patch clamp experiments, with a tip diameter of 1–2 μm. For more details see Reischig and Stengl (2002). After the injection, the head capsule was closed with wax to allow intracellular transport of the dye overnight.

PDH-immunocytochemistry and evaluation

The next day the injected brains of the cockroaches were removed and fixed for 4 h in 4 % paraformaldehyde/7.5 % saturated picric acid in PB at room

temperature. Fifteen brains were prepared for wholemount analysis as follows: The brains were washed in Tris-buffered saline (TBS; 0.1 M Tris-HCl/0.3 M NaCl, pH 7.4) containing 0.1 % Triton X-100 (TrX). Then, they were preincubated overnight in TBS with 0.5 % TrX, and 2 % normal goat serum (NGS). The brains were incubated with anti-β-PDH polyclonal antiserum (# 3B3; Dircksen et al., 1987) at a dilution of 1:80,000 in TBS containing 0.5 % TrX and 1 % NGS for 3 days. Then, the brains were washed three times in TBS with 0.1 % TrX. They were labelled overnight with dichlorotriazinyl aminofluorescein (DTAF)-conjugated goat anti rabbit IgG (Dianova, Hamburg, Germany) in TBS containing 0.5 % TrX and 1 % NGS. Subsequently, the brains were washed three times in TBS with 0.1 % TrX, then cleared and mounted in elvanol (Rodriguez and Deinhard, 1960; 5 g Moviol (Hoechst, Germany), 10 ml glycerine, 20 ml phosphate buffered saline, 1 mg/ml n-propyl-gallate). DTAF-immunofluorescence was detected with a 512–565 nm bandpass filter, and rhodamine fluorescence was detected with a 590 nm long-pass filter on a confocal laser scanning microscope (Zeiss), equipped with an argon (488 nm) and a helium/neon laser (543 nm).

The other 35 brains were embedded in gelatine/albumin (4.8 % gelatine and 12 % ovalbumin in pure water) and postfixed in 8 % formalin in PB. The brains were sectioned with a vibratome in a frontohorizontal plane to 40 μm thick slices. The free-floating sections were washed in PB and preincubated in 2 % NGS diluted in TBS containing 0.5 % TrX. The anti-β-PDH antiserum was diluted 1:10,000 in TBS containing 1 % NGS and 0.5 % TrX, and was applied to the sections for 18–20 h at room temperature. After washing in TBS with 0.1 % TrX, the sections were incubated for 1 h in 1:300 goat-anti-rabbit IgG coupled with DTAF or CY2 fluorescent dye (Dianova, Germany) in TBS containing 0.5 % TrX and 1 % NGS. After washing in TBS with 0.1 % TrX, the sections were mounted on chromalum/gelatine coated microscope slides, embedded in Entellan (Merck, Darmstadt, Germany) under covering slides and examined with a Leitz TCS SP2 confocal laser scan microscope equipped with a variable detection filtering system. Most scans were performed using a Leitz HPX PL apochromate 40x/1.25 oil immersion lens. To exclude crosstalk artefacts, the specimen were always scanned sequentially, and the detection ranges were separated as far as possible. DTAF or Cy2 was exited with a 488 nm argon laser; fluorescence light was detected between 505–525 nm. Rhodamin fluorescence was exited with the 543 nm line of a helium/neon laser and detected between 585–625 nm.

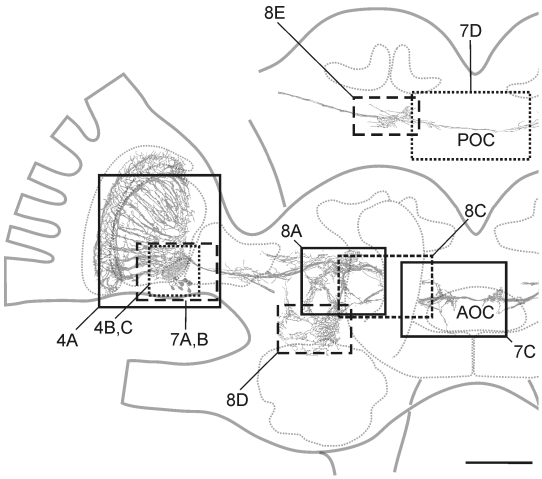

Fig. 2. Reconstruction of the PDH-ir neuron system contralaterally to the injected AMe, to demonstrate the scanning sites of the confocal laser scan images presented in Figs. 4, 7, and 8. AOC anterior optic commissure, POC posterior optic commissure. Scale bar = 200 μm.

Projection images of optical section series were accomplished as maximum projections. The respective scan regions for Figs. 5, 7, and 8 together with a reconstruction of the PDH-ir neuron system are indicated in Fig. 2. For a complete reconstruction of the PDH-ir fibre system embedded in a 3D model of the cockroach brain, see Reischig and Stengl (2002).

To perform a reconstruction drawing of double-labelled fibres and somata in one AMe (Fig. 6), all single images of two image stacks (derived from two consecutive physical sections of the AMe; z-distance of optical sections was 1 μm) were imported into one multi layer image in Adobe Photoshop 6.0. The red channel image (rhodamine fluorescence from the injected AMe) of optical section No. 1 followed the green channel image (PDH immunoreactivity) of optical section No. 1, red channel of optical section No. 2 the respective green channel, and so on. Double-labelled structures of one optical section could be detected, if the respective green channel was rendered semi-transparent, and the red channel below became visible; layers which otherwise covered visibility of the layers in examination were hidden. On additional image layers, double-labelled structures were traced using the drawing tools of Photoshop. After that, the layers containing the laser scan images were deleted, and the layers containing the drawings were merged.

RESULTS

To resolve the question whether PDH-ir medulla neurons (PDHMe) qualify for a direct and monosynaptic coupling pathway between both AMae, we

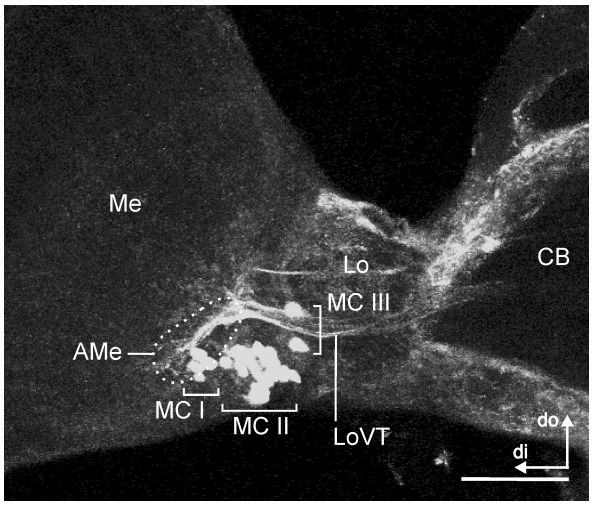

Fig. 3. In this wholemount preparation of a cockroach brain, all three groups of heterolaterally projecting medulla cells (MC I–III) are stained after injection of rhodamine-dextran in the contralateral accessory medulla (AMe). The dotted line indicates the position of the ipsilateral AMe. MC I contains four neurons. This group lies in the position of the somata of the anterior PDHMe. MC II is a cluster of up to 35 neurons. MC III lies close to the lobula valley tract (LoVT) posteriorly to the lobula (Lo). All three groups project *via* the LoVT into the central brain (CB) and to the contralateral optic lobe. Me medulla. Coordinates: di distal, do dorsal. Scale bar = 100 μm.

injected rhodamine-coupled dextran (Rh-D) as neuronal tracer in one AMe (Fig. 1), and counterstained the brains with anti-β-PDH antiserum (Dircksen et al., 1987). Fifteen brains were analysed as wholemounts, and 35 were sectioned with a vibratome at 40 μm prior examination. As described before (Reischig and Stengl, 2002), three different soma groups (medulla cells groups I–III (MC I–III; Fig. 3) and two distinct fibre arborisation patterns could regularly be observed in the optic lobe contralaterally to the injected AMe. Up to three MC I somata in altogether 17 experiments (3 wholemounts, 14 sectioned brains) showed additional PDH-ir staining (Figs. 4A, 5; the respective scanning regions of Figs. 4, 7, and 8 are shown in Fig. 2) and thus, are a subgroup of the anterior PDHMe. In the contralateral optic lobe, PDH-ir fibres originating from the injected ipsilateral AMe could only be observed in the sectioned brains, but not in the wholemounts ($N = 11$). They arborise in the anterior, the internodular, and shell neuropil of the AMe (Figs. 4B,C, 6), and extend in a fanshaped manner through the distalmost layer of the medulla (Figs. 4A,B) to the lamina (not shown; compare Reischig and Stengl 2002). The Rh-D-stained MC II and MC III somata never showed colocalised staining with PDH-ir (Fig. 5A,B), nor could colocalised staining be observed in the posterior PDHMe. In the central brain, most but not all arborisation sites of PDH-ir fibres are innervated by PDH-ir fibres of both optic lobes. The intensity of Rh-D staining varied between different animals and was largely dependent of the precision of Rh-D injections; best results, most notably concerning the staining intensity and the number of MC I somata and fibres, were obtained if the AMe was accurately hit (Fig. 4D). Remarkably, the staining intensity of MC I somata and fibres was always lower than that of MC II and III; particularly the respective fibres were often difficult to detect within the large background caused by intercellular distributed Rh-D. According to previous results obtained with biotinylated dextran (Reischig and Stengl, 2002), Rh-D labelled neurons in anterograde and retrograde manner.

Contralateral PDH-ir projections in the accessory medulla

In the following descriptions, numerical statements of counted cells always refer to the 35 experiments, where Rh-D injected brains were sectioned prior to the PDH immunostaining procedure, if not quoted otherwise. Mean numbers of stained fibres and somata are indicated as n_m. The injected optic lobe (always the left side in respect to the animal's body axis) is referred as ipsilateral, the opposite, untreated right optic lobe as contralateral (contralateral to the injection site).

In 14 of the sectioned brains, maximally 3 Rh-D stained MC I somata could be observed in the contralateral optic lobe, which showed colocalising PDH-ir (in 3 brains; 2 somata in 6 brains, 1 in 5 brains) and therefore, belong to the anterior PDHMe (Fig. 4A). As stated elsewhere (Reischig and Stengl, submitted), the anterior PDHMe are further divided into three subpopulations according to soma size and PDH-ir staining intensity, with about four somata in each subgroup (Fig. 5): the most intensely staining large somata ($n_m \pm$ S.D.: 19 ± 4 μm), weaker staining medium-sized somata (15 ± 3 μm), and faintly staining small somata (11 ± 2 μm). In many preparations, one of the large anterior PDHMe is conspicuously larger than the others (up to 26 μm) and takes the position most proximally to the central brain. Combining the results of the successful injection experiments, regularly one of the medium-sized and two of the large anterior PDHMe of the contralateral optic lobe could be stained by Rh-D injection in the AMe and thus, project to the AMe of the opposite optic lobe (Fig. 5). One of these two large anterior PDHMe is the most proximal, largest anterior PDHMe. The small anterior PDHMe never showed Rh-D staining.

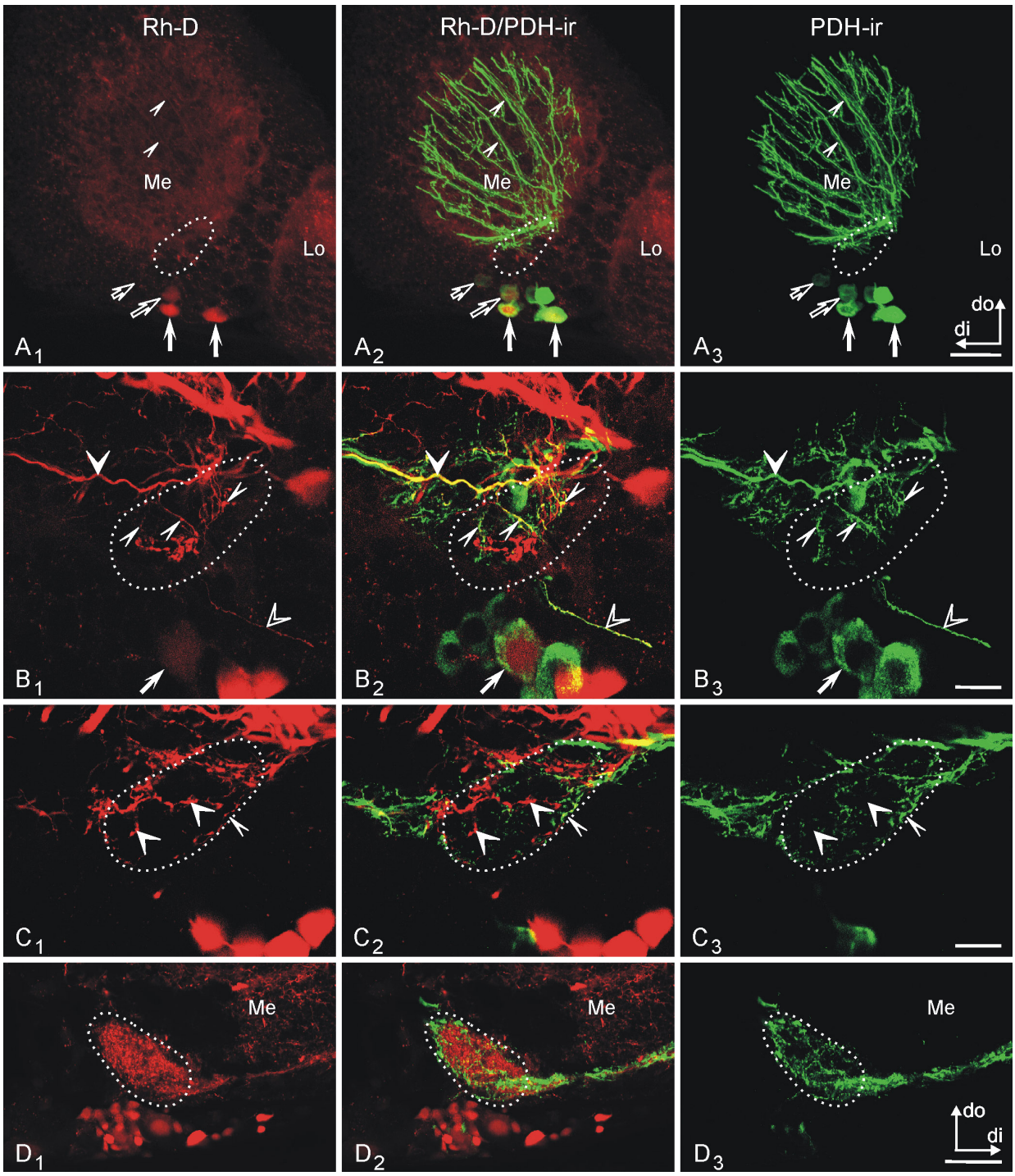

Fig. 4. Confocal laser scan images obtained from vibratome sections of the optic lobe contralaterally to the dextran-injected accessory medulla (AMe, A–C), and of an injected, ipsilateral AMe (D). Red shows rhodamine-dextran (Rh-D) fluorescence, green) shows PDH immunoreactivity. The respective overlay images in the middle column shows colocalisation in yellow. A shows projection images of 21 optical sections (z-distance between single sections = 2 μm), B–D show single optical sections. The dotted line indicates the position of the AMe. **A_{1-3}:** In this optic lobe all three AMe-connecting PDH-ir anterior medulla neurons (anterior PDHMe) are visible. Two of these neurons belong to the large anterior PDHMe (filled arrows), and one to the medium-sized anterior PDHMe (open large arrows). All belong to the MC I. The small and weakly staining anterior PDHMe (open small arrows) do not project to the contralateral optic lobe. Colabelled PDH-ir fibres project *via* the distal layer fibre fan of the medulla (arrowheads) to the lamina. **B_{1-3}:** Fibres from the injected, opposite AMe project *via* the lobula valley tract into the anterior neuropil of the AMe (slim arrowheads) and into the distal layer of the medulla (large filled arrowheads). Additionally, a characteristic colabelled fibre projects into the cell cortex (open arrowhead). Arrows: a weakly Rh-D-stained, contralaterally projecting large anterior PDHMe soma. The other three red but not colabelled somata belong to the MC II. **C_{1-3}:** A single optical section of the AMe further posterior to that shown in B. Few colabelled varicose PDH-ir fibres are visible in the shell neuropil of the proximal edge of the AMe (slim arrowheads). The not colabelled fibres (large arrowheads) appear to belong to the MC II somata. **D_{1-3}:** The injected AMe of the same preparation shown in B and C displays Rh-D-staining, which is largely confined to the AMe. Coordinates: A_3 valid also for B,C, D_3 only for D; di distal, do dorsal. Scale bars = 80 μm in A, 20 μm in B,C, 40 μm in D.

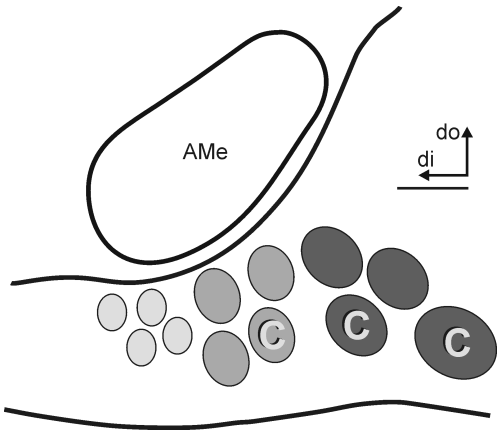

Fig. 5. Scheme of the accessory medulla (AMe) with the three groups of PDH-ir anterior medulla neurons (anterior PDHMe), three of which project to the contralateral AMe (indicated by C). The anterior PDHMe consist of four small and weakly immunoreactive somata (light grey), four medium-sized and more intensely staining somata (medium grey), and four large, most intensely staining somata (dark grey). The most proximal one of the latter is prominently larger than the others. Coordinates: di distal, do dorsal. Scale bar = 20 μm.

In the neuropil of the AMe contralaterally to the injected site, a subpopulation of the PDH-ir fibres showed colocalised Rh-D staining indicating connections to the injected AMe (Figs. 4B,C, Fig. 6). Most of these fibres were found in the anterior neuropil of the AMe, which covers the anterior face of the AMe, but extends more distally and gives rise to the fan-shaped anterior layer fibre system of the medulla (Reischig and Stengl, 1996). As shown previously (Reischig and Stengl, 2002), fibres emerging from the injected AMe run *via* the lobula valley tract (LoVT, Fig. 5A) through the anterior neuropil of the AMe and the contralateral distal layer fibre system of the medulla to the lamina. Here, a subpopulation of these fibres (Figs. 4A,B, Fig. 6) could be shown to belong to the PDH-ir neuron system. The AMe-portion posteriorly to the anterior neuropil consists of a core of dense nodular neuropil, which is interwoven by loose internodular neuropil and surrounded by a loose shell neuropil (Reischig and Stengl, 1996). Rh-D stained PDH-ir fibres were further found in the shell neuropil, preferentially at the proximal margin of the AMe (Fig. 4C), and, to a lesser extend, in the internodular neuropil of the AMe. Most of these double-labelled fibres showed very intense PDH-ir staining, which differs from that of a slightly weaker staining PDH-ir fibre population that is more common in the internodular neuropil (see PDH-ir labelling in Fig. $4C_3$). A conspicuous varicose PDH-ir fibre extending into the soma region ventrally and medially to the AMe also showed Rh-D staining. Due to the variable Rh-D staining results concerning number and staining intensity of fibres and somata, we were not able to assign any of the three anterior PDHMe with bilateral AMe projections to particular PDH-ir fibre populations.

The PDH-ir contralateral projection sites in the central brain

In the midbrains, both PDH-ir commissures contained double-labelled fibres, which could be traced to the contralateral optic lobes. In seven brains, we found up to three PDH-ir fibres with Rh-D staining in the anterior optic commissure (AOC; Fig. 7C); in each of 4 brains, one fibre was observed in the posterior optic commissure (POC; Fig. 7D). There was no clear correlation between the number of stained fibres in the commissures and the number of stained MC I somata. In four preparations with colocalising PDH-ir and Rh-D staining in MC I somata, we found no Rh-D staining at all in either commissure.

In the central brain halves contralaterally to the injected AMe, we examined all projection areas of the PDH-ir neuron system for double-labelled fibres deriving from the injected AMe. Double-labelled fibres were found in a prominent PDH-ir fibre arch of the anterior part of the superior lateral protocerebrum (SLP; Fig. 8A,B), in more posterior regions of the SLP and the superior median protocerebrum (SMP; Fig. 8C), in the inferior lateral protocerebrum (ILP; Fig. 8D), and in the posterior optic tubercle (Fig. 8E). No colocalisation was found in the ventrolateral protocerebrum (VLP). In most regions of the SLP and SMP, we found double-labelled fibres next to Rh-D stained fibres without PDH-ir, as well as PDH-ir fibres, which showed no Rh-D staining (Fig. 8B). The arborisation pattern of PDH-ir fibres in a conspicuous termination area dorsally to the prominent PDH-ir fibre arch of the anterior part of ther SLP differs from that of the other PDH-ir arborisation in the SLP and SMP: the fibres are more evenly distributed across this area, and stain less intensely. This area showed no double-labelled fibres, although some Rh-D stained fibres from the injected AMe arborise there (Fig. 8A). In the ILP, only few double-labelled fibres were found within an area showing otherwise dense innervation by PDH-ir varicose fibres (Fig. 8D).

Non-PDH-ir contralateral inputs in the AMe and optic lobe

Next to PDH-ir fibres, additional fibres from the injected AMe invade the contralateral AMe (Figs. 4B,C, 7A) and also the distal layer of the medulla, which show a similar arborisation pattern as the PDH-ir neurons and probably belong to the fourth

heterolateral but not PDH-ir MC I neuron. Moreover, very prominent in the non-injected AMe are fibres, which mainly belong to the MC II and, possibly, to the MC III somata. The MC II are the largest population of contralaterally projecting AMe neurons with up to 20 somata stained in 22 of 35 preparations ($n_m = 7.8 \pm 5.4$; Figs. 5A, 7A). They project through 1–2 bundles of neurites, the ventromedian bundles, dorso-posteriorly to the AMe, where they join the LoVT. In the AMe, they form prominent arborisations, which are concentrated in the internodular and shell neuropil of the distal face of the AMe (large arrowheads in Figs. 4B,C). These fibres have pronounced ramifications in median layers of the medulla (Fig. 5A), which do not reach the lamina (termed middle-layer fibre system of the medulla in Reischig and Stengl, 2002). Up to six cell bodies form the MC III, which lie posteriorly to the LoVT (Fig. 5B, 7A). They where found in 15 of 35 preparations ($n_m = 2.5 \pm 1.8$). Rh-D labelling of this group never colocalised with the posterior PDHMe. Mostly, the MC III somata lie slightly more posteriorly and more proximally to the central brain, where the posterior PDHMe have to been expected. Sometimes, one of these somata lies apart from the main group (Fig. 5B). None of the Rh-D stained fibre arborisations of the AMe and other parts of the optic lobe could be unequivocally assigned to these somata.

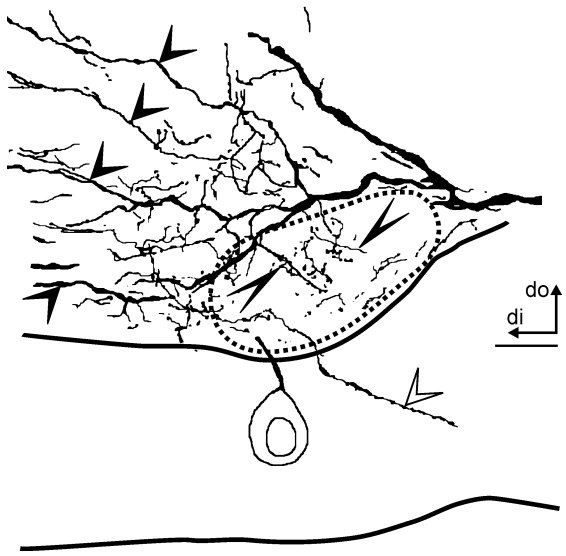

Fig. 6. Reconstruction of PDH-ir fibres and one cell body of an AMe stained after rhodamine-dextran injection into the contralateral AMe. The reconstruction was derived from the two confocal laser scan image stacks demonstrated in Fig. 4B and C (see also Material and Methods). Most contralateral PDH-ir fibres ramify in the anterior neuropil of the AMe (slim arrowheads) and project from there into the distal layer of the medulla (large filled arrowheads). Open large arrowhead: A fibre originating from a contralateral anterior PDHMe projects into the soma region of the AMe. Coordinates: di distal, do dorsal. Scale bar = 20 μm.

DISCUSSION

In search for the neuronal coupling pathways that mutually synchronise the bilaterally circadian pacemakers of the cockroach *L. maderae*, the AMae, we injected the neuronal tracer Rh-D into one AMe. Subsequent histological examination of the contralateral AMe additionally labelled with PDH immunocytochemistry revealed that three of the dozen anterior PDHMe of one optic lobe belong to the MC I somata that directly connect both AMae *via* both PDH-ir commissures, the AOC and POC. Except the VLP, nearly all of the arborisation sites of PDH-ir fibres in the contralateral central brain receive PDH-ir inputs from both AMae. Thus, we identified candidates for a direct mutual coupling pathway between the bilaterally symmetric circadian clocks of *L. maderae*.

Specificity and reliability of the tracer studies

Previous studies showed that dextran performed well as extracellularly applied neuronal tracer to stain heterolateral optic lobe projections in the cockroach *L. maderae* (Reischig and Stengl, 2002). Compared to horse raddish peroxidase, dextran was particularly advantageous to label the MC I neurons, and was therefore used in this study. However, we realised some conspicuous differences in Rh-D uptake and/or intracellular transport between the MC I and MC II cells. Generally, the MC I somata showed less Rh-D staining intensity compared to MC II somata. In addition, the processes of the MC I neurons were less frequently stained than compared to the MC II processes and were often hardly to detect against the background caused by unspecific migration of Rh-D in the intercellular space. Moreover, in some preparations that contained Rh-D-stained contralateral MC I somata, we could not discern corresponding fibres in the commissures or elsewhere. Apparently, the MC I and MC II groups differ strongly in their uptake and/or transport mechanisms. It appears that MC I cells take up dextran less efficiently, accumulate it very quickly in the somata, and thus, level the amount of the Rh-D signal in the fibres beyond the detection threshold. Thus, MC I neurons appear to preferentially employ retrograde transport of Rh-D in the MC I neurons. However, the staining of fibres indicated as axonal outputs by their beaded appearance clearly demonstrates an additional but weaker anterograde transport mechanism. This bidirectional transport allows to simultaneously detect neuron somata and axonal termina-

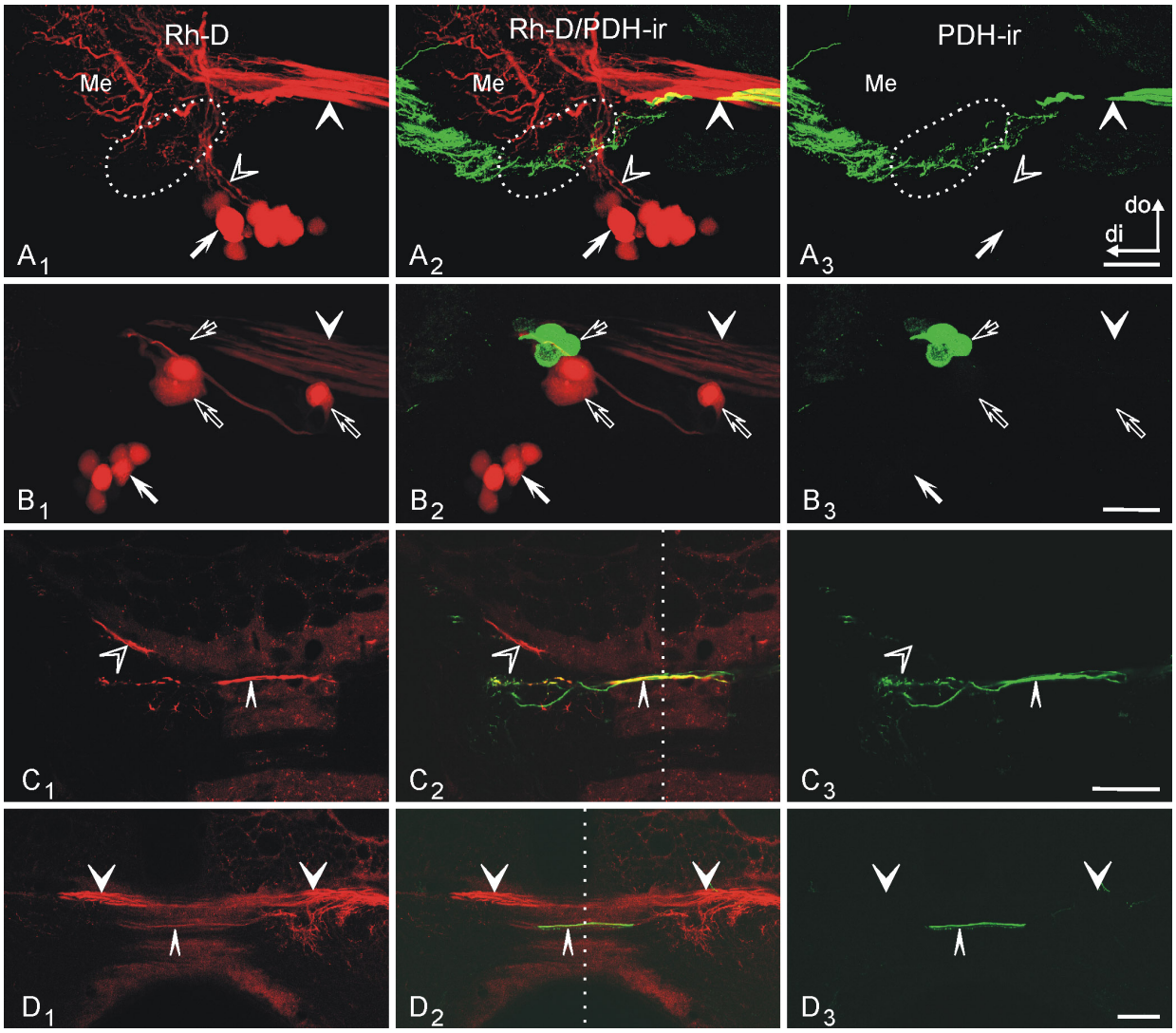

Fig. 7. Confocal laser scan images of posterior regions of the non-injected accessory medulla (A–B) and both PDH-ir commissures in the midbrain (C–D). Red shows Rh-D fluorescence, green shows PDH immunoreactivity. The respective overlay images in the middle column shows colocalisation in yellow. A shows projection images of 15 optical sections (z-distance of a single section = 2 μm), B–C show single optical sections. **A_{1-3}:** None of the contralaterally projecting medulla cells group II (MC II, arrow) colocalise with PDH immunostaining. The MC II project *via* the ventromedian bundle (open arrowhead) through the dorso-posterior part of the AMe to the lobula valley tract (filled arrowhead) and form the median-layer fibre system of the medulla (Me). Dotted line: position of the AMe. **B_{1-3}:** The contralaterally projecting MC III (open large arrows) are not identical to the posterior PDH-ir medulla cells (short arrows). Large filled arrow: Posterior portion of the MC II. Arrowheads: lobula valley tract. **C_{1-3}:** In the anterior optic commissure (AOC, slim arrowheads), double labelled fibres are visible projecting from the injected AMe to the contralateral optic lobe and AMe. Filled arrowheads: fibres from the AOC in the superior median protocerebrum. The open arrowheads point to the interoptical tract 3 (see Reischig and Stengl, 2002). **D_{1-3}:** The posterior optic commissure contains two PDH-ir fibres connecting both AMae (slim arrowheads). The large arrowheads point to the fibres of the POC that connect the MC II. Coordinates: A_3 valid also for B; di distal, do dorsal. The dotted line in C_2 and D_2 indicates the midline of the brain. Scale bars = 40 μm in A–D.

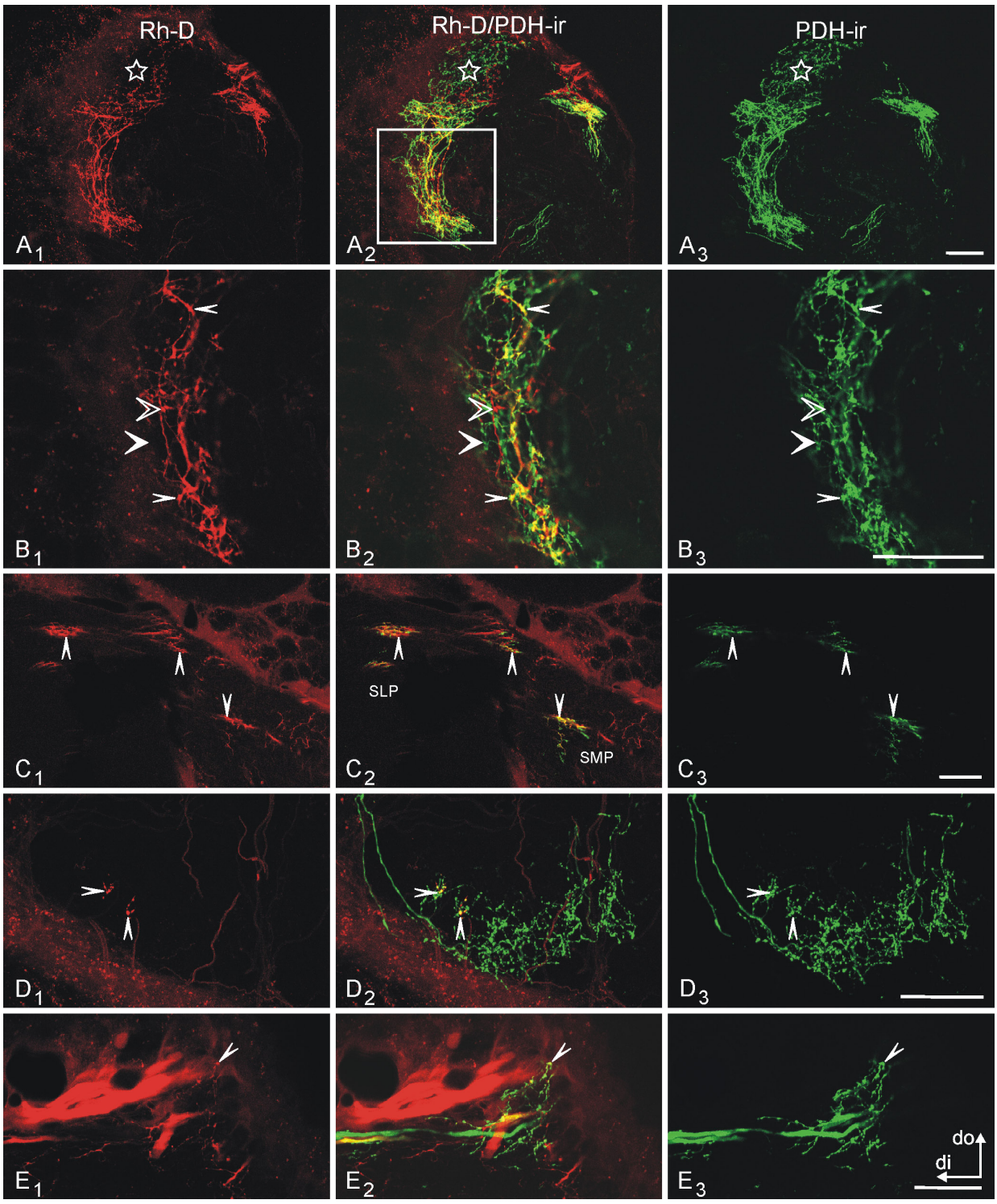

Fig. 8. Confocal laser scan images of typical projection areas of the PDHMe in the central brain, after injection of rhodamine-dextran (Rh-D) into the contralateral AMe. Red shows Rh-D fluorescence, green shows PDH immunoreactivity. The respective overlay images in the middle column shows colocalisation in yellow. A and D show projection images of 18 and 26 optical sections, respectively (z-distance of a single section = 1 μm), B–C and E show single optical sections. **A_{1-3}:** In the anterior part of the superior lateral protocerebrum contralaterally to the Rh-D-injected AMe, a prominent arc-like PDH-ir projection area overlaps with Rh-D staining. Another PDH-ir projection area with less intensely staining fibres (asterisk) shows partly overlap with RH-D labelled fibres, but without colocalisation in single fibres. Square: Detail enlarged in B. **B_{1-3}:** Optical section of the area indicated in A_2. PDH-ir fibres occur with (slim arrowheads) and without (large filled arrowheads) additional Rh-D-labelling, as well as Rh-D labelled fibres occur which are not PDH-ir (large open arrowheads). **C_{1-3}:** Also in the superior lateral protocerebrum (SLP) and in the superior medial protocerebrum (SMP) between the alpha lobe and the mushroom body peduncle contralaterally to the injected AMe, double labelled fibres occur (arrowheads). **D_{1-3}:** In the inferior lateral protocerebrum, only little colocalisation occurs (arrowheads). **E_{1-3}:** In the posterior optic tubercle contralaterally to the injected AMe, PDH-ir fibres are colabelled with Rh-D (slim arrowhead). Coordinates: di distal, do dorsal. Scale bars = 40 μm in A,C,E, 20 μm in B,D.

tions, but impedes the clear assignment of particular Rh-D-stained fibre patterns to the belonging cell bodies.

Since it could not be excluded that during injection tracer leaked into medulla neuropil next to the AMe, it is possible that some of the contralateral PDH-ir neurons rather arborise in the medulla. However, we recognised that the quality of Rh-D-staining particularly in MC I somata and fibres, strongly depended on the precision of the RH-D injections in the AMe. Therefore, it can be concluded that three anterior PDHMe, as well as at least a subpopulation of the MC II neurons, directly connect both AMae. Moreover, single MC II neurons were also observed in single cell stainings to directly connect both AMae (Loesel and Homberg, 1998; Loesel and Homberg, 2001).

Coupling pathways of the AMe

The first anatomical descriptions of neurons directly connecting both optic lobes in orthopteroid insects were provided by Roth and Sokolove (1975) in *L. maderae* and Honegger and Schürmann (1975) in crickets, and, for *L. maderae*, were discussed to be involved in the circadian system. In *L. maderae* however, only one posterior tract with two soma groups was reported, namely, tract 7 with the middle layer fibre system of the medulla (compare Reischig and Stengl, 2002), together with somata corresponding to MC II and III. A more detailed study involving horse radish peroxidase and dextran injections as well as backfills of the whole optic stalk (Reischig and Stengl, 2002) revealed seven tracts directly connecting both optic lobes, with four of them connecting the medullae. Tracts 4 and 7 were shown to connect both AMae and are formed by a group of four somata lying anterior-ventrally to the AMe, the MC I. The arborisation pattern of these neurons throughout the optic lobes and central brain closely resembles that of the PDH-ir medulla neurons. In this study we demonstrate, that tracts 4 and 7 indeed contain three PDH-ir neurons, which are a subgroup of the anterior PDHMe. Comparing the results of all experiments it can be concluded, that one of these heterolateral anterior PDHMe projects through tract 7 *via* the POC, the other two run through tract 4 *via* the AOC (Fig. 9). Thus, three anterior PDHMe (one medium-sized and two large) directly connect both AMae and are therefore strong candidates for a direct coupling pathway of the circadian pacemaker controlling locomotor behaviour in the cockroach.

The PDH-ir fibres that project into the contralateral AMe are not evenly distributed in the AMe. Their main arborisation area in the AMe is the anterior neuropil (Reischig and Stengl, 1996) of the AMe. To a lesser extend they project into the shell neuropil of the AMe, and only occasionally, they where found in the internodular neuropil. These projections have large varicosities, and show intense PDH-ir staining compared to PDH-ir fibres that are more distributed in the internodular neuropil (compare Fig. 4C). We therefore propose the anterior and shell neuropil as the most important site for receiving and processing mutual coupling signals between both AMae. Because the nodular neuropil of the AMe receives GABAergic input from the medulla, it appears rather to be involved in photic entrainment (Petri et al., 2002).

The identity of the fourth contralaterally projecting MC I neuron, which is not PDH-ir, remains so far unresolved, but we assume that it belongs to the FMRFamide-ir neuron system of the AMe. Next to the AMe reside about 30 neuronal somata, which are FMRFamid-ir (Petri et al., 1995). A subgroup of these FMRFamide-ir neurons share the positions of the cell bodies and arborisation patterns with the PDH-ir neurons, including contralateral projections *via* the POC, and, probably, also the AOC. Up to six of these neurons show colocalising PDH and FMRFamide immunoreactivity. Here we found an additional Rh-D labelled fibre without PDH immunoreactivity that appears to belong to the fourth MC I soma in the POC next to the PDH-ir fibres. In the POC, FMRFamid-ir fibres with no colocalising PDH immunoreactivity could indeed be traced connecting both AMae *via* the posterior optic tubercles (Petri et al., 1995). Thus, it is very likely that the fourth MC I soma is an FMRF-ir neuron, which projects *via* the POC, since an Rh-D-labelled non-PDH-ir fibre could be traced to the optic lobe contralaterally to the injected AMe.

However, fibres stained with Rh-D that are not PDH-ir, also occur parallel to the Rh-D labelled PDH-ir fibres in the SLP and SMP contralaterally to the injected AMe (Fig. 8A,B). These areas are reached through the AOC, not through the POC. Hence, these AOC-passing non PDH-ir fibres also could belong to the fourth MC I soma that is not PDH-ir. Since we have no indications about single neurons that send projections through both the AOC and POC, we assume that the projections in the anterior and posterior protocerebrum belong to different neurons. However, it is not very likely that more than four MC I neurons exist that have not been detected yet (this cannot be excluded, but is not very likely after 139 injections and optic stalk backfills reported in this and the previous work (Reischig and Stengl, 2002), where never more than four MC I somata could be detected). Hence, these Rh-D-stained non PDH-ir neurons(s) projecting through the AOC

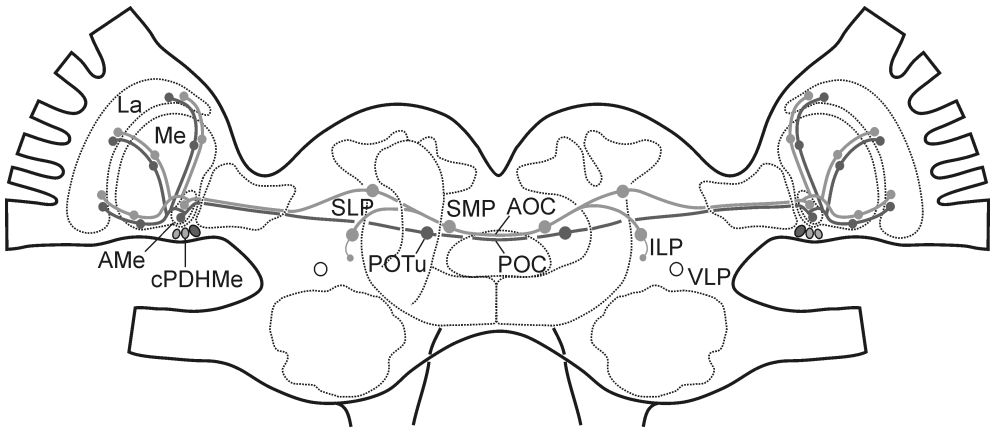

Fig. 9. In each optic lobe, three contralaterally projecting PDH-ir medulla neurons (cPDHMe) connect the accessory medulla (AMe) to various areas in both optic lobes, both midbrain halves, and to the contralateral AMe. This scheme demonstrates the pathways provided by these neurons. The filled circles represent the main sites of synaptic interactions of the two fibre systems. The prominent large cPDHMe (dark grey) appears to connect both AMae *via* the posterior optic commissure (POC) and both posterior optic tubercles (POTu). Thus, the remaining large and medium-sized cPDHMe (light grey) project *via* the anterior optic commissure (AOC) with arborisations in the anterior and proximal superior lateral protocerebra (SLP), the superior median protocerebra (SMP), and, to a lesser extend, the inferior lateral protocerebra (ILP). The ventrolateral protocerebra (VLP), however, seems not to receive inputs from the contralateral AMe, although it is a termination site of PDH-ir fibres, too (open circles).

might terminate in the contralateral midbrain without reaching the contralateral AMe. In this case, FMRFamide-ir AMe neurons passing the AOC either would not reach the contralateral AMe (which is also the case for at least one PDHMe; see below), or they might belong to the population with colocalising PDH- and FMRFamid immunoreactivity.

The comparison of anti-FMRFamide/PDH double-labellings of Petri et al. (1995) with our injection experiments leads to some further assumptions. We demonstrated, that one of the contralaterally projecting anterior PDHMe belongs to the subgroup of the medium-sized, and two to the subgroup of the large somata containing the prominent large cell body (Fig. 6). Among the PDH-ir/FMRFamide-ir colabelled neurons is obviously not the prominent large one. Hence, maximally two of the somata with colocalising PDH and FMRFamid immunoreactivity could connect both AMae. Since no colocalisation in PDH-ir and FMRFamide-ir fibres passing the POC was detected (for the AOC, this has not been explicitly reported), it is likely that the very large anterior PDHMe projects *via* the POC to the opposite AMe, while the remaining large and medium-sized anterior PDHMe use the AOC.

Thus, all anatomical and additional physiological data (Petri et al., 1995; Petri and Stengl, 1997, 2001) indicate that the PDH-ir pathway is paralleled by an FMRFamid-ir pathway which could also serve as coupling pathway between the two bilateral pacemakers. We will test our hypotheses with triple stainings by tracer injections into one AMe combined with simultaneous FMRFamid and PDH immunocytochemistry.

Additionally to the four MC I neurons, also the MC II, and, possibly, the MC III neurons connect both AMae. A direct connection by the MC II is further demonstrated by intracellular single cell recordings with subsequent dye injections (Loesel and Homberg, 2001). This group consists of up to 35 neurons in either optic lobe (Reischig and Stengl, 2002; in this work, up to 20 were found) and projects through a portion of the POC which lies slightly superiorly and anteriorly to the PDH-ir fibres projecting through the POC (Fig. 7D). Whether all MC II neurons indeed connect the AMae, or only a part of them, remains unclear. Neurons of this type react to stationary light stimuli with phasic-tonic excitation and, as also found in crickets (Labhart and Petzold, 1993), react to e-vector changes of polarised light. This reaction profile renders MC II neurons unlikely to be involved in a circadian synchronisation pathway that bases on transmission of pacemaker phase information. These neurons might rather participate in general light entrainment and/or time compensation of (or entrainment by) the polarisation vision system (Loesel and Homberg, 2001). Inputs of contralateral light entrainment pathways into the ipsilateral AMe, as well as input of phase information by the contralateral pacemaker *via* a coupling pathway have been proposed (Page et al., 1977; Page, 1983a,b). Whether these functionally different pathways use the same or different neuronal tracts could not be resolved. Here we present evidences for the anatomical correlates of these different pathways,

which lie to close together to be separated by lesion experiments.

The structure and function of the MC III neurons remains elusive; in our experiments, no arborisations can be assigned to them because of overlap with the prominent MC II arborisations. No single cell recordings or immunostainings are known to the authors that could be assigned to these cells. It is further unclear, whether these neurons indeed connect both AMae or arborise only in the AMe contralaterally to the soma site. Furthermore, it remains unresolved whether they indeed run through the POC, or whether they use tract 2, which merges with the LoVT and is therefore a further candidate to provide direct connections between the AMae (Reischig and Stengl, 2002). Further anatomical studies have to unravel the details of the pathways that couple the bilateral pacemakers.

Central brain projections of the AMe coupling MC I neurons

Next to serving for mutual pacemaker coupling, the PDHMe neurons are discussed to provide circadian output into the central brain (Stengl and Homberg, 1994), a role which is evident in *Drosophila* (Renn et al., 1999; Park et al., 2000; Helfrich-Förster et al., 2000). The processes of the three anterior PDHMe projecting to the contralateral optic lobe do not only connect both AMae, but also form beaded output terminals in the medulla and lamina of the contralateral optic lobe, and in most contralateral central brain areas that are additionally invaded by PDHMe from the same side. The contralateral central projections include the POTu, SMP, SLP, and, to a lesser extend, the ILP, but not the VLP. Additionally, in preliminary degeneration experiments one optic lobe in cockroaches was cut, and after one week allowing degeneration of fibres that were cut off their somata, the brains were removed and stained with anti-β-PDH antiserum. The results demonstrated a nearly mirror-symmetric arborisation pattern of the PDH-ir neurons in the central brain, but no arborisations in the VLP contralaterally to the remaining PDHMe (data not shown).

Because the AOC contains usually six PDH-ir fibres (i.e., from three PDHMe of either side; Stengl and Homberg, 1994), at least one additional PDHMe projects to contralateral central brain areas, but not to the contralateral optic lobe, since maximally two PDHMe were found to project *via* the AOC. This implicates that not only the clocks are synchronised by PDH-ir neurons, but also that output of timing information of both bilateral pacemakers is compared and processed in the clock's central brain output regions.

Page (1983a) proposed in *L. maderae* a functional separation of the pathway that serves for mutual pacemaker synchronisation on the one hand, and the pathway for pacemaker output on the other hand. Our results demonstrate additional midbrain terminations of the AMe coupling neurons. Thus, Page's hypothesis can only partly apply. Additionally, transplantations of the AMe with anterior PDHMe combined with PDH immunocytochemistry indicated that only innervations of the SMP and SMP with PDH-ir fibres might be crucial for sustaining circadian rhythmic locomotor activity (Reischig and Stengl, 2003). Thus, only for the one anterior PDHMe projecting through the POC *via* the POTu it can be assumed that these neurons solely serves for pacemaker coupling but not for central output of timing information. With behavioural experiments involving differential lesions of either the AOC or POC, we started to investigate whether both commissures are functionally indispensable, or whether one commissure alone is capable to sustain pacemaker synchronisation.

Functions of the PDH-ir MC I neurons

An input of the pigment-dispersing factor (PDF), which is most likely expressed by the PDHMe, into the circadian clock has been demonstrated by microinjection of PDF into one optic lobe resulting in a monophasic all-delay phase response curve (PRC) with a peak at the late subjective day (Petri and Stengl, 1997). This PRC differs considerably from the PRCs derived with light pulses, γ-aminobutyric acid, or *Mas*-allatotropin injections (Petri et al., 2002). Thus, PDF is most likely not involved in the light entrainment pathway but provides a non-photic input into the clock. Therefore, our results suggest that the three anterior PDHMe, which connect both AMae, are a part of the synchronising pathway of the bilateral pacemakers. Furthermore, computer models which simulated mutual coupling of *per*/*tim* feedback loops showed that a coupling interaction *via* a combination of all-delay and all-advance phase response curves allows for mutual pacemaker coupling and simulates all respective experimental results obtained from cockroaches (Petri and Stengl, 2001). Thus, we assume that synchronisation of both circadian pacemakers could be mediated by phase-delaying anterior PDH-ir medulla neurons projecting *via* the AOC and POC, together with another parallel, probably FMRFamide-ir neuronal pathway that may cause phase-advances. The effects of several FMRFamide related peptides on the circadian sys-

tem of *Leucophaea* are currently under survey in our laboratory. Moreover, intracellularly recorded neurons, which matched the morphology of an anterior PDHMe projecting through the POC, showed no response to short light pulses during daytime. This is a prerequisite for neurons mediating timing information, which should only be influenced by long-lasting light stimuli during nighttimes. Additionally, ultrastructural studies revealed input- as well as output synapses from PDH-ir neurons in the AMe (Reischig and Stengl, submitted), thus further demonstrating the monosynaptic nature of the AMe-coupling PDH-ir pathways.

Comparison with Drosophila

In *Drosophila*, the main circadian pacemaker driving locomotor and eclosion rhythms is composed of about nine *per*-expressing neurons, the "lateral neurons" (LN_vs), consisting of generally five small (sLN_vs) and four large (l-LN_vs) cell bodies (Frisch et al., 1994; Helfrich-Förster, 1998; Blanchardon et al., 2001; reviewed by Stanewsky, 2002). Both groups express the *pdf* gene (with the exception of one s-LN_v) and can be labelled with anti-β-PDH antiserum (Helfrich-Förster, 1995). Anatomical and physiological studies suggest a differential role between these two groups. The s-LN_vs project to the superior protocerebrum and are crucial for maintaining circadian regulated locomotor activity. The l-LN_vs project to the contralateral optic lobe *via* a posterior commissure without forming sidebranches in the central brain, and appear not to be able to drive locomotor rhythms without the s-LN_vs (Helfrich-Förster, 1995; Shafer et al., 2002). In *Leucophaea*, the situation is more complex. Three groups of anterior PDHMe, each of them consisting of about four neurons (Reischig and Stengl, 1996; Fig. 4), and a group of about four posterior PDHMe could be discerned in *Leucophaea*. Maximally 12 PDH-ir fibres could be found leaving or entering the optic lobe *via* the LoVT (Petri et al., 1995). As shown here, three of them originate from the opposite optic lobe; therefore, maximally nine fibres leave the optic lobe, while the remaining arborise only within the optic lobe ipsilaterally to the soma site. Because the type of faintly staining PDH-ir fibres that were observed within the AMe could not be recognised in the central brain, we propose that the small, faintly staining anterior PDHMe restrict their arborisations to the ipsilateral optic lobe. A subpopulation of nine of the eight medium-sized and large anterior PDHMe and the four posterior PDHMe together project to the protocerebrum. Five neurons arborise solely in the ipsilateral protocerebrum, while four project also to contralateral brain areas, whereby three of the latter project further to the optic lobe contralaterally to the soma site. Since members of both the medium-sized and large groups of anterior PDHMe contribute to contralateral projections, and only one of these cells projects *via* the POC, we cannot unequivocally homologise either of these groups, or the posterior PDHMe, which projection fields are not well known so far, to the s-LN_vs or l-LN_vs of *Drosophila*. We further showed, that apparently both the medium-sized and/or large anterior PDHMe are capable to sustain circadian rhythmic locomotor activity in *Leucophaea* (Reischig and Stengl, 2003). This raises the possibility, that in *Leucophaea* the same neurons may be circadian pacemakers, output and coupling neurons in one. Hence, the clear division of the PDH-ir neurons in two structurally as well as functionally separated units as in *Drosophila* seems not to apply to cockroaches.

ACKNOWLEDGEMENTS

We are very grateful to Heinrich Dircksen (University of Bonn, Germany) for providing the anti-β-PDH antiserum. This work was supported by the Deutsche Forschungsgemeinschaft (DFG) grants STE 531/7-1, 2, 3, and Human Science Frontier.

LITERATURE CITED

Blanchardon E, Grima B, Klarsfeld A, Chelot E, Hardin PE, Preat T, and Rouyer F. 2001. Defining the role of *Drosophila* lateral neurons in the control of circadian rhythms in motor activity and eclosion by targeted genetic ablation and PERIOD protein overexpression. Eur J Neurosci 13:871–888.

Chiba Y and Tomioka K. 1987. Insect circadian activity with special reference to the localisation of the pacemaker. Zool Sci 4:945–954.

Dircksen H, Zahnow CA, Gaus G, Keller R, Rao KR, and Riem JP. 1987. The ultrastructure of nerve endings containing pigment-dispersing hormone (PDH) in crustacean glands: identification by an antiserum against a synthetic PDH. Cell Tissue Res 250:377–387.

Frisch B, Hardin PE, Hamblen-Coyle MJ, Rosbash M, and Hall JC. 1994. A promoterless period gene mediates behavioural rhythmicity and cyclical per expression in a restricted subset of the *Drosophila* nervous system. Neuron 12:555–570.

Helfrich-Förster C. 1995. The period clock gene is expressed in central nervous system neurons which also produce a neuropeptide that reveals the projections of circadian pacemaker cells within the brain of *Drosophila melanogaster*. Proc Natl Acad Sci USA 92:612–616.

Helfrich-Förster C. 1998. Robust circadian rhythmicity of *Drosophila melanogaster* requires the presence of lateral neurons: a brain-behavioural study of disconnected mutants. J Comp Physiol A 182:435–453.

Helfrich-Förster C, Stengl M, and Homberg U. 1998. Organisation of the circadian system in insects. Chronobiol Int 15:567–594.

Helfrich-Förster C, Täuber M, Park JH, Muhlig-Versen M, Schneuwly S, and Hofbauer A. 2000. Ectopic expression of the neuropeptide pigment-dispersing factor alters behavioural rhythms in *Drosophila melanogaster*. J Neurosci 20:3339–3353.

Homberg U, Reischig T, and Stengl M. 2003. Neural organisation of the circadian system of the cockroach *Leucophaea maderae*. Chronobiol Int, in press

Homberg U, Würden S, Dircksen H, and Rao KR. 1991. Comparative anatomy of pigment-dispersing hormone-immunoreactive neurons in the brain of orthopteroid insects. Cell Tissue Res 266:343–357.

Honegger HW and Schürmann FW. 1975. Cobalt sulphide staining of optic fibres in the brain of the cricket, *Gryllus campestris*. Cell Tissue Res 159:213–225.

Labhart T and Petzold J. 1993. Processing of polarised light information in the visual system of crickets. In Wiese K, Gribakin FG, Popov AV, and Renninger G, editors. Sensory system of arthropods. Basel: Birkhäuser Verlag. p 158–169.

Loesel R and Homberg U. 1998. Sustained oscillations in an insect visual system. Naturwissenschaften 85:238–240.

Loesel R and Homberg U. 2001. Anatomy and physiology of neurons with processes in the accessory medulla of the cockroach *Leucophaea maderae*. J Comp Neurol 439:193-207.

Nishiitsutsuji-Uwo J and Pittendrigh CS. 1968. Central nervous system control of circadian rhytmicity in the cockroach. II. The optic lobes, locus of the driving oscillator? Z vergl Physiol 58:14–46.

Page TL. 1982. Transplantation of the cockroach circadian pacemaker. Science 216:73–75.

Page TL. 1983a. Effects of optic-tract regeneration on internal coupling in the circadian system of the cockroach. J Comp Physiol 153:353–363.

Page TL. 1983b. Regeneration of the optic tracts and circadian pacemaker activity in the cockroach *Leucophaea maderae*. J Comp Physiol A 152:231–240.

Page TL. 1984. Neuronal organisation of a circadian clock in the cockroach *Leucophaea maderae*. In: Photoperiodic regulation of insect and molluscan hormones, Ciba foundation symposium 104. London: Pitman. p 115–135.

Page TL, Caldarola PC, and Pittendrigh CS. 1977. Mutual entrainment of bilaterally distributed circadian pacemakers. Proc Natl Acad Sci USA 74:1277–1281.

Park JH, Helfrich-Förster C, Lee G, Liu L, Rosbash M, and Hall JC. 2000. Differential regulation of circadian pacemaker output by separate clock genes in *Drosophila*. Proc Natl Acad Sci USA 97:3608–3613.

Petri B and Stengl M. 1997. Pigment-dispersing hormone shifts the phase of the circadian pacemaker of the cockroach *Leucophaea maderae*. J Neurosci 17:4087–4093.

Petri B and Stengl M. 2001. Phase response curves of a molecular model oscillator: implications for mutual coupling of paired oscillators. J Biol Rhythms 16:125–141.

Petri B, Stengl M, Würden S, and Homberg U. 1995. Immunocytochemical characterisation of the accessory medulla in the cockroach *Leucophaea maderae*. Cell Tissue Res 282:3–19.

Petri B, Homberg U, Loesel R, and Stengl M. 2002. Evidence for a role of GABA and *Mas*-allatotropin in photic entrainment of the circadian clock of the cockroach *Leucophaea maderae*. J Exp Biol 205:1459–1469.

Reischig T and Stengl M. 1996. Morphology and pigment-dispersing hormone immunocytochemistry of the accessory medulla, the presumptive circadian pacemaker of the cockroach *Leucophaea maderae*: a light- and electron- microscopic study. Cell Tissue Res 285:305–319.

Reischig T and Stengl M. 2002. Optic lobe commissures in a three-dimensional brain model of the cockroach *Leucophaea maderae*: a search for the circadian coupling pathways. J Comp Neurol 443:388–400.

Reischig T and Stengl M. 2003. Ectopic transplantation of the accessory medulla restores circadian locomotor rhythms in arrhythmic cockroaches (*Leucophaea maderae*). J Exp Biol 206:1877–1886.

Renn SC, Park JH, Rosbash M, Hall JC, and Taghert PH. 1999. A *pdf* neuropeptide gene mutation and ablation of PDF neurons each cause severe abnormalities of behavioural circadian rhythms in *Drosophila*. Cell 99:791–802.

Roberts SK. 1974. Circadian rhythms in cockroaches: Effects of optic lobe lesions. J Comp Physiol 88:21–30.

Rodriguez J and Deinhard F. 1960. Preparation of a semipermanent mounting medium for fluorescent antibody studies. Virology 12:316–317.

Roth RL and Sokolove PG. 1975. Histological evidence for direct connections between the optic lobes of the cockroach *Leucophaea maderae*. Brain Res 87:23–39.

Shafer OT, Rosbash M, and Truman JW. 2002. Sequential nuclear accumulation of the clock proteins period and timeless in the pacemaker neurons of *Drosophila melanogaster*. J Neurosci 22:5946–5954.

Sokolove PG. 1975. Localisation of the cockroach optic lobe circadian pacemaker with microlesions. Brain Res 87:13–21.

Stanewsky R. 2002. Clock mechanisms in *Drosophila*. Cell Tissue Res 309:11–26.

Stengl M. 1995. Pigment-dispersing hormone-immunoreactive fibres persist in crickets which remain rhythmic after bilateral transection of the optic stalks. J Comp Physiol A 176:217–228.

Stengl M and Homberg U. 1994. Pigment-dispersing hormone-immunoreactive neurons in the cockroach *Leucophaea maderae* share properties with circadian pacemaker neurons. J Comp Physiol A 175:203–213.

Ushirogawa H, Abe Y, and Tomioka K. 1997. Circadian locomotor rhythms in the cricket, *Gryllodes sigillatus*. II. Interactions between bilaterally paired circadian pacemakers. Zoolog Sci 14:729–36.

Wiedenmann G and Loher W. 1984. Circadian control of singing in crickets: two different pacemakers for early-evening and before-dawn activity. J Insect Physiol 30:145–151.

Appendix

APPENDIX A. COMPARATIVE CONSIDERATIONS

Since the accessory medulla (AMe) of *Leucophaea* now is the one best characterised among all insects, some comparative studies in other insect groups still remain to come. It is a very interesting aspect that the AMe was first discovered in holometabolous insects where it functions, together with the accessory lamina, as visual integration centre throughout the larval development of the insect (Pflugfelder, 1936; Hanström, 1940; Ehnbohm, 1948). There, the three classical optic lobe neuropils lamina, medulla, and lobula not yet exist (Meinertzhagen, 1973). In primitive holometabolous insects, such as Trichoptera, the larval stemmata together with their connections to the AMe persist in the imago (Hagberg, 1986). The phylogenetic development of the AMe from an internal clock in hemimetabolous insects into a visual neuropil in the larvae of holometabolous insects, where it probably also function as internal clock at least in the adult stage, is quite astonishing. Detailed comparative studies remain to unravel the secrets of this exceptional career of the AMe. Further, the homology of the AMae in hemi- and holometabolous insects still remains to be established. To give a first impression about differences of the AMe morphology in insects, selected images of AMae and PDH-ir neurons of several insects belonging to different groups are added herein (Fig. 1). The nodular appearance of the AMe in some insects as crickets and hawkmoths is not as obvious as in *Leucophaea* or in the locust (Fig. 1A–C). In flys, the AMe is not as clear distinguishable as in other insects (Fig. 1D). The functional implications of these differences are so far completely unknown. Interestingly, in the primitive zygopteroid insect *Lepisma saccharina* the AMe is very prominent and lies between the lamina and the medulla (Fig. 1E). In all other investigated insects, the AMe is closer to the lobula, what is a result of an about 90° turn of the medulla around its vertical axis during development in the higher insects. Hence, one may speculate whether probably the complete distal layer of the medulla (which is quite continuous to the anterior neuropil of the AMe in *Leucophaea*) in fact belongs to the AMe, or, in other words, the AMe is a special differentiation of the distal layer of the medulla.

Such and related questions might additionally be answered by investigation of the AMe throughout the ontogenetic development of insects. For *Leucophaea*, studies on first instar nymphae show that the AMe is already developed, lies between medulla and lobula, and shows its typical nodular appearance (Meßner, 1998; Fig. 1F). The AMe is larger in respect to the other optic lobe neuropils than in the adult stage. In the locust *Schistocerca gregaria*, the development of PDH-ir medulla was investigated throughout embryonic development (Homberg and Prakash, 1996). Somata of the PDHMe appeared at stage 45 % of embryonic development. Between 50 and 55 %, the distal medulla layer fibre fan and the AMe differentiate together out of an arc of PDH-ir fibres originally extending over the distal surface of the medulla, thus supporting the assumption of a common origin of AMe and the distal medulla layer.

LITERATURE CITED

Ehnbohm K. 1948. Studies on the central and sympathetic nervous system and some sense organs in the head of neuropteroid insects. Opusc Entomol [Suppl] 8:1–162.

Hagberg M. 1986. Ultrastructure and central projections of extraocular photoreceptors in caddiesflies. Cell Tissue Res 245:643–648.

Hanström B. 1940. Inkretorische Organe, Sinnesorgane und Nervensystem des Kopfes einiger niedriger Insektenordnungen. Kungl Sven Vetensk Akad Handl Ser 3 18:1–265.

Homberg U and Prakash N. 1996. Development of pigment-dispersing hormone-like immunoreactivity in the brain of the locust *Schistocerca gregaria*: comparison with immunostaining for urotensin I and *Mas*-allatotropin. Cell Tissue Res 285:127–139.

Meinertzhagen IA. 1973. Development of the compound eye and optic lobe of insects. In Young D, editor. Developmental neurobiology of arthropods. Cambridge: Cambridge University Press. p 51–104.

Meßner AM. 1998. Untersuchungen zur Inneren Uhr von Insekten: Desoxyglucose-Markierung der akzessorischen Medulla in der Schabe *Leucophaea maderae* und PDH-immunzytochemische Untersuchungen. Teacher examination thesis: University of Regensburg, Germany.

Pflugfelder O. 1936. Vergleichend-anatomische, experimentelle und embryologische Untersuchungen über das Nervensystem und die Sinnesorgane der Rynchoten. Stuttgart: Schweizerbart'sche Verlagsbuchhandlung.

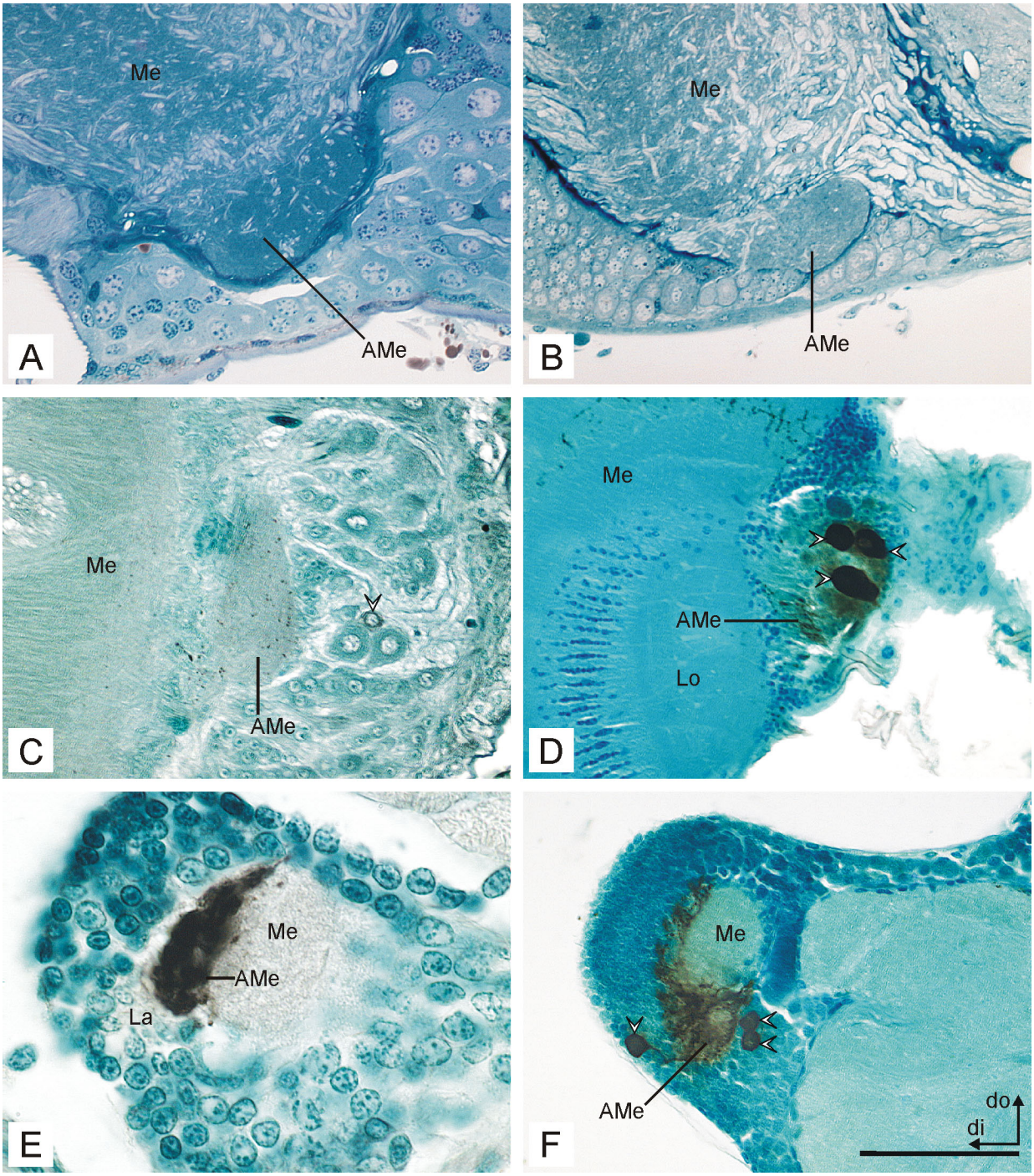

Fig. 1. Comparisons the of accessory medulla morphology and PDH-immunoreactivity among several insect species (A locust *Schistocerca gregaria*; B cricket *Teleogryllus commodus*; C hawkmoth *Manduca sexta*; D housefly *Musca domestica*; E silverfish *Lepisma saccharina*; F first larval stage of *Leucophaea maderae*; A,B show 3 μm resin sections stained with Richardson's blue, C–F show 10 μm paraffin sections stained with anti-βPDH-antiserum and methylene blue. AMe accessory medulla; La lamina; Lo lobula; Me medulla). **A:** The AMe of the locust shows a nodular appearance similar to the cockroach. **B:** The AMe of the cricket consists of dense neuropil, which however lacks the typical nodular structure that is apparent in cockroaches. **C:** Also, the AMe of the hawkmoth is evenly structured. Faint PDH-ir staining is scattered throughout the neuropil. Arrowhead: PDH-ir medulla soma. **D:** In the housefly, the AMe is far less conspicuous than in all other insect groups shown here, and is only recognisable by the location of PDH-ir fibres in the vicinity of the PDH-ir medulla somata (arrowheads). **E:** The silverfish has only 12 ommatidia in one compound eye and hence, possesses a quite small optic lobe. The large AMe is situated distally to the medulla. Of the lamina, only a small part is visible. **F:** As in the silverfish, the AMe of the cockroach larva is relatively large compared to the medulla. The position of the AMe ventrally to the medulla will later change to the typical ventro-medial position. Arrowheads: PDH-ir medulla somata. The preparations for Figs. 1E and 1F were performed by Andreas Meßner under supervision by the author. Coordinates: di distal, do dorsal. Scale bar in F = 100 μm in A–D and F, 30 μm in E.

APPENDIX B. ULTRASTUCTURE OF CONTRALATERAL AME-PROJECTIONS

In preliminary degeneration experiments, it was examined on the electron-microscopic (EM) level whether processes of AMe branch in the contralateral AMe. After cutting the processes off a neuron, the cut off neurits progressingly degenerate. Depending on the time elapsed after the cut, profiles of degenerating fibres can be recognised on EM micrographs. They appear darker than normal fibres, and undergo progressive structural disintegration until a total disassembly of the fibre. To examine whether neurons of one optic lobe project to the AMe of the contralateral optic lobe, the optic stalk on one side was sectioned (Fig. 2A). If neurons in the sectioned optic lobe form axonal projections in the contralateral AMe, degenerating fibres should there become visible in the EM-analysis. In these experiments, the degeneration time (the time between the cut of the optic lobe and sacrificing the animal) is crucial to obtain sufficient "staining" of the degenerating fibres without too much loss of intracellular structure. Hence, a series of experiments ($N = 21$) was performed to optimise degeneration times. After severance of one optic stalk of CO_2-anesthetised cockroaches, groups of animals were allowed to survive for different times (4 h, $n = 4$; 8 h, $n = 4$; 16 h, $n = 4$; 21 h, $n = 7$; 31 h; $n = 2$; one sham-operated control animal in every group). Then, the brains where processed for conventional EM-histology as described in the methods sections of Chapters I and II.

The best compromise between preservation and recognisability of fibres was achieved with a degeneration time of eight hours. Some fibres even retained their dense core vesicles and could be recognised due to darker staining of the cytoplasm. Degenerated fibres were preferentially distributed in the anterior, shell, and internodular neuropil of the AMe, thus supporting respective light microscopical observations (Chapters VI, VII). Most of the degenerated fibres in the internodular neuropil displayed no or few dense core vesicles (Fig. 2B). At these fibres, axo-axonal input synapses as well as output synapses onto dendritic processes could be found. Thus, heterolateral neurons are directly involed in neuronal circuitries of the AMe. The distribution pattern of these profiles in the AMe suggests that they originate from the contralateral MC II neurons, which at least partly directly connect the bilateral symmetric AMae (see Chapter VI, Fig. 5E; Chapter VII, Fig. 7A). In one case, a degenerated fibre with medium-sized dense core vesicles was observed in the shell neuropil of the AMe (Fig. 2C). Since this vesicle type is always associated with PDH-immunoreactivity (Chapter I, Fig. 6A,B; Chapter II, Fig. 9A,B) and belongs to the large anterior PDH-ir medulla neurons (PDHMe), it is very likely that this profile originates from a fibre of a contralateral large anterior PDHMe.

The evaluation of this experimental series was not fully completed and additional degeneration experiments were not undertaken in favour of other experimental approaches, which reveal more information about the overall assembly of the AMe coupling pathways (Chapters VI, VII). Therefore, the results were not included in a separate chapter of this dissertation. However, these preliminary experiments allow for a further exploration of the ultrastructure and synaptology of the coupling pathways of the AMe, and may be expanded in the future with immunocytochemical methods to reveal details about the synaptic connectivities of identified contralaterally projecting neurons like the anterior PDHMe.

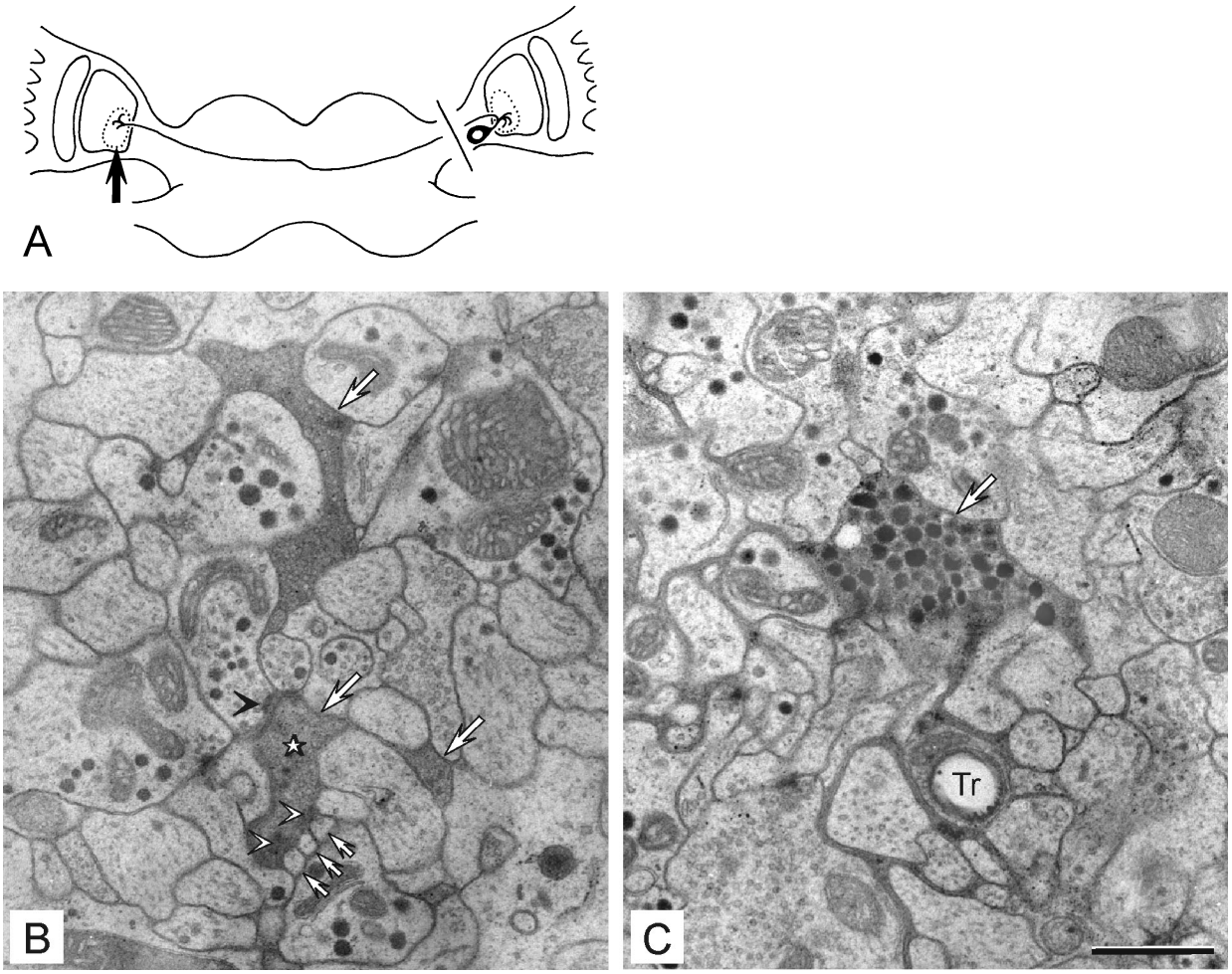

Fig. 2. Scheme of the experimental procedure of the degeneration experiments (A), and electron micrographs of degenerated fibres in the AMe contralaterally to the sectioned optic lobe after 16 (B) and 8 hours (C) of degeneration time. **A:** After sectioning of one optic stalk, fibres that where cut off from their somata will degenerate. Hence, axonal projections in the contralateral AMe (arrow) can be visualised in electron microscopical examinations. **B:** These degenerated profiles (white arrows) in the internodular neuropil of the AMe show only few dense core vesicles. One profile (asterisk) receives synaptic input (black arrowhead) from a profile with large dense core vesicles. This degenerated profile additionally forms output synapses (white arrowheads) to small dendritic processes (small arrows). **C:** This degenerated profile filled with medium-sized dense core vesicles (arrow) was found in the shell neuropil of the AMe. Tr trachea. Scale bar in C = 1 μm in B,C.

ACKNOWLEDGEMENTS

I'am very greatful to HD Dr. Monika Stengl for supervising my PhD study. In the long time of our fruitful cooperation I never missed her support. She always encouraged me to follow own ideas and enabled me to work very independently.

My special thank is dedicated to Sabine Hofer, who brought the necessary new turn into my life and therefore, largely contributed to the success of this work.

I also thank Prof. Dr. Roland Brandl to take the part of the second referee of this thesis, and Prof. Dr. Paul Galland and Prof. Dr. Uwe Homberg for their participation in the examination commission.

Further, I thank all people in the labs of Monika Stengl, Uwe Homberg, and Joachim Schachtner in Regensburg and Marburg for fruitful discussions and helpful suggestions in many regards, particularly Jan Dolzer, Frank Just, Rudi Lösel, Bernhard Petri, Joachim Schachtner, Gesa Thies, and Rita Zintl.

Ich versichere, daß ich meine Dissertation

Identification and characterisation of the circadian pacemaker of the cockroach *Leucophaea maderae*

selbstständig, ohne unerlaubte Hilfe angefertigt und mich dabei keiner anderen als der von mir ausdrücklich bezeichneten Quellen und Hilfen bedient habe.

Die Dissertation wurde in der jetzigen oder einer ähnlichen Form noch bei keiner anderen Hochschule eingereicht und hat noch keinen sonstigen Prüfungszwecken gedient.

Marburg, den

(Thomas Reischig)